Published for SISSA by Springer
Received: April 21, 2021
Revised: August 10, 2021
Accepted: August 15, 2021
Published: September 14, 2021

New physics explanations of a_μ in light of the FNAL muon $g-2$ measurement

Peter Athron,[a,b] **Csaba Balázs,**[b] **Douglas H.J. Jacob,**[b] **Wojciech Kotlarski,**[c] **Dominik Stöckinger**[c] **and Hyejung Stöckinger-Kim**[c]

[a] *Department of Physics and Institute of Theoretical Physics, Nanjing Normal University, Nanjing, Jiangsu 210023, China*
[b] *School of Physics and Astronomy, Monash University, Melbourne, Victoria 3800, Australia*
[c] *Institut für Kern- und Teilchenphysik, TU Dresden, Zellescher Weg 19, 01069 Dresden, Germany*

E-mail: peter.athron@coepp.org.au, csaba.balazs@monash.edu, douglas.jacob@monash.edu, wojciech.kotlarski@tu-dresden.de, dominik.stoeckinger@tu-dresden.de, hyejung.stoeckinger-kim@tu-dresden.de

Abstract: The Fermilab Muon $g-2$ experiment recently reported its first measurement of the anomalous magnetic moment $a_\mu^{\rm FNAL}$, which is in full agreement with the previous BNL measurement and pushes the world average deviation Δa_μ^{2021} from the Standard Model to a significance of 4.2σ. Here we provide an extensive survey of its impact on beyond the Standard Model physics. We use state-of-the-art calculations and a sophisticated set of tools to make predictions for a_μ, dark matter and LHC searches in a wide range of simple models with up to three new fields, that represent some of the few ways that large Δa_μ can be explained. In addition for the particularly well motivated Minimal Supersymmetric Standard Model, we exhaustively cover the scenarios where large Δa_μ can be explained while simultaneously satisfying all relevant data from other experiments. Generally, the a_μ result can only be explained by rather small masses and/or large couplings and enhanced chirality flips, which can lead to conflicts with limits from LHC and dark matter experiments. Our results show that the new measurement excludes a large number of models and provides crucial constraints on others. Two-Higgs doublet and leptoquark models provide viable explanations of a_μ only in specific versions and in specific parameter ranges. Among all models with up to three fields, only models with chirality enhancements can accommodate a_μ and dark matter simultaneously. The MSSM can simultaneously explain a_μ and dark matter for Bino-like LSP in several coannihilation regions. Allowing under abundance of the dark matter relic density, the Higgsino- and particularly Wino-like LSP scenarios become promising explanations of the a_μ result.

Keywords: Beyond Standard Model, Supersymmetric Standard Model

ArXiv ePrint: 2104.03691

https://doi.org/10.1007/JHEP09(2021)080

JHEP09(2021)080

Contents

JHEP09(2021)080

1 Introduction

Precision measurements of the anomalous magnetic moment of the muon, a_μ, provide excellent tests of physics beyond the Standard Model (BSM), and the results can give hints at what form it might take. Recently the E989 experiment [1] at the Fermi National Laboratory (FNAL) published the most precise measurement of the anomalous magnetic moment of the muon [2]. This result, and the previous result from Brookhaven National Laboratory (BNL) [3] (adjusted according to the latest value of μ_μ/μ_p as in ref. [4]) and the new world average [2] are

$$a_\mu^{\text{FNAL}} = (116\,592\,040 \pm 54) \times 10^{-11}, \tag{1.1}$$
$$a_\mu^{\text{BNL}} = (116\,592\,089 \pm 63) \times 10^{-11}, \tag{1.2}$$
$$a_\mu^{2021} = (116\,592\,061 \pm 41) \times 10^{-11}. \tag{1.3}$$

The FNAL measurement is fully compatible with the previous best measurement and has a smaller uncertainty. Compared to the BNL result, the new world average a_μ^{2021} has a slightly decreased central value and a 30% reduced statistics-dominated uncertainty. In parallel to the FNAL measurement, a worldwide theory initiative provided the White Paper [4] with the best estimate for the central theory prediction in the Standard Model (SM). Its value and uncertainty are

$$a_\mu^{\text{SM}} = (116\,591\,810 \pm 43) \times 10^{-11}. \tag{1.4}$$

This SM prediction is based on up-to-date predictions of QED [5, 6], electroweak [7, 8], hadronic vacuum polarization [9–15] and hadronic light-by-light contributions [16–30]. For further discussion of recent progress we refer to ref. [4].[1] The experimental measurements show the following deviations from the updated theoretical SM prediction:

$$\Delta a_\mu^{\text{FNAL}} = (23.0 \pm 6.9) \times 10^{-10}, \tag{1.5}$$
$$\Delta a_\mu^{\text{BNL}} = (27.9 \pm 7.6) \times 10^{-10}, \tag{1.6}$$
$$\Delta a_\mu^{2021} = (25.1 \pm 5.9) \times 10^{-10}. \tag{1.7}$$

In each case the uncertainties are combined by summing them in quadrature. In the last line Δa_μ^{2021} is the new, updated deviation based on the experimental world average and the SM White Paper result. The long standing discrepancy between the BNL measurement and the SM theory prediction is confirmed and sharpened. Its significance is increased from 3.7σ to 4.2σ by the combination with FNAL data.

This improvement has a significant impact on our understanding of BSM physics as it strengthens a major constraint on a variety of otherwise plausible SM extensions. In this paper we provide a comprehensive overview of this impact the FNAL measurement has on

[1] The White Paper also contains an extensive discussion of promising progress of lattice QCD calculations for the hadronic vacuum polarization. The lattice world average evaluated in ref. [4], based on [31–39], is compatible with the data-based result [9–15], has a higher central value and larger uncertainty. More recent lattice results are obtained in refs. [40, 41]. Scrutiny of these results is ongoing (see e.g. ref. [42]) and further progress can be expected.

JHEP09(2021)080

BSM physics. We examine the impact in minimal 1-, 2- and 3-field extensions of the SM, and in the well-motivated Minimal Supersymmetric Standard Model (MSSM). Within this theoretical framework we provide a thorough overview of the impact the FNAL measurement has and highlight promising scenarios that can explain it. In our investigation we use state-of-the-art a_μ calculations. For the simple SM extensions we use FlexibleSUSY [43, 44], which includes the universal leading logarithmic two-loop QED contributions in addition to the full one-loop calculation. For the MSSM we use `GM2Calc` [45], which implements a dedicated high-precision MSSM calculation including two-loop and higher-order contributions based on the on-shell scheme.

Reviews and general discussions of BSM contributions to a_μ have been given in refs. [25, 46–51]. Previously the deviation from BNL has been studied extensively in the literature. There was intensive activity proposing BSM explanations of the BNL result after its first discovery and in following years [52–163]. Many ideas came under pressure from results at the LHC, and scenarios were proposed which could resolve tensions between a_μ, LHC results and other constraints [164–376]. Many of these constructions use supersymmetry in some way and will be discussed in our section 6, but this list also includes solutions motivated by extra dimensions [108–113, 238, 239] and technicolor or compositeness [114–119, 240, 241], or even introducing unparticle physics [150], as well as just extending models with new states like the two-Higgs doublet models [120–123, 242–264] or adding leptoquarks [124, 125, 265–272], new gauge bosons (including sub-GeV gauge bosons, dark photons and generalizations) [126–133, 273–292], Higgs triplets [156, 157] and vector-like leptons [289, 293–304], or very light, neutral and weakly interacting scalar particles [305–313]. Some works have taken a systematic approach, classifying states according to representations and investigating a large set of them [152, 367–376].[2]

The deviation found already by the BNL measurement also gave rise to the question whether it could be due to hypothetical, additional contributions to the hadronic vacuum polarization.[3] If such additional effects would exist, they could indeed shift the SM prediction for a_μ towards the experimental value, but would at the same time worsen the fit for electroweak precision observables, disfavouring such an explanation of the deviation [411–415].

In spite of the vast number of works and the many varied ideas, for most models the same general principles apply. Typically the deviation requires new states with masses below the TeV scale or not much above 1 TeV to explain the experimental value with perturbative couplings. The models which allow large a_μ with particularly large masses involve very large couplings and/or introduce enhancements through new sources of muon chirality flips (as we will describe in the next section). Therefore the absence of BSM signals at the LHC has led to tensions with large a_μ in many models: either very large couplings and heavy masses are needed or the stringent LHC limits have to be evaded in other ways.

[2]Finally on the same day as the release of the FNAL result a very large number of papers were already released interpreting it [377–410]. This demonstrates what a landmark result this is and the intense interest it is generating within the particle physics community.

[3]This question is further motivated by lattice QCD results on the hadronic vacuum polarization, see footnote 1.

JHEP09(2021)080

Not only LHC, but also dark matter searches can lead to tensions in many models. The Planck experiment [416, 417] observed the dark matter abundance of the universe to be:

$$\Omega_{h^2} = 0.1200 \pm 0.001. \tag{1.8}$$

Since BSM contributions to a_μ are often mediated by new weakly interacting neutral particles, many interesting models also contain dark matter candidate particles. Any dark matter candidate particle with a relic density more than 0.12 is over abundant and therefore strongly excluded. Further, the negative results of direct dark matter searches can lead to strong additional constraints on the model parameter spaces.

In the present work we aim to provide a comprehensive picture of the impact the new FNAL measurement has on BSM physics. The models we investigate in detail represent a wide range of possibilities. They cover models with new strongly or weakly interacting particles, with extra Higgs or SUSY particles, with or without a dark matter candidate, with or without new chirality flips and with strong or weak constraints from the LHC. In all cases we provide a detailed description of the mechanisms for the contributions to a_μ; we then carry out detailed investigations of the model parameter spaces, including applicable constraints from the LHC and dark matter using state-of-the-art tools for evaluating constraints and LHC recasting. This allows us to answer which models and which model scenarios can accommodate the new FNAL measurement and the deviation Δa_μ^{2021} while satisfying all other constraints.

The rest of this paper is as follows. In section 2 we explain how the anomalous magnetic moment appears in quantum field theories and emphasise the most important aspects which both make it an excellent probe of BSM physics and make the observed anomaly very difficult to explain simultaneously with current collider limits on new physics. In sections 3, 4, and 5 we present results for minimal 1-, 2- and 3-field extensions of the SM respectively that show the impact the new FNAL result has on these models. To provide a more global picture for 1- and 2-field extensions, in section 3.1 and section 4.1 we also classify models of this type systematically by quantum numbers and use known results to summarise their status with respect to explaining the BNL result, showing that this measurement severely restricts the set of possible models. This allows us to select models with the best prospects for detailed investigation, presenting results for the two-Higgs doublet model (section 3.2), leptoquark models (section 3.3) and two field extensions with scalar singlet dark matter (section 4.2). For three field models we perform a detailed examination of models with mixed scalar singlet and doublet dark matter (section 5.1) and fermion singlet and doublet dark matter (section 5.2). In section 6 we discuss the impact of the sharpened deviation on the MSSM, which is widely considered one of the best motivated extensions of the SM. This section also contains a brief self-contained discussion of a_μ and the possible enhancement mechanisms in the MSSM and explains in detail our treatment of dark matter data and LHC recasting. All constraints are then applied on the general MSSM, allowing all kinds of neutralino LSPs. Finally we present our conclusions in section 7.

JHEP09(2021)080

2 Muon $g-2$ and physics beyond the SM

In quantum field theory, the anomalous magnetic moment of the muon is given by

$$a_\mu = -2m_\mu F_M(0)\,, \tag{2.1}$$

where m_μ is the muon pole mass and $F_M(0)$ is the zero-momentum limit of the magnetic moment form factor. The latter is defined via the covariant decomposition of the 1-particle irreducible muon-muon-photon vertex function $\Gamma^\mu(p,-p',q)$,

$$\bar{u}(p')\Gamma^\mu(p,-p',q)u(p) = -eQ\,\bar{u}(p')\left[\gamma^\mu F_V(q^2) + (p+p')^\mu F_M(q^2) + \ldots\right]u(p) \tag{2.2}$$

with the on-shell renormalized electric charge e, $Q=-1$, on-shell momenta $p^2 = p'^2 = m_\mu^2$, on-shell spinors $u(p)$, $u(p')$ and $q = p'-p$. The quantum field theory operator corresponding to a_μ connects left- and right-handed muons, i.e. it involves a chirality flip.

The observable a_μ is CP-conserving, flavour conserving, loop induced, and chirality flipping. These properties make it complementary to many other precision and collider observables. In particular the need for a muon chirality flip has a pivotal influence on the BSM phenomenology of a_μ. It requires two ingredients.

- Breaking of chiral symmetry. There must be a theory parameter breaking the chiral symmetry under which the left- and right-handed muon fields transform with opposite phases. In the SM and the MSSM and many other models this chiral symmetry is broken only by the non-vanishing muon Yukawa coupling y_μ.[4] In all these cases contributions to $F_M(0)$ are proportional to at least one power of the muon Yukawa coupling, where e.g. the MSSM Yukawa coupling is enhanced compared to the SM one.

  In some models, there are additional sources of breaking of the muon chiral symmetry. Examples are provided by the leptoquark model discussed below in section 3.3, where the simultaneous presence of left- and right-handed couplings $\lambda_{L,R}$ and the charm- or top-Yukawa coupling breaks the muon chiral symmetry and leads to contributions governed by $\lambda_L\lambda_R m_{c,t}$. Similar mechanisms can also exist in the three-field models discussed below.

- Spontaneous breaking of electroweak gauge invariance. Since the a_μ operator connects a left-handed lepton doublet and right-handed lepton singlet it is not invariant under electroweak (EW) gauge transformations. Hence any contribution to $F_M(0)$ also must be proportional to at least one power of some vacuum expectation value (VEV) breaking EW gauge invariance. In the SM, there is only a single VEV v, so together with the required chirality flip, each SM-contribution to $F_M(0)$ must be proportional to $y_\mu v$ and thus to the tree-level muon mass. However, e.g. in the MSSM, there are two VEVs $v_{u,d}$; hence there are contributions to a_μ governed by $y_\mu v_u$, while the tree-level muon mass is given via $y_\mu v_d$. This leads to the well-known enhancement by $\tan\beta = v_u/v_d$.

[4] For the MSSM this statement is true if one follows the customary approach to parametrize the trilinear scalar soft SUSY-breaking parameters as $T_f \equiv A_f y_f$ by explicitly factoring out the respective Yukawa couplings.

JHEP09(2021)080

In addition, the gauge invariant operators contributing to a_μ are (at least) of dimension six; hence any BSM contribution to a_μ is suppressed by (at least) two powers of a typical BSM mass scale. In conclusion, BSM contributions to a_μ can generically be parametrized as

$$\Delta a_\mu^{\text{BSM}} = C_{\text{BSM}} \frac{m_\mu^2}{M_{\text{BSM}}^2}, \tag{2.3}$$

where M_{BSM} is the relevant mass scale and where the coefficient C_{BSM} depends on all model details like origins of chirality flips and electroweak VEVs as well as further BSM coupling strengths and loop factors.[5]

An interesting side comment is that BSM particles will typically not only contribute to a_μ but also to the muon mass in similar loops, and those contributions depend on the same model details and scale as $\Delta m_\mu^{\text{BSM}}/m_\mu \sim \mathcal{O}(C_{\text{BSM}})$. The estimate $\Delta a_\mu^{\text{BSM}} \sim \mathcal{O}(\Delta m_\mu^{\text{BSM}}/m_\mu) \times \frac{m_\mu^2}{M_{\text{BSM}}^2}$ is therefore valid in many models [50, 53]. One may impose a criterion that these BSM corrections to the muon mass do not introduce fine-tuning, i.e. do not exceed the actual muon mass. In models where this criterion is satisfied, C_{BSM} can be at most of order unity and a generic upper limit,

$$\Delta a_\mu^{\text{BSM}} \lesssim \mathcal{O}(1) \frac{m_\mu^2}{M_{\text{BSM}}^2}, \tag{2.4}$$

is obtained [50, 53]. In this wide class of models, imposing this criterion then implies an order-of-magnitude upper limit on the mass scale for which the value Δa_μ can be accommodated:[6]

$$\text{BNL:} \qquad \Delta a_\mu^{\text{BSM}} = 27.9 \times 10^{-10} \quad \Rightarrow \quad M_{\text{BSM}} \lesssim \mathcal{O}(2)\text{TeV} \tag{2.5}$$

$$\text{Including FNAL:} \qquad \Delta a_\mu^{\text{BSM}} = 25.1 \times 10^{-10} \quad \Rightarrow \quad M_{\text{BSM}} \lesssim \mathcal{O}(2.1)\text{TeV} \tag{2.6}$$

In appendix A we collect the generic one-loop Feynman diagrams which can contribute to a_μ in a general renormalizable quantum field theory. The results are expressed in terms of generic masses and couplings and reflect the above discussion. Contributions containing the factor m_μ^2 correspond to chirality flips on the external muon line governed by the SM Yukawa coupling and VEV; the other contributions correspond to chirality flips via BSM couplings or fermion masses and require the simultaneous presence of BSM couplings to left- and right-handed muons, which in turn requires that some virtual states in the loop are not pure gauge eigenstates but mix via electroweak VEVs.

[5] We note that eq. (2.3) does not imply the naive scaling $\Delta a_e^{\text{BSM}} : \Delta a_\mu^{\text{BSM}} : \Delta a_\tau^{\text{BSM}} \approx m_e^2 : m_\mu^2 : m_\tau^2$ with the lepton generation since the coefficient C_{BSM} does not have to be generation-independent. Still, the prefactor m_l^2/M_{BSM}^2 in a_l implies that the muon magnetic moment is more sensitive to BSM physics than the electron magnetic moment and that typical models which explain e.g. the BNL deviation for a_μ give negligible contributions to a_e. For detailed discussions and examples for deviations from naive scaling in models with leptoquarks, two Higgs doublets or supersymmetry we refer to refs. [330, 418].

[6] The case of vector-like leptons provides an interesting exception with a slightly more complicated behaviour, see the discussions in refs. [293, 294, 303] and below in section 4.1. There, also tree-level BSM contributions to the muon mass exist, and the ratio between Δa_μ and $\Delta m_\mu^{\text{tree}}$ does not scale as $1/M_{\text{BSM}}^2$ as above but as $1/(16\pi^2 v^2)$. This might seem to allow arbitrarily high masses, circumventing the bounds (2.4), (2.5), (2.6). However, even using only tree-level effects in the muon mass, these references also find upper mass limits from perturbativity and constraints on the Higgs-muon coupling.

JHEP09(2021)080

3 Single field extensions

In this section we discuss the impact of a_μ on simple single field extensions of the SM. Such extensions can be interesting in their own right or representative for more elaborate models with many new fields and particles and illustrate the impact of the a_μ measurement. We begin in section 3.1 with a general overview of the status of one-field extensions, covering renormalizable models with new spin 0, spin 1/2 or spin 1 fields. In sections 3.2-3.3 we then show the impact of the latest data on the two most interesting cases — the two-Higgs doublet model and leptoquark models.

3.1 Overview

Before presenting our updated results for those cases in sections 3.2-3.3, we first classify the single field extensions according to their spin and their SM representations and charges, and discuss the known results to provide a very important overview of what is possible and put our new results in the appropriate context. Single field models have been classified or reviewed in a systematic manner in refs. [367, 369–371, 421], with the results summarized in table 1.

The confirmation of a large positive deviation from the SM prediction in the anomalous magnetic moment of the muon rules out most one-field extensions of the SM. The reasons for this are simple. First to explain the anomaly these models must provide a positive contribution to a_μ, and this constraint alone rules out a large number of the possible extensions. Secondly even if the sign of the contribution is positive, the models must have a chirality flip in order for the contribution to be large enough with perturbative couplings. Without a chirality flipping enhancement, contributions that explain a_μ require the masses of the new particles to be so light that they would already have been observed in collider experiments.

Ref. [367] considers scalars, fermions and vectors. For fermions and scalars they considered gauge invariant extensions with SU(3) singlets, which may be SU(2) singlets, doublets, triplets ($Y = -1$) and adjoint triplets ($Y = 0$) for fermions, and doublets and triplets for scalars. They do not consider scalars obtaining a VEV. They treated vector states as simplified models of neutral and charged vector states without specifying any gauge extension. They assume minimal flavour violating interactions with leptons (see 2.2 of ref. [367] for details) for LEP contact interaction limits and LHC searches, and perform the calculation of Δa_μ at the one-loop level. They obtained a negative contribution to a_μ from the scalar triplet, the neutral fermion singlet, and fermion triplets with hypercharge 0 or -1, and found that while a charged fermion singlet can give a positive contribution it is always too small to explain $\Delta a_\mu^{\rm BNL}$. They found scalar and fermion doublet scenarios that could accommodate $\Delta a_\mu^{\rm BNL}$ at the 1σ level were ruled out by LEP searches for neutral scalars and LEP limits on mixing with SM leptons respectively. For a single neutral vector boson, they find that the region where $\Delta a_\mu^{\rm BNL}$ can be explained within 1σ is entirely ruled out by LEP constraints from 4-fermion contact interactions and resonance searches. They also consider a single charged vector boson coupling to a right handed charged lepton and a

JHEP09(2021)080

Model	Spin	$SU(3)_C \times SU(2)_L \times U(1)_Y$	Result for $\Delta a_\mu^{\rm BNL}$, Δa_μ^{2021}
1	0	$(\mathbf{1},\mathbf{1},1)$	Excluded: $\Delta a_\mu < 0$
2	0	$(\mathbf{1},\mathbf{1},2)$	Excluded: $\Delta a_\mu < 0$
3	0	$(\mathbf{1},\mathbf{2},-1/2)$	Updated in section 3.2
4	0	$(\mathbf{1},\mathbf{3},-1)$	Excluded: $\Delta a_\mu < 0$
5	0	$(\overline{\mathbf{3}},\mathbf{1},1/3)$	Updated section 3.3
6	0	$(\overline{\mathbf{3}},\mathbf{1},4/3)$	Excluded: LHC searches
7	0	$(\overline{\mathbf{3}},\mathbf{3},1/3)$	Excluded: LHC searches
8	0	$(\mathbf{3},\mathbf{2},7/6)$	Updated section 3.3.
9	0	$(\mathbf{3},\mathbf{2},1/6)$	Excluded: LHC searches
10	1/2	$(\mathbf{1},\mathbf{1},0)$	Excluded: $\Delta a_\mu < 0$
11	1/2	$(\mathbf{1},\mathbf{1},-1)$	Excluded: Δa_μ too small
12	1/2	$(\mathbf{1},\mathbf{2},-1/2)$	Excluded: LEP lepton mixing
13	1/2	$(\mathbf{1},\mathbf{2},-3/2)$	Excluded: $\Delta a_\mu < 0$
14	1/2	$(\mathbf{1},\mathbf{3},0)$	Excluded: $\Delta a_\mu < 0$
15	1/2	$(\mathbf{1},\mathbf{3},-1)$	Excluded: $\Delta a_\mu < 0$
16	1	$(\mathbf{1},\mathbf{1},0)$	Special cases viable
17	1	$(\mathbf{1},\mathbf{2},-3/2)$	UV completion problems
18	1	$(\mathbf{1},\mathbf{3},0)$	Excluded: LHC searches
19	1	$(\overline{\mathbf{3}},\mathbf{1},-2/3)$	UV completion problems
20	1	$(\overline{\mathbf{3}},\mathbf{1},-5/3)$	Excluded: LHC searches
21	1	$(\overline{\mathbf{3}},\mathbf{2},-5/6)$	UV completion problems
22	1	$(\overline{\mathbf{3}},\mathbf{2},1/6)$	Excluded: $\Delta a_\mu < 0$
23	1	$(\overline{\mathbf{3}},\mathbf{3},-2/3)$	Excluded: proton decay

Table 1. Summary of known results for gauge invariant single field extensions with one-loop contributions to the anomalous magnetic moment of the muon. These results are rather exhaustive due to systematic investigations and classifications in ref. [367, 369–371]. Note however that while we present the results based on representations of SM gauge and Lorentz symmetries, the references make assumptions that can be important to the conclusions and are different in each paper. Thus the conclusions summarised in this table should be interpreted with care. For more information on models 1-2, 3-4, 5-9, 10-12, 13, 14-18 and 19-23 see references [124, 152, 152, 367, 367, 367, 370, 371, 371, 371, 371, 371, 371, 419–422] and [370], respectively. We use color highlighting to give a visual indication of the status of the model, namely green for viable explanations, red for excluded and purple for vector extensions excluded on the basis of their UV completions.

right handed neutrino,[7] and find that in this case the region where $\Delta a_\mu^{\rm BNL}$ can be explained within 1σ is ruled out by the combination of LEP limits on contact interactions and LHC direct searches. In summary they find that all gauge invariant one-field extensions they considered failed to explain the anomaly. This paper's findings are reflected in table 1, except for the cases of the scalar doublet (see section 3.2) and the neutral vector (see the

[7] Technically this is a two-field extension of the SM though they do not classify it as such.

JHEP09(2021)080

discussion in section 3.1.1 at the end of this overview), where there is a lot of dedicated literature and it is known that breaking the assumptions of ref. [367] can change the result.

Refs. [369, 371, 421] also take a systematic approach. Ref. [421] considers scalar bosons.[8] Compared to results in the other papers this adds the singly charged SU(2) singlets to table 1. This result was also used in the classification in ref. [371] (drawing also from ref. [419]), along with doubly charged SU(2) scalar singlets using results from ref. [420] and scalar leptoquarks (see section 3.3 for our update) originally proposed in ref. [124]. They also add a new result for a fermion SU(2) singlet with hypercharge $-3/2$, i.e. the fermion state $(\mathbf{1}, \mathbf{2}, -3/2)$, showing that the contribution is always negative above the LEP limit. Otherwise their classification overlaps with ref. [367] and the conclusions are effectively consistent.[9] Ref. [369] does not require $\mathrm{SU}(2)_L$ invariance and instead considers simplified models of Lorentz scalar, fermion and vector states with results presented in terms of axial and vector couplings, g_a and g_v and classify states according to electromagnetic charges and SU(3) representations. The reference presents plots of Δa_μ predictions against the mass of the new state for specific cases of the couplings. We checked that the results are consistent with what we present in table 1, but ref. [369] does not contain additional general conclusions on the viability of each case.

While refs. [367] and [369] used a simplified models treatment of vector states, ref. [370] systematically classified vector extensions according to SM gauge representations and considered the implications of embedding these into a UV complete gauge extension of the SM. They found that only $(\mathbf{1}, \mathbf{1}, 0)$ may provide a viable UV complete explanation of $\Delta a_\mu^{\mathrm{BNL}}$, depending on specific model dependent details (see section 3.1.1 below for more details on such explanations). Although the $(\mathbf{1}, \mathbf{2}, -3/2)$ vector state gives large contributions to a_μ, they rejected this since the UV completion into 331 models cannot provide a $\Delta a_\mu^{\mathrm{BNL}}$ explanation consistent with experimental limits [422]. A $(\mathbf{1}, \mathbf{3}, 0)$ vector state has no chirality flip, so explanations are ruled out by LHC limits [423]. $(\overline{\mathbf{3}}, \mathbf{1}, -2/3)$ and $(\overline{\mathbf{3}}, \mathbf{2}, -5/6)$ have chirality flipping enhancements, but they reject $(\overline{\mathbf{3}}, \mathbf{1}, -2/3)$ based on an $\mathrm{SU}(4)_C \times \mathrm{SU}(2)_L \times \mathrm{U}(1)_R$ UV completion and limits on the masses from rare decays [424], while the $(\overline{\mathbf{3}}, \mathbf{2}, -5/6)$ state is rejected based on an SU(5) UV completion and proton decay limits. Models without chirality flip enhancements ($(\overline{\mathbf{3}}, \mathbf{1}, -5/3)$, $(\overline{\mathbf{3}}, \mathbf{2}, 1/6)$ and $(\overline{\mathbf{3}}, \mathbf{3}, -2/3)$) can all be ruled out by collider constraints or because they give the wrong sign. A summary of the constraints excluding each of the vector leptoquarks are included in table 1.

3.1.1 Dark photon and dark Z explanations

Before concluding this overview we now briefly discuss the particularly interesting case of an additional gauge field Z_d with $(\mathbf{1}, \mathbf{1}, \mathbf{0})$ quantum numbers that arises from some additional $\mathrm{U}(1)_d$ gauge symmetry. The dark photon scenario assumes that the known quarks and leptons have no $\mathrm{U}(1)_d$ charge. The potential impact of dark photons on a_μ has been extensively studied, after the first proposal in ref. [132]. Models with a general

[8] They also consider vector states but assume additional fermions in that case.

[9] They do however comment that they obtained minor differences to those from ref. [367] in the a_μ calculation for the $(\mathbf{1}, \mathbf{1}, -1)$ and $(\mathbf{1}, \mathbf{2}, -1/2)$ fermions, which alter the reason why they are excluded. We checked these results and agree with the results of ref. [367].

JHEP09(2021)080

Higgs sector contain both kinetic mixing of the SM B-field and Z_d and the mass mixing of the SM Z-field and Z_d. As the mass mixing parameter is typically far smaller than the kinetic mixing one, the leading contribution to a_μ is proportional to the kinetic mixing parameter ϵ. The kinetic mixing term induces an interaction between the SM fermions and the dark photon, and the region relevant for significant Δa_μ has first been found to be $10^{-6} < \epsilon^2 < 10^{-4}$, with dark photon masses in the range between 1 MeV $\cdots$ 500 MeV [132]. However the electron anomalous magnetic moment result [425] reduces the mass range to 20 MeV $\cdots$ 500 MeV [289], and the remaining range is excluded by the following experimental results obtained from various dark photon production channels from A1 in Mainz [426] (radiative dark photon production in fixed-target electron scattering with decays into e^+e^- pairs), BaBar [427] (pair production in e^+e^- collision with subsequent decay into e^+e^- or $\mu^+\mu^-$ pairs), NA48/2 at CERN [428] (π^0 decay modes via dark photon and subsequent decay into e^+e^--pair) and from dark matter production via dark photon from NA46 at the CERN [429].

As a result, pure dark photon models cannot accommodate significant contributions to a_μ. Extensions, e.g. so-called "dark Z" models, open up new possibilities but are also strongly constrained [288–290, 292, 305]. Similarly, neutral Z' vector bosons with direct gauge couplings to leptons are also strongly constrained (as indicated in table 1); for examples of remaining viable possibilities with significant contributions to a_μ we mention the model with gauged $L_\mu - L_\tau$ quantum number and generalizations thereof, see refs. [273, 274, 277, 278, 283, 285, 430]. Even in such viable models only rather small parts of the parameter space are promising; in particular only specific windows for the new vector boson masses can lead to viable explanations of Δa_μ^{2021}. In case of the $L_\mu - L_\tau$ model, the recent ref. [393] has shown that essentially only the mass range between $0.01 \ldots 0.1$GeV remains, and that this parameter range can be further probed in the future by muon fixed-target experiments and even by neutrino and dark matter search experiments. For very heavy Z' masses in the TeV region, explanations of Δa_μ^{2021} are already disfavoured by LHC data, but further constraints can ultimately be obtained at a muon collider [278]. In case of "dark Z" models, the viable mass range is below the 1 GeV scale, and the promising parameter space can be probed by measurements of the running weak mixing angle at low energies at facilities such as JLab QWeak, JLab Moller, Mesa P2, see e.g. refs. [290, 383].

3.2 Two-Higgs doublet model

As can be seen in table 1, the two-Higgs doublet model is one of the very few viable one-field explanations of $\Delta a_\mu^{\text{BNL}}$. It is in fact the only possibility without introducing new vector bosons or leptoquarks. The two-Higgs doublet model (2HDM) contains a charged Higgs $H^\pm$, a CP-odd Higgs A, and two CP-even Higgs bosons H, h, where h is assumed to be SM-like (we assume here a CP-conserving Higgs potential, which is sufficient to maximize contributions to a_μ). To be specific we list here the Yukawa Lagrangian for the neutral Higgs bosons in a form appropriate for the 2HDM of type I, II, X, Y and the flavour-aligned 2HDM, in the form of ref. [251],

$$\mathcal{L}_Y = -\sum_{\mathcal{S}=h,H,A} \sum_f \frac{Y_f^{\mathcal{S}} m_f}{v} \mathcal{S} \bar{f} P_{\text{R}} f + \text{h.c.}, \tag{3.1}$$

JHEP09(2021)080

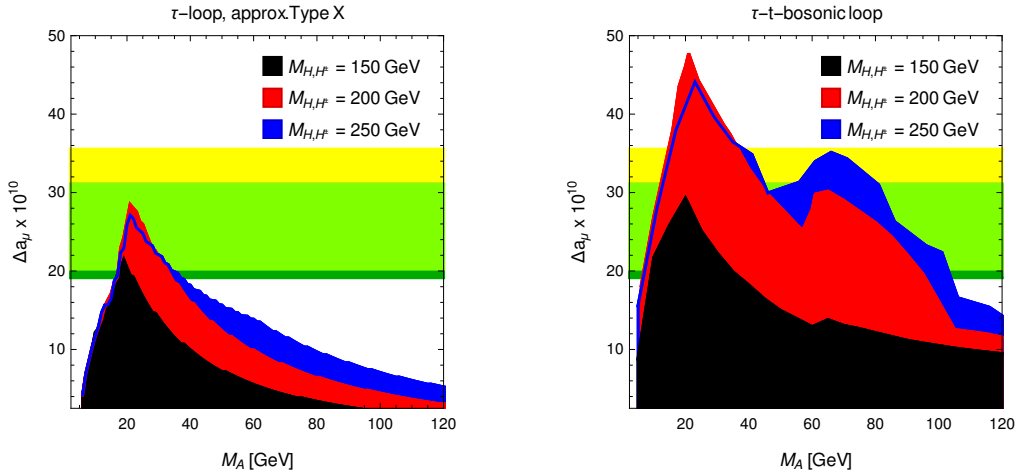

(a) (b)

Figure 1. The maximum results for Δa_μ in the two versions of the two-Higgs Doublet Model with minimal flavour violation, compared with the 1σ regions around $\Delta a_\mu^{\rm BNL}$ (yellow) and new world average Δa_μ^{2021} (green); light green shows the overlap between the two regions. The maximum results are shown as functions of M_A, for three different values of $M_{H,H^\pm}$, as indicated: (a) lepton-specific/type X model (b) flavour-aligned two-Higgs Doublet Model. The results are based on ref. [252]. The left plot is technically obtained in the framework of the flavour-aligned model but taking only τ-loop contributions, which coincides with the type X model.

$$Y_f^h = \sin(\beta-\alpha) + \cos(\beta-\alpha)\zeta_f, \qquad Y_{d,l}^A = -\zeta_{d,l}\,, \tag{3.2}$$

$$Y_f^H = \cos(\beta-\alpha) - \sin(\beta-\alpha)\zeta_f, \qquad Y_u^A = +\zeta_u\,. \tag{3.3}$$

where the Dirac fermions f run over all quarks and leptons, $(\beta-\alpha)$ is a mixing angle and $\sin(\beta-\alpha)=1$ corresponds to h being SM-like. The dimensionless Yukawa prefactors ζ_f depend on the 2HDM version and will be specialized later.

The 2HDM has a rich phenomenology with a plethora of new contributions to the Higgs potential and the Yukawa sector. It differs from the previously mentioned models in that two-loop contributions to a_μ are known to be crucial. Typically the dominant contributions arise via so-called Barr-Zee two-loop diagrams. In these diagrams an inner fermion loop generates an effective Higgs-γ–γ interaction which then couples to the muon via a second loop. If the new Higgs has a large Yukawa coupling to the muon and if the couplings in the inner loop are large and the new Higgs is light, the contributions to a_μ can be sizeable. The Higgs mediated flavour changing neutral currents in the 2HDM can be avoided by imposing either $\mathbb{Z}_2$ symmetry or flavour-alignment.

Figure 1 presents up-to-date results of the possible contributions Δa_μ in both of these versions of the 2HDM. The figure is based on results of ref. [252] and compares them to the new world average Δa_μ^{2021} obtained from including the FNAL value. It arises from scans of the model parameter space and shows the maximum possible Δa_μ as a function of the most important parameters, the two new Higgs masses M_A and M_H, where the choice $M_H = M_{H^\pm}$ maximises Δa_μ. The reason why there are absolute upper limits on Δa_μ is a combination of theoretical and experimental constraints, as discussed in the following.

JHEP09(2021)080

Figure 1(a) shows the results for the 2HDM type X, the so-called lepton-specific version of the 2HDM with $\mathbb{Z}_2$ symmetry. A general analysis of all types of the 2HDM with discrete $\mathbb{Z}_2$ symmetries and minimal flavour violation has been done in ref. [242], where only this lepton-specific type X model survived as a possible source of significant Δa_μ. In this model, the parameters of eq. (3.1) are $\zeta_l = -\tan\beta$ for all charged leptons, while $\zeta_{u,d} = \cot\beta$ for all quarks. The $\tan\beta$-suppression of quark Yukawa couplings helps evading experimental constraints from LEP, LHC and flavour physics. In the type X 2HDM the main contributions arise from Barr-Zee diagrams with an inner τ-loop, which are $(\tan\beta)^2$-enhanced. Hence important constraints arise from e.g. precision data on $Z \to \tau\tau$ and τ-decay [244, 246, 249, 253] as well as from LEP data on the mass range $M_A \lesssim 20\,\text{GeV}$ [252]. As figure 1(a) shows, only a tiny parameter space in the 2HDM type X remains a viable explanation of the observed Δa_μ^{2021}. For a 1σ explanation, M_A must be in the small interval $20 \ldots 40\,\text{GeV}$; the corresponding maximum values of the $\tan\beta$ parameter, which governs the lepton Yukawa couplings in this model, are in the range $50 \ldots 100$. The masses of the new heavier Higgs bosons $M_{H,H^\pm}$ vary between 150 and 250 GeV in the figure. Smaller values of these masses lead to stronger constraints (since loop contributions to τ-physics are less suppressed), while larger values lead to a larger hierarchy $M_A \ll M_{H,H^\pm}$ which leads to stronger constraints from electroweak precision physics and theoretical constraints such as perturbativity [249, 252]. We mention also that the 2HDM type X parameter space with particularly large contributions to a_μ can lead to peculiar τ-rich final states at LHC [247, 256] but can be tested particularly well at a future lepton collider [431] and is also compatible with CP violation and testable contributions to the electron electric dipole moment [255].

Figure 1(b) shows results for the so-called flavour-aligned two-Higgs doublet model, which is a more general but still minimal flavour violating scenario. Here the parameters ζ_l, ζ_u, ζ_d are independent, however assumed to be generation-universal. The contributions to a_μ were first discussed in ref. [245] and then scrutinized in refs. [243, 251, 252]. Here not only the τ-lepton loop contributes in essentially the same way as before, but also Barr-Zee diagrams with the top-quark in the inner loop may contribute. To a smaller extent, also purely bosonic two-loop diagrams can increase a_μ. The plot takes into account all contributions, based on refs. [251, 252]. In particular the top-quark loop leads to a larger possible value of a_μ. Its contributions are bounded by constraints from LHC data and B-physics. The LHC constraints are weaker for $M_A > 62\,\text{GeV}$, where the decay $h \to AA$ is kinematically impossible [252]. This is reflected in the behaviour of the maximum Δa_μ as a function of M_A in the plot. In case of the flavour-aligned 2HDM the world average deviation Δa_μ^{2021} can be accommodated for M_A up to 100 GeV, if the heavy and charged Higgs masses are in the region $M_H = M_{H^\pm} = 200 \ldots 250\,\text{GeV}$. In the parameter space which maximises Δa_μ in the flavour-aligned 2HDM the light A-boson has simultaneously significant Yukawa couplings to the top quark and to τ-leptons, leading to a significant rate for the process $gg \to A \to \tau\tau$, which might be tested at future LHC runs.

Hence among the 2HDM versions without tree-level FCNC, the well-known type I and type II versions are excluded as explanations of the deviation Δa_μ^{2021}. In contrast, the lepton-specific type X model and the more general flavour-aligned 2HDM can give sig-

JHEP09(2021)080

nificant contributions to Δa_μ. In both cases, two-loop Barr-Zee diagrams with A-boson exchange and τ-loop are important; in the flavour-aligned model also top-loops are important. The mass M_A is severely constrained and the new Yukawa couplings must be at their upper experimental limits. Because of this, the 2HDM explanations of Δa_μ^{2021} are going to be further scrutinized at ongoing and future experiments: any improvement of the LHC sensitivity to $gg \to A \to \tau\tau$ can either discover the A-boson or reduce the allowed parameter space visible in figure 1(b). Likewise, improved measurements of τ-decays can lead to reduced upper limits on the maximum $\tan\beta$ or ζ_l, respectively, and reduce the viable parameter space in both plots. As mentioned above, refs. [247, 256] have investigated how further future LHC measurements of processes such as HA or $H^\pm A$ production with decay into multi-lepton final states can impact the 2HDM explanations of Δa_μ^{2021}. Lepton colliders even with modest c.o.m. energy offer additional coverage of the 2HDM parameter space via the Yukawa process $e^+e^- \to \gamma^*/Z^* \to \tau\tau A$ [431], which is directly sensitive to the low-mass pseudoscalar Higgs boson relevant for a_μ.

Further, we mention that more exotic variants of the 2HDM which involve neither $\mathbb{Z}_2$-symmetric nor general flavour-aligned Yukawa couplings can open up additional possibilities. E.g. large non-flavour aligned Yukawa couplings to τ-leptons or top quarks can allow large contributions to a_μ even for masses of M_A above 100 GeV [256, 331]. In these cases, important constraints arise from lepton flavour violating processes [256] and B-physics [331]. Large, non-flavour aligned τ-Yukawa couplings also allow another window of significant contributions with a very light CP-even Higgs with $M_H \lesssim 1$ GeV [259]. And a muon-specific 2HDM can accommodate large Δa_μ with $\tan\beta$ of order 1000 [250].

3.3 Scalar leptoquarks

In this subsection we update the results for the other single field models which could explain $\Delta a_\mu^{\text{BNL}}$, i.e. the scalar leptoquarks. Scalar and vector leptoquarks that interact with SM leptons and quarks can appear as the only BSM particle in one-loop contributions to the anomalous magnetic moment of the muon. Scalar leptoquarks have been considered as a solution for the anomalous magnetic moment anomaly in refs. [124, 369, 371, 432, 433], while vector leptoquarks have also been considered in refs. [369, 370]. Here we focus on studying scalar leptoquarks in detail, since one would expect vector leptoquarks to be associated with an extension of the gauge symmetries, which complicates the construction of these models, and taking the simplified model approach they may yield results which are rather misleading compared to what can be achieved in a realistic model.

Requiring gauge invariant couplings to SM leptons and quarks restricts us to the five scalar leptoquarks [434] shown in table 1 (Models 5–9). Only two of these models,[10] S_1 $(\overline{\mathbf{3}}, \mathbf{1}, 1/3)$ and R_2 $(\mathbf{3}, \mathbf{2}, 7/6)$, have both left- and right-handed couplings to the SM fermions and can therefore have a chirality flip enhancing their one-loop contributions [124, 369, 371].

Leptoquarks can in general have complicated flavour structure in their couplings. Since our focus is on demonstrating the impact of the anomalous magnetic moment experiment and demonstrating the various ways to explain it, we prefer to simplify the flavour structure

[10] We follow the notation in ref. [434].

JHEP09(2021)080

and focus on the couplings that lead to an enhanced Δa_μ contribution. We therefore restrict ourselves to muon-philic leptoquarks that couple only to the second-generation of SM leptons, evading constraints on flavour violating processes such as $\mu \to e\gamma$. Leptoquarks that induce flavour violation in the quark sector have been widely considered in the literature as possible solutions to flavour anomalies, and sometimes simultaneous explanations of a_μ and these anomalies (see e.g. refs. [432, 433]). However we also do not consider these here for the same reasons we choose to avoid lepton flavour violating couplings and the same reasoning applies to simultaneous explanations of the more recent a_e anomaly [435].

We found that it is possible to explain the $\Delta a_\mu^{\text{BNL}}$ and Δa_μ^{2021} results with moderately sized perturbative couplings using leptoquarks that are both muon-philic *and* charm-philic, i.e. leptoquarks that only couple to second generation up-type quarks as well as only second generation charged leptons. Specifically we found $\Delta a_\mu^{\text{BNL}}$ could be explained while satisfying LHC limits from direct searches as long as $\sqrt{|\lambda_L \lambda_R|} \gtrsim 0.4$, where λ_L and λ_R are the leptoquark couplings to the muons and the quarks. However careful consideration of CKM mixing and flavour changing neutral currents (FCNC) reveals stringent constraints. While one may require that the new states couple only to the charm and not the up-quark or top-quark, CKM effects will then still generate couplings to the bottom and down-quark. This effect is very important and the impact of these for "charm-philic" leptoquark explanations of $\Delta a_\mu^{\text{BNL}}$ has been considered in ref. [267]. There they find that constraints from $\text{BR}(K^+ \to \pi^+ \nu\overline{\nu})$ for the S_1 leptoquark, or $\text{BR}(K_L \to \mu^+\mu^-)$ for the R_2 leptoquark, heavily restrict one of the couplings that enter the a_μ calculation. They find this excludes fitting $\Delta a_\mu^{\text{BNL}}$ within 1σ, but in the case of the first model an explanation within 2σ remained possible, while for the second model explanations well beyond 2σ were excluded. They also consider the possibility that it is the down-type couplings that are second generation only, and find even more severe constraints in that case. Finally for a limited case, they explore including a direct coupling to the top-quark and find that quite large couplings to the top quark are needed to explain $\Delta a_\mu^{\text{BNL}}$ within 1σ. Due to the strong flavour constraints from coupling the leptoquark to the second generation of SM quarks, we instead present results for top-philic leptoquarks, i.e. using scalar leptoquarks which couple to the second generation SM leptons, and the third generation of SM quarks.

Below is written the Lagrangian for both scalar leptoquarks, where here all fermions are written as 2-component left-handed Weyl spinors, for example $Q_3 = (t_L, b_L)^T$ and $\mu_R^\dagger$, which follows the notation of ref. [436]. For simplicity we also define $\mu, t, b := \mu_R^\dagger, t_R^\dagger, b_R^\dagger$ below

$$\begin{aligned}\mathcal{L}_{S_1} = &-\left(\lambda_{QL} Q_3 \cdot L_2 S_1 + \lambda_{t\mu} t \mu S_1^* + \text{h.c.}\right) \\ &- M_{S_1}^2 |S_1|^2 - g_{HS_1} |H|^2 |S_1|^2 - \frac{\lambda_{S_1}}{2}\left(|S_1|^2\right)^2, \qquad (3.4)\\ \mathcal{L}_{R_2} = &-\left(\lambda_{Q\mu} R_2^\dagger Q_3 \mu + \lambda_{tL} L_2 \cdot R_2 t + \text{h.c.}\right) \\ &- M_{R_2}^2 |R_2|^2 - g_{HR_2} |H|^2 |R_2|^2 - \frac{\lambda_{R_2}}{2}\left(|R_2|^2\right)^2. \qquad (3.5)\end{aligned}$$

where the dot product above denotes the $\text{SU}(2)_L$ product, so e.g. $Q_3 \cdot L_2 = t_L \mu_L - b_L \nu_{\mu L}$. For the S_1 leptoquark one could also include $\text{SU}(3)_C \times \text{SU}(2)_L \times \text{U}(1)_Y$ gauge invariant

JHEP09(2021)080

renormalizable operators, $S_1 Q_3 L_2$ and $S_1 tb$ but unless these diquark couplings are severely suppressed or forbidden, they will give rise to rapid proton decay when combined with the leptoquark operators we consider here [437, 438]. R_2 does not admit such renormalizable operators [437] though there remain dangerous dimension 5 operators that would need to be forbidden or suppressed [438]. Since we are focused on a_μ we again simplify things by assuming all parameters are real, but note that if we were to consider complex phases then electric dipole moments would also be of interest, see e.g. ref. [439].

Constraints on the masses of scalar leptoquarks with second and third generation couplings to the SM leptons and quarks respectively can be directly applied from 13 TeV CMS [440, 441] results, dependent on how strong they couple to those fermions. Given the above Lagrangians, one can see that the scalar leptoquark singlet S_1 can decay to either a top quark and muon or bottom quark and neutrino, while the upper and lower components of the scalar leptoquark doublet decay as R_2^u to a top quark and muon and R_2^d to either a top quark and neutrino or a bottom quark and muon. Thus for the leptoquark S_1 given in eqs. (3.4), the branching fraction $\beta_{S_1} = Br(S_1 \to t\mu)$, is given by:

$$\beta_{S_1} = \frac{\lambda_{QL}^2 + \lambda_{t\mu}^2}{2\lambda_{QL}^2 + \lambda_{t\mu}^2}. \tag{3.6}$$

For scalar leptoquark singlet S_1 the most stringent LHC limits when coupling to third generation quarks and second generation leptons are dependent on β_{S_1} [440]. Thus we can calculate β_{S_1} using selected values of the couplings between S_1 and the fermions, and interpolate between them to find the limits on the mass given in ref. [440]. Now for R_2 in eq. (3.5), limits can be placed on the upper component of the doublet, R_2^u, which decays solely to $t\mu$. In this case the mass limits from ref. [440] are applied where the branching ratio for R_2^u to decay to $t\mu$ is taken to be $\beta_{R_2^u} = 1$.

Further constraints can be placed on leptoquarks from the effective coupling of a Z boson to leptons. The experimentally measured effective couplings of the Z boson to a pair of muons are given as $g_L^{\mu\mu} = -0.2689 \pm 0.0011$, $g_R^{\mu\mu} = 0.2323 \pm 0.0013$ [417, 442] in the case of left- and right-handed couplings. The contribution from a scalar leptoquark with couplings to any flavour of the SM fermions to the effective couplings between Z and muon, $\delta g_{L,R}^{\mu\mu}$, is given by eqs. (22,23) in ref. [443] for the leptoquarks S_1 and R_2 respectively. Points with left-right effective couplings more than 2σ away from the measured values are treated as constrained.

Likewise, the effective coupling of the Z boson to any two neutrinos has been measured as the observed number of light neutrino species $N_\nu = 2.9840 \pm 0.0082$ [442]. The BSM contributions from a scalar leptoquark to this are given by [443]:

$$N_\nu = \sum_{i,j=e,\mu,\tau} \left(\left| \delta^{ij} + \frac{\delta g_{\nu L}^{ij}}{g_{\nu L}^{\mathrm{SM}}} \right|^2 + \left| \frac{\delta g_{\nu R}^{ij}}{g_{\nu L}^{\mathrm{SM}}} \right|^2 \right), \tag{3.7}$$

where $g_{\nu L}^{\mathrm{SM}}$ are the SM couplings, and $\delta g_{\nu L,R}^{ij}$ are the BSM couplings between the Z boson and the neutrinos given again in eqs. (22,23) from ref. [443].

Due to the large masses of the leptoquarks considered for this model, it is reasonable to consider fine-tuning in the mass of the muon. With large BSM masses and sizeable

JHEP09(2021)080

couplings to the SM, contributions to the muon can be generated as detailed in section 2. The specific constraint considered in this paper for when the contribution to the muon mass is considered not "fine-tuned" is

$$\frac{1}{2} < \frac{m_\mu^{\overline{\rm MS}}}{m_\mu} < 2, \tag{3.8}$$

i.e. the relative difference between the $\overline{\rm MS}$ and pole masses $m_\mu^{\overline{\rm MS}}$ and m_μ should not exceed 100%. While not forbidden, one may consider explanations of large a_μ via $\mathcal{O}(> 100\%)$ corrections to the pole mass m_μ as unattractive.

Since the chirality flip provides an enhancement to Δa_μ proportional to the squared mass of the heaviest quark that the leptoquark couples to, in the case of a leptoquark coupling to the SM's third quark generation the enhancement is m_t/m_μ. Note that we actually found that the m_c/m_μ enhancement for charm-philic leptoquarks was sufficient to allow explanations of $\Delta a_\mu^{\rm BNL}$ consistent with LHC limits (but not flavour constraints) with perturbative couplings, therefore this much larger enhancement should be more than sufficient, even with rather small couplings or quite heavy masses. In both cases of the leptoquark models, the leptoquark contributions to a_μ are given by two kinds of diagrams of the FFS and SSF type,

$$\Delta a_\mu^{LQ} = \Delta a_\mu^{\rm FFS} + \Delta a_\mu^{\rm SSF}\,. \tag{3.9}$$

For the scalar leptoquark singlet S_1, the contributions to a_μ specifically come from diagrams with top-leptoquark loops and are given by:

$$\Delta a_\mu^{\rm FFS} = \frac{3m_\mu^2 Q_t}{32\pi^2 M_{S_1}^2}\left(\frac{\lambda_{QL}^2+\lambda_{t\mu}^2}{6}E\left(\frac{m_t^2}{M_{S_1}^2}\right)+\frac{4\lambda_{QL}\lambda_{t\mu}}{3}\frac{m_t}{m_\mu}F\left(\frac{m_t^2}{M_{S_1}^2}\right)\right), \tag{3.10}$$

$$\Delta a_\mu^{\rm SSF} = \frac{3m_\mu^2 Q_{S_1}}{32\pi^2 M_{S_1}^2}\left(-\frac{\lambda_{QL}^2+\lambda_{t\mu}^2}{6}B\left(\frac{m_t^2}{M_{S_1}^2}\right)-\frac{2\lambda_{QL}\lambda_{t\mu}}{3}\frac{m_t}{m_\mu}C\left(\tfrac{m_t^2}{M_{S_1}^2}\right)\right), \tag{3.11}$$

where the charges $Q_t = 2/3$, $Q_{S_1} = 1/3$ and the one-loop functions $B(x)$, $C(x)$, $E(x)$, and $F(x)$ are defined in appendix A. These contributions are described by the fermion-fermion-scalar (FFS) diagram 19(a) and the scalar-scalar-fermion (SSF) diagram 19(b) of figure 19 with the generic F fermion lines replaced by a top quark and the scalar S ones by S_1. Similarly, the contributions from the scalar leptoquark doublet R_2 involving top/bottom and leptoquark loops are given by:

$$\begin{aligned}\Delta a_\mu^{\rm FFS} = \frac{3m_\mu^2}{32\pi^2 M_{R_2}^2}\Bigg(&Q_t\frac{4\lambda_{Q\mu}\lambda_{tL}}{3}\frac{m_t}{m_\mu}F\left(\frac{m_t^2}{M_{R_2}^2}\right)-Q_t\frac{\lambda_{Q\mu}^2+\lambda_{tL}^2}{6}E\left(\frac{m_t^2}{M_{R_2}^2}\right)\\&-Q_b\frac{\lambda_{Q\mu}^2}{6}E\left(\frac{m_b^2}{M_{R_2}^2}\right)\Bigg),\end{aligned} \tag{3.12}$$

$$\begin{aligned}\Delta a_\mu^{\rm SSF} = \frac{3m_\mu^2}{32\pi^2 M_{R_2}^2}\Bigg(&Q_{R_2}^u\frac{2\lambda_{Q\mu}\lambda_{tL}}{3}\frac{m_t}{m_\mu}C\left(\tfrac{m_t^2}{M_{R_2}^2}\right)-Q_{R_2}^u\frac{\lambda_{Q\mu}^2+\lambda_{tL}^2}{6}B\left(\frac{m_t^2}{M_{R_2}^2}\right)\\&-Q_{R_2}^d\frac{\lambda_{Q\mu}^2}{6}B\left(\frac{m_b^2}{M_{R2}^2}\right)\Bigg),\end{aligned} \tag{3.13}$$

JHEP09(2021)080

where $Q^d_{R_2} = 2/3$ is the charge of the lower component of the leptoquark doublet, and $Q^u_{R_2} = 5/3$ is the charge of the upper component, and $Q_b = -1/3$. Note the colour factor 3 in front of each of the leptoquark contributions. Each of the above contributions is produced by a pair of diagrams which are of the FFS diagram type 19(a) or the SSF diagram type 19(b) of figure 19 with the generic F fermion lines replaced by a top or bottom quark and the scalar S ones by R^d_2 and R^u_2, respectively.

The important parameters for determining the above contributions to a_μ from scalar leptoquarks are the couplings λ_L, λ_R between the leptoquarks and either the left- or right-handed top quarks, and the mass of the leptoquark M_{LQ}. For either of these leptoquarks the dominant contribution to a_μ, arises from the internal chirality flip enhancement and has the following approximate form,

$$\Delta a_\mu^{LQ} \approx \frac{\lambda_L \lambda_R m_\mu m_t}{8\pi^2 M_{LQ}^2}\left(Q_t\, F\left(\frac{m_t^2}{M_{LQ}^2}\right) \pm \frac{Q_{LQ}}{2}\, C\left(\frac{m_t^2}{M_{LQ}^2}\right)\right), \tag{3.14}$$

where the $-/+$ is for the singlet/doublet. Comparing this to eq. (2.3), we can see that $C_{BSM} = Q_t \lambda_L \lambda_R m_t/(8\pi^2 m_\mu)$, with the ratio $m_t/m_\mu \approx 1600$, gives the parametric enhancement to Δa_μ from the chirality flip. We can also see how allowing the leptoquark to couple to the top quark versus the charm quark leads to a larger value of Δa_μ. While this can be used to qualitatively understand our results, the numerical calculations were performed with `FlexibleSUSY` 2.5.0 [43, 44].[11] The `FlexibleSUSY` calculation of Δa_μ includes the full one-loop contribution and the universal leading logarithmic two-loop QED contribution [450], which tends to reduce the result by $\approx 6\% - 10\%$.

The contributions to a_μ from the introduction of the scalar leptoquarks S_1 and R_2 with Lagrangians given by eqs. (3.4), (3.5) are shown in figures 2 and 3, respectively. Results are shown in the M_{LQ}-λ_{QL} and M_{LQ}-$\lambda_{Q\mu}$ planes, scanning up to a leptoquark mass of $M_{LQ} = 4500\,\text{GeV}$. We find that for both S_1 and R_2 the observed a_μ discrepancy can be explained within 1σ using similar ranges of couplings and a leptoquark mass $M_{LQ} \gtrsim 1.1$–$1.5\,\text{TeV}$.

The left and middle panels of figure 2 show where $\Delta a_\mu^{\text{BNL}}$ and Δa_μ^{2021} can be explained when the coupling to the right-handed top quark is fixed to $\lambda_{t\mu} = 0.1, 0.2$ respectively. For $\lambda_{t\mu} = 0.1$, the black line showing points which exactly explain the Δa_μ^{2021} discrepancy is a parabolic curve, following the quadratic relationship between leptoquark mass and coupling in eq. (3.14). By increasing the coupling to $\lambda_{t\mu} = 0.2$, a lower value of the coupling λ_{QL} to the left-handed top quark is required to get the same contributions to Δa_μ, and the region which can explain Δa_μ^{2021} narrows and flattens as shown in the middle panel. In both cases the new Δa_μ^{2021} value can be explained with a marginally smaller coupling than the previous BNL value due to the small decrease in the discrepancy. CMS searches for scalar leptoquarks [440], shown by grey shading, exclude regions with masses $M_{S_1} \lesssim 1.1$–$1.5\,\text{TeV}$, dependent on the branching ratio β_{S_1} in eq. (3.6). For lower λ_{QL} couplings the strongest mass constraint of $M_{S_1} > 1420\,\text{GeV}$ arises, since $\beta_{S_1} \to 1$ as $\lambda_{QL} \to 0$. Additionally, the cyan region indicates points affected by the "fine-tuning" in the muon mass discussed in

[11] where `SARAH` 4.14.1 [444–447] was used to get expressions for masses and vertices, and `FlexibleSUSY` also uses some numerical routines originally from `SOFTSUSY` [448, 449].

JHEP09(2021)080

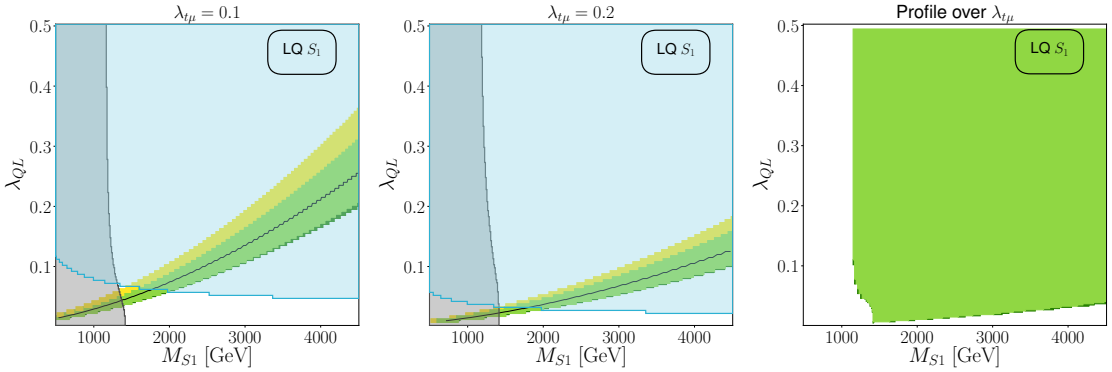

Figure 2. Scenarios which can explain $\Delta a_\mu^{\text{BNL}}$ and/or Δa_μ^{2021} in the model with an $\text{SU}(2)_L$ singlet scalar leptoquark S_1 defined in eq. (3.4). Results are shown in the M_{S1}-λ_{QL} plane for fixed $\lambda_{t\mu} = 0.1$ (left panel), $\lambda_{t\mu} = 0.2$ (middle panel) and by varying $\lambda_{t\mu} \in [0, 0.5]$ (right panel). In the latter case we *profile* to find the regions in the M_{S1}-λ_{QL} plane that for some value of $\lambda_{t\mu}$ in the scan, satisfy all experimental constraints and can explain the Δa_μ measurements within 1σ. Regions which can explain $\Delta a_\mu^{\text{BNL}}$ and Δa_μ^{2021} to within 1σ are yellow and green respectively, with the overlap between these two regions coloured lime. The black line indicates points which produce a Δa_μ contribution matching eq. (1.7). The grey regions are excluded by scalar leptoquark searches at the Large Hadron Collider [440]. Regions shaded cyan are disfavoured as they provide a relative contribution which shift the muon mass up by more than 100% or down by more than 50% as in eq. (3.8). In the right panel only solutions which have not been excluded by leptoquark searches or $Z \to \mu\mu$ or $Z \to \nu\nu$ constraints are displayed, i.e. any points ruled out by any of these experimental constraints are discarded.

section 2 and defined in eq. (3.8): here the loop contributions to muon mass calculated in `FlexibleSUSY` cause the muon mass to increase more than twice the pole mass or decrease less than half the pole mass. Satisfying this fine-tuning criteria, places a rough upper limit of $\lambda_{QL} \lesssim 0.06$ for $\lambda_{t\mu} = 0.1$ and $\lambda_{QL} \lesssim 0.04$ for $\lambda_{t\mu} = 0.2$. Note that these fine-tuning conditions allow only a small strip of the parameter space to remain.

In the right panel of figure 2, we profile over $\lambda_{t\mu}$ to find the best fits to a_μ, that is we vary the coupling $\lambda_{t\mu} \in [0, 0.5]$ and show the lowest number of standard deviation within which a_μ can be explained in the 2D plane, from all scenarios where $\lambda_{t\mu} \in [0, 0.5]$. This panel has the same constraints as before, except for the muon mass fine-tuning. The LHC leptoquark searches impose a limit of $M_{S_1} \gtrsim 1.1\,\text{TeV}$, with slightly higher mass limits implied by this for the lowest λ_{QL} values since the branching ratios depend on the leptoquark couplings. The exclusion in the bottom right of the plot is formed by our choice of restricting the $\lambda_{t\mu}$ to moderate values ≤ 0.5. If we allow $\lambda_{t\mu}$ to vary up to $\sqrt{4\pi}$ then no exclusion in the bottom right would be visible due to the large chirality flip enhancement.[12] As the mass M_{S_1} is increased, the minimum coupling λ_{QL} which produces a contribution that can explain a_μ within 1σ increases, in line with eq. (3.14), with the new world average result able to be explained in narrower region of the parameter space due to the reduction in the uncertainty.

[12] In contrast if we plotted the charm-philic case the combination of LHC and large Δa_μ constraints would lead to a much larger exclusion in the bottom right of the plot than can be seen here, even when the equivalent coupling is varied up to the perturbativity limit.

JHEP09(2021)080

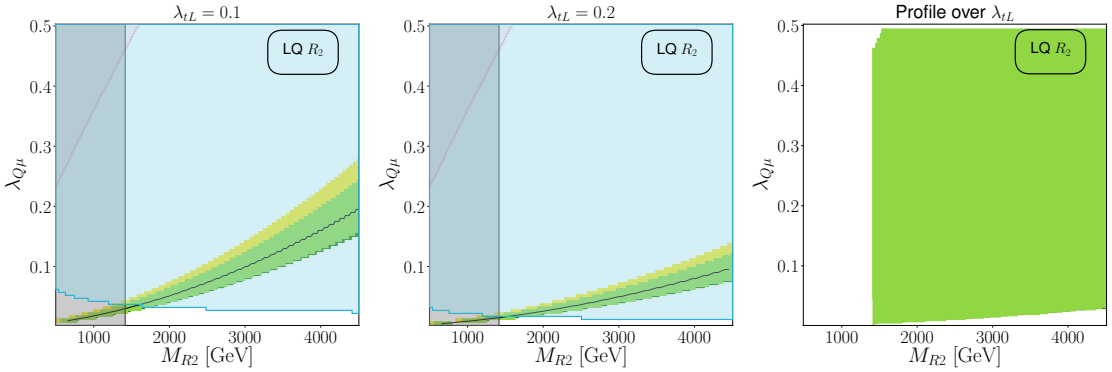

Figure 3. Scenarios which can explain $\Delta a_\mu^{\text{BNL}}$ and/or Δa_μ^{2021} in the model with a scalar leptoquark $\text{SU}(2)_L$ doublet R_2 defined in eq. (3.5). Results are shown in the M_{R2}-λ_{QL} plane for fixed $\lambda_{tL} = 0.1$ (left panel), $\lambda_{tL} = 0.2$ (middle panel) and by varying $\lambda_{tL} \in [0, 0.5]$ (right panel). In the latter case we *profile* to find the regions in the M_{R2}-λ_{QL} plane where these measurements can be explained for some value of λ_{tL} in the scan and satisfy experimental constraints. Colours are the same as in figure 2. Additional relevant exclusions in the parameter space from the constraint $Z \to \nu\nu$ are shaded in pink and in the right panel this is included in the list of experimental constraints that points must satisfy, in addition to those listed in figure 2.

Similarly, for the scalar leptoquark doublet R_2, Δa_μ contours for fixed values of the coupling to right-handed top quarks, $\lambda_{tL} = 0.1, 0.2$, are shown in left and middle panels of figure 3, with a profile over λ_{tL} shown in the right panel. Again, the Δa_μ contours for fixed $\lambda_{tL} = 0.1, 0.2$ follow the quadratic ratio given in eq. (3.14), with larger Δa_μ values from a given leptoquark mass being obtained with the larger coupling $\lambda_{tL} = 0.2$. This time, the mass constraints placed on the leptoquark R_2^u from the LHC are independent of the couplings, as R_2^u always decays to a top quark and muon. Again imposing the fine-tuning criteria has a huge impact, with the contributions from the leptoquark reducing the muon mass m_μ. For $\lambda_{tL} = 0.1$ only a small corner of parameter space can explain Δa_μ^{2021} without fine tuning, and for $\lambda_{tL} = 0.2$ this shrinks to a tiny region. From profiling over λ_{tL}, we find that again Δa_μ^{2021} can be explained within 1σ for masses $M_{R_2} \geq 1420\,\text{GeV}$. For higher couplings $\lambda_{Q\mu} \gtrsim 0.47$, constraints from $Z \to \nu\nu$ raise the minimum mass which can explain Δa_μ^{2021}. As with the previous model our choice to restrict ourselves to moderate $\lambda_{tL} \leq 0.5$ leads a lower bound on the $\lambda_{Q\mu}$ coupling that increases with mass as a smaller coupling $\lambda_{Q\mu}$ cannot produce a large enough Δa_μ^{2021}. As before there would be no exclusion in the bottom right region if we varied λ_{tL} up to $\sqrt{4\pi}$.

In figure 4 the Δa_μ predictions for both leptoquarks were profiled over the mass of the leptoquark with couplings ranging up to a cutoff of 0.5, where we have again excluded points ruled out by the LHC searches and the decays $Z \to \mu\mu$ or $\nu\nu$. The regions which can explain Δa_μ^{2021} follow the relationship given in eq. (3.14), where the contribution has identical dependence on the couplings to the left- and right-handed top quarks. As expected LHC limits on the leptoquark mass mean that there is a lower limit for the values of the couplings that can explain the observed a_μ disagreement within 1σ. However, this limit is extremely small so that only leptoquarks with couplings $\lambda_{QL} \times \lambda_{t\mu} \lesssim 0.003$ are unable to

JHEP09(2021)080

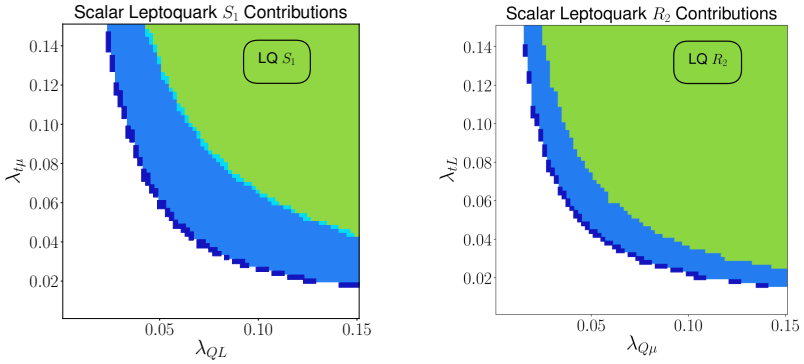

Figure 4. Results for Δa_μ^{2021} and $\Delta a_\mu^{\text{BNL}}$ in the planes of the leptoquark couplings where we profile over all possible scalar leptoquark masses up to 4.5 TeV. More specifically in the left panel we show results for the $\text{SU}(2)_L$ singlet S_1 defined in eq. (3.4) in the λ_{QL}–$\lambda_{t\mu}$ plane and in the right panel we show the scalar leptoquark $\text{SU}(2)_L$ doublet R_2 defined in eq. (3.5) in the $\lambda_{Q\mu}$–λ_{tL} plane. We show couplings between the leptoquark and the SM fermions that can satisfy direct LHC searches and $Z \to \mu\mu$ and $Z \to \nu\nu$ constraints and can simulteneously explain Δa_μ^{2021} (green) or both $\Delta a_\mu^{\text{BNL}}$ *and* Δa_μ^{2021} (lime green) within 1σ. Additionally points which can also avoid the fine-tuning constraints in eq. (3.8) on the muon mass are shaded in dark blue if they can explain Δa_μ^{2021}, aqua if they can explain $\Delta a_\mu^{\text{BNL}}$ within 1σ, and blue if they can explain *both*.

produce large enough contributions to a_μ with a mass that has not be excluded by LHC searches in the S_1 model. As can be seen in the plot we obtain slightly lower limits on the couplings in the R_2 model compared to the S_1 model. This is due to the higher limits from the LHC on the leptoquark singlet at low couplings, as seen in figures 2, 3. Note that if we try to explain $\Delta a_\mu^{\text{BNL}}$ or Δa_μ^{2021} while avoiding fine-tuning of the muon mass, then we get an upper limit on the couplings of $\lambda_{QL} \times \lambda_{t\mu} \lesssim 0.006$ for the S_1 model and $\lambda_{tL} \times \lambda_{Q\mu} \lesssim 0.004$ for the R_2 model. However, putting aside fine-tuning constraints the deviation between the SM prediction and the observed value of the anomalous magnetic moment of the muon can be explained within 1σ, needing couplings of reasonable size no smaller than ≈ 0.05 each.

There are many possibilities for detecting leptoquarks at collider experiments, including planned high-luminosity improvements at the LHC as well as several proposed colliders such as the HE-LHC [451], ILC [452], CLIC [453], CEPC [454], and the FCC-ee [455] and FCC-hh [456]. The contributions of scalar leptoquarks to decays and flavour-changing processes such as $Z \to l_i l_j$, $Z \to \nu\nu$, $W \to l_i \nu$, $h \to l_i l_j$, $l_i \to l_j \gamma$, $l_i \to l_j \nu\nu$, and $l_i \to 3l_j$ have been examined by ref. [272]. The authors found that the ILC, CLIC, CEPC, and FCC-ee may be sensitive to changes of the $Z \to l^+ l^-$ couplings at the level of $10^{-5} - 10^{-6}$ (relative to the standard coupling). They also estimated the ILC and FCC-ee sensitivity to branching fractions of $Z \to ll'$ to be $10^{-8} - 10^{-9}$. Ref. [457] examined the Higgs decays $h \to \gamma\gamma$, $h \to gg$ and $h \to Z\gamma$, and showed that the scalar leptoquarks contributions to these can generally be measured with increased precision at the ILC, CLIC, CEPC, FCC-ee and FCC-hh. They also showed that the value of the electroweak oblique observables, S and T (but not U), can change due to leading order contributions from scalar leptoquarks. They claimed that contributions to T of size 0.01 at the CEPC and 0.005 at the FCC-ee could

JHEP09(2021)080

be measured. Ref. [458] calculated the production cross-sections of scalar leptoquark pairs and a scalar leptoquark with a lepton in proton-proton collisions at the LHC, HL-LHC, and HE-LHC colliders. The cross sections of leptoquark pair production at the HE-LHC and FCC-hh were also given by ref. [459]. Ref. [435] was able to place an upper limit of $M_{LQ} < 65\,\text{TeV}$ on the mass of the leptoquarks if one requires them to explain Δa_e simultaneously with Δa_μ. Additionally, other leptoquarks have also been shown to be detectable at collider experiments ref. [460–464].

In summary leptoquarks are an exciting and well-motivated possibility for physics beyond the SM, which is not only motivated by a_μ but also by flavour anomalies. However, among all possible leptoquark quantum numbers, the S_1 and R_2 models are the only two viable explanations of $\Delta a_\mu^{\text{BNL}}$ and Δa_μ^{2021}. Furthermore, leptoquark couplings of the left- and the right-handed muon to top quarks are required. In this way, chirality flip enhancements by m_t/m_μ are possible. Under these conditions, leptoquark masses above the LHC-limit of around 1.4 TeV can accommodate Δa_μ^{2021} without violating flavour constraints. The large Δa_μ^{2021} can even be explained with leptoquark couplings to the left- and right-handed muon that are as small as ≈ 0.05, which is essentially unchanged from the BNL value, despite the small reduction in the central value. In principle, masses in the multi-TeV region can accommodate the measured a_μ, if the couplings are sufficiently increased. However, if one takes the fine tuning criteria on the muon mass seriously then only very narrow regions of parameter space remain for natural leptoquark solutions of the observed a_μ, just above the LHC limits.

4 Two-field extensions

In this section we consider simple extensions of the SM by two fields. We focus on models where the new particles can appear together in pure BSM loops that contribute to a_μ, in which case the new fields should have different spins. It is not possible to get an enhancement through internal chirality flips in these models, restricting explanations of a_μ to low mass regions, but compressed spectra in these regions may evade the LHC limits. In addition one of the new particles could be a stable dark matter candidate, and then simultaneous explanation of a_μ and dark matter is possible. For these reasons the case of two fields with different spins behaves very differently from the one-field extensions, and is representative for a range of more elaborate models.

We begin in section 4.1 with an overview of the status of two-field extensions. There we also comment on the case with two fields of the same spin, including the interesting case of vector-like leptons. From the overview we identify two specific models that are promising in view of a_μ, dark matter and LHC constraints. These models will be analysed in detail in section 4.2 and compared against the latest a_μ^{2021} result and results from LHC and dark matter experiments.

4.1 Overview

With the possibilities for one-field extensions essentially exhausted, it is natural to then consider including two new fields entering the one-loop diagrams for a_μ together. The one-

JHEP09(2021)080

$(\mathrm{SU}(3)_C \times \mathrm{SU}(2)_L \times \mathrm{U}(1)_Y)_{\mathrm{spin}}$	$+\mathbb{Z}_2$	Result for $\Delta a_\mu^{\mathrm{BNL}}$, Δa_μ^{2021}
$(\mathbf{1},\mathbf{1},0)_0 - (\mathbf{1},\mathbf{1},-1)_{1/2}$	No	Projected LHC 14 TeV exclusion, not confirmed
	Yes	Updated section 4.2
$(\mathbf{1},\mathbf{1},-1)_0 - (\mathbf{1},\mathbf{1},0)_{1/2}$	Both	Excluded: $\Delta a_\mu < 0$
$(\mathbf{1},\mathbf{2},-1/2)_0 - (\mathbf{1},\mathbf{1},0)_{1/2}$	Both	Excluded: $\Delta a_\mu < 0$
$(\mathbf{1},\mathbf{1},0)_0 - (\mathbf{1},\mathbf{2},-1/2)_{1/2}$	No	Excluded: LHC searches
	Yes	Updated section 4.2
$(\mathbf{1},\mathbf{2},-1/2)_0 - (\mathbf{1},\mathbf{1},-1)_{1/2}$	No	Excluded: LEP contact interactions
	Yes	Viable with under abundant DM
$(\mathbf{1},\mathbf{1},-1)_0 - (\mathbf{1},\mathbf{2},-1/2)_{1/2}$	Both	Excluded: $\Delta a_\mu < 0$
$(\mathbf{1},\mathbf{2},-1/2)_0 - (\mathbf{1},\mathbf{2},-1/2)_{1/2}$	Both	Excluded: LEP search
$(\mathbf{1},\mathbf{2},-1/2)_0 - (\mathbf{1},\mathbf{3},0)_{1/2}$	No	Excluded: LHC searches
	Yes	Viable with under abundant DM
$(\mathbf{1},\mathbf{2},-1/2)_0 - (\mathbf{1},\mathbf{3},-1)_{1/2}$	No	Excluded: LHC searches + LEP contact interactions
	Yes	Viable with under abundant DM
$(\mathbf{1},\mathbf{3},0)_0 - (\mathbf{1},\mathbf{2},-1/2)_{1/2}$	Both	Excluded: $\Delta a_\mu < 0$
$(\mathbf{1},\mathbf{3},0)_0 - (\mathbf{1},\mathbf{3},-1)_{1/2}$	No	Excluded: LHC searches
	Yes	Viable with under abundant DM
$(\mathbf{1},\mathbf{3},-1)_0 - (\mathbf{1},\mathbf{2},-1/2)_{1/2}$	Both	Excluded: $\Delta a_\mu < 0$
$(\mathbf{1},\mathbf{3},-1)_0 - (\mathbf{1},\mathbf{3},0)_{1/2}$	Both	Excluded: $\Delta a_\mu < 0$
$(\mathbf{1},\mathbf{1},-1)_{1/2} - (\mathbf{1},\mathbf{1},0)_1$	No	Excluded: $\Delta a_\mu < 0$
$(\mathbf{1},\mathbf{2},-1/2)_{1/2} - (\mathbf{1},\mathbf{1},0)_1$	No	Excluded: $\Delta a_\mu < 0$
$(\mathbf{1},\mathbf{2},-1/2)_{1/2} - (\mathbf{1},\mathbf{3},0)_1$	No	Excluded: LHC searches + LEP contact interactions
$(\mathbf{1},\mathbf{1},0)_{1/2} - (\mathbf{1},\mathbf{1},1)_1$	No	Excluded: LHC searches + LEP contact interactions
$(\mathbf{1},\mathbf{2},-1/2)_{1/2} - (\mathbf{1},\mathbf{1},-1)_1$	No	Excluded: LHC searches + LEP contact interactions
$(\mathbf{1},\mathbf{3},-1)_{1/2} - (\mathbf{1},\mathbf{3},0)_1$	No	Excluded: $\Delta a_\mu < 0$

Table 2. Summary of known results for gauge invariant extensions of two fields with different spin with one-loop contributions to the anomalous magnetic moment of the muon. These results are rather exhaustive due to systematic investigations and classifications in refs. [367, 372, 376]. Note that this summarises results in the literature where different assumptions have been made, see the text and the original references for details. When there are multiple reasons for ruling a scenario out, we mention the most model- independent constraint. We use color highlighting to give a visual indication of the status of the model, namely green for viable explanations, red for excluded and purple for extensions that are only viable with under abundant dark matter.

loop diagrams shown in figure 19 of appendix A, have topologies FFS, SSF, VVF, FFV, VSF and SVF (where F = fermion, S = scalar and V = vector boson). Clearly, having loops with only BSM particles requires that the two new states have different spin. One of the new states must be a fermion (allowed to be Dirac, Majorana or Weyl fermion),

JHEP09(2021)080

the other either a scalar or a vector boson. This means the new states can't mix and new fermions can't couple to both the left- and right-handed muon, so no new chirality flips may be introduced. Therefore $\Delta a_\mu^{\rm BNL}$ explanations like this are heavily constrained and this has now been strongly confirmed with Δa_μ^{2021} result. Nonetheless one important new feature is that these both states couple to the muon together in trilinear vertices. If this is the only way they couple to SM states, and the BSM states have similar masses, then LHC limits could be evaded due to compressed spectra. Furthermore if this is due to a $\mathbb{Z}_2$ symmetry where the BSM states transform as odd, then it predicts a stable particle that could be a dark matter candidate.

The status of $\Delta a_\mu^{\rm BNL}$ from a pair of BSM fields with different spins is summarised in table 2, and these results have simply been confirmed by the new world average Δa_μ^{2021}. This table draws extensively from refs. [367, 372, 376]. Ref. [367] considers models without dark matter candidates and requires minimal flavour violation, while refs. [372] and [376] consider models with $\mathbb{Z}_2$ symmetry and dark matter candidates. Many models can be immediately excluded because their contributions to a_μ are always negative[13] with results in the literature in reasonable agreement regarding this. Models with positive contributions to a_μ predict a sufficiently large contribution only for very light states, and as a result collider searches place severe constraints on these models. However the collider search limits depend on the model assumptions and need to be understood in this context. The $\mathbb{Z}_2$ symmetry is particularly important as it regulates the interaction between the SM and BSM particles. Therefore, when necessary/required, the models in table 2 are considered in two cases: with or without $\mathbb{Z}_2$ symmetry. Collider constraints effectively eliminate almost all the models without $\mathbb{Z}_2$ symmetry, while requiring that the $\mathbb{Z}_2$ symmetric models simultaneously explain dark matter and $\Delta a_\mu^{\rm BNL}$ effectively restricts us to just the two models that we update in section 4.2. However first, in the following, we explain the assumptions used in our main sources to eliminate the remaining models that give a positive contribution to a_μ and the important caveats to these findings.

The introduction of a vector-like fermion and a scalar or a vector without any additional symmetries was dealt with by ref. [367], considering different $\mathrm{SU}(2)_L$ representations, namely singlets, doublets, triplets or adjoint triplets. They quickly eliminate a scalar doublet and fermion doublet combination, i.e. $(\mathbf{1},\mathbf{2},-1/2)_0$ – $(\mathbf{1},\mathbf{2},-1/2)_{1/2}$, without considering LHC constraints because cancellations amongst the contributions mean Δa_μ is too small for a 1σ explanation of $\Delta a_\mu^{\rm BNL}$ while satisfying basic assumptions like perturbativity and the $\approx 100\,\mathrm{GeV}$ LEP limit [465, 466]. For LHC searches they look at Drell-Yan production, which depends only on the gauge structure, but for decays they rely on $\mathbb{Z}_2$ violating leptonic interactions where they assume a minimal flavour violating structure. They apply also LEP constraints on contact interactions, using the same assumptions for the lepton interactions. However one should again note the caveats described at the beginning of section 3.1 on minimal flavour violation and abscence of scalar VEV. Adding only 8 TeV LHC searches effectively eliminates three more $\Delta a_\mu^{\rm BNL}$ explanations: $(\mathbf{1},\mathbf{1},0)_0$ – $(\mathbf{1},\mathbf{2},-1/2)_{1/2}$,

[13]The sign of Δa_μ from the one-loop diagrams can be understood analytically and ref. [376] also presents general conditions for a positive contribution, based on the hypercharge and the SU(2) representations.

JHEP09(2021)080

$(\mathbf{1},\mathbf{2},-1/2)_0$ – $(\mathbf{1},\mathbf{3},0)_{1/2}$ and $(\mathbf{1},\mathbf{3},0)_0$ – $(\mathbf{1},\mathbf{3},-1)_{1/2}$.[14] Constraints on $ee\ell\ell$ contact interactions derived from LEP observables alone further excludes $(\mathbf{1},\mathbf{2},-1/2)_0$ – $(\mathbf{1},\mathbf{1},-1)_{1/2}$, and in combination with LHC searches excludes $(\mathbf{1},\mathbf{2},-1/2)_0$ – $(\mathbf{1},\mathbf{3},-1)_{1/2}$ and fermion-vector extensions $(\mathbf{1},\mathbf{2},-1/2)_{1/2}$ – $(\mathbf{1},\mathbf{3},0)_1$, $(\mathbf{1},\mathbf{1},0)_{1/2}$ – $(\mathbf{1},\mathbf{1},-1)_1$ and $(\mathbf{1},\mathbf{2},-1/2)_{1/2}$ – $(\mathbf{1},\mathbf{1},-1)_1$. It is important to also note that the limits from contact interactions can also be avoided by cancellations from the contributions of heavy states that may appear as part of a more elaborate model, and are therefore quite model dependent.

Ref. [372] considered scenarios with a new fermion and scalar, where there is a $\mathbb{Z}_2$ symmetry under which the BSM fields are odd, so that the models have a stable dark matter candidate. In all cases the dark matter candidate was the scalar. The new couplings they introduce are renormalizable, perturbative, CP conserving, gauge invariant and muon-philic (meaning that muons are the only SM fermions the BSM states couple to). For the scalar-fermion $(\mathbf{1},\mathbf{1},0)_0$ – $(\mathbf{1},\mathbf{1},-1)_{1/2}$ pair with charged fermion singlet, they find a region where $\Delta a_\mu^{\text{BNL}}$ and the relic density can both be explained within 2σ. LHC constraints exclude much of the parameter space, but significant regions with compressed spectra survive. The results for the pair $(\mathbf{1},\mathbf{1},0)_0$ – $(\mathbf{1},\mathbf{2},-1/2)_{1/2}$ are essentially the same. We update both models in section 4.2. For an inert scalar doublet, coupled with fermions that are $\text{SU}(2)_L$ singlets, doublets, triplets, i.e. $(\mathbf{1},\mathbf{2},-1/2)_0$ – $(\mathbf{1},\mathbf{1},-1)_{1/2}$, $(\mathbf{1},\mathbf{2},-1/2)_0$ – $(\mathbf{1},\mathbf{2},-1/2)_{1/2}$ and $(\mathbf{1},\mathbf{2},-1/2)_0$ – $(\mathbf{1},\mathbf{3},-1)_{1/2}$, they find a narrow region at, or just below, the Higgs resonance region ($m_s \approx m_h/2$), that is consistent with both the relic density and a_μ^{BNL} within 2σ.[15] LHC searches almost exclude these scenarios, but in all cases a tiny region where the fermion is about 100 GeV survives. Since these regions are so small, in table 2 we only report that these models are viable with under abundant dark matter. For an inert scalar doublet coupled with an adjoint triplet fermion ($(\mathbf{1},\mathbf{2},-1/2)_0$ – $(\mathbf{1},\mathbf{3},0)_{1/2}$) they find no region can be consistent a_μ^{BNL} and the observed DM relic density.

Ref. [376] considered the same type of models, but substantially expanded the number by including a wider range of dark matter candidates and systematically classifying the representations in a manner similar to that shown in our table 2. For a given mass of the dark matter candidate that is sufficiently heavier than the W-boson mass, higher $\text{SU}(2)_L$ representations will have a comparatively large dark matter annihilation cross-section, they use this to place further analytically derived constraints on the models. Beyond the very fine tuned regions near the Higgs resonance[16] the only models that could explain $\Delta a_\mu^{\text{BNL}}$ and the relic abundance of dark matter are scalar singlet dark matter with either a fermion singlet or fermion doublet, i.e. $(\mathbf{1},\mathbf{1},0)_0$ – $(\mathbf{1},\mathbf{1},-1)_{1/2}$ and $(\mathbf{1},\mathbf{1},0)_0$ – $(\mathbf{1},\mathbf{2},-1/2)_{1/2}$. For these two surviving explanations of dark matter and $\Delta a_\mu^{\text{BNL}}$ they further apply constraints

[14] There is a very small 5 GeV gap in the exclusion for $(\mathbf{1},\mathbf{1},0)_0$ – $(\mathbf{1},\mathbf{2},-1/2)_{1/2}$ and a small corner of parameter space of $(\mathbf{1},\mathbf{3},0)_0$ – $(\mathbf{1},\mathbf{3},-1)_{1/2}$ escaped 8 TeV searches, but given the LHC run-II projection in ref. [367], this should now be excluded unless there is a large excess in the data. For this reason we describe these models as excluded in table 2.

[15] Explaining a_μ^{BNL} within 2σ requires only adding a small part of the deviation. As the authors comment in their text, for the doublet case the BSM Δa_μ contribution is very small. A 1σ explanation should not be possible, so we regard this explanation excluded by LEP.

[16] As an example of this they also present results with explanations near the Higgs resonance for the scalar-fermion $(\mathbf{1},\mathbf{2},-1/2)_0$ – $(\mathbf{1},\mathbf{1},-1)_{1/2}$ case.

JHEP09(2021)080

from the 8 TeV and 13 TeV LHC searches and LEP limit on electroweak states. While in the latter model one can also get a neutral dark matter candidate if the fermion is lighter than the scalar, direct detection rules this out. They find that LHC searches heavily constrain the regions where relic density and $\Delta a_\mu^{\rm BNL}$ may be simultaneously explained, but cannot entirely exclude the possibility.

4.1.1 Vector-like leptons

Before ending this overview we briefly also discuss the case of models with two fields of the same spin. In this case mixing of fields and enhanced chirality flips are allowed, but a dark matter candidate is precluded. Particularly interesting examples are extensions with vector-like leptons (VLLs), i.e. extension by two new vector-like fermions with the same quantum numbers as the left- and right-handed SM leptons. The muon-philic VLLs can couple both to left- and right-handed muons and to the Higgs boson; the contributions to a_μ behave similarly to the ones of leptoquarks in eq. (3.14), but the chirality flip at the top quark is replaced by the new Yukawa coupling of the VLL to the Higgs boson. Such models have been discussed in detail in refs. [293, 294, 296].

A distinguishing property of such models is that significant new contributions to the muon mass arise at tree level via the mixing with the new VLL. The relation between loop contributions to a_μ and to the tree-level muon mass is therefore more complicated than in the discussion of section 2 leading to eq. (2.4): for Higgs-loop contributions to a_μ, the ratio between Δa_μ and $\Delta m_\mu^{\rm tree}$ does not behave as $1/M_{\rm BSM}^2$ but rather as $1/(16\pi^2 v^2)$ [293, 294]. Nevertheless, for couplings in line with electroweak precision constraints and perturbativity, only masses up to the TeV scale are able to provide significant contributions to a_μ, similar to the bound of eq. (2.5).

Currently these models with a single VLL can accommodate all existing limits, but there are two noteworthy constraints. On the one hand, bounds from $\mu \to e\gamma$ require the VLL couplings to be non-universal, i.e. very much weaker to the electron than to the muon (to allow large enough contributions for a_μ^{2021}) [296]. On the other hand, the muon-Higgs coupling is modified by the large tree-level contributions to the muon mass. Already the current LHC constraints on the Higgs decay rate $h \to \mu^+\mu^-$ imply upper limits on the possible contributions to a_μ, and if future experiments measure the $h \to \mu^+\mu^-$ rate to be in agreement with the SM prediction, a deviation as large as $\Delta a_\mu^{\rm BNL}$ cannot be explained [296]. However extensions with more fields may relax the mass limits and constraints from $h \to \mu^+\mu^-$ [303, 304], given the lowest-order calculations of these references.

Slightly generalized models, where vector-like fermions may also carry quantum numbers different from ordinary leptons, have been examined in refs. [293, 367]. Ref. [367] examined the introduction of a vector-like fermion $\mathrm{SU}(2)_L$ doublet $(\mathbf{1},\mathbf{2},-1/2)_{1/2}$ with either an $\mathrm{SU}(2)_L$ singlet ($(\mathbf{1},\mathbf{1},0)_{1/2}$ or $(\mathbf{1},\mathbf{1},-1)_{1/2}$) or a $\mathrm{SU}(2)_L$ triplet ($(\mathbf{1},\mathbf{3},0)_{1/2}$ or $(\mathbf{1},\mathbf{3},-1)_{1/2}$). Each BSM fermion state is coupled to the Higgs boson and either the SM lepton $\mathrm{SU}(2)_L$ doublet L_i, the SM lepton $\mathrm{SU}(2)_L$ singlet e_i with a flavour-universal coupling, or another BSM vector-like fermion. BSM and SM fermions of the same charge then mix together, with the amount of mixing between the SM and fermion states constrained by LEP limits [467]. Thus they allow minimal flavour violation between the SM lepton

JHEP09(2021)080

generations, and some of the main constraints on the masses of the vector-like fermions comes from minimal flavour violation. Ref. [293] additionally considered the introduction of a vector-like fermion $\mathrm{SU}(2)_L$ doublet with hypercharge $Y = -3/2$ with either a charged fermion singlet or triplet (either $(\mathbf{1},\mathbf{2},-3/2)_{1/2}$ – $(\mathbf{1},\mathbf{1},-1)_{1/2}$ or $(\mathbf{1},\mathbf{2},-3/2)_{1/2}$ – $(\mathbf{1},\mathbf{3},-1)_{1/2}$). Ultimately both consider that these mixing vector-like fermions can produce positive contributions to a_μ and cannot be ruled out even by 14-TeV LHC projections.

4.2 Scalar singlet plus fermion explanations

Our overview has resulted in two kinds of two-field models of particular interest, shown in table 2. Both models are heavily constrained by LHC, but have not been excluded yet in the literature. We denote the two models as Model L and Model R, which extend the SM by adding the following fields:

$$\text{Model L:}\quad \phi,\ \psi_d = \begin{pmatrix}\psi_d^+\\ \psi_d^0\end{pmatrix}, \qquad\qquad \text{Model R:}\quad \phi,\ \psi_s \equiv \psi_s^-, \tag{4.1}$$

where $\phi = \phi^0$ is an $\mathrm{SU}(2)_L$ singlet scalar field with representation $(\mathbf{1},\mathbf{1},0)_0$, ψ_d a doublet fermion field with representation $(\mathbf{1},\mathbf{2},1/2)_{1/2}$, and ψ_s a singlet fermion field with representation $(\mathbf{1},\mathbf{1},-1)_{1/2}$. These new fermions are vector-like, or Dirac fermions, thus not only are the Weyl spinors ψ_d and ψ_s introduced but also their Dirac partners $\psi_d^c = (\psi_d^{+c\dagger}, \psi_d^{0c\dagger})$ and $\psi_s^c \equiv \psi_s^{-c\dagger}$. In Model L the new fields couple only to the left-handed muon, and in Model R to the right-handed muon.

The two models add the following terms to the SM Lagrangian, using Weyl notation as in eq. (3.5):

$$\mathcal{L}_\mathrm{L} = \left(\lambda_L L\cdot\psi_d\phi - M_\psi\psi_d^c\psi_d + \text{h.c.}\right) - \frac{M_\phi^2}{2}|\phi|^2, \tag{4.2}$$

$$\mathcal{L}_\mathrm{R} = \left(\lambda_R\mu\phi\psi_s - M_\psi\psi_s^c\psi_s + \text{h.c.}\right) - \frac{M_\phi^2}{2}|\phi|^2, \tag{4.3}$$

which can be written out into their $\mathrm{SU}(2)_L$ components:

$$\mathcal{L}_\mathrm{L} = \left(\lambda_L\nu_{\mu L}\psi_d^0\phi^0 - \lambda_L\mu_L\psi_d^+\phi^0 - M_\psi\psi_d^{0c\dagger}\psi_d^0 - M_\psi\psi_d^{+c\dagger}\psi_d^+ + \text{h.c.}\right) - \frac{M_\phi^2}{2}|\phi^0|^2, \tag{4.4}$$

$$\mathcal{L}_\mathrm{R} = \left(\lambda_R\mu_R^\dagger\psi_s^-\phi^0 - M_\psi\psi_s^{-c\dagger}\psi_s^- + \text{h.c.}\right) - \frac{M_\phi^2}{2}|\phi^0|^2. \tag{4.5}$$

We have not included additional renormalisable terms involving the scalar singlet in the Higgs potential, which are not relevant for a_μ, but we do briefly comment on the impact they would have later on, as they can affect the dark matter phenomenology. This leaves both models with just three parameters.

In the following we therefore present a detailed update of the phenomenology of Model L and Model R, scanning over all three parameters in each case to test whether or not dark matter and large Δa_μ can be simultaneously explained. We include the latest data from Fermilab, and the most recent LHC collider searches included in `SModelS` 1.2.3 in ref. [468–474] and `CheckMate` 2.0.26 [475–481]. It should be noted that we deal only with BSM fields

JHEP09(2021)080

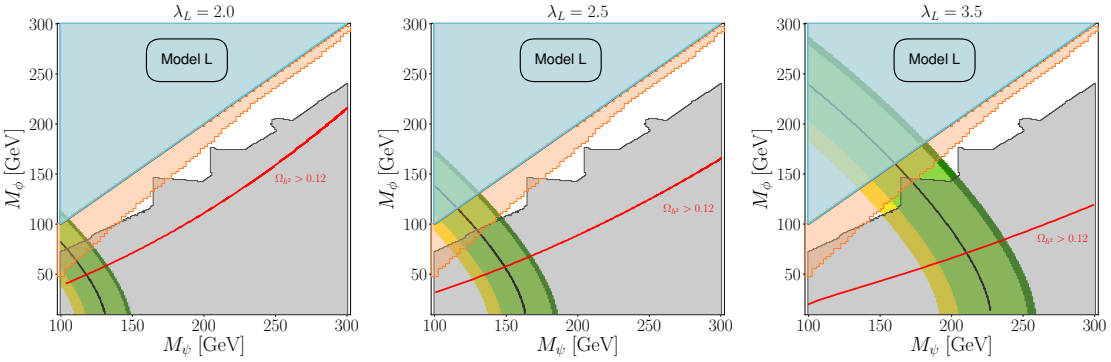

Figure 5. Results from Model L, scanning over the masses of the new fermion and scalar which couple to the left-handed muon. Regions which can explain Δa_μ in eq. (1.7) or eq. (1.6) to within 1σ are coloured green and yellow respectively, with the overlap between the two regions is coloured lime. The black line indicates masses which produce a Δa_μ contribution matching eq. (1.7). The points where a dark matter candidate particle produces the observed relic abundance of 0.1200, eq. (1.8), are shown in red, with the region below being excluded due to having an over abundance of dark matter. The region where $M_\psi < M_\phi$ is shaded cyan. Regions excluded by 13-TeV results at the LHC are shaded grey, with the exclusions from the soft leptons search [482] obtained using `CheckMate` shaded in orange. Thus a_μ can only be explained in small slices of parameter space between the grey and orange regions. As the coupling between the left-handed muon and the BSM particles is increased, higher masses are required to explain a_μ.

that couple to second generation SM fermions. Thus, flavour violation constraints on our models can safely be ignored, including limits from contact interactions. This is in line with the methodology in ref. [376], but not [367].

The BSM contributions from both of the two field dark matter models come from the FFS diagram 19(a) of figure 19 with the generic F fermion lines replaced by ψ^- and the scalar S one by ϕ^0. The contributions to a_μ from both of these models are given by identical expressions (where $\lambda_{L,R}$ are generally denoted by λ). The result is given by

$$\Delta a_\mu^{\text{Model L}} = \Delta a_\mu^{\text{Model R}} = -Q_\psi \frac{\lambda^2}{32\pi^2} \frac{m_\mu^2}{6M_\phi^2} E\left(\frac{M_\psi^2}{M_\phi^2}\right), \tag{4.6}$$

where $Q_\psi = -1$. It does not involve a chirality flip enhancement, which has a large impact on the ability of these models to explain a_μ whilst avoiding collider constraints.

The results for the first of the two field dark matter models, Model L, are shown in figures 5, 6. Scans were performed over a grid of scalar mass $M_\phi \in [0, 400]$ GeV and fermion masses of $M_\psi \in [100, 400]$ GeV, taking into consideration the LEP limit $M_\psi > 100$ GeV [465, 466] on charged fermion masses. Before showing results of the full scan, in figure 5 we show Δa_μ in three slices of the parameter space in the M_ψ–M_ϕ (M_ψ over $100 \ldots 300$ GeV and M_ϕ over $0 \ldots 300$ GeV) with fixed $\lambda_L = 2, 2.5, 3.5$. Due to the lack of enhanced chirality flips a sufficiently large Δa_μ is obtained only when the coupling constant is large and the masses are relatively small. However due to the new reduced measurement of a_μ, the discrepancy can be explained with heavier masses than before as indicated in the green curve. For $\lambda_L \leq 2$, the model cannot provide large enough Δa_μ to explain the

JHEP09(2021)080

anomaly within 1σ while avoiding the LEP $M_\psi > 100\,\text{GeV}$ limit and LHC limits (discussed below), while for very large values of $\lambda_L = 2.5$ or $\lambda_L = 3.5$ it is possible to explain the anomaly but even when λ_L is close to $\sqrt{4\pi}$, Δa_μ^{2021} can only be explained within 1σ for masses below 260 GeV. These results can be approximately reproduced using eq. (4.6), though we have again performed the calculation with `FlexibleSUSY` 2.5.0 [43, 44], which includes the full one-loop calculation and the universal leading logarithmic two-loop QED contribution [450].

We do not consider scenarios with $M_\psi < M_\phi$ because such cases are like Higgsino dark matter or the doublet case of minimal dark matter and as such will be under abundant when the mass is below about 1 TeV (see e.g. Ref. [483]). Without a chirality flipping enhancement it will not be possible to explain $\Delta a_\mu^{\text{BNL}}$ or Δa_μ^{2021} with masses that are heavy enough to explain dark matter. Hence the dark matter candidate is given by the scalar singlet ϕ. Direct detection of dark matter constraints then depend on the parameters of Higgs potential terms involving the singlet. By including such terms, we found that direct detection constraints rule out significant parts of the parameter space but can always be evaded by choosing the additional parameters to be small. Therefore, for simplicity, we neglect these parameters in our final numerical results and do not show direct detection constraints.

The collider constraints are shown with overlayed shading. The lower grey shaded region comes from searches for charginos, neutralinos, sleptons, and long-lived particles, using leptonic final states in the 8-TeV searches [423, 484–486] and the 13-TeV searches [487–490], included in `SModelS` 1.2.3 [491, 492] and excludes most of the light mass parameter space where a_μ can be explained. Nonetheless there is still a considerable gap close to the $M_\phi = M_\psi$ line, which escapes these constraints, but may be closed by searches for compressed spectra. We therefore also show in shaded orange the CMS search for the compressed spectra of soft leptons [482], which was obtained using `CheckMate` 2.0.26 [475, 476] using `MadAnalysis` [493] and `PYTHIA` [472, 473] to generate event cross-sections. As a result of these constraints there is little room for the model to evade collider constraints and explain the observed value of a_μ, though some gaps do evade the collider constraints we apply.

Finally we also consider the relic density of dark matter in this model using `micrOMEGAs` 5.2.1 [494]. The red line in figure 5 indicates where the model's dark matter candidate particle produces the Planck-observed relic density of $\Omega_{h^2} = 0.1200$, eq. (1.8). Along this red line the relic abundance of dark matter is depleted to the observed value through t-channel exchange of the BSM fermions. This mechanism is less effective below the line, where the mass splitting between the BSM scalar and fermion is larger, leading to over abundance. All points below the red line are strongly excluded by this over abundance, though this does not rule out any scenarios that are not already excluded by collider constraints. Above the line the relic density is under abundant. Our results show that it is not possible for any of these λ_L values to simultaneously explain a_μ^{2021} and the relic density, while evading collider limits.

To give a more global picture of the status of the model in figure 6 we also vary $\lambda_L \in [0, 3.5]$. In the left panel we show where on the M_ϕ–M_ψ plane it is possible to

JHEP09(2021)080

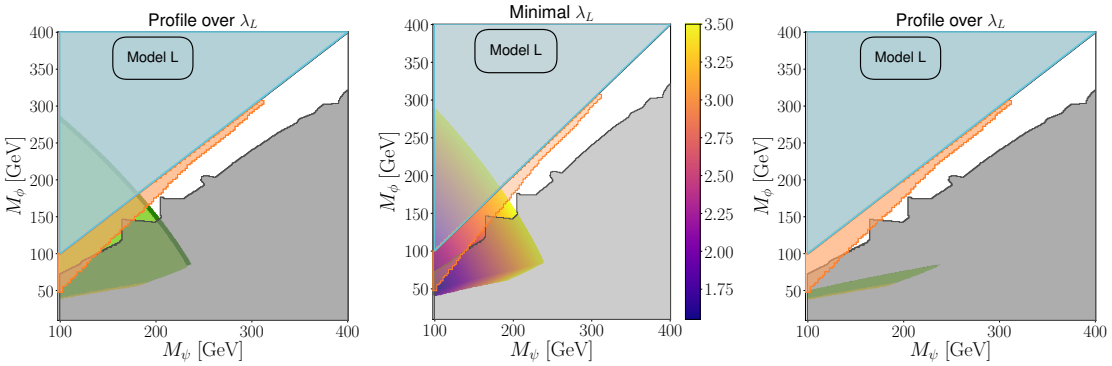

Figure 6. Several profiles of Model L. Colours for the first and third panels are the same as figure 5, and the same LHC limits (which do not depend on the coupling) are overlaid. The left panel shows the best contributions to a_μ for each value of the BSM masses, without having a dark matter candidate particle with an over abundant relic density. Likewise, the right panel only shows points which have a dark matter relic density within 1σ of the Planck observation [416]. The middle panel shows the smallest value of the coupling λ_L which can explain a_μ^{2021} (eq. (1.7)) within 1σ without producing over abundant dark matter.

simultaneously fit the BNL measurement or the new world average for a_μ and avoid an over abundant relic density, for some value of λ_L within this range. As expected this shows that λ_L may be adjusted so that for very light masses one may always explain a_μ within 1σ, but as the masses are raised past $200 - 300\,\text{GeV}$, this is no longer possible. As a result the combination of collider constraints shown in grey, cyan and orange exclude all but two narrow regions of parameter space in the compressed spectra region between the M_ϕ and M_ψ masses. As shown in the middle panel of figure 6, where we plot the minimum value of λ_L consistent with a 1σ explanation of Δa_μ^{2021}, explaining the observed value requires a very large coupling $\lambda_L \geq 2.5$. One may question the precision of our calculation for such large values of λ_L, however given the mass reach of the collider experiments which extends well past the 1σ region it is unlikely that including higher orders in the BSM contributions will change anything significantly. Finally the right panel of figure 6 shows a_μ results that are compatible with explaining the full observed dark matter relic density within 1σ, having obtained this data from a targeted scan using `MultiNest` 3.10 [495–498]. Our results show that it is now impossible to simultaneously explain dark matter and $\Delta a_\mu^{\text{BNL}}$ and the same is true with the updated Δa_μ^{2021} measurement.

Compared to the results for this model shown in ref. [376], we find that the most recent collider search(es) [485, 488], are the most important for narrowing the gaps in the exclusion. Currently, there is very little room for the model to survive.

Results for Model R are shown in figures 7, 8. Since the contributions to a_μ for this model are also governed by eq. (4.6), the behaviour of Δa_μ is the same. However as one can see in figures 7, 8 the collider constraints for Model R, which has no $\text{SU}(2)_L$ interactions, are weaker than those for Model L, with the exclusions again coming from `SModelS` 1.2.3 through the 8-TeV searches [485, 486, 499, 500] and the 13-TeV searches [487–490, 501]. The searches providing most of the constriction on the parameter space of Model R are

JHEP09(2021)080

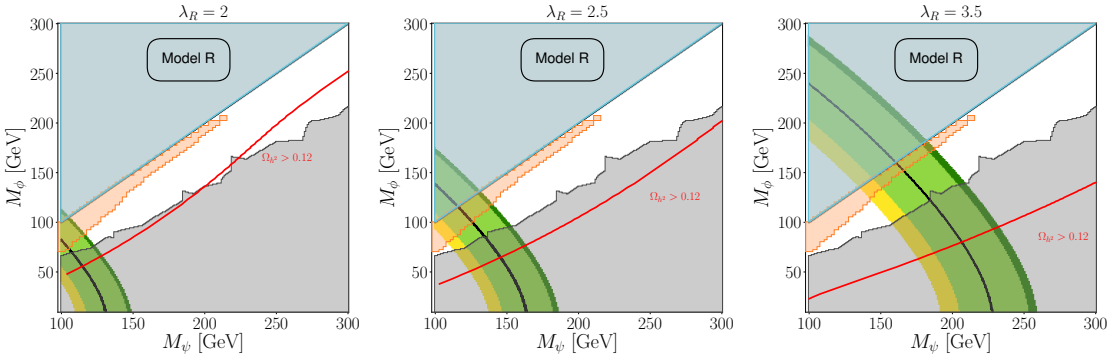

Figure 7. Results from Model R, scanning over the masses of the new fermion and scalar which couple to the right-handed muon. Colours are the same as figure 5.

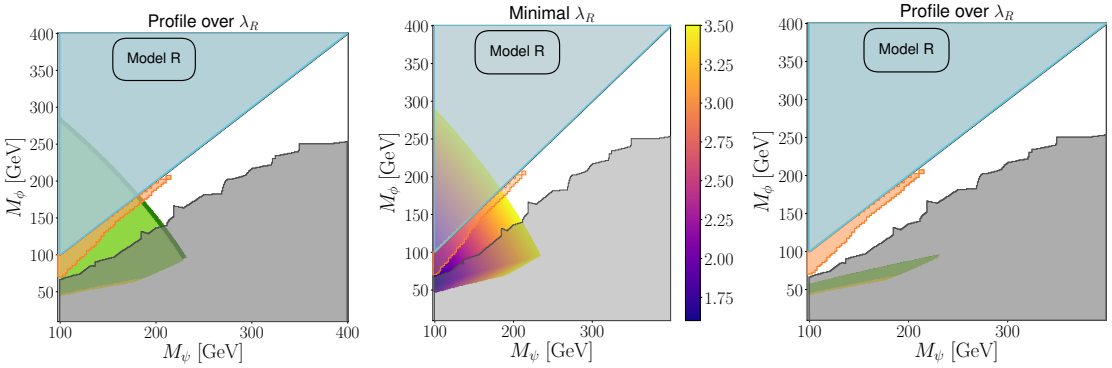

Figure 8. Several profiles of Model R. Colours for the first and third panels are the same as figure 5. The middle panel shows the lowest value of λ_R which can explain a_μ^{2021} from eq. (1.7) within 1σ. The panels are constructed in the same way as those in figure 6. The same LHC limits as figure 7 (which do not depend on the coupling) are overlaid.

the ATLAS searches [485, 490] and the CMS searches [488, 501]. As a result in the case of Model R there is still some room to explain the a_μ measurement within currently applied collider constraints. However as can be seen in the left panel of figure 7 even with $\lambda_R = 2.0$, there is only a little room to escape the combination of the standard electroweakino searches shaded grey and the soft lepton compressed spectra search shaded orange. In the middle panel when $\lambda_R = 2.5$ one can see a significantly larger, but still narrow region where a_μ^{2021} can be explained within 1σ while evading the collider limits. In the right panel as λ_R approaches the perturbative limit both the value and area of the viable parameter space are larger. In the left panel of figure 8, where λ_R is allowed to vary, one can see the full region of the $M_\phi - M_\psi$ plane where a_μ^{2021} is explained within 1σ, while avoiding giving a relic density of dark matter which is too over abundant. With the overlaid collider limits we can see the complete picture of parameter space where it remains possible to explain this observed a_μ, while evading limits from colliders. Avoiding collider constraints from the LHC requires compressed spectra, and comparing the green and lime green regions, one can see that the situation with the new world average has just marginally increased the masses that can be accommodated. However as shown by the middle panel of figure 8,

JHEP09(2021)080

evading these limits requires a coupling of $\lambda_R \gtrsim 1.8$. One can also see that the relic density cannot be explained simultaneously with a_μ^{2021} in any of the slices shown in figure 7, and the right panel of figure 8 does show that the regions which can explain dark matter relic density and Δa_μ^{2021} to within 1σ are fully ruled out by collider constraints.

In summary, two-field models with different spin do not contain new sources of chirality flipping enhancements, and many models of this class are not able to generate significant positive contributions to a_μ, see table 2. However the Model L and Model R investigated here do give positive contributions, and our results show they remain viable explanations of the new world average deviation Δa_μ^{2021} after the FNAL measurement, as can be seen from figures 5-8, with small parts of the parameters space escaping LHC constraints. Model R is found to be slightly more viable due to reduced impact of LHC constraints, in particular those from compressed spectra searches. In both models, however, it is not possible to simultaneously explain Δa_μ^{2021} whilst producing the observed dark matter relic density [416] and satisfying LHC collider constraints. It is only possible to explain Δa_μ^{2021} within 1σ with an under abundant dark matter candidate particle. Further, the lack of chirality flip for either of these models constrain the masses to be $M_\psi, M_\phi \leq 210\,\text{GeV}$ to both avoid collider constraints and explain the value of Δa_μ^{2021}, where compressed spectra searches are important for the viability of these models. Future data from a_μ experiments and LHC might entirely exclude these models.

5 Three-field extensions

As we saw in section 4 introducing two fields with different spins is the simplest way to explain dark matter and give new contributions to muon $g-2$, but collider constraints heavily constrain the region where such models can explain the observed muon $g-2$. This is because in those cases it is not possible to induce a chirality flip in the muon $g-2$ diagram's loop, as both the new fermion and scalar only couple to either the left- or right-handed muon.

We therefore now consider the simplest models that can both have an enhanced contribution to muon $g-2$ from a chirality flip and explain dark matter. These are models with two fields of the same spin that mix together and a third field with a different spin and a $\mathbb{Z}_2$ symmetry under which these new fields are odd, while the SM fields are even. The leading contributions in supersymmetric models are in fact of this kind, as will be discussed in section 6, but here we also consider three-field models that do not arise as part of the MSSM. As in previous sections we will restrict ourselves to renormalizable models with new scalars and new fermions. Models of this nature have previously been classified in ref. [376], and there it is demonstrated that due to the chirality flip contribution there are many models which can explain the a_μ anomaly in eq. (1.6), with models that have a new field with a much higher $\text{SU}(2)_L$ representation (up to 20) being able to produce sizable contributions to a_μ. Likewise, the larger contributions to a_μ from the chirality flip enables three field models to simultaneously produce a dark matter candidate with the observed dark matter relic abundance [502] also with much higher $\text{SU}(2)_L$ representations compared to the two field models. This chirality flip enhancement also enables one to examine much higher mass scales compared to two field models, evading LHC collider constraints.

JHEP09(2021)080

In this section we present a detailed discussion of the phenomenology of two kinds of three-field models, which we denote as 2S1F and 2F1S, with two scalars and one fermion or vice versa. The quantum numbers will be chosen such that the models represent a variety of possible dark matter candidates. In model 2S1F, the dark matter is a scalar singlet or doublet (or mixture) and may be compared to generic scalar singlet or inert doublet models or to left- or right-handed sneutrinos. In model 2F1S, the dark matter is a singlet or doublet fermion (or a mixture) and may be compared to Bino or neutral Higgsino. Model 2S1F has some similarities to the BLR contribution in the MSSM, but the spin of the dark matter candidate is different. Model 2F1S contains the same states as the BHL contribution in the MSSM. In both cases, the couplings are treated as arbitrary, not respecting SUSY-like relations, which leads to a different phenomenology, and we compare and contrast these two models with their respective MSSM scenarios. Both of these models were considered in ref. [376], showing particular slices of the parameter space. Here we update these models with the latest a_μ^{2021} result and direct detection constraints, and perform a thorough sampling of the whole parameter space to show how the data leads to meaningful constraints on the parameters of these models.

5.1 Three-field model with two scalars, one charged fermion and scalar dark matter

We begin with the Model 2S1F which is the SM extended with three $\mathbb{Z}_2$-odd fields: one electrically charged fermion and two scalar fields,

$$\psi_s, \quad \phi_s^0, \quad \phi_d = \begin{pmatrix} \frac{\phi_d^0 + iA_\phi}{\sqrt{2}} \\ \phi_d^- \end{pmatrix}, \tag{5.1}$$

where ψ_s is an SU(2) singlet charged Dirac fermion expressed in Weyl spinors with representation $(\mathbf{1},\mathbf{1},1)_{1/2}$, ϕ_s^0 a scalar singlet with representation $(\mathbf{1},\mathbf{1},0)_0$, and ϕ_d a scalar doublet with representation $(\mathbf{1},\mathbf{2},-\frac{1}{2})_0$. The relevant interactions are:

$$\begin{aligned}\mathcal{L}_{\text{2S1F}} = &\left(a_H H\cdot\phi_d\phi_s^0 + \lambda_L\phi_d\cdot L\psi_s + \lambda_R\phi_s^0\mu\psi_s^c - M_\psi\psi_s^c\psi_s + \text{h.c.}\right)\\ &- M_{\phi_d}^2|\phi_d|^2 - \frac{M_{\phi_s}^2}{2}|\phi_s^0|^2.\end{aligned} \tag{5.2}$$

The new scalars couple to one of the left- and right-handed muons each, along with the new fermion. Then using a trilinear scalar coupling between the two scalars and the Higgs boson, the VEV of the Higgs bosons gives rise to mass mixing terms between the two scalars, and induces a chirality flip in the loop of muon $g-2$ processes. The relevant parameter combination for invoking this chirality flip enhancement is $a_H\lambda_L\lambda_R$.

For Model 2S1F in eq. (5.2), the neutral scalar singlet ϕ_s^0 and the CP-even part of the neutral component of ϕ_d mix together into two flavours of a neutral scalar ϕ_i^0 for $i=1,2$:

$$\mathcal{L}_{\text{2S1F}} \ni -\frac{1}{2}\begin{pmatrix}\phi_s^0 & \phi_d^0\end{pmatrix}\begin{pmatrix}M_{\phi_s}^2 & a_H v\\ a_H v & M_{\phi_d}^2\end{pmatrix}\begin{pmatrix}\phi_s^0\\ \phi_d^0\end{pmatrix} = -\frac{1}{2}\sum_{i=1,2} M_{\phi_i^0}^2|\phi_i^0|^2,$$

JHEP09(2021)080

where the mass eigenstates relate to the gauge eigenstates through the mixing matrix U_S as

$$\begin{pmatrix}\phi_1^0\\ \phi_2^0\end{pmatrix} = U_S^T \begin{pmatrix}\phi_s^0\\ \phi_d^0\end{pmatrix} . \tag{5.3}$$

The dark matter candidate is then the lightest neutral scalar ϕ_1^0. For this mixing to avoid producing a tachyon, the limit $a_H v < M_{\phi_s} M_{\phi_d}$ must be respected. As in the previous section on two-field extensions, we do not consider additional renormalisable terms involving the new scalars that could appear in the Higgs potential, but would not affect the a_μ prediction. These terms can change the dark matter phenomenology though, adding additional mechanisms to deplete the relic density, and new interactions that can mediate direct detection. However we do not expect these to substantially modify our conclusions.

In this model the one-loop BSM contribution to the anomalous magnetic moment is given by:

$$\begin{aligned}\Delta a_\mu^{\text{2S1F}} =& \frac{m_\mu^2}{32\pi^2}\left(\frac{\lambda_L^2}{12M_{\phi_d}^2}\,E\left(\tfrac{M_\psi^2}{M_{\phi_d}^2}\right) + \sum_{i=1,2}\frac{\lambda_L^2|U_{S\,2i}|^2 + 2\lambda_R^2|U_{S\,1i}|^2}{12M_{\phi_i^0}^2}\,E\left(\tfrac{M_\psi^2}{M_{\phi_i^0}^2}\right)\right.\\ &\left. + \frac{M_\psi}{m_\mu}\sum_{i=1,2}\frac{2\sqrt{2}\lambda_L\lambda_R U_{S\,1i}U_{S\,2i}}{3M_{\phi_i^0}^2}\,F\left(\tfrac{M_\psi^2}{M_{\phi_i^0}^2}\right)\right).\end{aligned} \tag{5.4}$$

These contributions come in the form of the FFS diagram 19(a) of figure 19 with the generic F fermion lines replaced by ψ^- the conjugate of ψ_s, and the scalar S one by ϕ_i^0 and A_ϕ, respectively.

The second line of eq. (5.4) provides the contribution with the chirality flip enhancement, and is therefore typically the dominant contribution. While a cursory glance at eq. (5.4) might lead one to believe that this model's chirality flip provides an apparent enhancement according to the ratio M_ψ/m_μ, the actual behaviour is more complicated. The actual form of this enhancement can be seen by using the simplification of the mixing angles $U_{S\,11}U_{S\,21} = -U_{S\,12}U_{S\,22} \to a_H v/(M_{\phi_1^0}^2 - M_{\phi_2^0}^2)$. Plugging this into eq. (5.4) generates a difference between loop functions which, together with the mass difference in the denominator, can be written in terms of the loop function $\tilde{F}_a$ of the appendix eq. (A.16). In this way, for $M_\psi \gg m_\mu$, the contribution from this model simplifies to the chirality flip contribution as:

$$\Delta a_\mu^{\text{2S1F}} \approx \frac{m_\mu^2}{32\pi^2}\frac{M_\psi}{m_\mu}\sum_{i=1,2}\frac{2\sqrt{2}\lambda_L\lambda_R U_{S\,1i}U_{S\,2i}}{3M_{\phi_i^0}^2}\,F\left(\frac{M_\psi^2}{M_{\phi_i^0}^2}\right) \tag{5.5}$$

$$\approx \frac{m_\mu^2}{32\pi^2}\frac{M_\psi}{m_\mu}\frac{2\sqrt{2}\lambda_L\lambda_R a_H v}{3(M_{\phi_1^0}^2 - M_{\phi_2^0}^2)}\left(\frac{1}{M_{\phi_1^0}^2}\,F\left(\frac{M_\psi^2}{M_{\phi_1^0}^2}\right) - \frac{1}{M_{\phi_2^0}^2}\,F\left(\frac{M_\psi^2}{M_{\phi_2^0}^2}\right)\right), \tag{5.6}$$

$$\approx -\frac{m_\mu^2}{32\pi^2}\frac{M_\psi}{m_\mu}\frac{2\sqrt{2}\lambda_L\lambda_R a_H v}{M_\psi^4}\,\tilde{F}_a\left(\frac{M_\psi^2}{M_{\phi_1^0}^2}, \frac{M_\psi^2}{M_{\phi_2^0}^2}\right). \tag{5.7}$$

Thus the final result for this chirality-enhanced contribution can be written in the form

$$\Delta a_\mu^{\text{2S1F}} \approx -\frac{m_\mu^2}{32\pi^2 M_\psi^2}\,\frac{2\sqrt{2}\lambda_L\lambda_R a_H v}{m_\mu M_\psi}\,\tilde{F}_a\left(\frac{M_\psi^2}{M_{\phi_1^0}^2}, \frac{M_\psi^2}{M_{\phi_2^0}^2}\right), \tag{5.8}$$

JHEP09(2021)080

where e.g. $\tilde{F}_a(1,1) = 1/12$. We see that the actual enhancement factor, beyond the typical loop and mass suppression factor, is given by the ratio $\lambda_L \lambda_R a_H v/(m_\mu M_\psi)$. As announced earlier it relies on the factor $\lambda_L \lambda_R a_H$ and requires all three of these couplings to be non-zero.

We have presented this discussion of how the parametric behaviour of the chirality flip can be extracted from the exact result eq. (5.4) in quite some detail, and we remark that similar discussions can also be applied to other models, e.g. to the model 2F1S discussed later, or to MSSM contributions discussed in section 6.[17]

If either λ_L or λ_R are zero then clearly the above contribution vanishes, while it will also vanish if there is no mixing between the scalars, i.e. $a_H = 0$, so that $U_{S\,1i} U_{S\,2i}$ vanishes. If $\lambda_L = a_H = 0$ or $\lambda_R = a_H = 0$ then eq. (5.4) reduces to the same result for two fields with different spin, i.e. eq. (4.6), while if a_H is non-zero, then one gets a similar result, but with some dilution from the mixing. Similarly if both λ_L and λ_R are non-zero, but $a_H = 0$ then we simply get two copies of eq. (4.6), with different couplings that are summed. Finally note that the mixing will also be heavily suppressed just by having a large enough mass splitting between the two scalar states, i.e. making the ratio $(v a_H)^2/(M^2_{\phi_s} M^2_{\phi_d})$ sufficiently small.

In the following we provide a detailed phenomenological analysis of the Model 2S1F. The underlying question is whether the model can accommodate the new a_μ^{2021} value simultaneously with current constraints from dark matter and LHC. The model is complicated and depends on three masses and three couplings in a relevant way. We focus on the parameter space where λ_L, λ_R and a_H are all non-zero, such that the model behaves differently from the models of the previous section. Eq. (5.8) then provides the dominant contribution and can be used to understand our results. As in previous sections we do however use `FlexibleSUSY` 2.5.0 [43, 44] to obtain the numerical results, where we augment the full one-loop BSM calculation with the universal leading logarithmic photonic 2-loop contributions [503].

Before entering details, we briefly explain relevant dark matter processes. Without the a_H, λ_L and λ_R interactions that are important for a_μ, dark matter could behave either as pure scalar singlet or as pure inert scalar doublet dark matter. In the inert doublet case, already the standard $\mathrm{SU}(2)_L$ electroweak gauge interactions are sufficient to deplete the relic density to (below) the observed value when it has a mass of (less than) about 600 GeV [504]. The preferred mass of scalar singlet dark matter depends on the Higgs portal coupling, but outside of fine tuned parameter regions and for couplings $\lambda_{L,R} < 1$, the best fit for the data is found when the pure scalar singlet dark matter has a mass of $\approx$ 1–3 TeV[18] [505]. Beyond these simple special cases, the model here allows many additional depletion mechanisms: significant $\lambda_{L,R}$ allow t-channel exchange of the new fermion, through λ_L or λ_R if the scalar dark matter is doublet or singlet dominated (or both if there is mixing). If the new fermion mass is sufficiently close, coannihilations through λ_L

[17] The enhancement may be compared to the enhancement factor for the MSSM BLR contribution shown in eq. (6.6) in section 6, where $a_H v$ corresponds to $m_\mu \mu \tan\beta$. In the corresponding MSSM contribution, the couplings analogue to $\lambda_{L,R}$ are gauge couplings, while these couplings are independent here.

[18] We do not consider the Higgs portal coupling needed for this, in our analysis, but the well studied phenomenology of scalar singlet dark matter may be useful in showing the kind of scenarios that we neglect here.

JHEP09(2021)080

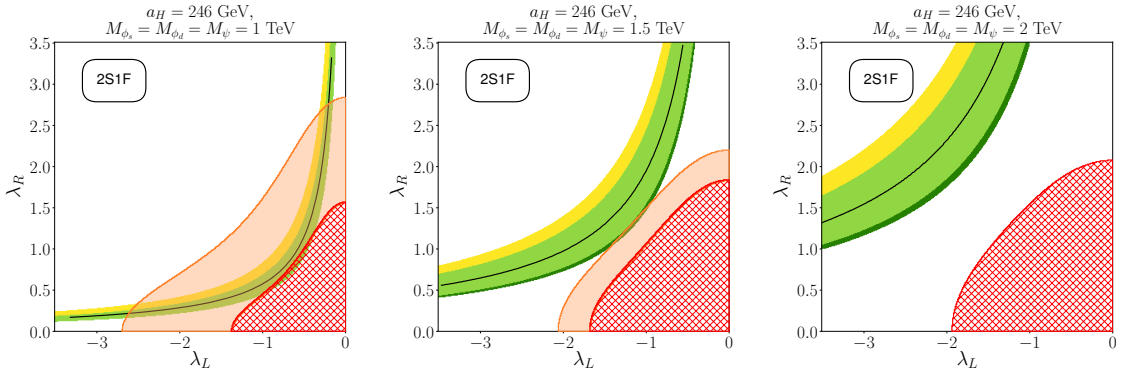

Figure 9. Results from Model 2S1F, scanning over the couplings of the new scalars and fermion to the left- and right-handed muon. All BSM fields have identical masses as specified in the subfigures. The trilinear coupling which parametrises the mixing of the neutral BSM scalars is fixed to $a_H = 246\,\text{GeV}$. Regions which can explain $\Delta a_\mu^{\text{BNL}}$ and Δa_μ^{2021} to within 1σ are coloured yellow and green respectively, while the overlap between these two regions is coloured lime. The black line marks couplings which produce a contribution which exactly matches eq. (1.7). The points where a dark matter candidate particle produces the observed relic abundance of 0.1200, eq. (1.8), are at the boundary of the hatched region shown in red, with the hatched region below and to the right being excluded due to having a relic abundance greater than 0.12. Regions excluded by searches for the direct detection of dark matter at the Xenon1T experiment [506, 507] are shaded in orange.

and λ_R can also be active in depleting the relic density. The coupling a_H between singlet, doublet, and the SM Higgs can lead to singlet-doublet coannihilation processes. This same coupling a_H is also relevant for direct detection constraints on dark matter, which depend particularly on Higgs-mediated processes. Importantly, the mentioned additional depletion processes can compensate general suppressions of cross sections for heavier masses. As a result even heavier dark matter masses than for the inert doublet can become possible.

As we will see from detailed scans, the dark matter constraints indeed only allow rather heavy masses, which are above LHC limits. For this reason we do not explicitly consider LHC constraints in the following.

In figure 9 we begin our numerical analysis of this model. The figure represents a baseline behaviour. In order to maximize contributions to a_μ via a large chirality flip and mixing (see eq. (5.8) and following discussion) we choose equal masses $M_{\phi_s} = M_{\phi_d}$ and fix $a_H = v = 246\,\text{GeV}$ as a reference value, similar to scenarios examined by ref. [376]. We also choose M_ψ to be equal to the scalar masses. This is a rather special choice for dark matter, as all mechanisms for depleting the relic density can be active here, including scalar-fermion coannihilation. As a result, the relic density will be quite suppressed and the Planck-observed value can only be explained for small couplings. On the other hand, the dark matter direct detection will not be suppressed due to the large mixing between the scalar and doublet, allowing interactions with the nucleons through the moderately sized a_H coupling.

The behaviour of Δa_μ in the three panels of figure 9 clearly reflects the $\lambda_L \lambda_R a_H / M^2$ dependence of the chirality-flipping contributions shown in eq. (5.8). In each panel the

JHEP09(2021)080

coupling dependence is approximately hyperbolic. Specifically, in the left panel for TeV-scale masses it is possible to explain Δa_μ^{2021} with couplings $|\lambda_L \lambda_R| \approx 0.8^2$. As the masses are increased to 1.5 TeV and 2 TeV in the middle and right panels respectively, the contribution to a_μ is suppressed. Therefore at higher masses to explain $\Delta a_\mu^{\text{BNL}}$ and Δa_μ^{2021} to within 1σ either larger couplings are required, as shown in the plot, or alternatively a larger value of a_H (which is fixed to 246 GeV on this plot) could be chosen.

Each panel in figure 9 also shows a red hatched region, which is excluded by over abundance of the dark matter relic density. At the boundary the observed value [416] can be explained. In the non-hatched region the predicted relic density is under abundant. Further, the orange shaded regions are excluded by direct detection searches using `DDCalc` 2.2.0 [508, 509].[19] As mentioned above, the equal mass scenario is constructed to maximize the impact of relic density depletion mechanisms. The dark matter candidate has significant singlet and doublet components, and the depletion mechanisms are equally sensitive to both λ_L and λ_R, see the Lagrangian eq. (5.2). If either coupling is sufficiently large the relic density becomes under abundant. As a result the red lines are approximately parabolic in the $\lambda_L - \lambda_R$ plane, and for $\mathcal{O}(1)$ values of the couplings the relic density can be explained. As the overall mass scale is increased, the required couplings become slightly larger.

The dark matter direct detection limits depend on spin-independent cross sections between dark matter and nucleons in the detector. These cross sections are mediated particularly by the Higgs boson, and the relevant coupling of dark matter to the Higgs boson is particularly sizeable in the present equal mass case with strong singlet-doublet mixing and a significant value of a_H. It does not depend on λ_L and λ_R, but via the rescaling according to relic density, the resulting direct detection limits do vary across the λ_L–λ_R plane. These limits are generally strong, because of the unsuppressed coupling to the Higgs boson. They become however significantly weaker for increasing masses because of the suppression of the cross sections, despite the slight increase of the relic density.

The combination of all these constraints means that for our baseline case, with equal masses, shown in the three panels of figure 9 it is impossible to explain Δa_μ^{2021} simultaneously with the dark matter relic density. For masses of 1 TeV, Δa_μ^{2021} could be explained simultaneously with the dark matter relic density, however direct detection constraints exclude a large part of the Δa_μ band and the entire region where the relic density is explained. For masses of 1.5 TeV, the direct detection limits constrain only a very little of the region which can explain Δa_μ^{2021}, however the direct detection constraints still rule out an explanation of the relic density. For masses of 2 TeV the full relic density can be explained, however not simultaneously with Δa_μ^{2021}. One may ask whether just changing the value of the trilinear coupling a_H between the Higgs boson and the two BSM scalar bosons could

[19] In the calculation we have correctly rescaled the direct detection spin-independent (SI) cross-sections according to the abundance of dark matter as

$$\sigma_{\text{SI,eff}} = \sigma_{\text{SI}} \times \frac{\Omega_{h^2}}{\Omega_{h^2,\text{Planck}}},$$

where $\Omega_{h^2,\text{Planck}} = 0.1200$ is the dark matter relic abundance as observed by the Planck experiment, see eq. (1.8), and Ω_{h^2} is the relic abundance produced by the dark matter candidate particle.

JHEP09(2021)080

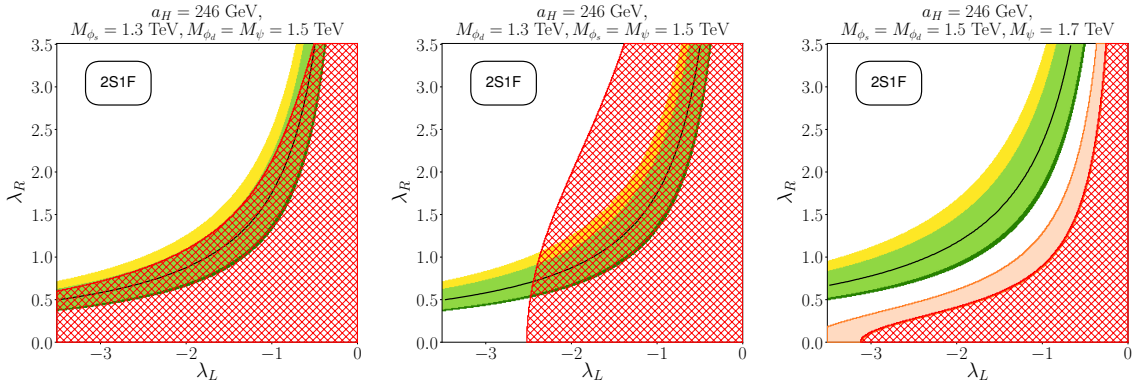

Figure 10. Results from Model 2S1F, scanning over the couplings of the new scalars and fermion to the left- and right-handed muon. The trilinear coupling which parametrises the mixing of the neutral BSM scalars is fixed to $a_H = 246\,\text{GeV}$. Colours are the same as in figure 9. In these scenarios the mass of either the scalar singlet ϕ_s, scalar doublet ϕ_d, or fermion ψ_s is displaced by 200 GeV from the other BSM masses at 1500 GeV.

allow the simultaneous explanation of large Δa_μ and dark matter. As eq. (5.8) shows, increasing the value of a_H increases the size of the BSM contributions to a_μ, while the dark matter relic density is essentially independent of a_H in these scenarios. Therefore the a_μ-bands in figure 9 would move down and to the right, to smaller couplings, while the red hatched regions would remain largely unchanged from adjusting a_H. However the direct detection constraints become stronger if a_H is increased, because it increases Higgs-nucleon interactions via the SM Higgs. As a result the strengthened direct detection limits would rule out points with the observed dark matter relic density. Decreasing a_H has the opposite effect: the band of parameter space where Δa_μ is explained moves up and to the left, further away from the observed relic density, and weakening the direct detection constraint will not help. So in summary it is not possible in these equal mass scenarios to explain both the measured value Δa_μ and the observed value of the relic density of dark matter at the same time, while avoiding constraints from direct detection. In the following we therefore consider further parameter slices to obtain additional insight into the phenomenology of the model.

The situation can be changed substantially if we split the masses of the new states. The relic density of each point will in general be larger, since mass splittings will suppress several relic density depletion mechanisms such as coannihilation channels. Figure 10 investigates this for three example cases. In each of the three panels the mass of the fermion singlet is 200 GeV away from the dark matter scalar, which in turn is either singlet- or doublet-dominated or a mixture. All panels of figure 10 can be compared to the middle panel of figure 9, where all masses were equal to 1500 GeV. The contribution to a_μ is similar in all cases, with slight changes of the required couplings depending on the increased/decreased masses.

The dark matter phenomenology changes more dramatically. Both the relic density and the direct detection constraints differ strongly between the panels of figure 10 and compared to the middle panel of figure 9. Specifically the direct detection constraint ruled

JHEP09(2021)080

out a full explanation of the relic density in the equal mass case of the middle panel of figure 9. The same still happens in the third panel of figure 10, where the scalar doublet and singlet masses are equal. The reason in all these cases is the doublet-singlet mixing and the unsuppressed coupling of dark matter to the Higgs boson via the doublet-singlet-Higgs coupling a_H. In contrast, as soon as the scalar doublet and singlet masses are different (left and middle panels of figure 10), the direct detection constraints are weakened, and as a result a full explanation of the observed relic density is viable.

In detail the left panel of figure 10 illustrates the case where the dark matter candidate is dominantly a scalar singlet with only about a 1% admixture of doublet. The singlet mass is set 200 GeV lighter than the scalar doublet and the fermion masses. The relic density is driven up compared to the middle panel of figure 9 since several dark matter depletion mechanisms are suppressed. Generally, the scalar singlet participates only in few interactions and mostly annihilates through t-channel exchange of the BSM fermion.[20] Although the singlet couples to BSM fermions only through λ_R, in the cross-section for t-channel exchange of the muon, contributions that depend only on λ_L (or only on λ_R) are suppressed by either m_μ^2/M_F^2 or by the relative velocity in comparison to the contribution proportional to $\lambda_L^2\lambda_R^2$. This leads to the shape of the red line that can be seen in the plot, where it follows a similar trajectory to the a_μ contours, which is approximately a hyperbola.

Strikingly in the left panel of figure 10 we find that the red curve, where the observed relic density can be explained, and the black curve, where Δa_μ^{2021} can be explained are very close to each other and follow the same trajectory. However while a 1σ explanation of $\Delta a_\mu^{\text{BNL}}$ could have been accommodated, the slightly higher couplings required to explain relic density measurements means that the over abundance of dark matter now rules out most of the parameter space where Δa_μ^{2021} (eq. (1.7)) can be explained, except for a small slice of parameter space with $\lambda_R > 2.5$. Nonetheless this could be changed with small adjustments to the mass splitting and in general it is possible to explain Δa_μ^{2021} and relic density at the same time. Explanations of Δa_μ^{2021} are possible for masses above 1 TeV, as long as the product $\lambda_L\lambda_R a_H$ is sufficient.

In the middle panel of figure 10 we instead focus on doublet-dominated dark matter, by setting the scalar doublet mass 200 GeV lighter than both the scalar singlet and fermion (and again compared to the middle panel of figure 9). The impact on Δa_μ is very similar to what happened in the left plot as expected from eq. (5.8). However, the change in the behaviour of dark matter is very different. Now the dark matter candidate has generally many more interaction channels via the $\text{SU}(2)_L$ gauge interactions of the doublet component. Hence the relative importance of the $\lambda_{L,R}$ parameters is reduced compared to the singlet-dominated case. Although not visible in the plot, the overall variation of the relic density is much reduced compared to the left panel or the middle panel of figure 9. The residual dependence on λ_L is still important to deplete the relic density sufficiently, but the residual dependence on λ_R via the singlet-admixture is of minor importance. In this case the constraints from the relic density and from Δa_μ are essentially orthogonal in the

[20] Other processes also play a significant role including e.g. t-channel exchanged of scalar, which occurs through the small doublet admixture.

JHEP09(2021)080

parameter space and thus complementary. Both constraints can be fulfilled, but agreement can only be achieved for very large values of $|\lambda_L|$ ($\approx$ between 2.4 and 2.5 when Δa_μ^{2021} is explained with 1σ).

In the right panel of figure 10 we raise the fermion mass by 200 GeV, compared to the middle panel of figure 9. Here we can see that this slightly increases the size of the couplings required to explain the measured Δa_μ values. As mentioned before, however, in this case with equal scalar singlet and doublet masses the relic density must be under abundant because of direct detection constraints. Raising the fermion mass suppresses the coannihilation mechanisms involving the fermion, which are strongly dependent on the couplings λ_L and λ_R, but t-channel fermion exchange can still be active as suggested by the fact that the relic density curve is again a hyperbola similar to the left panel. However since the singlet and doublet masses are equal in this case, the usual SU(2) scalar doublet (co)annihilations have greater impact, reducing the required size of $\lambda_L\lambda_R$. Due to the rescaling, the direct detection constraints reflect this behaviour. With the chosen value of $a_H = 246\,\text{GeV}$ Δa_μ^{2021} can be explained with an under abundant relic density.

Just as for figure 9, we can change a_H to see if we can simultaneously explain a_μ and dark matter. Currently in the middle panel of figure 10, as well as the left panel with very large λ_R, we can already explain a_μ^{2021} and dark matter simultaneously. As we saw previously increasing a_H increases the constraints from direct detection. For the left panel as nearly all of the parameter space that can explain Δa_μ^{2021} to within 1σ is ruled out by over abundant dark matter, we can decrease a_H to push the parameter space up into the under abundant regions. However, by increasing a_H for the middle panel, the observed dark matter relic density line would become more dependent on λ_R, as the two scalars mix more. For the right panel, again increasing a_H would cause the regions ruled out by direct detection to become more prevalent, while pulling the space which can explain Δa_μ^{2021} closer to it. However, while decreasing a_H would shrink the regions constrained by direct detection, the red line does not shift close enough to the band which can explain Δa_μ^{2021}, which itself would move away up and to the left as a_H is decreased. So in the scenario with M_ψ increased slightly from $M_{\phi_s} = M_{\phi_d} = 1.5\,\text{TeV}$, it is never possible to explain Δa_μ^{2021} and the dark matter relic density simultaneously, even if we adjust a_H.

In all the two-dimensional slices of parameter space we presented, explaining Δa_μ^{2021} and dark matter is only possible with sizable interactions between the BSM states and muons, λ_L and λ_R. Indeed the relic density is over abundant when both λ_L and λ_R, are small because both the t-channel exchange of the BSM fermion and coannihilations with the BSM fermion are driven by these λ_L and λ_R couplings. At lighter masses both these processes and (co)annihilation processes involving SU(2) interactions of the scalar doublet will become more efficient as the mass suppression is reduced, with the SU(2) interactions becoming more significant relative to λ_L and λ_R. These effects imply that at much lighter masses it should be possible to also deplete the relic density with much smaller λ_L and λ_R. At the same time, explaining $\Delta a_\mu^{\text{BNL}}$ or Δa_μ^{2021} with smaller couplings is also possible when all the masses are small. However because it is possible for the observed relic density to be obtained through SU(2) interactions of a 600 GeV scalar doublet, it is not clear that with small couplings large Δa_μ and dark matter can be explained simultaneously as the

JHEP09(2021)080

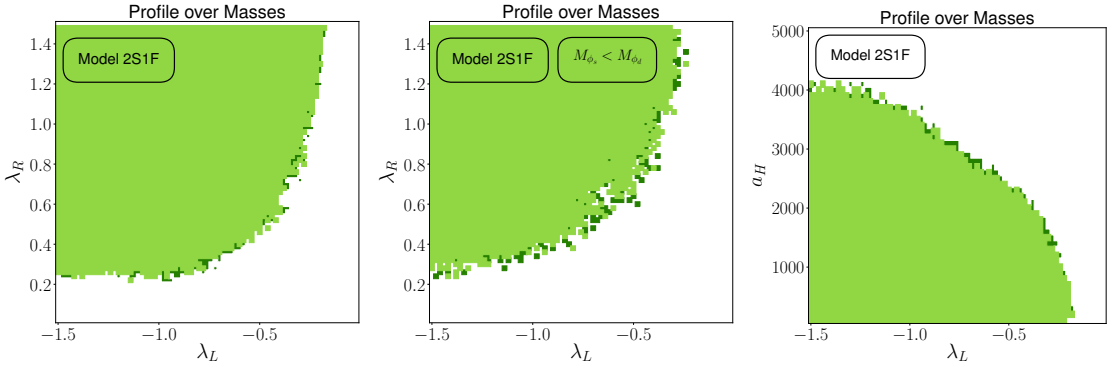

Figure 11. Profile over the $\lambda_L - \lambda_R$ plane or the $\lambda_L - a_H$ plane for Model 2S1F, scanning over the masses of the new scalars and fermion between 0 and 5000 GeV, as well as the mixing $a_H \leq 5000\,\text{GeV}$ and coupling $\lambda_R \in [0, 1.5]$. Colours are the same as in figure 9. The scan targeted the observed value of the dark matter relic density 0.1200, eq. (1.8), the value of Δa_μ in eq. (1.6), and the direct detection log likelihood provided by `DDCalc` [508, 509], where points which are excluded by direct detection or are more than 3σ away from the Planck observation are thrown away.

a_μ explanation may then require larger values of λ_L and λ_R (or smaller masses) than what is required for fitting the relic density. Whether dark matter and the a_μ anomalies can be simultaneously explained for all λ_L, λ_R or if there is a lower bound on these couplings just from these requirements remains an open question.

Therefore we now turn to a complete exploration of the parameter space of this model, varying M_{ϕ_s}, M_{ϕ_d}, M_ψ, a_H, λ_L, and λ_R to see the impact of the new Δa_μ^{2021} measurements and address the question posed above. We vary $M_i \in [0, 5000]$, $a_H \in [0, 5000]$, $\lambda_{L,R} \in [0, 1.5]$ in a number of `MultiNest` [495–498] scans with a likelihood constructed to target $\Omega_{h^2} = 0.1200$, different possible[21] values of a_μ and solutions which evade direct detection limits. In total we collected about 15 million samples targeting several different values in the range $\Delta a_\mu \lesssim [0, 42 \times 10^{-10}]$.

In the left panel of figure 11 we present results in the λ_L–λ_R plane. This shows that it is only possible to explain the a_μ^{BNL} measurement and dark matter simultaneously when $|\lambda_L \lambda_R| \geq 0.22$. With the new a_μ^{FNAL} measurement this limit update changes very little. Couplings smaller than this cannot simultaneously explain a_μ^{2021} and dark matter. For the case of scalar doublet dominated dark matter the SU(2) interactions will deplete the relic density to below the observed value whenever $m_{\phi_d} \lesssim 600\,\text{GeV}$ and this limit on the lightest mass makes explaining large Δa_μ impossible for such small couplings. For pure scalar singlet dark matter, note that if the scalar doublet is so heavy it completely decouples, then the model effectively reduces to that of Model R from the two field section. There we already found that a simultaneous explanation of dark matter and the a_μ measurements is only possible for very large λ_R (higher than the values shown in figure 11) and not possible at all when collider limits are also taken into account.

[21] Due to the time required for such large dimensional scans, these were performed before the release of the FNAL Muon g-2 results [2] and without knowledge of the result. Therefore for we performed scans for a range of results that we considered plausible given the previous a_μ^{BNL} measurement.

JHEP09(2021)080

If instead the dark matter has a significant admixture of both the scalar singlet and the scalar doublet, then the situation is a bit more complicated. With both singlet and doublet mixing, the relic density can deplete through processes involving both λ_L and λ_R couplings and a_H in addition to the SU(2) interactions of the doublet component. One can compensate increased splitting in the masses by raising a_H to keep Δa_μ fixed to the measured value, or similarly one can reduce the mass splitting to compensate for reducing a_H but in either case the relic density is still depleted too efficiently since both raising a_H and reducing the mass splitting can enhance annihilation cross-sections. Increasing a_H and reducing the mass splitting also increases direct detection cross-sections, increasing the tension with large Δa_μ further. Therefore when there is significant mixing between the scalar singlet and doublet, requiring that the measured relic density is obtained implies masses that are too large (for any given a_H value) for large Δa_μ to be explained with small couplings. We also looked at scenarios where the dark matter is more singlet or more doublet in nature separately. We found quite similar limits on $\lambda_L \lambda_R$ emerge in both cases, though the more singlet DM case had a marginally higher limit, as can be seen in the middle panel of figure 11.

The tension with a_H is also shown in the plot on the right panel of figure 11. There one can see that there is an upper limit on a_H, coming from the dark matter constraints discussed above. The value of a_H can also be restricted by the need to avoid tachyonic scalars that would appear when $a_H v < M_{\phi_s} M_{\phi_d}$. However we find it is the limits from dark matter that leads to the constraint shown in the right panel of figure 11.

As a result we find a lower limit on $|\lambda_L \lambda_R|$ that increases with the value for Δa_μ used as a constraint. In this way we directly see the impact of the new Δa_μ^{2021} result on this model. We do not expect collider limits to affect our results here, since we do not find any solutions explaining both dark matter and $\Delta a_\mu^{\rm BNL}$ or Δa_μ^{2021} where the lightest of the two scalar masses $M_{\phi_1^0}$ is below around 500 GeV for our choice of coupling range ($\lambda_{L,R} \leq 1.5$). Our scan results also indicate interesting structure in the mass planes. We reserve the detailed discussion and presentation of such mass plane results for a future dedicated global fit of the model. Nonetheless it is clear from our results that the combination of parameters and masses that are allowed are significantly impacted by the interplay between dark matter and a_μ constraints. The $a_\mu^{\rm BNL}$ and $a_\mu^{\rm FNAL}$ measurements are therefore very important for the phenomenology of models like this and should be included in all such studies, and in any future global fits of any models like this.

5.2 Three-field model with two fermions, one charged scalar and fermionic dark matter

Having looked at scalar dark matter in the previous section we now consider a model with a fermionic dark matter candidate. For this we choose a minimal three-field model with two new fermions and one new scalar field, which we call Model 2F1S. Specifically this model extends the SM by adding three $\mathbb{Z}_2$-odd fields

$$\phi_d = \begin{pmatrix} \phi_d^+ \\ \phi_d^0 \end{pmatrix}, \ \psi_d = \begin{pmatrix} \psi_d^0 \\ \psi_d^- \end{pmatrix}, \ \psi_s^0 \,, \tag{5.9}$$

JHEP09(2021)080

where ϕ_d is a scalar doublet with representation $(\mathbf{1},\mathbf{2},\frac{1}{2})_0$, ψ_d a Dirac fermion doublet with representation $(\mathbf{1},\mathbf{2},-\frac{1}{2})_{1/2}$ expressed in Weyl spinors ψ_d and its Dirac partner $\psi_d^c = (\psi_d^{0c\dagger}, \psi_d^{-c\dagger})$, and ψ_s^0 a neutral singlet Weyl fermion with representation $(\mathbf{1},\mathbf{1},0)_{1/2}$.

In principle the model allows scenarios with scalar dark matter, however we do not consider such scenarios here. We use the model as an illustration of fermionic dark matter, in which case the dark matter candidate is predicted to be a mixture of the fermion singlet and the neutral doublet component. Ref. [376] also studied the model in certain parameter slices. Here we intend to determine the full status of the model, studying the detailed parameter dependence and performing general scans of the parameter space.

The relevant interactions are:

$$\mathcal{L}_{\text{2F1S}} = \Big(\lambda_1 H\cdot\psi_d\psi_s^0 - \lambda_2\psi_d^c\psi_s^0 H + \lambda_L L_2\cdot\phi_d\psi_s^0 + \lambda_R\psi_d\mu\phi_d^\dagger - M_{\psi_d}\psi_d^c\psi_d - \frac{M_{\psi_s}}{2}\psi_s^0\psi_s^0 + \text{h.c.}\Big) - M_\phi^2|\phi_d|^2, \tag{5.10}$$

where the sign in front of the λ_2 term reflects our definition of ψ_d^c as an SU(2) anti-doublet.

The model has four new coupling parameters. $\lambda_{L,R}$ are the couplings to the left- and right-handed muon, similarly to the case of the previous Model 2S1F. The couplings $\lambda_{1,2}$ govern the mixing of the BSM fermions via the Higgs VEV, similarly to the a_H parameter in the previous case. The products $\lambda_i\lambda_L\lambda_R$ are responsible for the new source of muon chirality flips (for $i = 1, 2$). To reiterate, this model can also be compared to the Bino-Higgsino-left smuon (BHL) system for the MSSM, see eq. (6.6) below. There ψ_d corresponds to the Higgsino, ψ_s to the Bino, and ϕ_d to the left smuon doublet, and the couplings λ_1, λ_2 and λ_L would all correspond to the Bino coupling g_1, while λ_R would correspond to the muon yukawa coupling. A difference is that the MSSM counterparts of the couplings $\lambda_{1,2}$ would couple the Higgsinos to the up-type and down-type Higgs doublets, and the resulting contributions to the mass mixings would involve the $\tan\beta$ parameter, while here there is just one single Higgs doublet and the mass mixing is simpler.

The mixing of the BSM fermions affects the singlet ψ_s^0 and the neutral components of the fermion doublet ψ_d^0 and its Dirac partner $\psi_d^{0c\dagger}$. They mix into three different flavours of neutral fermions ψ_i^0 with Majorana mass terms via the mixing matrix V_F:

$$\mathcal{L}_{\text{2F1S}} \ni -\frac{1}{2}\begin{pmatrix}\psi_s^0 & \psi_d^0 & \psi_d^{0c\dagger}\end{pmatrix}\begin{pmatrix} M_{\psi_s} & \frac{\lambda_1 v}{\sqrt{2}} & \frac{\lambda_2 v}{\sqrt{2}} \\ \frac{\lambda_1 v}{\sqrt{2}} & 0 & M_{\psi_d} \\ \frac{\lambda_2 v}{\sqrt{2}} & M_{\psi_d} & 0\end{pmatrix}\begin{pmatrix}\psi_s^0 \\ \psi_d^0 \\ \psi_d^{0c\dagger}\end{pmatrix} = -\frac{1}{2}\sum_{i=1,2,3} M_{\psi_i^0}\psi_i^0\psi_i^0\,, \tag{5.11}$$

where

$$\begin{pmatrix}\psi_1^0 \\ \psi_2^0 \\ \psi_3^0\end{pmatrix} = V_F^T\begin{pmatrix}\psi_s^0 \\ \psi_d^0 \\ \psi_d^{0c\dagger}\end{pmatrix}. \tag{5.12}$$

The contribution to a_μ from this model comes from two diagrams, the FFS diagram of figure 19(a) and the SSF diagram of figure 19(b), with the generic F fermion lines replaced

JHEP09(2021)080

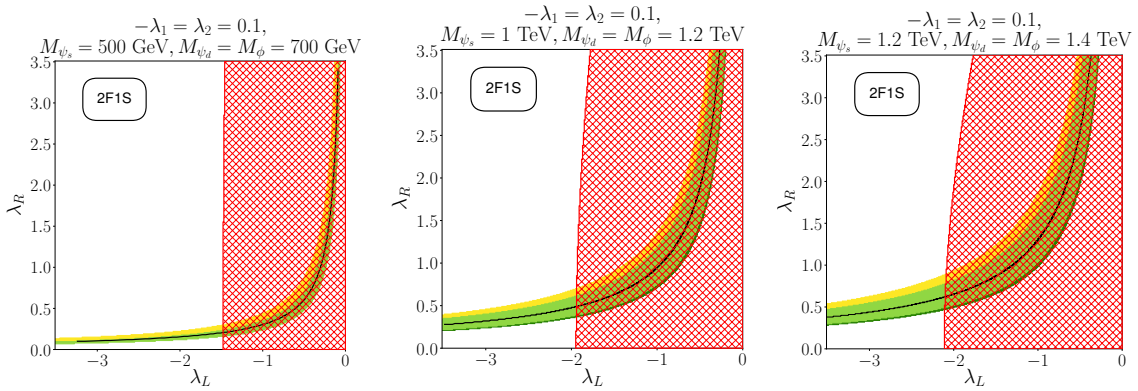

Figure 12. Results from Model 2F1S, scanning over the couplings of the new fermions and scalar to the left- and right-handed muon. Colours are the same as in figure 9. The mixing couplings are fixed to $-\lambda_1 = \lambda_2 = 0.1$. In this scenario the masses of the scalar doublet ϕ_d and fermion doublet ψ_d are raised by 200 GeV above the mass of the fermion singlet ψ_S. Points to the right of the red line produce an over abundance of dark matter and are strongly excluded.

by ψ^- and ψ_i^0 and the scalar S ones by ϕ_d^0 and ϕ_d^{+*}, respectively. Among these diagrams, only the SSF diagram with neutral fermion exchange can lead to an enhanced chirality flip. The full contributions are given by:

$$\Delta a_\mu^{\text{2F1S}} = \frac{m_\mu^2}{32\pi^2 M_\phi^2}\left(\frac{\lambda_R^2}{6}E\left(\frac{M_{\psi_d}^2}{M_\phi^2}\right) - \sum_{i=1}^{3}\frac{\lambda_R^2|V_{F\,2i}|^2 + \lambda_L^2|V_{F\,1i}|^2}{6}B\left(\frac{M_{\psi_i^0}^2}{M_\phi^2}\right) + \sum_{i=1}^{3}\frac{M_{\psi_i^0}}{m_\mu}\frac{2\lambda_L\lambda_R V_{F\,1i}V_{F\,2i}}{3}C\left(\frac{M_{\psi_i^0}^2}{M_\phi^2}\right)\right). \tag{5.13}$$

The term in the second line corresponds to the additional source of chirality flip in the model. It can be analyzed similarly to the term in eq. (5.8). The actual enhancement factor, beyond the loop and mass suppression factor, is given by the coupling combination $\lambda_{1,2}\lambda_L\lambda_R/y_\mu$ where the $\lambda_{1,2}$ are contained in the product of the mixing matrix elements $V_{F\,1j}V_{F\,2j}$ of the neutral fermions. If this coupling combination vanishes, the new chirality flip contribution and the third term disappear, and we end up with the contribution of Model L from section 4, eq. (4.6).

The case of a pure fermion SU(2) doublet dark matter candidate is very well known as this corresponds to Higgsino dark matter in the MSSM, or the lowest representation of minimal dark matter [510]. In that case it is possible to deplete the relic density to the measured value, using only SU(2) gauge interactions, when the fermion doublet has a mass of 1 TeV [483] while above (below) it will be over (under) abundant. This can be adjusted by mixing with singlet, to obtain well-tempered dark matter [483] where the rapid depletion of dark matter from SU(2) interactions are diluted through mixing with the singlet, though well-tempered dark matter is heavily constrained by direct detection (see e.g. figure 8 of ref. [511]). As in the previous example explaining $\Delta a_\mu^{\text{BNL}}$ and Δa_μ^{2021} after including the FNAL result will require significant values of the λ_L, λ_R and λ_i couplings, leading to additional depletion mechanisms. Therefore scenarios where all the input masses are set to be equal will only explain dark matter at very heavy masses.

JHEP09(2021)080

Instead we first focus on scenarios where the dark matter is dominantly singlet in nature in figure 12, showing two dimensional parameter slices in the λ_L–λ_R plane, with the overall mass scale increasing between the panels from left to right. Specifically each of the three panels shows scenarios where the fermion doublet ψ_d and scalar doublet ϕ_d are always 200 GeV higher than the mass of the fermion singlet ψ_s^0. To simplify things further, we choose fairly small values for the mixing parameters $-\lambda_1 = \lambda_2 = 0.1$, since large singlet-doublet mixing increases dark matter direct detection constraints and depletes the relic density. The other couplings are varied in the range $-\lambda_L, \lambda_R \in [0, 3.5]$.

As a function of λ_L, λ_R, we get a similar curve for a_μ^{2021} to the ones shown in figures 9, 10, due to the dominant chirality flip contribution of eq. (5.13) having the same dependence on $\lambda_L\lambda_R$ as eq. (5.8). The nearly vertical red lines indicate points in agreement with the Planck observed [416] dark matter relic abundance; points to the right are over abundant and excluded. As can be seen in all panels of figure 12, all points allowed by the dark matter relic density are also in agreement with direct detection constraints due to the small values of the λ_i coupling.[22]

Going from left to right in the three panels of figure 12, the singlet mass is increased from 500 GeV to 1000 GeV and 1200 GeV, while the mass splitting remains 200 GeV. In the left panel the dark matter relic abundance depends only on λ_L, the coupling of the singlet to the muon and the BSM scalar, due to the large mixing suppression of any λ_R contribution through the fermion doublet component of the dark matter.[23] In the middle and right panels the relative doublet content of the dark matter candidate rises, opening up additional annihilation mechanisms through the SU(2) interactions and the λ_R coupling. Thus when λ_R is large t-channel exchange of the BSM scalars may play a role through λ_R, leading to the curvature of the red line, which is most pronounced in the right panel. Therefore, while in the left panel avoiding an over abundance of dark matter gives a simple bound of $\lambda_L < -1.5$, in the middle and right panel larger values of $|\lambda_L|$ are required to deplete the relic density to the observed value or below, and the precise limit also depends on λ_R. In all panels Δa_μ^{2021} can be explained simultaneously with the relic density if λ_R has the rather small values $\lambda_R \in [0.1, 0.7]$.

The mass splitting between the singlet fermion ψ_s and the scalar doublet ϕ has a large impact on the relic density. In figure 13 we show this impact by varying this mass splitting over three λ_L–λ_R planes, specifically we fix $M_{\psi_s} = 500$ GeV and set $M_\phi = 500$ GeV, 550 GeV and 600 GeV in the left, middle and right panels respectively. At the same time we keep the fermion doublet mass fixed at a heavy scale $M_{\psi_d} = 3000$ GeV, well above that of the dark matter candidate, so that in this case it will not play any role in the depletion of dark matter relic density.[24] This choice also suppresses the Δa_μ prediction and means that very

[22] This can be compared to MSSM scenarios where such a small mass splitting between the Bino and Higgsino would face more severe constraints from direct detection since the gauge interactions that control the Bino-Higgsino-Higgs vertices are larger than λ_i couplings chosen for this example.

[23] Note that in contrast to the scalar dark matter case discussed in the previous section, in the annihilation cross-section for the t-channel of the BSM scalar, terms that depend only on λ_L are not suppressed compared to terms that depend on both λ_L and λ_R.

[24] The exact choice for the mass is not important and, for this reason, the plots of figure 13 actually allow understanding of the behaviour of the model in a wider range of doublet masses.

JHEP09(2021)080

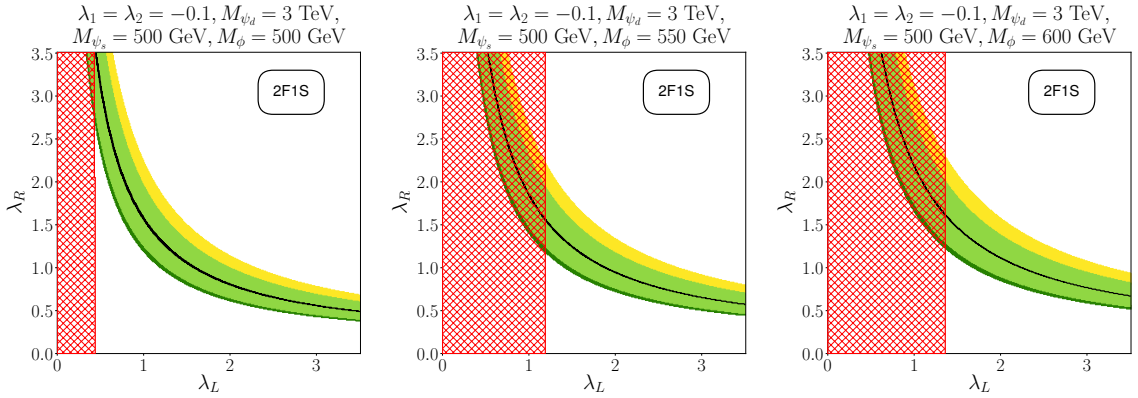

Figure 13. Results from Model 2F1S, scanning over the couplings of the new scalars and fermion to the left- and right-handed muon. Colours are the same as in figure 9. The mixing couplings are fixed to $\lambda_1 = \lambda_2 = -0.1$. In this scenario the fermion doublet has its mass fixed at $M_{\psi_d} = 3000$ GeV, the fermion singlet is fixed at $M_{\psi_s} = 500\,\text{GeV}$, and the scalar doublet has its mass slowly increased from M_{ψ_s}. Points below or to the left of the red line produce an over abundance of dark matter and are strongly excluded.

large couplings are required to explain $\Delta a_\mu^{\text{BNL}}$ and Δa_μ^{2021}. We also choose $\lambda_{1,2} = -0.1$ and $\lambda_L > 0$. The relative sign change between λ_1 and λ_2 leads to destructive interference between different terms and thus a further slight suppression of the overall contributions to Δa_μ.

In all three panels of figure 13 the relic density depends only on λ_L due to the decoupling of the doublet state, while Δa_μ depends on both λ_L and λ_R since the chirality flip enhancement is proportional to $\lambda_L \lambda_R$. Just as before, in all cases we can explain the discrepancy in a_μ and provide a dark matter candidate particle simultaneously. Between the three panels the Δa_μ result only changes a little, as expected due to the small mass increases. However the dark matter relic density depends strongly on the value of the mass splitting. In the left panel where $M_\phi = M_{\psi_s}$, most of the parameter space has an under abundance of dark matter. The very small mass splitting between the dark matter fermion ψ_1^0 and the BSM scalar opens up coannihilation channels which were suppressed in figure 12. Due to these highly efficient coannihilations the relic density is depleted for much smaller values of λ_L than in the previous figures. When M_ϕ is increased to 550 GeV in the middle panel, the (co)annihilations through λ_L become less efficient. As a result a much larger $\lambda_L \approx 1.1$ is required to deplete the relic density to the observed value via t-channel processes as in the case of figure 12. Increasing the scalar mass further to 600 GeV (right panel) an even larger $\lambda_L \approx 1.4$ is required to produce a relic abundance that matches the Planck observation. However while the bound from an over abundant relic density changed a lot between 500 GeV and 550 GeV, as we move away from the optimal window for coannihilations, subsequently increasing M_ϕ above 600 GeV has a much weaker impact. If we increase the scalar mass further the relic density limit gradually increases until somewhere between 2.3–2.4 TeV it is no longer possible to deplete the relic density to the observed value or below with perturbative couplings.

JHEP09(2021)080

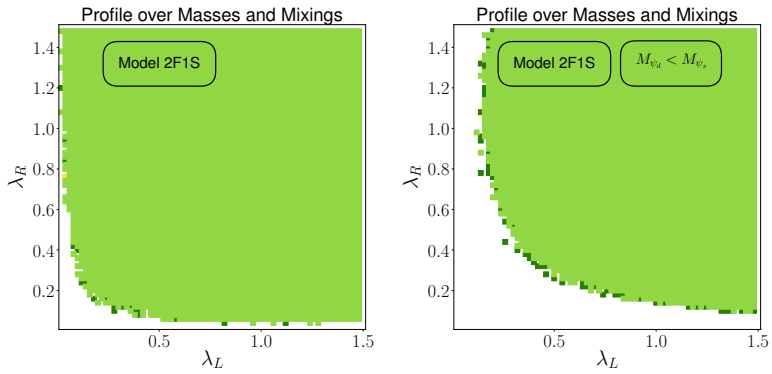

Figure 14. Viable points in the $\lambda_L - \lambda_R$ plane obtained from scanning over the masses of the new scalar and fermions between 0 and 5000 GeV, as well as the Yukawa couplings $\lambda_{L,R} \in [0, 1.5]$ and $\lambda_{1,2} \in [0, 3.5]$ for Model 2F1S. Colours are the same as in figure 9. Scan targeted the observed value of the dark matter relic density 0.1200, eq. (1.8), the a_μ value in eq. (1.6), and the direct detection log likelihood provided by DDCalc [508], where points which are excluded by direct detection limits or are more than 3σ away from the Planck observation are thrown away.

In section 5.1 the fact that a 600 GeV scalar dark matter candidate naturally depletes the relic density to the observed value played a critical role in leading to a lower bound on $|\lambda_L \lambda_R|$ from the combination of Δa_μ and dark matter constraints. Since a pure fermion doublet naturally depletes the relic density to the observed value when it has a mass of about 1.1 TeV, we may anticipate a similar result in this model. In addition we have also seen that when the doublet fermion is very heavy, large couplings are required, while mixed singlet-doublet fermion dark matter scenarios should be strongly constrained by direct detection. Therefore we now perform a scan over the full parameter space of the Model 2F1S to see if this also leads to a lower bound on $|\lambda_L \lambda_R|$.

We sample all free parameters in this model ($\lambda_1, \lambda_2, \lambda_L$, λ_R, M_ϕ, M_{ψ_d}, and M_{ψ_s}) using `MultiNest` [495–498], with mass range $M_i \in [0, 5000]$ GeV, and the BSM Yukawa couplings having the values $\lambda_{L,R} \in [0, 1.5]$ and $\lambda_{1,2} \in [0, 3.5]$, with the results shown in figure 14. Again, several values of Δa_μ where targeted in the range $[0, 42] \times 10^{-10}$, with a total of 62 million points scanned. In the left panel of the figure, we can see that there is a lower bound on the couplings $|\lambda_L \lambda_R| \gtrsim 0.036$ below which we cannot simultaneously explain the measured value of a_μ whilst producing a dark matter candidate particle with the observed relic density that escapes direct detection limits. As we anticipated in the discussion above, pure singlet fermion dark matter requires larger couplings to explain large Δa_μ, while fermion doublet dark matter annihilates too effectively for light masses.

Significant singlet-doublet fermion mixing can dilute the SU(2) gauge interactions of the doublet, but does not avoid this problem as it means that t-channel exchange of the BSM scalars will be active through both λ_L and λ_R, and increasing the mixing also increases direct detection. Reducing $\lambda_L \lambda_R$ while increasing λ_i to keep the Δa_μ prediction fixed makes direct detection limits more relevant. As a result the combination of these constraints leads to the lower limit $|\lambda_L \lambda_R|$ shown in the plot. Interestingly we also find a more severe limit on $|\lambda_L \lambda_R| \approx 0.14$ for dark matter that is mostly doublet in nature, as shown in the right panel of figure 14.

JHEP09(2021)080

As in the previous case this shows how the a_μ measurements have a significant impact on the model, implying a siginifcant constraint on the couplings. However since the new world average is quite close to the BNL value there is little difference between the limits implied by the $\Delta a_\mu^{\text{BNL}}$ and Δa_μ^{2021} results. The masses in our samples are mostly heavy enough to easily evade collider limits.[25] However collider limits should be included in a full global fit of the model, but we leave that and a presentation of the full impact of all constraints on all parameters and masses to future work. Again we stress that our results demonstrate that the FNAL measurement plays a critical role in the phenomenology of these models and should be included in all phenomenological studies of models of this type and future global fits.

As discussed earlier this model can be compared to the BHL scenario of the MSSM. There since $\lambda_L \lambda_R \lambda_i$ corresponds to $g_1^2 y_\mu$, a_μ can only be explained with masses less than 200 GeV, due to the weaker enhancement [217]. Similarly the $|\lambda_L \lambda_R|$ bound corresponds to $g_1 y_\mu$, which should be well below the bound for this model and would suggest that the BHL scenario alone cannot explain both the measured a_μ and dark matter. However it is important to note that the comparison is not perfect due to the fact that the MSSM contains two Higgs doublets, which gives an additional enhancement from the ratio of the two Higgs VEVs, $\tan\beta$. As a result in the BHL scenario, a dominantly bino dark matter candidate can simultaneously explain dark matter and account for $\Delta a_\mu^{\text{BNL}}$ and Δa_μ^{2021} despite having couplings below the lower bound for this in the Model 2F1S. On the other hand, the Model 2F1S has much greater freedom to explain dark matter and large Δa_μ at much higher masses than is possible in the BHL scenario. The fact that the $\lambda_R \neq y_\mu$ in this model is of great significance, but on top of that the freedom to push all couplings up to values much larger than that of g_1 and to vary the interactions independently, gives rise to a rich and distinct phenomenology.

Therefore our results show that this class of simple models provide an interesting way to explain both dark matter and large Δa_μ. They are complementary to the explanations that come from the MSSM and appear to be significantly less constrained. However these models have not been constructed from any principle other than to explain the phenomenology, and as a result the deeper motivation is unclear. It would be very interesting to consider whether models that are motivated from more fundamental principles can have such scenarios as a low energy effective field theory.

6 Supersymmetry and the Minimal Supersymmetric Standard Model

In the present section we consider the Minimal Supersymmetric Standard Model (MSSM). It is one of the most promising extensions of the SM and offers potential explanations of EW naturalness and of dark matter as the lightest supersymmetric particle (LSP), it is

[25] The lightest mass scenarios in our samples *are* relevant for the lower bound on the couplings we obtained and our samples include some points where the lightest BSM fermion is between 300–500 GeV. In principle therefore LHC data could imply further constraints on our surviving samples. However we tested all such points from the scan targetting the a_μ^{BNL} with `SModelS` 1.2.3 and did not find any further exclusion. Therefore we expect our limit from just dark matter and Muon g-2 to be robust.

JHEP09(2021)080

compatible with unification of gauge couplings — and it could easily explain the deviation Δa_μ based on the initial BNL measurement. However a tension has developed because of LHC and dark matter searches, which severely constrain the MSSM parameter space. The tension remains in place in view of the new FNAL result (1.1) if the MSSM is required to accommodate the deviation Δa_μ^{2021}.

Here we present an update and investigate the parameter space of the MSSM which can accommodate this deviation, given the new FNAL measurement eq. (1.1) and the SM theory update (1.4). We focus particularly on the combined constraints from LHC and dark matter direct detection (DMDD) searches.

The MSSM contributions have been extensively studied in the past. For analyses and reviews of the basic behaviour we refer to refs. [49, 74, 166, 512]; higher-precision calculations were done in refs. [86, 87, 159–165]. For recent studies in the light of LHC run-II data we refer to refs. [200–204] (which involve a detailed recasting of LHC data) and [205–236] (which involve model building, the construction of specific scenarios and/or constraints from dark matter or electroweak precision observables). Earlier studies of the SUSY phenomenology of a_μ of the LHC run 1 era can be found in refs. [166–199]. Refs. [334, 336] study simultaneous SUSY explanations of $(g-2)$ of both the muon and the electron.[26] We will provide more detailed comparisons to the literature in the following subsections.

The MSSM contributions to a_μ are mainly generated by left- and right-handed smuons $\tilde{\mu}_{\mathrm{L,R}}$, sneutrino $\tilde{\nu}_{\mu\mathrm{L}}$, Bino $\tilde{B}$, Winos $\tilde{W}_{1,2,3}$, and Higgsinos $\tilde{H}_{u,d}$ which are the SUSY partners of the muon, muon-neutrino, and the electroweak SM gauge and Higgs bosons. $\tilde{B}$, $\tilde{W}_{1,2,3}$ and $\tilde{H}_{u,d}$ form neutralinos $\chi^0_{1,2,3,4}$ and charginos $\chi^\pm_{1,2}$ mass eigenstates. They appear in the one-loop diagrams of figure 19(a) (with charginos and sneutrinos) and of figure 19(b) (with neutralinos and smuons).

To provide a brief overview and set the stage for the following discussion we present figure 15 and the following approximation of the leading MSSM contributions to a_μ,

$$\Delta a_\mu^{\mathrm{1L}}(\mathrm{WHL}) \approx 21\times 10^{-10}\mathrm{sign}(\mu M_2)\left(\frac{500\ \mathrm{GeV}}{M_{\mathrm{SUSY}}}\right)^2\frac{\tan\beta}{40}, \tag{6.1a}$$

$$\Delta a_\mu^{\mathrm{1L}}(\mathrm{BHL}) \approx 1.2\times 10^{-10}\mathrm{sign}(\mu M_1)\left(\frac{500\ \mathrm{GeV}}{M_{\mathrm{SUSY}}}\right)^2\frac{\tan\beta}{40}, \tag{6.1b}$$

$$\Delta a_\mu^{\mathrm{1L}}(\mathrm{BHR}) \approx -2.4\times 10^{-10}\mathrm{sign}(\mu M_1)\left(\frac{500\ \mathrm{GeV}}{M_{\mathrm{SUSY}}}\right)^2\frac{\tan\beta}{40}, \tag{6.1c}$$

$$\Delta a_\mu^{\mathrm{1L}}(\mathrm{BLR}) \approx 2.4\times 10^{-10}\mathrm{sign}(\mu M_1)\left(\frac{500\ \mathrm{GeV}}{M_{\mathrm{SUSY}}}\right)^2\frac{\tan\beta}{40}\frac{\mu}{500\ \mathrm{GeV}}. \tag{6.1d}$$

The letters B,W,H,L, and R are the abbreviations for Bino, Winos, Higgsinos, and Left-and Right-handed smuons respectively. As indicated by the letters in brackets, each contribution depends on three of these states and their respective masses. In each formula the

[26] There used to be a slight disagreement between the experimental number for the electron $g-2$ [425] and the SM theory evaluation [513, 514] based on the measurement of the fine-structure constant of ref. [515]. However, a more recent measurement of the fine-structure constant of ref. [516] leads to good agreement between theory and experiment for the electron $g-2$. Here we do not consider the electron $g-2$ further.

JHEP09(2021)080

three appropriate masses have been set to a common scale $M_{\rm SUSY}$ and $M_{\rm SUSY} \gg M_Z$ is assumed. The approximations highlight the linearity in $\tan\beta = v_u/v_d$, the ratio of the two MSSM Higgs VEVs.

The physics of the individual contributions is as follows. In the first three lines the muon chirality is flipped at the Yukawa coupling to a Higgsino; the Higgsino is then converted to a gaugino via a Higgs vacuum expectation value. The appearance of the enhanced VEV is always accompanied by a factor of the Higgsino mass μ. This explains the appearance of one Higgsino, one gaugino (Bino or Wino) and of the factors $\tan\beta$ and μ in the numerators.

The BLR contribution in the fourth line is special. Here the muon chirality is flipped at the smuon line via the insertion of a smuon-left-right flip, which is governed by a product of the Higgsino mass μ and the enhanced VEV in the smuon mixing matrix. This explains the appearance of left- and right-handed smuons and of the factors $\tan\beta$ and μ in the numerator. In contrast to the other contributions, the BLR contribution is approximately linearly enhanced by the Higgsino mass μ since this parameter does not appear as the mass of a virtual Higgsino. The signs of all contributions are determined by the signs of μ and the gaugino masses $M_{1,2}$. In the following we will only consider positive signs of all these parameters, leading to positive MSSM contributions to a_μ.

Figure 15 shows the theoretical maximum of the SUSY contributions (i.e. MSSM minus SM contributions) $a_\mu^{\rm SUSY,Max}$ in the plane of $m_{\chi_2^\pm}$ and $m_{\tilde\mu_1}$, where $\chi_2^\pm$ is the heavier chargino and $\tilde\mu_1$ the lighter smuon (for similar plots in different planes see refs. [49, 139, 182]). It fixes $\tan\beta = 40$ and allows all SUSY masses to vary independently between 100 GeV and 4 TeV, for further details see the caption.[27] The red dashed lines and the yellow/green coloured regions correspond to the indicated values of $a_\mu^{\rm SUSY,Max}$; specifically the yellow and green colours correspond to the 1σ regions for the BNL deviation and the new deviation including FNAL in eqs. (1.6), (1.7), respectively; the bright green colour corresponds to the overlap region. As indicated on the right of the legend plot, an alternative interpretation of the contour lines and regions is possible. Thanks to the approximate linearity in $\tan\beta$, each value for $a_\mu^{\rm SUSY}$ with $\tan\beta = 40$ can be translated into approximate $\tan\beta$-values for which the other values of $a_\mu^{\rm SUSY}$ can be obtained. In the legend plot this translation is done for $\Delta a_\mu^{2021} = 25.1 \times 10^{-10}$, the new experimental average deviation from the SM. E.g. on the contour labeled "20" we have $a_\mu^{\rm SUSY,Max} = 20 \times 10^{-10}$ for $\tan\beta = 40$, and equivalently we would get $a_\mu^{\rm SUSY,Max} = \Delta a_\mu^{2021}$ for $\tan\beta \approx 50$. On the contour labeled "50", we have $a_\mu^{\rm SUSY,Max} = 50 \times 10^{-10}$ for $\tan\beta = 40$, and the world average deviation can be explained for $\tan\beta \approx 20$.

The figure and the formulas show that large contributions in the ballpark of the BNL deviation are of course possible but require upper limits on the SUSY masses. E.g. $a_\mu^{\rm SUSY} > 20 \times 10^{-10}$ (which is just at the lower 1σ level of the deviation) can only be explained (for $\tan\beta = 40$ and $\mu \leq 4$ TeV) if:

[27] Widening the range of masses would not change the plot since the maximum $a_\mu^{\rm SUSY}$ is obtained in the bulk of the mass range, not at its boundary. This is a reflection of the fact that the leading contributions approximated in eq. (6.1) are suppressed if Bino, Wino or Higgsino masses are too small.

JHEP09(2021)080

- either both chargino masses are lighter than around 1.1 TeV (vertical black line in figure 15),
- or one smuon is lighter than around 700 GeV (horizontal black line in figure 15).

This already illustrates the potential tension between a_μ and LHC data since the LHC-searches are sensitive to chargino and smuon masses above these values. In addition to LHC, constraints from dark matter searches enforce lower limits on combinations of the chargino and neutralino masses. In more detail, the WHL contributions (6.1a) are by far most important in the largest part of parameter space. However for large μ, the BLR contribution can become sizable as well. In figure 15 the slight rise of $a_\mu^{\text{SUSY,Max}}$ with increasing $m_{\chi_2^\pm}$ is due to the BLR contribution. In contrast, the BHR and particularly the BHL contributions are not important for the maximum value $a_\mu^{\text{SUSY,Max}}$, and in general they are practically always strongly suppressed, unless there are extremely large mass splittings between left- and right-handed smuons. We do not consider such cases in the present paper; hence in the following only the WHL and BLR contributions are important.[28]

In the following subsections we will first introduce the SUSY contributions to a_μ in more detail (section 6.1), survey relevant LHC and dark matter constraints (section 6.2) and present a detailed phenomenological analysis and brief summary (sections 6.3, 6.4 and section 6.5).

6.1 SUSY parameters and contributions to a_μ

In the following we define our notation and provide details on the MSSM contributions to a_μ. Our notation is essentially the same as e.g. in refs. [49, 74, 166]. To fix it we provide the mass matrices of the charginos and neutralinos and the smuons:

$$X = \begin{pmatrix} M_2 & M_W\sqrt{2}\sin\beta \\ M_W\sqrt{2}\cos\beta & \mu \end{pmatrix}, \tag{6.2}$$

$$Y = \begin{pmatrix} M_1 & 0 & -M_Z s_\text{W}\cos\beta & M_Z s_\text{W}\sin\beta \\ 0 & M_2 & M_Z c_\text{W}\cos\beta & -M_Z c_\text{W}\sin\beta \\ -M_Z s_\text{W}\cos\beta & M_Z c_\text{W}\cos\beta & 0 & -\mu \\ M_Z s_\text{W}\sin\beta & -M_Z c_\text{W}\sin\beta & -\mu & 0 \end{pmatrix}, \tag{6.3}$$

$$M_{\tilde{\mu}}^2 = \begin{pmatrix} m_\mu^2 + m_\text{L}^2 + M_Z^2\cos 2\beta\left(-\frac{1}{2} + s_\text{W}^2\right) & m_\mu(-\mu\tan\beta + A_\mu^*) \\ m_\mu(-\mu^*\tan\beta + A_\mu) & m_\mu^2 + m_\text{R}^2 + M_Z^2\cos 2\beta\ (-s_\text{W}^2) \end{pmatrix}, \tag{6.4}$$

where the fundamental SUSY parameters appearing in these expressions are $\tan\beta$ and the two gaugino (Bino and Wino) mass parameters $M_{1,2}$, the Higgsino mass μ and the left-/right-handed smuon masses $m_{\text{L,R}}$. The smuon mass matrix also involves the trilinear soft

[28] Specifically the BHR contribution can be decisive if $\tan\beta \gg 50$ and if $m_\text{L} \gg m_\text{R}$ [186]. For further dedicated investigations focusing on parameter situations in which the BHL or BHR contributions dominate we refer to ref. [217].

JHEP09(2021)080

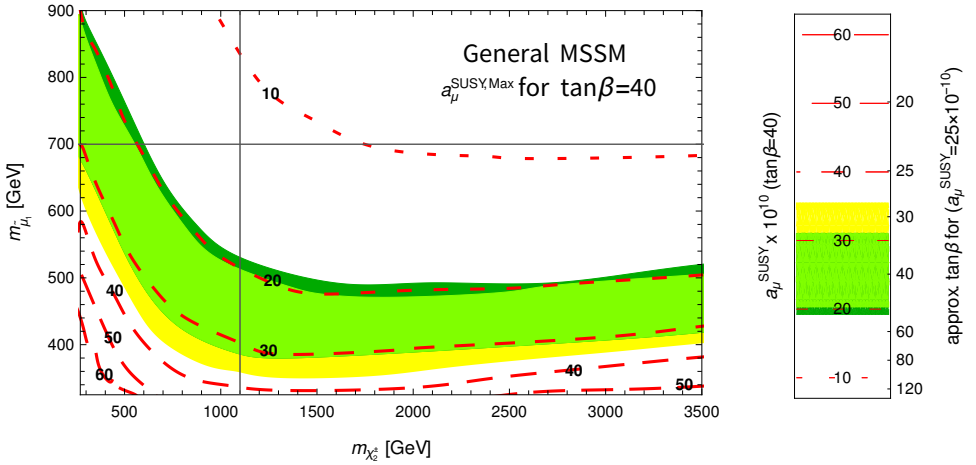

Figure 15. The theoretical maximum MSSM contribution $a_\mu^{\rm SUSY,Max}$ for $\tan\beta = 40$ in the plane of the heaviest chargino and the lightest smuon mass. (For each point in the plane, the actual value of the MSSM contribution can take any value between 0 and $\pm a_\mu^{\rm SUSY,Max}$, depending on the signs of parameters and details such as other masses and mixings.) The yellow/green coloured regions show where $a_\mu^{\rm SUSY,Max}$ (for $\tan\beta = 40$) is within the 1σ bands corresponding to the BNL and new deviations $\Delta a_\mu^{\rm BNL}$ and Δa_μ^{2021}, see eqs. (1.6), (1.7), and their overlap. The red dashed contour lines can be interpreted in two ways. Firstly, they directly correspond to certain values of $a_\mu^{\rm SUSY,Max}$ for $\tan\beta = 40$, as indicated in the left axis of the legend plot. Secondly, thanks to the approximate linearity in $\tan\beta$, each contour can be used to estimate the required $\tan\beta$ value for which $a_\mu^{\rm SUSY,Max}$ agrees with the deviation Δa_μ^{2021} (keeping other input parameters fixed). These $\tan\beta$ values can be read off from the right axis of the legend plot (the values are approximate since the linearity is not exact). As an example of the reinterpretation we take the point $m_{\chi_2^\pm} = 1750\,\text{GeV}$ and $m_{\tilde{\mu}_1} = 700\,\text{GeV}$. For $\tan\beta = 40$ we get $a_\mu^{\rm SUSY,Max} = 10\times10^{-10}$. The required $\tan\beta$ value to get Δa_μ^{2021} would be around 100, as read off from the right axis. The results for $a_\mu^{\rm SUSY,Max}$ were obtained from a scan using GM2Calc [45] in which all relevant SUSY masses are varied independently between 100 GeV and 4 TeV. The black lines indicate the maximum LHC reach for charginos and sleptons of 1100 and 700 GeV reported in refs. [487, 490], respectively.

SUSY-breaking parameter A_μ, which however will not play any role in the present paper. The other appearing parameters are the SM parameters $m_\mu, M_{W,Z}$ and $s_{\rm W} = \sqrt{1-c_{\rm W}^2}$. In our numerical treatment the fundamental SUSY parameters are defined as running $\overline{\rm DR}$-parameters at the scale 1 TeV, and the `MSSMEFTHiggs_mAmu` spectrum generator, created with[29] `FlexibleSUSY` [43, 44] and incorporated in `GAMBIT`-1.3, is used for the precise evaluation of the spectrum of mass eigenvalues including higher-order corrections.

The 1-loop contributions of the MSSM to a_μ have been systematically and comprehensively studied in ref. [512], for reviews see refs. [49, 74, 166]. A wide range of higher-precision calculations of 2-loop contributions is available. Including higher-order corrections, the full known SUSY contributions (i.e. the difference between MSSM and SM contributions) to

[29] `FlexibleSUSY` is a generic spectrum generator generator, and the FlexibleEFTHiggs extension [44, 517, 518] improves the Higgs mass calculation by resummation of large logarithms. The version used within `GAMBIT` is the one of ref. [44]. `FlexibleSUSY` also uses some numerical routines originally from [448, 449] and uses `SARAH` 4.14.1 [444–447].

JHEP09(2021)080

a_μ can be written as

$$a_\mu^{\text{SUSY}} = \left[a_\mu^{\text{1L SUSY}} + a_\mu^{\text{2L(a)}} + a_\mu^{\text{2L, photonic}} + a_\mu^{\text{2L},f\tilde{f}}\right]_{t_\beta\text{-resummed}}, \tag{6.5}$$

refs. [86, 87, 154, 159, 160] evaluated all 2-loop diagrams $a_\mu^{\text{2L(a)}}$ in which a SUSY loop is inserted into a SM-like loop, including so-called Barr-Zee diagrams. Given current experimental constraints these diagrams are very small. Refs. [163, 450] computed leading QED-logarithms and the full 2-loop QED corrections $a_\mu^{\text{2L, photonic}}$; refs. [162, 186] showed how to take into account n-loop higher-order terms enhanced by $(\tan\beta)^n$, i.e. carry out a $\tan\beta$-resummation. Finally refs. [164, 165] computed genuine SUSY 2-loop corrections $a_\mu^{\text{2L},f\tilde{f}}$ to the SUSY 1-loop diagrams which include non-decoupling effects from e.g. heavy squarks. Each of these three kinds of corrections can shift the 1-loop contributions by around 10%. All mentioned 1-loop and 2-loop contributions in eq. (6.5) are implemented in the code GM2Calc [45], which is used in our later phenomenological evaluations.[30]

The exact one-loop expression for $a_\mu^{\text{1L SUSY}}$ can be found in most mentioned references; a full overview of all contributions including higher orders is given in ref. [45]. Here we provide the 1-loop contributions in mass-insertion approximation, which allows to directly read off the main parameter dependences. Following the form given e.g. in refs. [165, 166, 186] they read

$$a_\mu^{\text{1L SUSY}} \approx \Delta a_\mu^{\text{1L}}(\text{WHL}) + \Delta a_\mu^{\text{1L}}(\text{BHL}) + \Delta a_\mu^{\text{1L}}(\text{BHR}) + \Delta a_\mu^{\text{1L}}(\text{BLR}),$$

with

$$\begin{aligned}
\Delta a_\mu^{\text{1L}}(\text{WHL}) &= \frac{g_2^2}{8\pi^2}\frac{m_\mu^2 M_2}{m_{\text{L}}^4}\,\mu\tan\beta\,F_a\left(\frac{M_2^2}{m_{\text{L}}^2},\frac{\mu^2}{m_{\text{L}}^2}\right) \\
&\quad - \frac{g_2^2}{16\pi^2}\frac{m_\mu^2 M_2}{m_{\text{L}}^4}\,\mu\tan\beta\,F_b\left(\frac{M_2^2}{m_{\text{L}}^2},\frac{\mu^2}{m_{\text{L}}^2}\right), && \text{(6.6a)} \\
\Delta a_\mu^{\text{1L}}(\text{BHL}) &= \frac{g_1^2}{16\pi^2}\frac{m_\mu^2 M_1}{m_{\text{L}}^4}\,\mu\tan\beta\,F_b\left(\frac{M_1^2}{m_{\text{L}}^2},\frac{\mu^2}{m_{\text{L}}^2}\right), && \text{(6.6b)} \\
\Delta a_\mu^{\text{1L}}(\text{BHR}) &= -\frac{g_1^2}{8\pi^2}\frac{m_\mu^2 M_1}{m_{\text{R}}^4}\,\mu\tan\beta\,F_b\left(\frac{M_1^2}{m_{\text{R}}^2},\frac{\mu^2}{m_{\text{R}}^2}\right), && \text{(6.6c)} \\
\Delta a_\mu^{\text{1L}}(\text{BLR}) &= \frac{g_1^2}{8\pi^2}\frac{m_\mu^2}{M_1^3}\,\mu\tan\beta\,F_b\left(\frac{m_{\text{L}}^2}{M_1^2},\frac{m_{\text{R}}^2}{M_1^2}\right). && \text{(6.6d)}
\end{aligned}$$

For SUSY masses significantly above M_Z this is a very good approximation (of the 1-loop contributions). Physics explanations and numerical examples have already been given around eq. (6.1). Next to $\tan\beta$ and the $\text{SU}(2)\times\text{U}(1)$ gauge couplings $g_{1,2}$, these contributions depend on the five independent SUSY mass parameters $M_{1,2}$, μ and $m_{\text{L,R}}$ introduced above. The appearing loop functions are normalized as $F_a(1,1) = 1/4$, $F_b(1,1) = 1/12$ and can be found in the mentioned references as well as in appendix A.

[30] For higher-order calculations in extensions of the MSSM see refs. [227, 237, 338, 519].

JHEP09(2021)080

The linear enhancement in $\tan\beta$ already explained in section 2 is apparent.[31] The $\tan\beta$ enhancement is accompanied by explicit factors of the Majorana gaugino masses $M_{1,2}$ and the MSSM Higgsino mass parameter μ.[32]

As indicated, all contributions in eq. (6.6) involve three different SUSY masses; the generic behaviour is $\propto 1/M^2_{\rm SUSY}$. The BLR-contribution in eq. (6.6) is special because it is linearly enhanced by large μ; this enhancement arises via the smuon mixing off-diagonal element in eq. (6.4).

Specific constraints on this BLR-contribution have been very thoroughly investigated in ref. [176]. Most importantly, vacuum stability requires that staus, the superpartners of τ-leptons, do not receive a charge-breaking vacuum expectation value, and this provides a constraint on the relation between the off-diagonal and diagonal elements of the stau mass matrix similar to eq. (6.4). As a quantitative example, ref. [176] finds that in case of universal left- and right-handed stau masses, the Higgsino mass has an upper limit, specifically

$$m_{\tilde\tau_{\rm L}} = m_{\tilde\tau_{\rm R}} = 300\ \text{GeV}\ (600\ \text{GeV}) \qquad \Rightarrow \qquad \mu \lesssim 1\ \text{TeV}\ (2\ \text{TeV})\,. \tag{6.7}$$

In our later plots we will show the appropriate constraint in the approximate form of eq. (14) of ref. [176].

6.2 LHC and dark matter constraints on explanations of Δa_μ^{2021}

Our aim is to analyze MSSM contributions to a_μ in the context of constraints from LHC and dark matter searches. Here we list the relevant constraints.

The relevant LHC constraints can be grouped into "standard" searches for electroweak particles (charginos/neutralinos and sleptons) and searches optimized for compressed spectra. The relevant searches are the following:

- Chargino/neutralino searches with decay into sleptons: the strongest chargino/neutralino mass limits are obtained from the pair production channel $pp \to \chi_1^\pm\chi_2^0$ with subsequent decay via on-shell sleptons into three charged leptons and two LSPs. In simplified-model interpretations, in which 100% decay branching ratios are assumed and the slepton mass is halfway between the LSP- and the chargino mass, the limits extend up to [487, 520]

  Chargino/slepton channel:

$$\chi_1^\pm\chi_2^0 \to \tilde l_{\rm L}\nu\tilde l_{\rm L} l(\tilde\nu\nu), \quad l\tilde\nu\tilde l_{\rm L} l(\tilde\nu\nu) \to l\nu\chi_1^0, \quad ll(\nu\nu)\chi_1^0 \tag{6.8a}$$

$$m_{\chi_1^\pm} \approx 1100\ \text{GeV} \qquad (\text{for } m_{\rm LSP} \approx 0\ldots 500\ \text{GeV}), \tag{6.8b}$$

$$m_{\rm LSP} \approx 700\ \text{GeV} \qquad (\text{for } m_{\chi_1^\pm} \approx 900\ldots 1000\ \text{GeV}). \tag{6.8c}$$

[31] The leading higher-order effects from QED-logarithms and from n-loop $(\tan\beta)^n$-effects can be approximately taken into account by multiplying the formulas by [162, 163, 186, 450] $\left(1 - \frac{4\alpha}{\pi}\log\frac{M_{\rm SUSY}}{m_\mu}\right)/(1+\Delta_\mu)$, where Δ_μ is a correction to the muon Yukawa coupling and $M_{\rm SUSY}$ the appropriate SUSY mass scale.

[32] As a side remark, in SUSY models with continuous R-symmetry such as the MRSSM, such Majorana gaugino masses and the μ-parameter are zero. Hence $a_\mu^{\rm SUSY}$ is not $\tan\beta$-enhanced, leading to distinctly different a_μ phenomenology [226].

JHEP09(2021)080

Further important, slightly weaker limits are obtained from the pair production channel $pp \to \chi_1^\pm \chi_1^\mp$ with subsequent decay via on-shell sleptons into two charged leptons and two LSPs. The limits in simplified-model interpretations reach up to $m_{\chi_1^\pm} \approx 1000\,\text{GeV}$ [490]. All limits of this kind depend on a significant mass splitting $\gtrsim 100\,\text{GeV}$ between the chargino and LSP masses; for smaller mass splittings the limits become much weaker.

- Chargino/neutralino searches with decay into other particles: the above limits are absent if the charginos cannot decay into sleptons e.g. because sleptons are too heavy. In such cases further limits are applicable. One such limit is obtained from the channel $pp \to \chi_1^\pm \chi_2^0$ assuming subsequent decays into on-shell W and Higgs bosons plus LSP. This limit extends up to [521]

  Chargino/Wh-channel:

$$\chi_1^\pm \chi_2^0 \to W h \chi_1^0 \chi_1^0, \quad W \to l\nu, \quad h \to b\bar{b} \tag{6.9a}$$
$$m_{\chi_1^\pm} \approx 750\ \text{GeV} \quad (\text{for } m_{\text{LSP}} \approx 0 \ldots 100\ \text{GeV}), \tag{6.9b}$$
$$m_{\text{LSP}} \approx 250\ \text{GeV} \quad (\text{for } m_{\chi_1^\pm} \approx 600\ \text{GeV}), \tag{6.9c}$$

  where Wino-like charginos and Bino-like LSP are assumed. If this assumption is not met, the production cross section is lower and/or the decay branching ratios are reduced [522]. Similar but slightly weaker limits are obtained in ref. [523]. A complementary limit is obtained in ref. [524] which searched for $pp \to \chi_1^\pm \chi_1^\mp, \chi_1^\pm \chi_2^0$ with subsequent decays via $\tilde{\tau}$-sleptons (staus) into τ-leptons. The limit in a simplified-model interpretation assuming Wino-like chargino reaches up to

  Chargino/stau-channel:

$$\chi_1^\pm \chi_2^0 \to \tilde{\tau}\nu\tilde{\tau}\tau(\tilde{\nu}\nu), \quad \tau\tilde{\nu}\tilde{\tau}\tau(\tilde{\nu}\nu) \to \tau\nu\chi_1^0, \tau\tau(\nu\nu)\chi_1^0, \tag{6.10a}$$
$$\chi_1^\pm \chi_1^\mp \to 2 \times \tilde{\tau}\nu(\tilde{\nu}\tau) \to 2 \times \tau\nu\chi_1^0 \tag{6.10b}$$
$$m_{\chi_1^\pm} \approx 760\ \text{GeV} \quad (\text{for } m_{\text{LSP}} \approx 0 \ldots 200\ \text{GeV}), \tag{6.10c}$$
$$m_{\text{LSP}} \approx 300\ \text{GeV} \quad (\text{for } m_{\chi_1^\pm} \approx 600 \ldots 700\ \text{GeV}). \tag{6.10d}$$

  Figure 8 of ref. [524] and the recasting study of ref. [201] show that the limit is rather robust against changes of the stau masses and mixings and against the Higgsino content of the chargino. There exist further chargino searches with decays into W and Z bosons [487, 490, 525–527], however the resulting limits are weaker and do not lead to excluded regions of the parameter spaces we will consider.

- Slepton searches: searches for the direct production of slepton pairs $\tilde{l}\tilde{l}, (\tilde{l} = \tilde{e}, \tilde{\mu})$ with subsequent decay into leptons plus LSP have been analyzed in ref. [490] (based on $139\,\text{fb}^{-1}$ data) and [487, 488] (based on $36\,\text{fb}^{-1}$ data). The limits extend up to

  Slepton [490] : (6.11a)

$$\tilde{l}_{\text{L,R}} \tilde{l}_{\text{L,R}} \to l^+ l^- \chi_1^0 \chi_1^0, \tag{6.11b}$$
$$m_{\tilde{l}} \approx 700\ \text{GeV} \quad (\text{for } m_{\text{LSP}} \approx 0 \ldots 300\ \text{GeV}), \tag{6.11c}$$
$$m_{\text{LSP}} \approx 400\ \text{GeV} \quad (\text{for } m_{\chi_1^\pm} \approx 550 \ldots 650\ \text{GeV}), \tag{6.11d}$$

JHEP09(2021)080

$$\text{Slepton [487, 488]}: \tag{6.11e}$$

$$m_{\tilde{l}} \approx 500 \text{ GeV} \quad (\text{for } m_{\text{LSP}} \approx 0 \ldots 300 \text{ GeV}), \tag{6.11f}$$

$$m_{\text{LSP}} \approx 300 \text{ GeV} \quad (\text{for } m_{\chi_1^\pm} \approx 500 \text{ GeV}). \tag{6.11g}$$

- Searches for SUSY particles with compressed-mass spectra: the compressed mass spectrum scenarios are investigated through the chargino-neutralino pair production modes $\chi_1^\pm\chi_2^0/\chi_1^\pm\chi_1^\mp$ with decays via virtual W/Z bosons and slepton pair production $\tilde{l}\tilde{l}$ with decays into leptons. In simplified-model analyses the limits depend on the nature of the charginos/neutralinos (Higgsino- or Wino-like) and reach up to masses of around 250 GeV and mass splittings to the LSP between $1 \ldots 50$ GeV [482, 528, 529].

Our technical setup for checking against these constraints is as follows. The LHC searches with the highest mass reach, i.e. the chargino/neutralino searches of refs. [487, 520, 525], and the slepton searches of ref. [487], and the compressed-mass searches of ref. [482] are checked using `ColliderBit` [530], a recasting tool within the `GAMBIT`-1.3 software framework [508, 530–534]. This framework was extended and applied to the chargino/neutralino sector already in ref. [535], where also a full description of all included analyses can be found. For each signal region (SR) of each analysis, `GAMBIT/ColliderBit` evaluates the theory prediction of the signal yield S_{SR}. It then constructs the log-likelihood differences $\ln \mathcal{L}_{\text{SR}} \equiv \ln \mathcal{L}(n|s = S_{\text{SR}}, b) - \ln \mathcal{L}(n|s = 0, b)$ for the computed signal yield and the observed event number n and background expectation b reported by the experiments. It also determines for each analysis which signal region SR^{max} has the highest expected sensitivity. For each given analysis `GAMBIT/ColliderBit` outputs a single "effective" log-likelihood difference $\ln \mathcal{L}_{\text{eff}} \equiv \ln \mathcal{L}_{\text{SR}^{\text{max}}}$. We refer to refs. [508, 530–534] for a detailed description of the procedure and cross-checks with original LHC analyses. To obtain a conservative LHC exclusion contour in the following plots of this section we proceed as follows. For each parameter point we take the largest effective $(-2 \ln \mathcal{L}_{\text{eff}})$ of any implemented analysis and employ $(-2 \ln \mathcal{L}_{\text{eff}})^{\text{Max}} \geq 6$ as the criterion for exclusion by the LHC recasting analysis.

In appendix B we provide further extensive details on the behaviour of the recasting for the parameter regions and the LHC analyses most relevant for our discussion. We discuss both cases with high sensitivity and low sensitivity. In particular we validate the recasting procedure by reproducing the exclusion contour of the ATLAS chargino/neutralino search of ref. [487], figure 8c. We further verify that the exclusion contour obtained as described above via $(-2 \ln \mathcal{L}_{\text{eff}})^{\text{Max}}$ is also fully consistent with the contour where the predicted signal yield for at least one signal region is equal to the respective ATLAS 95% C.L. upper limit. We checked that the same would be true for all following plots of the paper.[33]

As we will see the remaining mentioned LHC searches affect only a minor portion of the relevant SUSY parameter space. Hence we do not implement them in `GAMBIT/ColliderBit` but take them into account by directly using the simplified-model interpretations of the original ATLAS/CMS references. This is a very conservative approach which likely slightly

[33] In exceptional cases the comparison is not possible. In particular, the CMS analysis of ref. [482] for compressed spectra gives the maximum contribution $(-2 \ln \mathcal{L}_{\text{eff}})^{\text{Max}}$ in some parameter regions; for this analysis no individual 95% C.L. upper signal limits are available.

JHEP09(2021)080

overestimates the true LHC constraints on the MSSM, but it is motivated by the desire to find parameter regions which are definitely viable. Specifically, we apply the following constraints. Figures 14, 16 of ref. [528] are applied for Wino- or Higgsino-like charginos or sleptons as appropriate. Figure 6 of ref. [521] based on the Wh-channel chargino/neutralino search is applied to the lightest chargino in case of the hierarchy $M_1 < M_2 < \mu$ and if the chargino is lighter than sleptons and staus. Figure 7b of ref. [524] based on the stau-channel search is applied to the lightest chargino if its decay into stau is dominant and to the heavier chargino in case $\mu > M_2$ if the decay into stau is kinematically possible. As a further check we also directly apply the strong constraints of figures 7b, 7c of ref. [490] based on direct slepton searches (see eq. (6.11a)) and chargino searches with decays to sleptons; however as we will see they have no impact on our parameter spaces.

The following constraints from dark matter physics are relevant:

- Dark Matter Relic Density (DMRD): we assume the LSP to be the lightest neutralino, and unless noted otherwise we assume the LSP to be stable. In this case the LSP contributes to the dark matter relic density, and we require that the LSP relic density is in agreement with or smaller than the observed dark matter relic density. We have to distinguish the cases of dominantly Bino- or Wino- or Higgsino-like LSP. In the case of Wino- or Higgsino-like LSP and LSP-masses below 1 TeV, the relic density is always smaller than the observed value, thus leading to no constraints for our analysis (but to the requirement of additional, non-MSSM components of dark matter, see e.g. ref. [536, 537] for recent reviews). Ref. [214] has shown that coannihilation effects can increase the Higgsino- or Wino-like relic density if the mass splitting between sleptons and the LSP is significantly below 10%. However the extent is not sufficient to be of interest in the parameter regions of interest for a_μ, where we consider LSP masses below around 500 GeV.

  In the case of a Bino-like LSP in the considered mass range, the relic density is typically too large unless a specific mechanism acts to enhance the dark matter annihilation and to suppress the relic density. In the mass range of Bino masses of around 200...600 GeV there are three possibilities: stau-coannihilation, other slepton-coannihilation, and Wino-coannihilation [537–541]. As we will see, in each of our scenarios with Bino-like LSP, one of these possibilities can be realized without further impact on LHC-exclusion of parameters or on values of a_μ. Hence in summary we do not need to explicitly apply DMRD-constraints on our analysis of a_μ in the MSSM.

- Dark Matter Direct Detection (DMDD): if the LSP is stable there are constraints from the non-observation of dark matter in direct detection experiments. The most stringent constraints are obtained from the XENON1T experiment [506]; similar but weaker limits are obtained from XENON100, PandaX-II and LUX [542–544]. We evaluate these constraints using `DarkBit` and `DDCalc` [508, 509][34] within the `GAMBIT`

[34]The actual calculations can be done using internal code as well as interfaces to the public codes DarkSUSY [545] and `micrOMEGAs` [494]. For the calculations presented here we choose internal code and the interface to DarkSUSY.

JHEP09(2021)080

software framework [508, 530–534], using the provided log-likelihood functions as described in ref. [508]. Since the XENON1T limits are the strongest, we will only use those in our phenomenological analysis and consider a parameter point excluded at the 90% confidence level if $2\ln\mathcal{L}(\sigma=0) - 2\ln\mathcal{L}(\sigma, m_{\rm LSP}) > 1.64$ for the XENON1T analysis. The required calculations depend on the dark matter relic density. In the case of a Bino-like LSP, which allows an explanation of the observed value, we set the relic density to the observed value. In the case of Higgsino- or Wino-like LSP, in which case the relic density is smaller than the observed one, we use the relic density computed by `DarkBit`.

It is well known that the phenomenological impact of these constraints is that strong gaugino-Higgsino mixing of the LSP is not viable, except in "blind spots" which are characterized by particular ratios $\mu/m_{\rm LSP}$, require negative μ and depend on $\tan\beta$ and the CP-odd Higgs boson mass M_A [546]. As we will see, in case of a Bino-like LSP, lower limits on the Higgsino mass, and in case of a Higgsino-like LSP, lower limits on the Wino mass M_2 are implied. In contrast, the limits obtained in case of a Wino-like LSP turn out to be weaker.[35]

6.3 Setup of the phenomenological analysis

Our phenomenological analysis focuses on a wide parameter space of the MSSM (without flavour mixing in the sfermion sector). Our setup is as follows (all input parameters are defined as $\overline{\rm DR}$-parameters at the scale 1 TeV):

- The SUSY 1-loop contributions to a_μ depend on five mass parameters M_1, M_2, μ, $m_{\rm L}$, $m_{\rm R}$. We treat them as independent, except for setting the two slepton masses equal, $m_{\rm L} = m_{\rm R}$. Allowing different smuon masses would neither lead to enhanced $a_\mu^{\rm SUSY}$ nor significantly alter LHC and dark matter limits unless the mass splittings are extreme (see footnote 28). Since the influence of the trilinear scalar A-parameters is very small, we set $A_f = 0$ for all sfermion flavours.

- In all plots we fix

$$\tan\beta = 40 \tag{6.12}$$

as a reference value. Since $a_\mu^{\rm SUSY}$ is essentially linear in $\tan\beta$ it is easily possible to re-interpret plots for other values of $\tan\beta$, as already explained in the caption of figure 15.

[35] Technically, we determined these limits from dark matter direct detection in a separate computation using the `GAMBIT/DarkBit` framework. The limits may be of interest in their own right. In the parameter space relevant for our later plots with $\tan\beta = 40$ we obtained the following simple functional forms of the limits, correct to within 2%:

Bino-like LSP:	$\mu > 467\ \text{GeV} + 0.157 M_1 (1 + M_1/159\ \text{GeV})$
Wino-like LSP:	$\mu > 34.2\ \text{GeV} + 1.46 M_2$
Higgsino-like LSP:	$M_2 > 207\ \text{GeV} + 1.83\mu$

JHEP09(2021)080

- We assume R-parity conservation, such that the lightest SUSY particle (LSP) is stable and forms (a component of) dark matter. We assume the LSP to be the lightest neutralino.

- The selectron masses are set equal to the smuon masses, and generally we assume absence of flavour mixing in the slepton sector.[36] This is taken into account in evaluating the LHC search limits. The precise values of stau masses and mixings are not important for any of the considered observables except for the dark matter relic density in case of a Bino-like LSP. In the case of a Bino-like LSP, the LSP-relic density is generally too high, and we assume coannihilation with either staus, other sleptons or Winos to suppress the relic density to an acceptable value. Stau-coannihilation is generally possible as long as the Bino-mass is below around 600 GeV [538, 539]. It requires that one stau is sufficiently light but it does not fix the stau-masses and mixings uniquely. Since no other considered observables depend on their precise values, we fix the stau mass parameters to $2M_1$ in cases where stau-coannihilation is relevant. Due to stau mixing one mass eigenvalue is then close to the LSP mass. In cases where stau-coannihilation is not relevant we fix the stau mass parameters to 2 TeV, representing heavy staus. In the first case the chargino/neutralino limits based on ref. [524], see eq. (6.10), are relevant and taken into account.

- Squark and gluino masses are set to 6 TeV and the CP-odd Higgs mass is set to $M_A = 2\,\text{TeV}$. In this way, all respective LHC limits are evaded, and the mass of the SM-like Higgs boson is in the right ball-park. Such heavy squarks imply small, positive 2-loop corrections to a_μ^{SUSY} [164, 165]; we do not finetune the squark masses and mixings to fit the SM-like Higgs mass to agree with the measured values exactly, since there is no unique way to do it and since the impact on a_μ^{SUSY} and all other observables considered here is negligible.

Thus the essential parameters for our discussion are the four mass parameters

$$M_1, M_2, \mu, m_{\text{L,R}}, \tag{6.13}$$

where M_1 will be similar to the LSP-mass m_{LSP} in case the LSP is Bino-like; the two chargino masses are essentially given by M_2 and μ, respectively.

Despite having only four parameters, the parameter space is complex and there are many possible organizing principles. We may distinguish 24 different mass orderings and compressed or non-compressed spectra. We may classify according to the nature of the LSP and how dark matter is generated and according to which contributions to a_μ^{SUSY}

[36] Possible slepton flavour mixing between staus and smuons can lead to additional contributions to a_μ via enhanced chirality flips of the kind $\tilde{\mu}_{\text{L}} \to \tilde{\tau}_{\text{L}} \to \tilde{\tau}_{\text{R}} \to \tilde{\mu}_{\text{R}}$. Such effects have been studied in refs. [193, 512]; they enhance in particular the BLR-contributions and thus allow explanations of large a_μ with higher values of M_1, without conflict to bounds from the non-observation of $\tau \to \mu\gamma$. In contrast, slepton flavour mixing between selectrons and smuons does not enhance a_μ, but it leads to specific correlations to flavour-violating decays like $\mu \to e\gamma$ and $\mu \to e$ conversion, which in turn show interesting differences between the MSSM [83, 180, 547] and other models such as the MRSSM which does not allow a $\tan\beta$ enhanced dipole contributions [226].

JHEP09(2021)080

(WHL and/or BLR in eqs. (6.1), (6.6)) are dominant. We find that a very effective way to organize the discussion is to divide the parameter space in three distinct kinds of scenarios, denoting $m_{\tilde{l}} \equiv m_{\mathrm{L,R}}$ as the generic 1st and 2nd generation slepton mass, see also table 3:

- *Scenario with heavy chargino and smuons:*

$$m_{\tilde{l}} > 700 \text{ GeV}, \qquad m_{\chi^{\pm}_{1,2}} > 1100\,\mathrm{GeV}\,. \tag{6.14}$$

  These mass ranges correspond to the maximum reach of the LHC searches for sleptons and charginos found in refs. [487, 490] and are indicated by black lines in figure 15. The scenario thus evades all LHC constraints in the simplest possible way and is denoted as "LHC-unconstrained" in table 3. The following scenarios are defined to allow lighter SUSY particles.

- *Scenarios with lighter sleptons:* first we consider scenarios with slepton masses significantly below 700 GeV, which is possible if the sleptons are close in mass with the LSP, i.e.

$$m_{\mathrm{LSP}} \lessapprox m_{\tilde{l}} < 700\,\mathrm{GeV}\,, \tag{6.15}$$

  where the $\lessapprox$ symbol here denotes "lighter but not much lighter" to evade LHC limits, i.e. within around 100 GeV.[37] There are three sub-scenarios depending on the nature of the LSP, which we denote as

$$(\tilde{B}\tilde{l}),\ (\tilde{W}\tilde{l}),\ (\tilde{H}\tilde{l}) \tag{6.16}$$

  scenarios, respectively. In all these scenarios the chargino masses are obviously either heavier than the slepton masses or lighter but not by a significant amount.

- *Scenarios with charginos lighter than sleptons:* next we consider scenarios where both charginos are lighter than the sleptons:

$$m_{\mathrm{LSP}} < m_{\chi^{\pm}_{1,2}} < m_{\tilde{l}}\,. \tag{6.17}$$

  Here weaker LHC limits on charginos apply, such that chargino masses below 700 GeV are viable. We assume slepton masses to be non-compressed with the LSP, such that the LHC constraints on sleptons of refs. [487, 488, 490] are relevant (although the simplified-model interpretations illustrated in eqs. (6.11) do not necessarily apply). Again we can distinguish several sub-scenarios, depending on the nature of the LSP. We denote them as

$$(\tilde{B}\tilde{W}\tilde{H}),\ (\tilde{H}\tilde{W}/\tilde{W}\tilde{H}) \tag{6.18}$$

  scenarios. In the $(\tilde{B}\tilde{W}\tilde{H})$ scenario, no particular mass-ordering between the two chargino mass parameters M_2 and μ is implied; the $(\tilde{H}\tilde{W}/\tilde{W}\tilde{H})$ scenarios will be discussed together; the LSP is either Wino- or Higgsino-like and no particular value of M_1 is implied except that the Bino is not the LSP.

[37] More explicitly, the notation $m_{\mathrm{LSP}} \lessapprox m_{\tilde{l}}$ may be written as $m_{\mathrm{LSP}} < m_{\tilde{l}} < m_{\mathrm{LSP}} + \Delta m_{\mathrm{LHC}}$, where Δm_{LHC} is the mass gap allowed by LHC searches. The value of this allowed mass gap depends on the details of the considered spectrum but is typically of order 100 GeV.

JHEP09(2021)080

Scenario	Hierarchy	LSP/DM	Dominant a_μ
"LHC-unconstrained"	$m_{\tilde{l}} > 700\,\text{GeV}$, $m_{\chi^\pm_{1,2}} > 1100\,\text{GeV}$	Bino, Wino, Higgsino	WHL+BLR
$(\tilde{B}\tilde{l})$	$M_1 \lessapprox m_{\text{L,R}} \lesssim \mu, M_2$	Bino/$\tilde{\tau}$- or $\tilde{l}$- or $\chi^\pm$-coann.	WHL+BLR
$(\tilde{W}\tilde{l})$	$M_2 \lessapprox m_{\text{L,R}} \lesssim \mu, M_1$	Wino	WHL+BLR
$(\tilde{H}\tilde{l})$	$\mu \lessapprox m_{\text{L,R}} \lesssim M_1, M_2$	Higgsino	WHL
$(\tilde{B}\tilde{W}\tilde{H})$	$M_1 < M_2, \mu < m_{\text{L,R}}$	Bino/$\tilde{\tau}$- or $\chi^\pm$-coann.	WHL
$(\tilde{W}\tilde{H})$	$M_2 < \mu, M_1 < m_{\text{L,R}}$	Wino	WHL
$(\tilde{H}\tilde{W})$	$\mu < M_2, M_1 < m_{\text{L,R}}$	Higgsino	WHL

Table 3. Overview of the scenarios defined in section 6.3 and analysed in section 6.4. Here the $\lessapprox$ symbol denotes "lighter but not much lighter", i.e. sufficiently close to evade LHC limits, see main text; the $\lesssim$ symbol denotes "lighter or slightly heavier". In each case, the nature of the dark matter candidate is indicated. In cases of Bino-like LSP we assume the dark matter density to agree with observation, which in turn requires one of the indicated coannihilation mechanisms to be present. In the other cases we only assume that the predicted dark matter density does not surpass the observed one.

6.4 Phenomenological analysis

We will now discuss each scenario of table 3 in turn. In each case we will evaluate the possible values for a_μ^{SUSY} and the constraints from LHC and dark matter, and we will determine resulting viable parameter regions. Before explaining our results we briefly discuss the status of related studies in the literature. The general, phenomenological MSSM was analyzed in view of the BNL result $\Delta a_\mu^{\text{BNL}}$ versus LHC run-II in refs. [201–203, 220, 225], in refs. [203, 220, 225] including dark matter. All these references require a Bino-like LSP and consider parameter regions similar to our $(\tilde{B}\tilde{l})$ scenario.[38] Refs. [201, 202] also consider the general $(\tilde{B}\tilde{W}\tilde{H})$ scenario but do not consider dark matter. The LHC run-II data is treated with an increasing level of detail, and slightly different restrictions on the allowed masses are employed. Ref. [203] uses LHC recasting of a similar set of constraints as discussed in section 6.2, but with different recasting tools. It assumes stau-masses equal to the other slepton masses, i.e. generation universality, but allows differences between left- and right-handed sfermions $m_{\text{L}} \neq m_{\text{R}}$. This leads to slightly weaker LHC limits on M_2. Ref. [201] carries out a recasting of chargino search channels via staus, as mentioned in section 6.2. Refs. [202, 220, 225] treat LHC-data in different simplified ways without recasting. Ref. [225] focuses on scans of two parameter regions (both within our $(\tilde{B}\tilde{l})$ scenario), in which different states are decoupled. Ref. [202] focuses on the two cases $\mu = M_2$ and $\mu = 2M_2$ but allows for arbitrary slepton masses. The results of these references are that Bino-like LSP with either chargino-coannihilation or slepton/stau-coannihilation can provide viable explanations of dark matter and $\Delta a_\mu^{\text{BNL}}$, and refs. [203, 225] specify upper limits on the LSP mass.

[38] While finalizing this paper, ref. [548] appeared, which also contains results on the general MSSM, comparing a_μ to results from dark matter and LHC experiments in cases with Wino-like and Higgsino-like LSP. It uses the same approach as ref. [203] and shows similar complementarities to our study.

JHEP09(2021)080

Our study aims to provide an up-to-date and coherent analysis of the general MSSM in view of the Fermilab result for a_μ, dark matter data and our LHC recasting. We will treat all scenarios of table 3 including Bino-, Wino- or Higgsino-like LSP and provide details on allowed and preferred patterns of SUSY masses.

6.4.1 Scenario with heavy charginos and smuons, above all LHC limits

As a first basic scenario we consider sleptons and charginos heavier than 700 GeV and 1100 GeV, respectively, denoted as "LHC-unconstrained" in table 3. In figure 15 this region corresponds to the upper right quadrant of the plot, delineated by the black lines. The choice of this region is motivated by the maximum LHC reach for charginos and sleptons found in refs. [487, 490]. In other words, in the considered region the LHC limits are trivially fulfilled. Of course, the maximum LHC constraints were obtained for the simple special case of a massless Bino-like LSP χ_1^0, intermediate sleptons, and heavier charginos. The scenarios discussed later on will involve smaller masses and evade the LHC limits through choices of specific mass patterns, hierarchies and mass splittings.

Here we will first discuss the behaviour of $a_\mu^{\rm SUSY}$ in the upper right quadrant of figure 15, i.e. for $m_{\tilde{\mu}_1} \geq 700\,\text{GeV}$, $m_{\chi_2^\pm} \geq 1100\,\text{GeV}$. The figure already shows that $a_\mu^{\rm SUSY}$ is severely limited for such high masses. Overall we obtain $a_\mu^{\rm SUSY} \leq 13\times10^{-10}$ (for $\tan\beta = 40$ and $\mu \leq 4\,\text{TeV}$), and the maximum $a_\mu^{\rm SUSY}$ quickly drops for even heavier slepton masses. Hence the deviation observed at BNL (1.6) could at most be explained at the 2σ-level. for these values of $\tan\beta$ and μ. This remains the case also with the slightly smaller value and uncertainty of Δa_μ^{2021}.[39]

Despite the small contributions to a_μ, scenarios with heavy sparticles can be well motivated. E.g. the original focus point scenario [549, 550] naturally involve sleptons above the TeV scale, and in models with universality boundary conditions below the GUT scale, squarks and sleptons are rather close in mass [551] and LHC-constraints on squarks imply sleptons above the TeV scale [552]. Another attractive scenario where all sparticle masses are above the TeV scale is given by a Higgsino-like LSP with Higgsino mass around 1 TeV. This case leads to an explanation of the observed dark matter relic density without further tuning of masses or mass splittings and can be realized in the constrained MSSM or in more general variants of the MSSM (see e.g. Ref. [537]). However all such scenarios restrict $a_\mu^{\rm SUSY}$ to values below around 10×10^{-10} for $\tan\beta \lesssim 50$.

In the following we will focus on the alternative, "non-standard" scenarios which allow lighter sparticle masses.

6.4.2 $(\tilde{B}\tilde{l})$-scenario with light sleptons and Bino

The $(\tilde{B}\tilde{l})$-scenario is characterized by a Bino-like LSP and sleptons significantly lighter than 700 GeV. Given current LHC constraints it is viable if the mass splitting between

[39] Allowing for $\tan\beta \to \infty$ [186] or ultra-high values of μ [176] changes the picture. In both cases the linearity in $\tan\beta$ and μ visible in eqs. (6.6) is replaced by a saturation resulting from resummed higher-order effects. In such extreme parameter regions it is possible to obtain $a_\mu^{\rm SUSY} \approx 20\times10^{-10}$ for LSP masses above 1 TeV with $\mu = 100\,\text{TeV}$ and $\tan\beta = 40$ [176] or even $a_\mu^{\rm SUSY} > 30\times10^{-10}$ for LSP masses above 1 TeV with $\tan\beta \to \infty$ [186]. Similarly, the scenario of ref. [158] realizes radiative muon mass generation in the MSSM with non-holomorphic soft SUSY breaking parameters and allows LSP masses above 1 TeV while explaining $\Delta a_\mu^{\rm BNL}$.

JHEP09(2021)080

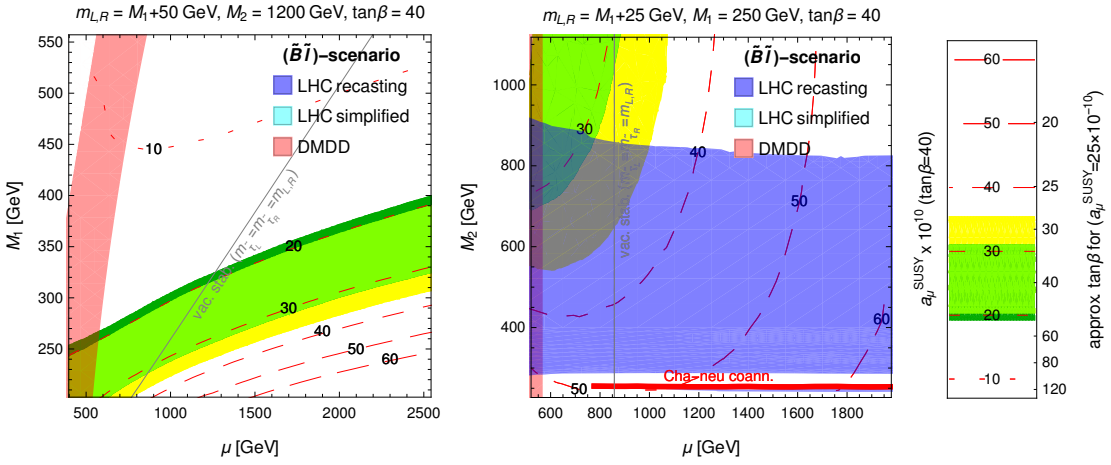

(a) (b)

Figure 16. $(\tilde{B}\tilde{l})$-scenario with either $M_2 = 1200\,\text{GeV}$ fixed or $M_1 = 250\,\text{GeV}$ fixed. For the remaining parameter values see the plots. The red dashed contours correspond to values of a_μ as indicated in the legend on the right; the yellow/green coloured regions correspond to the 1σ bands corresponding to the BNL deviation (1.6) and the new deviation including FNAL (1.7), and their overlap. For the $\tan\beta$-reinterpretation see caption of figure 15. The (light) red shaded regions are excluded by dark matter direct detection if the LSP is assumed stable; the blue shaded region corresponds to the limits from the LHC recasting, see figure 20 and text for details. These plots do not contain regions excluded by the additional LHC limits implemented in a simplified way. The red thick solid line in the right plot corresponds to the parameter strip where chargino-neutralino coannihilation is possible; directly below this strip a tiny region is excluded by the LHC-constraint from compressed masses, ref. [482], but we verified that this does not exclude the chargino-neutralino coannihilation region. The gray thin line corresponds to the vacuum stability constraint of ref. [176]; it applies in case the left- and right-handed stau-masses are set equal to the smuon/selectron masses and excludes the points to the right, i.e. with larger μ.

sleptons and the LSP is sufficiently small, $m_{\text{L,R}} - M_1 \lesssim 100\,\text{GeV}$ (for masses below around 200 GeV and very small splittings additional constraints from compressed-mass searches become relevant). The dark matter relic density can be correctly achieved by either $\tilde{l}/\tilde{\tau}$ or $\chi^\pm$-coannihilation by appropriate fine-tuning of parameters as discussed below. The scenario is illustrated in figure 16. The left plot figure 16(a) shows results in the μ–M_1-plane. The Wino mass is fixed to the rather high value $M_2 = 1200\,\text{GeV}$, safely but not too far above the chargino mass limit (6.8b), and the mass splitting $m_{\text{L,R}} - M_1 = 50\,\text{GeV}$. The right plot figure 16(b) shows results in the μ–M_2-plane, while the Bino and slepton masses are fixed to the rather light values $M_1 = 250\,\text{GeV}$ and $m_{\text{L,R}} = 275\,\text{GeV}$. In both plots the shown quantities are not very sensitive to the choice of the mass splitting, so the plots are representative for a wider range of values for $m_{\text{L,R}} - M_1$.

The red dashed lines and yellow/green coloured regions show the contours of a_μ and 1σ regions corresponding to the measurements from BNL only and the average including FNAL. The behaviour of a_μ in this $(\tilde{B}\tilde{l})$-scenario is dominated by the WHL and BLR contributions of eqs. (6.1), (6.6) and can be well understood via these approximations. The WHL contributions dominate in the left plot at large M_1 and very small μ and in

JHEP09(2021)080

the right plot at $\mu \lesssim 1\,\text{TeV}$; in these regions a_μ^{SUSY} decreases with increasing μ. The BLR contributions are linearly enhanced by μ and dominate at large μ in both plots. As the plots show very large a_μ^{SUSY} can be obtained both for large μ, where the BLR-contribution dominates, and for small μ with WHL-dominance.

LHC-constraints obtained by the recasting described in section 6.2 are displayed by the blue shaded region in the plots. The parameter space of the left plot figure 16(a) is entirely allowed (more details on the recasting are exhibited in the appendix), even where the Higgsino-like chargino is light. The right plot figure 16(b) shows the expected large excluded region approximately for $300\,\text{GeV} < M_2 < 900\,\text{GeV}$. It is excluded by the chargino/slepton channel search of refs. [487, 520], see eq. (6.8). The recasting shows again that the Wino-like charginos are significantly more constrained than Higgsino-like charginos and that the exclusion region is smaller than in the simplified-model interpretation of eq. (6.8b). An additional strip of parameter space at around $M_2 \approx M_1 - 5\,\text{GeV}$ (in which case the mass eigenvalues satisfy $m_{\chi_1^\pm} - m_{\chi_1^0} \approx 15\,\text{GeV}$) is excluded by the recasting of the CMS compressed-mass search of ref. [482].

Regarding dark matter it is well known that in case of a Bino-like LSP in the considered mass range the relic density is too high unless some coannihilation mechanism is active. In our case there are three options: chargino-, stau- or slepton-coannihilation (see also the review [537]). The possibility of chargino-coannihilation takes place in the parameter space where $m_{\chi_1^\pm} - m_{\chi_1^0} \approx 25\,\text{GeV}$ in the right plot, shown as the thick red line around $M_2 = 255\,\text{GeV}$. Here the relic density takes the measured value (1.8) without further tuning of the slepton masses. Everywhere else in the two plots the relic density can be correctly explained via slepton- or stau-coannihilation by slightly finetuning the slepton and/or stau masses. Since there is no unique way to achieve the required coannihilation we do not carry out this finetuning but fix the parameters as described above for the evaluation of all other observables. In this way the plot is representative for all these cases.[40]

Assuming now that the relic density is correctly explained, constraints from dark matter direct detection become relevant. The constraints from direct detection experiments are shown as the (light) red shaded bands; they exclude a large portion of the parameter space with small μ, implying $\mu \gtrsim 600 \ldots 800\,\text{GeV}$ in the plot. This reflects the well-known need for small gaugino-Higgsino mixing and a significant mass gap between the LSP and the Higgsino mass μ, see also section 6.2 and footnote 35.

The thin solid gray line in the plots corresponds to the vacuum stability constraint of ref. [176] on stau-mixing already explained around eq. (6.7). It excludes the large-μ region to its right under the condition that both left- and right-handed stau masses are as light as the smuon/selectron masses. This upper limit on μ thus applies in particular if stau-coannihilation and $m_{\tilde{\tau}_\text{L}} \approx m_{\tilde{\tau}_\text{R}}$ is assumed. Then the limit on μ significantly reduces

[40] The other observables have been evaluated by setting the stau masses to $2M_1$ in figure 16(a) and to 2000 GeV in figure 16(b). In order to achieve stau-coannihilation at least one stau mass has to be small and close to the LSP-mass. None of the plotted observables would change significantly, except that the LHC-constraints in the right plot would become slightly weaker since a larger variety of decay modes would exist for the charginos [203]. In this sense both plots are representative for a variety of cases and conservative in case of stau-coannihilation.

JHEP09(2021)080

the region in which the BLR-contributions to $a_\mu^{\rm SUSY}$ dominate. The vacuum stability constraint can be evaded and larger μ and large $a_\mu^{\rm SUSY}$ for heavier M_1 remain possible under the assumption that one stau or both staus are heavier. This can be compatible with a dark matter explanation either in the case of selectron/smuon-coannihilation, or in the case of stau-coannihilation with strongly non-universal left-/right-handed staus.

In summary, the $(\tilde{B}\tilde{l})$-scenario allows the following three parameter regions with large $a_\mu^{\rm SUSY}$. The first region is in the lower left of figure 16(a) and the upper left of figure 16(b) between the dark matter and vacuum stability constraints on μ. It involves μ around the 1 TeV scale and is allowed by all constraints even if we assume completely universal sleptons $m_{\rm L,R} \approx m_{\tilde{\tau}_{\rm L,R}}$. Here dark matter constraints can be explained by stau and/or slepton coannihilation and the a_μ result can be accommodated easily via the large BLR contributions. The new world average result for Δa_μ including FNAL can be explained well for $M_1 \lesssim 300\,\text{GeV}$ and $\tan\beta = 40$. As shown by figure 16(b), M_2 can be as low as around 900 GeV for our choice of $M_1 = 250\,\text{GeV}$, while for larger M_1 the LHC-limit on M_2 would relax slightly, and WHL-contributions could further increase $a_\mu^{\rm SUSY}$. The second region is to the right of the vacuum stability lines where μ is in the multi-TeV region and $a_\mu^{\rm SUSY}$ is further increased by the BLR contributions. The region is viable if at least one stau is sufficiently heavier. The dark matter relic density can then be generated via slepton or $\tilde{\tau}_1$ coannihilation. Here an explanation of Δa_μ is widely possible. The LSP mass can be heavier than 300 GeV, and the large white regions in figure 16(b) and lower right corner of figure 16(a) mean that Δa_μ^{2021} can be explained for $\tan\beta < 40$ according to the right axis of the legend plot. The third region is the patch of parameter space close to the lower border of figure 16(b). Here the Bino-like LSP, the Wino and the sleptons are all light and close in mass. This patch of parameter space allows in particular to generate dark matter via chargino-coannihilation, and it leads to very large $a_\mu^{\rm SUSY}$ for any value of μ above the dark matter limit. Here again the updated deviation Δa_μ^{2021} can be explained for $\tan\beta < 40$.

The recent model-building literature has put forward a variety of constructions leading to our second parameter region with light sleptons and very heavy μ, where $a_\mu^{\rm SUSY}$ is dominated by the BLR-contributions. These constructions are particularly motivated in view of the LHC constraints on the coloured SUSY particles and the Higgs mass. Clearly, a straightforward conclusion from such constraints is that gluino and top-squark masses are in the (multi-)TeV region. Via renormalization effects these masses can enter the electroweak symmetry breaking relations, and in many models very large μ in the multi-TeV region is then necessary in order to cancel such effects and allow a Higgs-VEV compatible with observations [215, 228, 230].

Many concrete constructions are inspired by universality ideas but involve some degree of non-universality to accommodate all existing constraints. One class of such models with multi-TeV-scale μ involves non-universal sfermion masses. General models with non-universal sfermion masses (but universal gaugino masses) have been constructed and investigated in refs. [196, 223], where $(\tilde{B}\tilde{l})$-like scenarios with $\mu \sim 10\,\text{TeV}$ were identified as promising. A specific kind of sfermion non-universality was considered in refs. [173, 207, 228], where the third generation of sfermions is assumed heavier than the first two, but universality between squarks and sleptons at some high scale is retained. Up-

JHEP09(2021)080

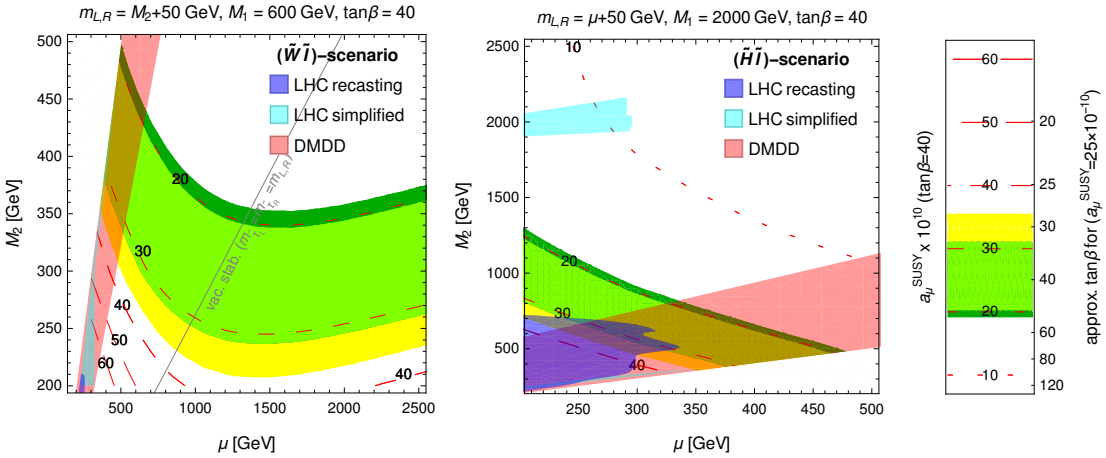

(a) (b)

Figure 17. (a) $(\tilde{W}\tilde{l})$-scenario. (b) $(\tilde{H}\tilde{l})$-scenario. For parameter values see the plots and the text. The red dashed contours correspond to values of $a_\mu^{\rm SUSY}$ as indicated in the legend on the right; the yellow/green coloured regions correspond to the 1σ bands corresponding to the BNL deviation (1.6) and the new deviation including FNAL (1.7), and their overlap. For the $\tan\beta$-reinterpretation see caption of figure 15. The red shaded region is excluded by dark matter direct detection if the LSP is assumed stable; the blue shaded regions correspond to the limits from the LHC recasting, see figure 20 for details. The cyan shaded region corresponds to the additional LHC limits implemented in a simplified way; in both plots the slepton search (6.11), ref. [490] excludes a narrow strip at small μ and M_2, where the slepton-LSP mass splitting is largest. In the right plot the compressed-mass searches of ref. [528] exclude another small region at large M_2, which enters the LSP mass via mixing. The thin solid gray line corresponds to the vacuum stability constraint of ref. [176]; it applies in case the left- and right-handed stau-masses are set equal to the smuon/selectron masses and excludes the points to its right, i.e. with larger μ.

to-date LHC constraints on gluino and Wino masses then imply that non-universal gaugino masses are almost unavoidable unless one allows an unstable charged slepton LSP [228].

Another class of models retains universality of all scalar soft SUSY-breaking masses but allows non-universal gaugino masses. In this case again, the scenario of figure 16 with very large μ is the only option to obtain significant $a_\mu^{\rm SUSY}$ [174, 181, 184, 224].

We mention that the scenario with μ in the multi-TeV region is also important to obtain large $a_\mu^{\rm SUSY}$ in the context of various specific model constructions, such as models based on Pati-Salam symmetry [194] (here, at the same time light Winos are preferred), models with usual GUT constraints but extra vectorlike matter fields [200, 216], and in a hybrid gauge-gravity mediation model with only four free parameters [206].

6.4.3 $(\tilde{W}\tilde{l})$-scenario with light sleptons and Wino

The $(\tilde{W}\tilde{l})$-scenario involves a Wino-like LSP and sleptons significantly lighter than 700 GeV. Current LHC-constraints on sleptons allow this scenario provided the slepton-LSP mass splitting is sufficiently small. The scenario is illustrated in figure 17(a) in the μ–M_2-plane. The mass splitting is chosen as $m_{\rm L,R} = M_2 + 50\,{\rm GeV}$, but the plotted quantities are not very sensitive to this choice. By definition of the scenario, the Bino mass is assumed to be

JHEP09(2021)080

heavier than the Wino mass. Since the Bino mass is also not strongly constrained by LHC data we fix it to $M_1 = 600\,\text{GeV}$, an intermediate value which is always heavier than M_2 in the plot but still allows significant BLR-contributions to a_μ^{SUSY}.

The behaviour of a_μ^{SUSY} (red dashed lines and yellow/green coloured regions) in this scenario with a Wino-like LSP is similar to the previous one in the case of a Bino-like LSP. The a_μ^{SUSY}-contours in figures 16(a), 16(b) and 17(a) have a similar shape. For small μ the WHL-contributions of eqs. (6.1), (6.6) dominate, and for $\mu \gtrsim 1500\,\text{GeV}$ the BLR-contributions to a_μ^{SUSY} dominate. An important difference is that the Wino-like LSP scenario allows very low Wino masses without the need for finetuning $M_1 \approx M_2$ as e.g. in figure 16(b). Hence the WHL-dominance region is wider in the $(\tilde{W}\tilde{l})$-scenario. In all of this WHL-dominance region the actual choice of $M_1 = 600\,\text{GeV}$ is inconsequential. This choice is important for $\mu \gtrsim 1500\,\text{GeV}$, where the BLR-contributions dominate and a_μ^{SUSY} rises with μ. Higher choices of M_1 would reduce a_μ^{SUSY} in this region.

The recasting of the ATLAS chargino search [487] excludes only a tiny blue shaded region in the plot at $M_2, \mu \lesssim 220\,\text{GeV}$, where both charginos and the sleptons are similar in mass. In addition the cyan shaded narrow strip at small μ corresponds to the additional LHC limits implemented in a simplified way as discussed in section 6.2. The specific analysis relevant here is the slepton search (6.11), ref. [490]. It excludes this cyan parameter strip, where the splitting between the slepton and LSP mass eigenvalues is largest.

The plot shows the dark matter direct detection limit as a red shaded band. It is well-known that a Wino-like LSP cannot produce the observed relic density unless the Wino mass is in the multi-TeV region, for a recent account see ref. [553]. In the mass region of interest for us, we obtained a Wino-LSP relic density which is typically a factor $10 \ldots 100$ smaller than the observed relic density. Nevertheless, the LSP-nucleon cross sections depend on the Wino-Higgsino mixing and are rather high. Hence the dark matter direct searches imply significant lower limits on the Higgsino mass μ of around $300 \ldots 800\,\text{GeV}$, see also footnote 35. This limit could only be circumvented by dropping the assumption of a stable LSP, e.g. by assuming R-parity violation of LSP-decays into light gravitinos.

The thin solid gray line in the plot corresponds to the vacuum stability constraint of ref. [176]. It applies if the left- and right-handed stau-masses are both set equal to the smuon/selectron masses. In such a case of slepton universality an upper limit on μ exists which essentially eliminates the region in which the BLR-contribution to a_μ^{SUSY} dominates.

In summary, the $(\tilde{W}\tilde{l})$-scenario can easily accommodate Δa_μ as large as the deviation Δa_μ^{2021} or even larger. Specifically e.g. the new world average (1.7) can be explained for $\tan\beta = 40$ with universal slepton masses and an LSP mass around $M_2 = 350\,\text{GeV}$ and $\mu = 800\,\text{GeV}$. Higher masses, in particular higher μ are also possible. For lower masses much smaller values of $\tan\beta$ can be sufficient. There are essentially no LHC constraints on this scenario as long as the mass splitting between sleptons and the LSP are sufficiently small. Dark matter direct detection enforces lower limits on μ, still leaving a wide parameter space in which the WHL-contributions to a_μ^{SUSY} are dominant and large. If slepton universality is assumed including staus, vacuum stability imposes an upper limit on μ; larger μ is possible if (at least one) heavy stau is assumed and provides further parameter space with large a_μ^{SUSY}.

JHEP09(2021)080

Again we provide a brief survey of model building efforts which lead to constructions like the $(\tilde{W}\tilde{l})$-scenario with a Wino-like LSP, light sleptons and very large μ. Ref. [230] has constructed an extreme variant of such a model with Wino-like LSP and slepton masses around 500 GeV based on Higgs-anomaly mediated SUSY-breaking [178, 205, 230]; that construction produces $\mu \gtrsim 25$ TeV. Ref. [221] shows that a similar scenario which involves both light Wino and Bino can follow from gaugino+Higgs-mediated SUSY breaking. Ref. [336] has also embedded a $(\tilde{W}\tilde{l})$-like scenario in a UV-model based on Higgs-mediated SUSY breaking. Such scenarios also had the potential to explain not only Δa_μ but also the smaller deviation in the electron magnetic moment a_e [334, 336] (see however footnote 26).

6.4.4 $(\tilde{H}\tilde{l})$-scenario with light sleptons and Higgsino

The $(\tilde{H}\tilde{l})$-scenario is characterized by a Higgsino-like LSP and sleptons significantly lighter than 700 GeV. Again, in view of current LHC-constraints the slepton-LSP mass splitting cannot be much larger than 100 GeV. The scenario is illustrated in figure 17(b) in the μ–M_2-plane. We again fix the mass splitting $m_{\text{L,R}} = \mu + 50$ GeV and we set the Bino mass to $M_1 = 2000$ GeV as reference values, although the considered observables are not very sensitive to this choice (except that significantly lower M_1 can lead to conflict with dark matter direct detection limits).

The behaviour of a_μ^{SUSY} shown by the red dashed lines and yellow/green coloured regions is quite different from the one in the previous two scenarios. Since the Higgsino mass μ is small, only the WHL-contributions of eqs. (6.1), (6.6) are important. For this reason the result shows the generic $1/M_{\text{BSM}}^2$-behaviour explained in section 2 and drops quickly both with increasing μ or increasing M_2, while the choice of M_1 has not much influence. Still, e.g. if $\mu = 300$ GeV the BNL deviation can be explained at the 1σ level even for $M_2 = 1$ TeV.

The constraints from LHC-recasting, shown in blue, are rather strong. They originate from the chargino/slepton channel searches of eq. (6.8), refs. [487, 520]. Compared to e.g. figure 20 now μ instead of M_1 takes the role of the LSP-mass, and the recasting shows that the resulting limits on the Wino-like chargino mass and thus on M_2 are weaker than in figure 20, extending only up to $M_2 = 700$ GeV in figure 17(b). The plot also shows additional cyan shaded parameter regions, which are subject to additional LHC-constraints implemented in a simplified way. Here, both the slepton search of ref. [490] and the compressed-mass searches of ref. [528] exclude small regions at small M_2 close to the $M_2 = \mu$ boundary and at large $M_2 \approx 2$ TeV, close to the bino mass. In both regions, neutralino mixing happens to lead to LSP-next-to-LSP mass splittings which are excluded. Though not visible in the plot we mention that the same compressed-mass searches also impose limits on the Higgsino-like chargino/neutralino system and thereby exclude parameter space with $\mu < 200$ GeV.

It is well known that a Higgsino-like LSP cannot produce the observed relic density for such light Higgsinos as considered here. Still there are relevant limits from dark matter direct detection experiments [554]. In the mass region of interest for us, we find that the Higgsino-LSP relic density is typically a factor 10 smaller than the observed relic density. This value is higher than the relic density in the previous case of a Wino-like LSP. As

JHEP09(2021)080

a result, stronger dark matter direct detection limits are obtained on M_2, shown as the red shaded band. In the plot they require $M_2 \gtrsim 500 \ldots 1500\,\text{GeV}$, depending on μ. As before, the dark matter direct detection limits apply only under the assumption that the Higgsino-like LSP is stable.

In summary, the $(\tilde{H}\tilde{l})$-scenario is strongly constrained by LHC chargino searches and by dark matter direct detection constraints (if the LSP is assumed to be stable). Still it allows values of M_2 as small as around 700 GeV and μ around 200 GeV which lead to a_μ^{SUSY} as large as 30×10^{-10}, but outside this small corner of parameter space the values of a_μ^{SUSY} quickly drop. The average deviation can be explained at the 1σ level for LSP masses up to 350 GeV for $\tan\beta = 40$. At the 2σ level, much higher LSP masses are possible.

In the model building literature, ref. [231] has considered a scenario of the $(\tilde{H}\tilde{l})$-type with significant mass gap between the Higgsino-LSP and the two gauginos, motivated within the context of a model with seesaw mechanism and SO(10) GUT constraints on the gaugino masses but non-universal scalar masses. Although electroweak LHC and DMDD constraints are not considered, this reference also finds only small viable contributions to a_μ^{SUSY} as a result of model-specific correlations to flavour-violating observables.

6.4.5 $(\tilde{B}\tilde{W}\tilde{H})$-scenario with light charginos

The remaining scenarios differ from the previous ones in that they involve two light charginos, while the sleptons are not assumed particularly light. The $(\tilde{B}\tilde{W}\tilde{H})$-scenario discussed here assumes both charginos to be lighter than the sleptons, but the Bino-like neutralino to be the LSP. Hence $M_1 < M_2, \mu$ with no particular order between M_2 and μ. The scenario is illustrated in figure 18(a). In the figure we set $m_{\text{L,R}} = 700\,\text{GeV}$, safely but not too far above the maximum LHC-limit of ref. [490]. We also fix $M_1 = 200\,\text{GeV}$ and show a_μ^{SUSY} versus LHC and dark matter constraints as a function of M_2 and μ.

The behaviour of a_μ^{SUSY} is dominated by the WHL-contributions of eqs. (6.1), (6.6) which are suppressed by the heavy slepton masses and further suppressed if μ and/or M_2 become heavy. The maximum contribution to a_μ^{SUSY} in figure 18(a) is around 30×10^{-10}; if μ and M_2 are heavier than 500 GeV, a_μ^{SUSY} reaches at most 15×10^{-10} for $\tan\beta = 40$ (which is just within the 2σ region of the updated deviation Δa_μ^{2021}. The chosen value of $M_1 = 200\,\text{GeV}$ has almost no influence on a_μ^{SUSY}. However the parameter space of this $(\tilde{B}\tilde{W}\tilde{H})$-scenario is subject to an interesting interplay of LHC and dark matter constraints.

First, since we assume the dark matter relic density to be correctly explained, the limits from dark matter direct detection are applicable, similarly to the plots in figure 16. In the present case with $M_1 = 200\,\text{GeV}$, the region with $\mu \lesssim 540\,\text{GeV}$ is excluded by this constraint. The constraint is shown by the red shaded band (partially overlaid with other coloured regions). As a result the entire region with $a_\mu^{\text{SUSY}} > 20 \times 10^{-10}$ is excluded, independently of other details.

Second, in order to achieve the correct relic density for this case of a Bino-like LSP in the given mass range, some coannihilation mechanism must act. Since sleptons are heavy, the two options are either chargino-coannihilation or stau-coannihilation. Chargino-coannihilation requires a specific chargino-LSP mass splitting. In figure 18(a) the thick red line denotes the one-dimensional contour along which chargino-coannihilation is possible

JHEP09(2021)080

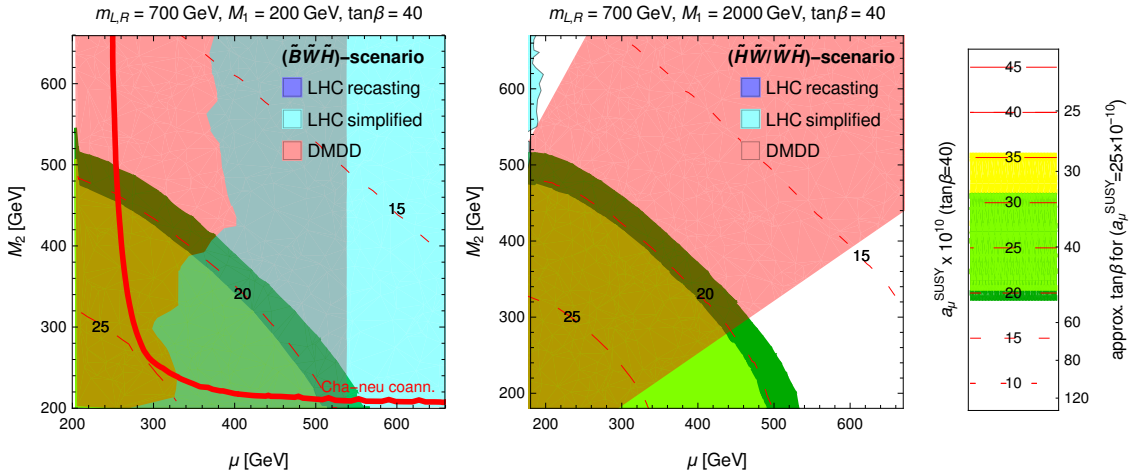

Figure 18. (a) $(\tilde{B}\tilde{W}\tilde{H})$-scenario. (b) $(\tilde{H}\tilde{W}/\tilde{W}\tilde{H})$-scenario. For parameter values see the plots and the text. The red dashed contours correspond to values of $a_\mu^{\rm SUSY}$ as indicated in the legend on the right; the yellow/green coloured regions correspond to the 1σ bands corresponding to the BNL deviation (1.6) and the new deviation including FNAL (1.7), and their overlap. For the $\tan\beta$-reinterpretation see caption of figure 15. The red shaded region is excluded by dark matter direct detection if the LSP is assumed stable; in the left plot this red region is the rectangle extending up to $\mu \approx 540\,\text{GeV}$. Both plots do not contain regions excluded by the LHC recasting. The cyan shaded regions correspond to the additional LHC limits implemented in a simplified way. In the left plot the cyan region is the large region extending from $\mu \gtrsim 300\ldots400\,\text{GeV}$ to the right (it is partially overlaid with dark matter and $a_\mu^{\rm SUSY}$-regions), it mainly arises from the stau-channel chargino search (6.10), ref. [524]; it is valid if light staus are assumed for stau-coannihilation. The red thick line in the left plot corresponds to the parameter strip where chargino-neutralino coannihilation is possible; in this region the dark matter relic density can be correctly described without light staus and the LHC-constraint does not apply.

due to appropriately small mass splittings between the lightest chargino and the LSP. Along this red contour we may assume staus to be heavy (e.g. degenerate with 1st and 2nd generation sleptons or even heavier). Anywhere outside the red line we must assume at least one or both staus to be light and close to the LSP in mass for stau-coannihilation.

Finally, we can apply LHC-constraints. The constraints depend on the coannihilation mechanism and the stau masses. Along the red contour for chargino-coannihilation we assume the staus to be heavy. Then the LHC-limit from chargino searches with Wh-channel [521], see eq. (6.9), is relevant. It turns out, however, that these limits do not exclude the chargino-coannihilation contour due to the small mass splittings. The scenario with Bino-like LSP and light charginos but heavier sleptons and staus has also been investigated thoroughly in ref. [535], where these scenarios were found to be not constrained and in some cases fitted excesses in the data.

Everywhere outside the red contour, we need to assume stau-coannihilation and light stau(s). In this case, the constraint from chargino searches with stau-channel [524], see eq. (6.10), applies. If we apply this LHC-constraint as described in section 6.2, the cyan

JHEP09(2021)080

shaded region in the plot is excluded, which is essentially the entire region with $\mu \gtrsim 350\,\text{GeV}$.[41]

As a result, the combination of dark matter and LHC-constraints exclude the entire scenario with stau-coannihilation for $M_1 = 200\,\text{GeV}$. Larger values of M_1 above around 300 GeV would relax LHC limits but lead to stronger dark matter direct detection limits (see footnote 35), thus leaving little room for large contributions to a_μ. If in the future the deviation decreases, this parameter region with significantly higher LSP masses M_1 and stau-coanihilation may become more promising.

Ref. [201] has considered a_μ versus LHC in the same scenario as well, however evaluated for $M_1 \leq 50\,\text{GeV}$. This smaller value of M_1 leads to larger a_μ^{SUSY} and weaker dark matter constraints, but also to stronger LHC exclusion limits (assuming stau masses in between M_1 and the chargino masses) essentially excluding the entire (μ, M_2)-region of interest for a_μ. Our larger value $M_1 = 200\,\text{GeV}$ reduces a_μ^{SUSY} but also leads to a parameter region with low chargino mass allowed by LHC; however our parameter region is challenged by DMDD constraints. This comparison highlights the complementarity between a_μ, LHC and dark matter constraints.

In summary, the entire $(\tilde{B}\tilde{W}\tilde{H})$-scenario with light staus turns out to be strongly under pressure. A remaining possibility in this $(\tilde{B}\tilde{W}\tilde{H})$-scenario is chargino-coannihilation and heavier staus: the small part of the red thick line at $\mu > 540\,\text{GeV}$ is viable. Here Δa_μ reaches up to 20×10^{-10} for $\tan\beta = 40$, which is just sufficient to accommodate the deviation (1.7) at the 1σ level.

The $(\tilde{B}\tilde{W}\tilde{H})$-scenario appears in an elaborate model building construction of ref. [213] based on the Pati-Salam model with inverse seesaw mechanism for neutrino masses. The benchmark points of that reference are very similar to the region of figure 18(a) with $\mu \sim 450\,\text{GeV}$, $M_2 \sim 300\,\text{GeV}$; however that reference does not consider DMDD constraints, which exclude such masses in our figure 18(a). In that model the right-handed sneutrinos provide significant additional contributions to a_μ, enlarging the parameter space with large a_μ^{SUSY}. A variant of the scenario has been considered in ref. [212]. This reference investigates dark matter generation via resonances, the so-called "Z/h-funnel" regions. It shows that LHC-constraints allow the h-funnel region, i.e. an LSP-mass around 60 GeV, together with large $\tan\beta \gtrsim 20$ and $\mu \gtrsim 390\,\text{GeV}$, which opens up additional parameter space similar to the one of figure 18(a).

6.4.6 $(\tilde{H}\tilde{W}/\tilde{W}\tilde{H})$-scenarios with light charginos

In the $(\tilde{H}\tilde{W}/\tilde{W}\tilde{H})$-scenarios again both charginos are lighter than the sleptons, but now the Bino mass is also heavier, so the LSP is either Wino- or Higgsino-like. Both scenarios are illustrated in figure 18(b) in the μ–M_2-plane. Like in the previous case we set $m_{\text{L,R}} = 700\,\text{GeV}$, safely but not too far above the LHC limit. We also set $M_1 = 2000\,\text{GeV}$. This

[41] As mentioned in the context of eq. (6.10) the LHC-constraint of ref. [524] is rather robust against changes of the stau masses and mixings and against the Higgsino content of the chargino. Hence we apply literally the constraints obtained in the simplified-model interpretation of ref. [524] to charginos with dominant decay into staus.

JHEP09(2021)080

choice is not critical — it neither influences LHC-limits nor a_μ, but it avoids limits from dark matter direct detection (which would be similar to the limits on M_2 discussed below).

The figure shows that the values of $a_\mu^{\rm SUSY}$ are very similar to the previous $(\tilde{B}\tilde{W}\tilde{H})$-case. This is no surprise since $a_\mu^{\rm SUSY}$ is dominated by the WHL-contributions and the higher value of M_1 is inconsequential. Hence the new a_μ deviation can be generally explained if $\tan\beta$ is around 40 or higher.

In fact, the main difference between the present scenarios and the previous $(\tilde{B}\tilde{W}\tilde{H})$-scenario is the nature of the LSP and the resulting very different dark matter and LHC constraints.

The LHC-constraints on the previous scenario were strong in case of light staus. Since now in the $(\tilde{H}\tilde{W}/\tilde{W}\tilde{H})$-scenarios there is no need to assume light staus we assume the staus to be at least as heavy as the other sleptons. As a result there are essentially no LHC constraints on the scenarios, in line with the previous case and the findings of ref. [535]. Only the regions with very small μ or $M_2 \lesssim 200\,\text{GeV}$ are subject to constraints from compressed-spectrum searches for the Higgsino- or Wino-like chargino/neutralino system. In the plot only a tiny cyan region at $\mu \approx 200\,\text{GeV}$ is excluded in this way, but the largest part of parameter space is allowed by LHC.

The dark matter direct detection limits apply under the assumption that the LSP is stable. As also mentioned in the context of figure 17 in sections 6.4.3 and 6.4.4, the LSP relic density is smaller than the observed value in the displayed parameter region, hence only a fraction of the observed dark matter can be explained. Nevertheless, the LSP-nucleon cross sections are sufficiently high to imply significant lower limits on the chargino masses. The limits are stronger in case of a Higgsino-like LSP and exclude the largest part of parameter space in the upper left part of the plot. The fact that current direct detection constraints exclude a large fraction of the parameter space with Higgsino-like dark matter has already been observed in ref. [554], where also scenarios with non-thermal dark matter production and additional dark matter candidates such as axions were considered. In the case of a Wino-like LSP the dark matter relic density is smaller and the constraints from direct detection are weaker, leaving open a larger triangular region in the lower right part of the plot.

In summary, therefore, almost the entire Higgsino-like LSP region of the $(\tilde{H}\tilde{W}/\tilde{W}\tilde{H})$-scenario is excluded by the combination of LHC compressed-mass searches and dark matter direct detection. Only a small region in the upper left part of the plot around $\mu \sim 250\,\text{GeV}$ and $M_2 \sim 600\,\text{GeV}$ remains viable. In this region, $a_\mu^{\rm SUSY}$ is always smaller than 20×10^{-10} for $\tan\beta = 40$ and outside the 1σ region of the new deviation Δa_μ^{2021}. The Wino-like LSP region of the $(\tilde{H}\tilde{W}/\tilde{W}\tilde{H})$-scenario in the triangular bottom right region of the plot allows a larger viable parameter space, in which a 1σ explanation of Δa_μ^{2021} is possible for $\tan\beta = 40$ and even a full explanation $a_\mu^{\rm SUSY} = 25\times10^{-10}$ can be reached. However for smaller $\tan\beta$, the current deviation is harder to explain. In case the dark matter constraints are not applied (by assuming unstable LSP) both scenarios can accommodate Δa_μ higher than 30×10^{-10}.

In the literature, several model-building efforts have led to specific constructions with mass patterns of the $(\tilde{H}\tilde{W}/\tilde{W}\tilde{H})$ kind. The scenario with either Higgsino- or Wino-like

JHEP09(2021)080

LSP can be motivated in gauge-mediated SUSY breaking [219], extended by non-minimal contributions to the soft-breaking parameters which allow the Higgs, squark and slepton scalar mass parameters to be non-universal. In addition, in the context of gauge-mediated SUSY breaking the lightest neutralino can decay into gravitinos; hence the DMDD constraints of figure 18(b) do not apply and the scenario of ref. [219] provides a viable SUSY model explaining Δa_μ. The Higgsino-like LSP scenario can be motivated within anomaly-mediated SUSY breaking [188], gaugino-mediated SUSY breaking [191] or in the context of electroweak finetuning considerations [185, 195]. The scenario has also been constructed in ref. [187] as a focus-point scenario (called FPNUS or FPHGM) based on gravity mediation with non-universal scalar masses or on Higgs-gaugino mediation. All these references do not apply DMDD constraints, which may be justified by assuming R-parity violation [187]. Similar scenarios were considered in a model with pseudo-Dirac gluino [211]; there, also DMDD constraints were investigated based only on the weaker limits from LUX and PandaX, however also leading to significant constraints on parameter space. Ref. [207] also considers the $(\tilde{H}\tilde{W})$-scenario with Higgsino-like LSP, but here universality between squarks and sleptons and quark flavour constraints imply only small contributions to a_μ.

6.5 Summary

Here we briefly summarize our main results on SUSY explanations of Δa_μ^{2021}. Like for other BSM scenarios, negative results from LHC and dark matter searches have significantly reduced the viable SUSY parameter space. Simple traditionally considered cases such as the Constrained MSSM are already excluded as explanations of $\Delta a_\mu^{\text{BNL}}$ and now also of Δa_μ^{2021} [555–558].

In our detailed phenomenological analysis we focused on the general MSSM without restrictions from GUT scale assumptions or specific SUSY breaking mechanisms. The only restrictions imposed by our analysis are a stable neutralino-like LSP which constitutes (part or all of) dark matter and the absence of flavour-violating soft SUSY-breaking parameters. For simplicity we also consider equal masses of left- and right-handed selectrons and smuons (called sleptons for short), while the stau-masses are left arbitrary. In a series of footnotes 28, 32, 36, 39 we commented on alternative cases with ultra-high $\tan\beta$ or μ, enhancements via lepton-flavour violation, and the MRSSM without $\tan\beta$ enhancement. The results of our analysis are as follows.

- *Scenario with heavy charginos and smuons*: the MSSM scenario with generally heavy masses, corresponding to the upper right quadrant of figure 15 where LHC limits are trivially avoided is disfavoured as an explanation of Δa_μ^{2021}. For such SUSY heavy masses, the current a_μ deviation can at most be explained if $\tan\beta \gg 40$ and/or $\mu \gg 4\,\text{TeV}$.

- $(\tilde{B}\tilde{l})$*-scenario*: a promising MSSM scenario is the $(\tilde{B}\tilde{l})$-scenario with Bino-like LSP and close-by sleptons to evade LHC limits. We identified three allowed parameter regions particularly promising in view of Δa_μ^{2021}: (1) Wino mass above LHC limits of around 900 GeV (for LSP mass of 250 GeV) and Higgsino mass μ of order 1 TeV. Here all slepton and stau masses may be universal. (2) Wino mass as before but μ in the

JHEP09(2021)080

multi-TeV region. Here at least one stau must be heavier to avoid vacuum stability constraints. (3) Light Wino with mass similar to the Bino and slepton masses. In all regions dark matter data implies a lower mass limit on μ. The relic density can be generated via stau/slepton coannihilation; in region (3) also Wino coannihilation is possible. In all these cases the result for Δa_μ^{2021} after the FNAL measurement can be easily explained in a wide range of masses and $\tan\beta$ values.

- *$(\tilde{W}\tilde{l})$- and $(\tilde{H}\tilde{l})$-scenarios*: the $(\tilde{W}\tilde{l})$- and $(\tilde{H}\tilde{l})$-scenarios are characterized by Wino- or Higgsino-like LSP; the sleptons are sufficiently close to the LSP to evade LHC limits. Specifically the $(\tilde{W}\tilde{l})$-scenario can lead to the largest a_μ^{SUSY} of any MSSM scenario in a wide parameter space via the WHL and BLR contributions: the DMDD constraints are weak and there are essentially no additional LHC constraints. The new updated a_μ deviation can be accommodated in a wide range of masses and $\tan\beta$ values, see figure 17(a). At the 1σ level and for $\tan\beta = 40$ LSP masses above 400 GeV are possible.

  In the $(\tilde{H}\tilde{l})$-scenario a_μ^{SUSY} is dominated only by WHL contributions, and DMDD and LHC constrain the Wino mass to be rather heavy. Hence there is an upper limit to the possible values of a_μ^{SUSY}, but a 1σ explanation of the current a_μ deviation is possible for $\tan\beta = 40$ and for LSP masses below 350 GeV. However, in both cases of Wino- or Higgsino-like LSP, the dark matter relic density cannot be fully accommodated simultaneously with Δa_μ^{2021}, necessitating additional non-MSSM components of dark matter such as gravitinos.

- *$(\tilde{B}\tilde{W}\tilde{H})$- and $(\tilde{H}\tilde{W}/\tilde{W}\tilde{H})$-scenarios*: in the $(\tilde{B}\tilde{W}\tilde{H})$- and $(\tilde{H}\tilde{W}/\tilde{W}\tilde{H})$-scenarios both charginos are assumed to be lighter than the sleptons, which in turn are constrained by LHC data. a_μ is rather limited in both scenarios. In the $(\tilde{B}\tilde{W}\tilde{H})$-scenario the Bino-like neutralino is the LSP and even lighter than both charginos. Outside the Bino-Wino coannihilation region this scenario is very strongly constrained by the combination of dark matter and LHC constraints. In the Bino-Wino coannihilation region, all constraints can be fulfilled for sufficiently large μ, however in this region and for $\tan\beta = 40$ a_μ^{SUSY} is almost always at least 1σ lower than the observed deviation. In the $(\tilde{H}\tilde{W}/\tilde{W}\tilde{H})$-scenarios either the Wino- or Higgsino-like neutralino is the LSP. Assuming staus as heavy as the other sleptons, there are no relevant LHC constraints. Although the full dark matter relic density is below the observed one (similarly to the $(\tilde{W}\tilde{l})$- and $(\tilde{H}\tilde{l})$-cases), direct detection constraints exist and require a mass splitting between the Higgsinos and Winos. The resulting a_μ^{SUSY} can be larger in case of a Wino-like LSP. Such a scenario is well able to explain the observed deviation for $\tan\beta = 40$ or slightly smaller $\tan\beta$ values.

The discussion and the plots show that the general MSSM can explain the current Δa_μ^{2021} in large parameter regions which will remain hard to test at the LHC alone. More sensitive LHC measurements will however sharpen the limits on SUSY particle masses; depending on the scenario, the mass of the LSP, of the dark matter coannihilation partner, or of

JHEP09(2021)080

the Wino-like chargino mass will be further scrutinized. If the LHC search results remain negative, this, together with theoretical constraints such as the stau vacuum stability constraints, will particularly help to eliminate motivated high-scale scenarios beyond the Constrained MSSM.

Future dark matter direct detection experiments are very promising in view of MSSM explanations of Δa_μ^{2021}. Both the LUX-ZEPLIN (LZ) experiment [559] and the XENONnT experiment [560] have the potential to increase the sensitivity to DMDD cross sections by more than an order of magnitude, reaching close to the irreducible neutrino background. These experiments have the potential to discover evidence for SUSY dark matter if the MSSM explanation of Δa_μ^{2021} is correct, or to significantly reduce the available parameter space. For the longer-term future, e^+e^- colliders offer great potential of testing MSSM explanations of Δa_μ^{2021} more conclusively, and we refer to refs. [203, 548] for more details. These references have shown that some part of the dark matter coannihilation parameter space can be tested at an e^+e^- linear collider with 500 GeV center-of-mass energy, while a very large part of the parameter space can be tested at a multi-TeV e^+e^- collider such as CLIC [561].

7 Conclusions

15 years after the BNL a_μ measurement showed a tantalizing deviation from the SM theory value and following tremendous theoretical work on improving and stabilizing the SM prediction, the Fermilab E989 experiment has published its first measurement of a_μ. The result is a strong confirmation of the BNL result and the existence of a deviation to the SM. After including the FNAL result, the new world average results in $\Delta a_\mu^{2021} = 25.1 \times 10^{-10}$, a 4.2σ deviation. It strengthens the indications for the existence of BSM physics in the lepton sector, possibly related to the muon mass generation mechanism.

Which BSM scenarios can accommodate the new Fermilab a_μ measurement, and what are the required parameter values? The present paper provides a detailed survey of possible explanations to answer this question. We focused on renormalizable models which were already promising in view of the previous BNL result. We asked particularly in what parameter space the models can accommodate the a_μ results, taking into account up-to-date constraints from LHC and dark matter searches, as well as other relevant constraints. Our survey covered simple extensions of the SM by one, two, or three new fields (required to be full SM gauge multiplets), including e.g. leptoquark and Two-Higgs doublet models, as well as a general version of the MSSM. Sections 3, 4 also contain detailed overviews of the status of models, and summaries of our phenomenological results can be found at the end of each section.

A useful background information is that the observed deviation Δa_μ^{2021} is larger than the electroweak contributions $a_\mu^{\rm EW} = 15.36(0.10) \times 10^{-10}$. BSM contributions to a_μ are typically suppressed as $1/M_{\rm BSM}^2$. Hence BSM models explaining the deviation must have nontrivial properties, and many models are excluded as explanations. The common nontrivial feature of most viable explanations is enhancements in the muon left-right chirality flip via new couplings and interactions. As explained around eq. (2.3) the chirality flip en-

JHEP09(2021)080

hancement is strongly related to the muon mass generation mechanism and causes related loop contributions to the muon mass. As a side note, one obtains a quite model-independent order-of-magnitude relationship: models in which the muon mass correction does not exceed 100% can explain Δa_μ^{2021} only for $M_{\rm BSM}^{\rm FNAL} \lesssim 2.1$ TeV according to eq. (2.6). But even in such models with chirality flip enhancements an explanation of Δa_μ^{2021} requires specific, often "non-traditional" regions of parameter space.

Examples of excluded models include the red highlighted models in tables 1, 2, many versions of leptoquark models or the familiar type I, II versions of the 2HDM. In the context of supersymmetry, familiar scenarios such as the Constrained MSSM cannot explain the deviation. Certain leptoquark and vector-like lepton models are examples which generate very large chiral enhancements, but they need non-flavour universal couplings, e.g. direct leptoquark couplings of muon to top-quark in the left- and right-handed sector.

An important outcome of the present study is that once the a_μ result is combined with current data from LHC and dark matter experiments, we obtain strong constraints on the detailed ways how BSM models can be realized. The only viable models of the kind discussed in section 4 that do not have chirality enhancements, are particularly strongly constrained. In these models, LHC data and Δa_μ^{2021} can be accommodated simultaneously in a small slice of parameter space, however it is impossible to also account for the full dark matter relic density, see figures 5–8. In contrast the simple 3-field models 2F1S and 2S1F of section 5 are least constrained and can accommodate a_μ and dark matter in a wide parameter region. The required values of the new coupling constants, however, are large and it remains to be seen how such scenarios can arise in more complete theories.

The 2HDM can accommodate the observed Δa_μ^{2021} while preserving minimal flavour violation, but only in the lepton-specific type X version or the generalized flavour-aligned 2HDM. Even in these scenarios only a tiny parameter space remains, where the new Yukawa couplings are close to their upper experimental limits and the new Higgs masses in a very narrow range below 100 GeV, see figure 1. Leptoquark masses are strongly constrained by LHC to be significantly above 1 TeV, pushing the explanation of Δa_μ^{2021} close to the region violating the fine tuning criterion on the muon mass, see figures 2–4.

For SUSY scenarios, the general tension between LHC mass limits and explanations of Δa_μ^{2021} is illustrated in figure 15. Still, the MSSM with Bino-like LSP and either stau/slepton-coannihilation or chargino coannihilation can fully explain Δa_μ^{2021} and the dark matter relic density, see figure 16. Apart from the constraints implied by the coannihilation mechanisms, the parameter space is wide open in the M_1–μ plane. LHC and dark matter constraints however imply mass patterns, e.g. lower limits on the Higgsino mass and two windows for the Wino mass. The case where both charginos are lighter than sleptons is very strongly constrained and may be excluded by future data from a_μ, LHC and dark matter experiments (figure 18(a)). Further, in the largest part of viable parameter space the simple GUT constraint on gaugino masses $M_1/M_2 \approx 1/2$ is strongly violated. The scenarios with a Higgsino-like LSP are strongly constrained and can accommodate the current a_μ only in a limited range of masses. Scenarios with Wino-like LSP emerge as particularly interesting (figures 17, 18(b)). They can accommodate a_μ in a vast parameter space without significant constraints; however in these scenarios the dark matter relic density can only be partially explained without additional contributions to the relic density.

JHEP09(2021)080

These results and discussions highlight the importance of a_μ not only as a potential proof of BSM physics but also of a crucial constraint on models. Particularly in combination with current LHC and dark matter data, it points to specific parameter regions of models and gives crucial clues on how BSM physics can (or cannot) be realized. Since many models involve muon chirality flip enhancements and/or flavour non-universality, further experiments testing lepton flavour violation, electric dipole moments, or lepton universality are promising to uncover further properties of BSM physics. Since the muon chirality flip enhancements are related to the mass generation mechanism for the muon, also the measurement of the Higgs-muon coupling at LHC or future lepton colliders can provide a test of various explanations of Δa_μ^{2021}. Further ultimate tests may be performed at a multi-TeV muon collider [562–567].

The new Fermilab a_μ measurement provides the best possible starting point for future a_μ determinations. Exciting further progress can be expected from the Run-2-4 results of the FNAL $g-2$ experiment, the planned JPARC $g-2$ experiment [568, 569], and from further progress on SM theory including the MUonE initiative to provide alternative experimental input to the determination of the hadronic contributions to a_μ [570, 571].

Acknowledgments

We thank the ColliderBit group from GAMBIT (and in particular Anders Kvellestad) for helpful discussions about available analyses and the statistical interpretation of their likelihoods and we also thank Felix Kahlhoefer for helpful comments on the statistical interpretation of both ColliderBit and DDCalc likelihoods. We also thank Adriano Cherchiglia for the consent to use internal results and data of ref. [252]. H.S-K. and D.S thank Hyesung Lee for the helpful discussion and comments on dark photon models. P.A. and D.J. thank Innes Bigaran for helpful discussions regarding leptoquark constraints applied in ref. [435]. D.J. thanks Susanne Westhoff for helpful clarifications regarding details about ref. [367], and Ursula Laa for her helpful support with `SModelS` and `micrOMEGAs`. The work of P.A. is supported by the Australian Research Council Future Fellowship grant FT160100274. P.A. also acknowledges the hospitality of Nanjing Normal University while working on this manuscript. The work of P.A. and C.B. is also supported with the Australian Research Council Discovery Project grant DP180102209. The work of C.B. was supported by the Australian Research Council through the ARC Centre of Excellence for Particle Physics at the Tera-scale CE110001104. This project was also undertaken with the assistance of resources and services from the National Computational Infrastructure, which is supported by the Australian Government. We thank Astronomy Australia Limited for financial support of computing resources, and the Astronomy Supercomputer Time Allocation Committee for its generous grant of computing time. The work has further been supported by the high-performance computing cluster Taurus at ZIH, TU Dresden. The research placement of D.J. under which this work was done was supported by the Australian Government Research Training Program (RTP) Scholarship and the Deutscher Akademischer Austauschdienst (DAAD) One-Year Research Grant. The work of H.S. and D.S. is supported by DFG grant STO 876/7-1.

JHEP09(2021)080

A General a_μ contributions

Here we collect generic one-loop results for BSM contributions to a_μ. We consider a generic new fermion F, a new scalar S and a new vector field V with masses $m_{F,S,V}$. The muon can have the following general couplings to SM and these BSM particles:

$$\mathcal{L}_{\text{muon}} = \lambda_L \overline{F_R}.S.L + \lambda_R \overline{F_L}.S.\mu + g_L \overline{F_L}\gamma^\nu V_\nu L + g_R \overline{F_R}\gamma^\nu V_\nu \mu + \text{h.c.}, \tag{A.1}$$

where $L = (\nu_{\mu_L}, \mu_L)^T$ corresponds to the $\text{SU}(2)_L$ left-handed lepton doublet, and $\mu = \mu_R^\dagger$ corresponds to the conjugate of the right-handed muon. From this Lagrangian, we can generate 6 generic one-loop contributions, as shown in figure 19, where charge flows from left-to-right and the fermions and scalars in the loop are assumed to have a negative charge. Using these couplings one can calculate (through Package-X in ref. [572])the general one-loop contributions in the $\xi = 1$ (t'Hooft Feynman) gauge of the general R-ξ class of gauges (see ref. [573]) read in the heavy BSM limit $M_{BSM} \gg m_\mu$:

$$a_\mu^{\text{FFS}} = \frac{Q_F m_\mu^2}{16\pi^2 m_S^2}\left(-\frac{2\lambda_L\lambda_R}{3}\frac{m_F}{m_\mu} F\left(\frac{m_F^2}{m_S^2}\right) - \frac{(\lambda_L^2+\lambda_R^2)}{12} E\left(\frac{m_F^2}{m_S^2}\right)\right), \tag{A.2}$$

$$a_\mu^{\text{SSF}} = \frac{Q_S m_\mu^2}{16\pi^2 m_S^2}\left(\frac{\lambda_L\lambda_R}{3}\frac{m_F}{m_\mu} C\left(\frac{m_F^2}{m_S^2}\right) + \frac{(\lambda_L^2+\lambda_R^2)}{12} B\left(\frac{m_F^2}{m_S^2}\right)\right), \tag{A.3}$$

$$a_\mu^{\text{FFV}} = \frac{Q_F m_\mu^2}{16\pi^2 m_V^2}\left(\frac{4(g_L g_R)}{3}\frac{m_F}{m_\mu} C\left(\frac{m_F^2}{m_V^2}\right) - \frac{(g_L^2+g_R^2)}{3} M\left(\frac{m_F^2}{m_V^2}\right)\right), \tag{A.4}$$

$$a_\mu^{\text{VVF}} = \frac{Q_V m_\mu^2}{16\pi^2 m_V^2}\left(-3(g_L g_R)\frac{m_F}{m_\mu} K\left(\frac{m_F^2}{m_V^2}\right) - \frac{(g_L^2+g_R^2)}{6} J\left(\frac{m_F^2}{m_V^2}\right)\right), \tag{A.5}$$

$$a_\mu^{\text{VSF}} = \frac{Q_V m_\mu^2}{16\pi^2 m_V}\left(\frac{(\lambda_R g_L + \lambda_L g_R)}{2m_\mu} N\left(\frac{m_F^2}{m_V^2}, \frac{m_F^2}{m_S^2}\right)\right), \tag{A.6}$$

$$a_\mu^{\text{SVF}} = \frac{Q_V m_\mu^2}{16\pi^2 m_V}\left(\frac{(\lambda_L g_L + \lambda_R g_R)}{2m_\mu} N\left(\frac{m_F^2}{m_V^2}, \frac{m_F^2}{m_S^2}\right)\right). \tag{A.7}$$

The one-loop functions are defined as:[42]

$$B(x) = \frac{2(1-6x+3x^2+2x^3-6x^2\log x)}{(1-x)^4}, \tag{A.8}$$

$$C(x) = \frac{3(1-x^2+2x\log x)}{(1-x)^3}, \tag{A.9}$$

$$E(x) = \frac{2(2+3x-6x^2+x^3+6x\log x)}{(1-x)^4}, \tag{A.10}$$

$$F(x) = \frac{3(-3+4x-x^2-2\log x)}{2(1-x)^3}, \tag{A.11}$$

[42]The loop functions are defined in agreement to loop functions familiar from the MSSM literature, see e.g. ref. [165] also for relationships to further loop functions. The SSF loop functions correspond to MSSM diagrams involving neutralinos and satisfy $B(x) = F_1^N(x)$, $C(x) = F_2^N(x) = 6G_4(x)$. The FFS loop functions correspond to loops involving charginos and satisfy $E(x) = F_1^C(x)$ and $F(x) = F_2^C(x) = 3G_3(x)$.

JHEP09(2021)080

$$J(x) = \frac{7 - 33x + 57x^2 - 31x^3 + 6x^2(3x-1)\log x}{(1-x)^4}, \tag{A.12}$$

$$K(x) = \frac{(1 - 4x + 3x^2 - 2x^2\log x)}{(1-x)^3}, \tag{A.13}$$

$$M(x) = \frac{(4 - 9x + 5x^3 + 6(1-2x)x\log x)}{(1-x)^4}, \tag{A.14}$$

$$N(x,y) = \frac{y}{(y-1)}\frac{x(x-y)^2\log x + (x-1)((x-y)*(y-1) - (x-1)x\log(x/y))}{(1-x)^2(x-y)^2}. \tag{A.15}$$

Here $x = m_F^2/m_S^2$ for FFS and SSF diagrams, $x = m_F^2/m_V^2$ for FFV, VVF, VSF, and SVF diagrams, and $y = m_F^2/m_S^2$ for VSF and SVF diagrams. The above one-loop functions with one argument have the limits $\lim_{x\to 1}\text{OneLoop}(x) = 1$ (Except for $J(x)$, $K(x)$, and $M(x)$ which have the limits 7/5, 2/3, and 3/2) and $\lim_{x\to\infty}\text{OneLoop}(x) = 0$, and have the following limits as $x \to 0$:

$$\lim_{x\to 0} B(x) \to 2, \qquad \lim_{x\to 0} C(x) \to 3, \qquad \lim_{x\to 0} E(x) \to 4, \qquad \lim_{x\to 0} F(x) \to \infty,$$
$$\lim_{x\to 0} J(x) \to 7, \qquad \lim_{x\to 0} K(x) \to 1, \qquad \lim_{x\to 0} M(x) \to 4.$$

The formulas needed e.g. for SUSY diagrams in mass-insertion approximation are given by

$$F_a(x,y) = -\frac{F(x) - F(y)}{3(x-y)}, \tag{A.16a}$$

$$F_b(x,y) = -\frac{C(x) - C(y)}{6(x-y)}, \tag{A.16b}$$

$$\tilde{F}_a(x,y) = -\frac{xF(x) - yF(y)}{3\left(\frac{1}{x} - \frac{1}{y}\right)}. \tag{A.16c}$$

They have the limits $F_a(1,1) = 1/4$ and $F_b(1,1) = \tilde{F}_a(1,1) = 1/12$.

B Details on LHC-constraints on SUSY parameter regions

In section 6.2 we described our procedure for recasting LHC-constraints on the SUSY parameter space; the procedure was then applied in section 6.4 to investigate the impact of LHC-constraints on the SUSY parameter space. Here we provide further details on the recasting.

In figure 20 we illustrate the recasting by reproducing the exclusion contour of the ATLAS chargino/neutralino search of ref. [487], figure 8c. Like in that reference, we have generated MSSM parameter points with mass hierarchy $M_1 < m_{\text{L,R}} < M_2 < \mu$, i.e. Bino-like LSP, intermediate sleptons of the 1st and 2nd generation, and a Wino-like pair of $\chi_2^0/\chi_1^\pm$. We allowed the slepton mass ratio parameter $x = (m_{\text{L,R}} - m_{\chi_1^0})/(m_{\chi_1^\pm} - m_{\chi_1^0})$ to be in the range $1/3 < x < 2/3$, while ref. [487] fixed $x = 1/2$. The thick solid blue contour in our figure 20 corresponds to points where the predicted signal yield for at least one signal

JHEP09(2021)080

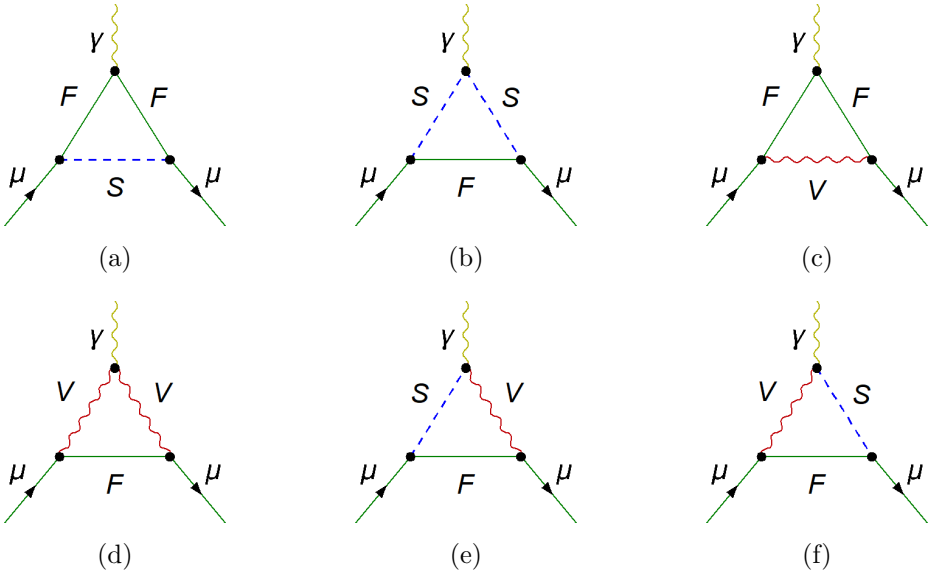

Figure 19. Diagrams producing general contributions to a_μ. Reading left-to-right, top-to-bottom, the FFS diagram 19(a), the SSF diagram 19(b), the FFV diagram 19(c), the VVF diagram 19(d), the VSF diagram 19(e), and the SVF diagram 19(f).

region is equal to the respective ATLAS 95% C.L. upper limit. It can be seen that this contour tracks the corresponding 95% C.L. contour of ref. [487], figure 8c, very well, i.e. to within 50 GeV. To illustrate the gradient we also show the thick dashed blue contour, corresponding to points where the predicted signal yield is three times higher than the respective ATLAS upper limit. Finally we also show blue coloured regions corresponding to different values of the largest effective $(-2\ln\mathcal{L}_{\rm eff})$ of any implemented analysis (in this figure, this is always the 3-lepton channel analysis of ref. [487]). We find that numerically the contour with $(-2\ln\mathcal{L}_{\rm eff})^{\rm Max} = 6$ tracks very well the 95% C.L. contour. We checked that the same would be true for most plots of our section 6.4 (the exceptions are very few cases where such a comparison is not possible because the relevant contribution to $(-2\ln\mathcal{L}_{\rm eff})^{\rm Max}$ comes from the CMS analysis of ref. [482] for compressed spectra, which does not provide individual 95% C.L. upper signal limits).

Figure 20 shows that the recasting reproduces the corresponding original ATLAS exclusion contour very well. On the other hand, several of the scenarios presented in section 6.4, particularly Figures 16(a), and 18 turned out to be entirely unconstrained by the LHC recasting. Hence we present here quantitative results of our recasting analysis, to confirm these statements and to expose further details.[43]

We confirmed that out of all ATLAS and CMS analyses implemented in `GAMBIT/ColliderBit`, the ATLAS electroweakino search of ref. [487] is most sensitive in the parameter regions in figures 16 and 18. Within this ATLAS search, the 3-lepton channel is most sensitive. The 3-lepton channel in turn is divided into 11 signal regions. Hence we will mainly focus on the results for these 11 signal regions in the following.

[43] Our results are compatible with related results of ref. [535] applying the `GAMBIT/ColliderBit` framework on chargino and neutralino searches with heavy sleptons, and we refer to that reference for further explanations of the weak LHC sensitivity to many realistic SUSY scenarios.

JHEP09(2021)080

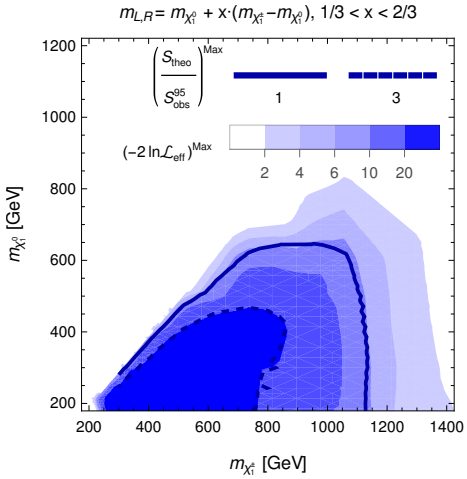

Figure 20. Recasting of the exclusion limits corresponding to ref. [487], figure 8c. The generated MSSM parameter points have the mass hierarchy $M_1 < m_{\mathrm{L,R}} < M_2 < \mu$, i.e. Bino-like LSP, intermediate sleptons of the 1st and 2nd generation, and a Wino-like pair of $\chi_2^0/\chi_1^\pm$. The slepton masses satisfy $x = (m_{\mathrm{L,R}} - m_{\chi_1^0})/(m_{\chi_1^\pm} - m_{\chi_1^0})$ with $1/3 < x < 2/3$. The thick solid blue contour can be directly compared to the 95% C.L. exclusion contour of ref. [487], figure 8c; the thick dashed blue contour corresponds to points where the predicted signal yield is three times higher than the respective ATLAS upper limit in at least one signal region. The blue coloured regions correspond to various values of the maximum effective $(-2\ln\mathcal{L}_{\mathrm{eff}})$ of any analysis implemented in `GAMBIT/ColliderBit`. The plots in section 6.4 show only the region corresponding to $(-2\ln\mathcal{L}_{\mathrm{eff}}) = 6$, which is very close to the line where $\left(S_{\mathrm{theo}}/S_{\mathrm{obs}}^{95\%}\right) \geq 1$ for at least one signal region; see text for more details.

Point	M_1	M_2	μ	$m_{L,R}$	$\ln\mathcal{L}_{\mathrm{eff}}^{\mathrm{ATLAS\_3Lep}}$	$\ln\mathcal{L}_{\mathrm{eff}}^{\mathrm{ATLAS\_2Lep0Jets}}$	$\ln\mathcal{L}_{\mathrm{eff}}^{\mathrm{ATLAS\_2LepPlusJets}}$	$\ln\mathcal{L}_{\mathrm{eff}}^{\mathrm{CMS\_2SSLep}}$	$\ln\mathcal{L}_{\mathrm{eff}}^{\mathrm{CMS\_3Lep}}$
$(\tilde{B}\tilde{l})_1$	200	1200	630	250	−0.45	0.33	0.003	0.002	0.25
$(\tilde{B}\tilde{W}\tilde{H})_1$	200	296	346	700	0.50	0.07	0.04	0.05	−0.24
$(\tilde{B}\tilde{W}\tilde{H})_2$	200	329	388	700	1.05	0.16	−0.37	0.05	−0.35
$(\tilde{H}\tilde{W})_1$	2000	239	162	700	−0.83	0.17	−0.04	−0.04	−0.1
(figure 20)$_1$	500	1039	2000	800	−3.4	−0.2	0	0	−0.13
(figure 20)$_2$	204	350	2000	300	−55.8	−15.9	0	−6.3	−56.9

Table 4. Definitions and basic properties of sample parameter points. The first four points represent the $(\tilde{B}\tilde{l})$-, $(\tilde{B}\tilde{W}\tilde{H})$-, and $(\tilde{H}\tilde{W})$-scenarios and correspond to points in figures 16 and 18 with particularly bad fit to experiment (though not excluded). The last two points represent the excluded region in figure 20. The columns $\ln\mathcal{L}_{\mathrm{eff}}^{\mathrm{analysis}}$ display effective analysis-specific log-likelihood differences obtained by `GAMBIT/ColliderBit` as described in section 6.2 and in ref. [530]. They correspond to the ATLAS analyses of ref. [487] for the 3-lepton, 2-lepton 0-jet and 2-lepton+jets channels, and to the CMS analyses of ref. [520] for the 2-same sign lepton and 3-lepton channels.

Tables 4 and 5 define example SUSY parameter points and present detailed results. The first four parameter points represent the $(\tilde{B}\tilde{l})$-, $(\tilde{B}\tilde{W}\tilde{H})$-, and $(\tilde{H}\tilde{W})$-scenarios. They are examples obtained in a parameter scan with particularly bad fit to experiment, i.e. particularly small likelihood ratio (but they are still not excluded). The other two points represent the excluded region in figure 20 with high or low chargino mass.

JHEP09(2021)080

Region	N_{obs}	N_{exp}	S^{95}_{obs}	$(\tilde{B}\tilde{l})_1$	$(\tilde{B}\tilde{W}\tilde{H})_1$	$(\tilde{B}\tilde{W}\tilde{H})_2$	$(\tilde{H}\tilde{W})_1$	(figure 20)$_1$	(figure 20)$_2$
				S	S	S	S	S	S
				$\ln \mathcal{L}_{\text{SR}}$	$\ln \mathcal{L}_{\text{SR}}$	$\ln \mathcal{L}_{\text{SR}}$	$\ln \mathcal{L}_{\text{SR}}$	$\ln \mathcal{L}_{\text{SR}}$	$\ln \mathcal{L}_{\text{SR}}$
WZ-0Ja	21	21.70 ± 2.90	12.80	0.02	0.41	2.11	1.31	0	8.98
				0.	−0.	−0.11	−0.05	0	−1.33
WZ-0Jb	1	2.70 ± 0.50	3.70	0.03	0.37	**1.47**	**1.24**	0	12.0
				−0.02	−0.23	**−1.0**	**−0.83**	0	−10.2
WZ-0Jc	2	1.60 ± 0.30	4.80	0.12	0.26	0.78	0.53	0.02	10.9
				0.03	0.04	0.02	0.05	0	−6.69
WZ-1Ja	1	2.20 ± 0.50	3.20	0.	0.15	0.33	0.06	0	0.19
				0.	−0.08	−0.18	−0.03	0	−0.1
WZ-1Jb	3	1.80 ± 0.30	5.60	0.11	0.46	1.17	0.54	0	3.55
				0.07	0.22	0.32	0.24	0	−0.28
WZ-1Jc	4	1.30 ± 0.30	7.20	0.13	0.33	**0.87**	0.24	0.03	5.59
				0.21	0.49	**1.05**	0.37	0.05	0.94
slep-a	4	2.20 ± 0.80	6.80	0.12	**1.95**	0.60	0.44	0	13.00
				0.07	**0.50**	0.29	0.22	0	−5.13
slep-b	3	2.80 ± 0.40	5.20	0.11	**2.30**	0.94	0.55	0.10	**76.6**
				0.	**−0.48**	−0.06	−0.	0	**−66.5**
slep-c	9	5.40 ± 0.90	10.50	0.52	0.94	1.30	0.68	0.14	**81.0**
				0.26	0.43	0.54	0.33	0.07	**−55.8**
slep-d	0	1.40 ± 0.40	3.00	0.30	0.39	0.50	0.24	0.35	42.2
				−0.29	−0.38	−0.48	−0.23	−0.34	−42.1
slep-e	0	1.10 ± 0.20	3.30	**0.45**	0.27	0.34	0.24	**3.41**	12.5
				−0.45	−0.27	−0.33	−0.23	**−3.40**	−12.5

Table 5. Detailed results for the sample parameter points defined in table 4 versus the 3-lepton channel of the ATLAS analysis [487]. The first four columns are taken from ref. [487], table 15, and show the names of the signal regions, the observed and expected background yields $N_{\text{obs,exp}}$ as well as the model-independent signal upper limits S^{95}_{obs}. The other columns show for each parameter point the predicted signal yield S and the resulting log-likelihood difference as defined in ref. [530] (the signal uncertainties estimated by `ColliderBit` are at the level of 10% of the signal or less). Numbers highlighted in boldface correspond to the entries with the highest significance and to the entries selected by `ColliderBit` for the overall $\ln \mathcal{L}^{\text{ATLAS\_13TeV\_MultiLEP\_3Lep}}_{\text{eff}}$ of table 4 (selected "on the basis of the signal region *expected* to give the strongest limit" [530]).

The columns $\ln \mathcal{L}^{\text{analysis}}_{\text{eff}}$ of table 4 display effective analysis-specific log-likelihood differences $\ln \mathcal{L}^{\text{analysis}}_{\text{eff}} \equiv \ln \mathcal{L}^{\text{analysis}}_{\text{SR}^{\text{max}}}$, where SR^{max} denotes the signal region of the respective analysis with the highest expected sensitivity, see section 6.2 and ref. [530]. The analyses are the ATLAS analyses of ref. [487] for the 3-lepton, 2-lepton 0-jet and 2-lepton+jets channels, and to the CMS analyses of ref. [520] for the 2-same sign lepton and 3-lepton channels. The table shows that the ATLAS and CMS 3-lepton channels are most sensitive for all parameter points.

JHEP09(2021)080

Table 5 shows the results obtained by `ColliderBit` for the 11 invidual signal regions of the ATLAS 3-lepton analysis and compares to the ATLAS results. The most important observation is that all signal yield predictions of the first four parameter points are far smaller than the ATLAS signal 95% C.L. upper limits. The entries which come relatively closest, i.e. which lead to the smallest negative log-likelihood difference, are highlighted in boldface. A second observation is that these entries are not always identical to the ones selected by `ColliderBit` for evaluating the effective log-likelihood difference for the next-to-last column of table 4. The reason [530] is that the selection is done assuming that the observed counts match the background expectation; however for the WZ-1Jc and slep-a signal regions this assumption is not true ($N_{\text{obs}} : N_{\text{exp}} = 4 : 1.3 \pm 0.3$ and $N_{\text{obs}} : N_{\text{exp}} = 4 : 2.2 \pm 0.8$ respectively).

On the other hand, for the two parameter points of the excluded region in figure 20 we observe that the high-mass point is indeed excluded by the slep-e signal region, and the low-mass point is excluded by a variety of signal regions by a large margin.

References

[1] Muon g-2 collaboration, *Muon* $(g-2)$ *technical design report*, arXiv:1501.06858 [INSPIRE].

[2] Muon g-2 collaboration, *Measurement of the positive muon anomalous magnetic moment to* 0.46 *ppm*, *Phys. Rev. Lett.* **126** (2021) 141801 [arXiv:2104.03281] [INSPIRE].

[3] Muon g-2 collaboration, *Final report of the muon E821 anomalous magnetic moment measurement at BNL*, *Phys. Rev. D* **73** (2006) 072003 [hep-ex/0602035] [INSPIRE].

[4] T. Aoyama et al., *The anomalous magnetic moment of the muon in the standard model*, *Phys. Rept.* **887** (2020) 1 [arXiv:2006.04822] [INSPIRE].

[5] T. Aoyama, M. Hayakawa, T. Kinoshita and M. Nio, *Complete tenth-order QED contribution to the muon* $g-2$, *Phys. Rev. Lett.* **109** (2012) 111808 [arXiv:1205.5370] [INSPIRE].

[6] T. Aoyama, T. Kinoshita and M. Nio, *Theory of the anomalous magnetic moment of the electron*, *Atoms* **7** (2019) 28 [INSPIRE].

[7] A. Czarnecki, W.J. Marciano and A. Vainshtein, *Refinements in electroweak contributions to the muon anomalous magnetic moment*, *Phys. Rev. D* **67** (2003) 073006 [*Erratum ibid.* **73** (2006) 119901] [hep-ph/0212229] [INSPIRE].

[8] C. Gnendiger, D. Stöckinger and H. Stöckinger-Kim, *The electroweak contributions to* $(g-2)_\mu$ *after the Higgs boson mass measurement*, *Phys. Rev. D* **88** (2013) 053005 [arXiv:1306.5546] [INSPIRE].

[9] M. Davier, A. Hoecker, B. Malaescu and Z. Zhang, *Reevaluation of the hadronic vacuum polarisation contributions to the Standard Model predictions of the muon* $g-2$ *and* $\alpha(m_Z^2)$ *using newest hadronic cross-section data*, *Eur. Phys. J. C* **77** (2017) 827 [arXiv:1706.09436] [INSPIRE].

JHEP09(2021)080

[10] A. Keshavarzi, D. Nomura and T. Teubner, *Muon $g-2$ and $\alpha(M_Z^2)$: a new data-based analysis*, *Phys. Rev. D* **97** (2018) 114025 [arXiv:1802.02995] [INSPIRE].

[11] G. Colangelo, M. Hoferichter and P. Stoffer, *Two-pion contribution to hadronic vacuum polarization*, *JHEP* **02** (2019) 006 [arXiv:1810.00007] [INSPIRE].

[12] M. Hoferichter, B.-L. Hoid and B. Kubis, *Three-pion contribution to hadronic vacuum polarization*, *JHEP* **08** (2019) 137 [arXiv:1907.01556] [INSPIRE].

[13] M. Davier, A. Hoecker, B. Malaescu and Z. Zhang, *A new evaluation of the hadronic vacuum polarisation contributions to the muon anomalous magnetic moment and to $\alpha(m_Z^2)$*, *Eur. Phys. J. C* **80** (2020) 241 [*Erratum ibid.* **80** (2020) 410] [arXiv:1908.00921] [INSPIRE].

[14] A. Keshavarzi, D. Nomura and T. Teubner, *$g-2$ of charged leptons, $\alpha(M_Z^2)$, and the hyperfine splitting of muonium*, *Phys. Rev. D* **101** (2020) 014029 [arXiv:1911.00367] [INSPIRE].

[15] A. Kurz, T. Liu, P. Marquard and M. Steinhauser, *Hadronic contribution to the muon anomalous magnetic moment to next-to-next-to-leading order*, *Phys. Lett. B* **734** (2014) 144 [arXiv:1403.6400] [INSPIRE].

[16] K. Melnikov and A. Vainshtein, *Hadronic light-by-light scattering contribution to the muon anomalous magnetic moment revisited*, *Phys. Rev. D* **70** (2004) 113006 [hep-ph/0312226] [INSPIRE].

[17] P. Masjuan and P. Sanchez-Puertas, *Pseudoscalar-pole contribution to the $(g_\mu-2)$: a rational approach*, *Phys. Rev. D* **95** (2017) 054026 [arXiv:1701.05829] [INSPIRE].

[18] G. Colangelo, M. Hoferichter, M. Procura and P. Stoffer, *Dispersion relation for hadronic light-by-light scattering: two-pion contributions*, *JHEP* **04** (2017) 161 [arXiv:1702.07347] [INSPIRE].

[19] M. Hoferichter, B.-L. Hoid, B. Kubis, S. Leupold and S.P. Schneider, *Dispersion relation for hadronic light-by-light scattering: pion pole*, *JHEP* **10** (2018) 141 [arXiv:1808.04823] [INSPIRE].

[20] A. Gérardin, H.B. Meyer and A. Nyffeler, *Lattice calculation of the pion transition form factor with $N_f = 2+1$ Wilson quarks*, *Phys. Rev. D* **100** (2019) 034520 [arXiv:1903.09471] [INSPIRE].

[21] J. Bijnens, N. Hermansson-Truedsson and A. Rodríguez-Sánchez, *Short-distance constraints for the HLbL contribution to the muon anomalous magnetic moment*, *Phys. Lett. B* **798** (2019) 134994 [arXiv:1908.03331] [INSPIRE].

[22] G. Colangelo, F. Hagelstein, M. Hoferichter, L. Laub and P. Stoffer, *Longitudinal short-distance constraints for the hadronic light-by-light contribution to $(g-2)_\mu$ with large-N_c Regge models*, *JHEP* **03** (2020) 101 [arXiv:1910.13432] [INSPIRE].

[23] V. Pauk and M. Vanderhaeghen, *Single meson contributions to the muon's anomalous magnetic moment*, *Eur. Phys. J. C* **74** (2014) 3008 [arXiv:1401.0832] [INSPIRE].

[24] I. Danilkin and M. Vanderhaeghen, *Light-by-light scattering sum rules in light of new data*, *Phys. Rev. D* **95** (2017) 014019 [arXiv:1611.04646] [INSPIRE].

[25] F. Jegerlehner, *The anomalous magnetic moment of the muon*, *Springer Tracts Modern Physics volume 274*, Springer, Germany (2017).

JHEP09(2021)080

[26] M. Knecht, S. Narison, A. Rabemananjara and D. Rabetiarivony, *Scalar meson contributions to a μ from hadronic light-by-light scattering*, *Phys. Lett. B* **787** (2018) 111 [arXiv:1808.03848] [INSPIRE].

[27] G. Eichmann, C.S. Fischer and R. Williams, *Kaon-box contribution to the anomalous magnetic moment of the muon*, *Phys. Rev. D* **101** (2020) 054015 [arXiv:1910.06795] [INSPIRE].

[28] P. Roig and P. Sanchez-Puertas, *Axial-vector exchange contribution to the hadronic light-by-light piece of the muon anomalous magnetic moment*, *Phys. Rev. D* **101** (2020) 074019 [arXiv:1910.02881] [INSPIRE].

[29] T. Blum, N. Christ, M. Hayakawa, T. Izubuchi, L. Jin, C. Jung et al., *Hadronic light-by-light scattering contribution to the muon anomalous magnetic moment from lattice QCD*, *Phys. Rev. Lett.* **124** (2020) 132002 [arXiv:1911.08123] [INSPIRE].

[30] G. Colangelo, M. Hoferichter, A. Nyffeler, M. Passera and P. Stoffer, *Remarks on higher-order hadronic corrections to the muon $g-2$*, *Phys. Lett. B* **735** (2014) 90 [arXiv:1403.7512] [INSPIRE].

[31] Fermilab Lattice, LATTICE-HPQCD, MILC collaboration, *Strong-isospin-breaking correction to the muon anomalous magnetic moment from lattice QCD at the physical point*, *Phys. Rev. Lett.* **120** (2018) 152001 [arXiv:1710.11212] [INSPIRE].

[32] Budapest-Marseille-Wuppertal collaboration, *Hadronic vacuum polarization contribution to the anomalous magnetic moments of leptons from first principles*, *Phys. Rev. Lett.* **121** (2018) 022002 [arXiv:1711.04980] [INSPIRE].

[33] RBC, UKQCD collaboration, *Calculation of the hadronic vacuum polarization contribution to the muon anomalous magnetic moment*, *Phys. Rev. Lett.* **121** (2018) 022003 [arXiv:1801.07224] [INSPIRE].

[34] D. Giusti, V. Lubicz, G. Martinelli, F. Sanfilippo and S. Simula, *Electromagnetic and strong isospin-breaking corrections to the muon $g-2$ from lattice QCD+QED*, *Phys. Rev. D* **99** (2019) 114502 [arXiv:1901.10462] [INSPIRE].

[35] PACS collaboration, *Hadronic vacuum polarization contribution to the muon $g-2$ with $2+1$ flavor lattice QCD on a larger than $(10\,fm)^4$ lattice at the physical point*, *Phys. Rev. D* **100** (2019) 034517 [arXiv:1902.00885] [INSPIRE].

[36] Fermilab Lattice, LATTICE-HPQCD, MILC collaboration, *Hadronic-vacuum-polarization contribution to the muon's anomalous magnetic moment from four-flavor lattice QCD*, *Phys. Rev. D* **101** (2020) 034512 [arXiv:1902.04223] [INSPIRE].

[37] A. Gérardin et al., *The leading hadronic contribution to $(g-2)_\mu$ from lattice QCD with $N_f = 2+1$ flavours of $O(a)$ improved Wilson quarks*, *Phys. Rev. D* **100** (2019) 014510 [arXiv:1904.03120] [INSPIRE].

[38] C. Aubin, T. Blum, C. Tu, M. Golterman, C. Jung and S. Peris, *Light quark vacuum polarization at the physical point and contribution to the muon $g-2$*, *Phys. Rev. D* **101** (2020) 014503 [arXiv:1905.09307] [INSPIRE].

[39] D. Giusti and S. Simula, *Lepton anomalous magnetic moments in Lattice QCD+QED*, PoS(LATTICE2019)104 [arXiv:1910.03874] [INSPIRE].

[40] S. Borsányi et al., *Leading hadronic contribution to the muon magnetic moment from lattice QCD*, *Nature* **593** (2021) 51 [arXiv:2002.12347] [INSPIRE].

JHEP09(2021)080

[41] C. Lehner and A.S. Meyer, *Consistency of hadronic vacuum polarization between lattice QCD and the R-ratio*, *Phys. Rev. D* **101** (2020) 074515 [arXiv:2003.04177] [INSPIRE].

[42] G. Colangelo, M. Hoferichter and P. Stoffer, *Constraints on the two-pion contribution to hadronic vacuum polarization*, *Phys. Lett. B* **814** (2021) 136073 [arXiv:2010.07943] [INSPIRE].

[43] P. Athron, J.-h. Park, D. Stöckinger and A. Voigt, *FlexibleSUSY — A spectrum generator generator for supersymmetric models*, *Comput. Phys. Commun.* **190** (2015) 139 [arXiv:1406.2319] [INSPIRE].

[44] P. Athron et al., *FlexibleSUSY 2.0: extensions to investigate the phenomenology of SUSY and non-SUSY models*, *Comput. Phys. Commun.* **230** (2018) 145 [arXiv:1710.03760] [INSPIRE].

[45] P. Athron et al., *GM2Calc: precise MSSM prediction for* $(g-2)$ *of the muon*, *Eur. Phys. J. C* **76** (2016) 62 [arXiv:1510.08071] [INSPIRE].

[46] K. Melnikov and A. Vainshtein, *Theory of the muon anomalous magnetic moment*, Springer, Germany (2006) [INSPIRE].

[47] F. Jegerlehner and A. Nyffeler, *The Muon g-2*, *Phys. Rept.* **477** (2009) 1 [arXiv:0902.3360] [INSPIRE].

[48] A. Czarnecki and W.J. Marciano, *The muon anomalous magnetic moment: a harbinger for 'new physics'*, *Phys. Rev. D* **64** (2001) 013014 [hep-ph/0102122] [INSPIRE].

[49] D. Stöckinger, *The muon magnetic moment and supersymmetry*, *J. Phys. G* **34** (2007) R45 [hep-ph/0609168] [INSPIRE].

[50] D. Stöckinger, *Muon* $(g-2)$ *and physics beyond the standard model*, *Adv. Ser. Direct. High Energy Phys.* **20** (2009) 393 [INSPIRE].

[51] M. Lindner, M. Platscher and F.S. Queiroz, *A call for new physics: the muon anomalous magnetic moment and lepton flavor violation*, *Phys. Rept.* **731** (2018) 1 [arXiv:1610.06587] [INSPIRE].

[52] R.L. Arnowitt, B. Dutta, B. Hu and Y. Santoso, *Muon* $g-2$*, dark matter detection and accelerator physics*, *Phys. Lett. B* **505** (2001) 177 [hep-ph/0102344] [INSPIRE].

[53] A. Czarnecki and W.J. Marciano, *The Muon anomalous magnetic moment: A Harbinger for 'new physics'*, *Phys. Rev. D* **64** (2001) 013014 [hep-ph/0102122] [INSPIRE].

[54] E.A. Baltz and P. Gondolo, *Implications of muon anomalous magnetic moment for supersymmetric dark matter*, *Phys. Rev. Lett.* **86** (2001) 5004 [hep-ph/0102147] [INSPIRE].

[55] L.L. Everett, G.L. Kane, S. Rigolin and L.-T. Wang, *Implications of muon g-2 for supersymmetry and for discovering superpartners directly*, *Phys. Rev. Lett.* **86** (2001) 3484 [hep-ph/0102145] [INSPIRE].

[56] J.L. Feng and K.T. Matchev, *Supersymmetry and the anomalous magnetic moment of the muon*, *Phys. Rev. Lett.* **86** (2001) 3480 [hep-ph/0102146] [INSPIRE].

[57] U. Chattopadhyay and P. Nath, *Upper limits on sparticle masses from g-2 and the possibility for discovery of SUSY at colliders and in dark matter searches*, *Phys. Rev. Lett.* **86** (2001) 5854 [hep-ph/0102157] [INSPIRE].

[58] D. Choudhury, B. Mukhopadhyaya and S. Rakshit, *Muon anomalous magnetic moment confronts exotic fermions and gauge bosons*, *Phys. Lett. B* **507** (2001) 219 [hep-ph/0102199] [INSPIRE].

JHEP09(2021)080

[59] S. Komine, T. Moroi and M. Yamaguchi, *Recent result from E821 experiment on muon $g-2$ and unconstrained minimal supersymmetric standard model*, *Phys. Lett. B* **506** (2001) 93 [hep-ph/0102204] [INSPIRE].

[60] U. Mahanta, *Constraining new physics in the TeV range by the recent BNL measurement of $(g-2)\mu$*, *Phys. Lett. B* **511** (2001) 235 [hep-ph/0102211] [INSPIRE].

[61] P. Das, S. Kumar Rai and S. Raychaudhuri, *Anomalous magnetic moment of the muon in a composite model*, hep-ph/0102242 [INSPIRE].

[62] K.-m. Cheung, *Muon anomalous magnetic moment and leptoquark solutions*, *Phys. Rev. D* **64** (2001) 033001 [hep-ph/0102238] [INSPIRE].

[63] T.W. Kephart and H. Pas, *Muon anomalous magnetic moment in string inspired extended family models*, *Phys. Rev. D* **65** (2002) 093014 [hep-ph/0102243] [INSPIRE].

[64] E. Ma and M. Raidal, *Neutrino mass, muon anomalous magnetic moment, and lepton flavor nonconservation*, *Phys. Rev. Lett.* **87** (2001) 011802 [*Erratum ibid.* **87** (2001) 159901] [hep-ph/0102255] [INSPIRE].

[65] J. Hisano and K. Tobe, *Neutrino masses, muon $g-2$, and lepton flavor violation in the supersymmetric seesaw model*, *Phys. Lett. B* **510** (2001) 197 [hep-ph/0102315] [INSPIRE].

[66] Z.-z. Xing, *Nearly bimaximal neutrino mixing, muon $g-2$ anomaly and lepton flavor violating processes*, *Phys. Rev. D* **64** (2001) 017304 [hep-ph/0102304] [INSPIRE].

[67] T. Ibrahim, U. Chattopadhyay and P. Nath, *Constraints on explicit CP-violation from the Brookhaven muon $g-2$ experiment*, *Phys. Rev. D* **64** (2001) 016010 [hep-ph/0102324] [INSPIRE].

[68] J.R. Ellis, D.V. Nanopoulos and K.A. Olive, *Combining the muon anomalous magnetic moment with other constraints on the CMSSM*, *Phys. Lett. B* **508** (2001) 65 [hep-ph/0102331] [INSPIRE].

[69] A. Dedes and H.E. Haber, *A light higgs boson explanation for the $g-2$ crisis*, in the proceedings of the 36th *Rencontres de Moriond on Electroweak Interactions and Unified Theories*, March 10–17, Les Arcs, France (2001) [hep-ph/0105014] [INSPIRE].

[70] M.B. Einhorn and J. Wudka, *Model independent analysis of g(muon)−2*, *Phys. Rev. Lett.* **87** (2001) 071805 [hep-ph/0103034] [INSPIRE].

[71] K. Choi, K. Hwang, S.K. Kang, K.Y. Lee and W.Y. Song, *Probing the messenger of supersymmetry breaking by the muon anomalous magnetic moment*, *Phys. Rev. D* **64** (2001) 055001 [hep-ph/0103048] [INSPIRE].

[72] S.K. Kang and K.Y. Lee, *Implications of the muon anomalous magnetic moment and Higgs mediated flavor changing neutral currents*, *Phys. Lett. B* **521** (2001) 61 [hep-ph/0103064] [INSPIRE].

[73] J.E. Kim, B. Kyae and H.M. Lee, *Effective supersymmetric theory and (g-2)(muon with R-parity violation*, *Phys. Lett. B* **520** (2001) 298 [hep-ph/0103054] [INSPIRE].

[74] S.P. Martin and J.D. Wells, *Muon anomalous magnetic dipole moment in supersymmetric theories*, *Phys. Rev. D* **64** (2001) 035003 [hep-ph/0103067] [INSPIRE].

[75] S. Rajpoot, *Muon anomalous magnetic moment in models with singlet fermions*, hep-ph/0103069 [INSPIRE].

[76] C.A. de S. Pires and P.S. Rodrigues da Silva, *Scalar scenarios contributing to $(g-2)$(muon) with enhanced Yukawa couplings*, *Phys. Rev. D* **64** (2001) 117701 [hep-ph/0103083] [INSPIRE].

JHEP09(2021)080

[77] S. Komine, T. Moroi and M. Yamaguchi, *No scale scenarios in the light of new measurement of muon anomalous magnetic moment*, *Phys. Lett. B* **507** (2001) 224 [hep-ph/0103182] [INSPIRE].

[78] K.-m. Cheung, C.-H. Chou and O.C.W. Kong, *Muon anomalous magnetic moment, two Higgs doublet model, and supersymmetry*, *Phys. Rev. D* **64** (2001) 111301 [hep-ph/0103183] [INSPIRE].

[79] S. Baek, P. Ko and H.S. Lee, *Muon anomalous magnetic moment, $B \to X_s\gamma$ and dark matter detection in the string models with dilaton domination*, *Phys. Rev. D* **65** (2002) 035004 [hep-ph/0103218] [INSPIRE].

[80] M. Raidal, *Enhancement of radiatively induced magnetic moment form-factors of muon: an effective lagrangian approach*, *Phys. Lett. B* **508** (2001) 51 [hep-ph/0103224] [INSPIRE].

[81] D.F. Carvalho, J.R. Ellis, M.E. Gomez and S. Lola, *Charged lepton flavor violation in the CMSSM in view of the muon anomalous magnetic moment*, *Phys. Lett. B* **515** (2001) 323 [hep-ph/0103256] [INSPIRE].

[82] H. Baer, C. Balázs, J. Ferrandis and X. Tata, *Impact of muon anomalous magnetic moment on supersymmetric models*, *Phys. Rev. D* **64** (2001) 035004 [hep-ph/0103280] [INSPIRE].

[83] Z. Chacko and G.D. Kribs, *Constraints on lepton flavor violation in the MSSM from the muon anomalous magnetic moment measurement*, *Phys. Rev. D* **64** (2001) 075015 [hep-ph/0104317] [INSPIRE].

[84] Y.-L. Wu and Y.-F. Zhou, *Muon anomalous magnetic moment in the standard model with two Higgs doublets*, *Phys. Rev. D* **64** (2001) 115018 [hep-ph/0104056] [INSPIRE].

[85] S. Baek, T. Goto, Y. Okada and K.-i. Okumura, *Muon anomalous magnetic moment, lepton flavor violation, and flavor changing neutral current processes in SUSY GUT with right-handed neutrino*, *Phys. Rev. D* **64** (2001) 095001 [hep-ph/0104146] [INSPIRE].

[86] C.-H. Chen and C.Q. Geng, *The Muon anomalous magnetic moment from a generic charged Higgs with SUSY*, *Phys. Lett. B* **511** (2001) 77 [hep-ph/0104151] [INSPIRE].

[87] A. Arhrib and S. Baek, *Two loop Barr-Zee type contributions to $(g-2)$(muon) in the MSSM*, *Phys. Rev. D* **65** (2002) 075002 [hep-ph/0104225] [INSPIRE].

[88] K. Enqvist, E. Gabrielli and K. Huitu, *$g-2$ of the muon in SUSY models with gauge multiplets in the bulk of extra dimensions*, *Phys. Lett. B* **512** (2001) 107 [hep-ph/0104174] [INSPIRE].

[89] D.G. Cerdeno, E. Gabrielli, S. Khalil, C. Muñoz and E. Torrente-Lujan, *Muon anomalous magnetic moment in supersymmetric scenarios with an intermediate scale and nonuniversality*, *Phys. Rev. D* **64** (2001) 093012 [hep-ph/0104242] [INSPIRE].

[90] Y.G. Kim and M.M. Nojiri, *Implications of muon anomalous magnetic moment for direct detection of neutralino dark matter*, *Prog. Theor. Phys.* **106** (2001) 561 [hep-ph/0104258] [INSPIRE].

[91] T. Blazek and S.F. King, *Muon anomalous magnetic moment and $\tau \to \mu\gamma$ in a realistic string inspired model of neutrino masses*, *Phys. Lett. B* **518** (2001) 109 [hep-ph/0105005] [INSPIRE].

[92] G.-C. Cho and K. Hagiwara, *Supersymmetric contributions to muon $g-2$ and the electroweak precision measurements*, *Phys. Lett. B* **514** (2001) 123 [hep-ph/0105037] [INSPIRE].

JHEP09(2021)080

[93] S. Barshay and G. Kreyerhoff, *Stronger neutrino interactions at extremely high-energies and the muon anomalous magnetic moment*, *Eur. Phys. J. C* **23** (2002) 191 [hep-ph/0106047] [INSPIRE].

[94] R.L. Arnowitt, B. Dutta and Y. Santoso, *SUSY phases, the electron electric dipole moment and the muon magnetic moment*, *Phys. Rev. D* **64** (2001) 113010 [hep-ph/0106089] [INSPIRE].

[95] G. Bélanger, F. Boudjema, A. Cottrant, R.M. Godbole and A. Semenov, *The MSSM invisible Higgs in the light of dark matter and* $g-2$, *Phys. Lett. B* **519** (2001) 93 [hep-ph/0106275] [INSPIRE].

[96] W. de Boer, M. Huber, C. Sander and D.I. Kazakov, *A Global fit to the anomalous magnetic moment,* $b \to X_s\gamma$ *and Higgs limits in the constrained MSSM*, hep-ph/0106311 [INSPIRE].

[97] L. Roszkowski, R. Ruiz de Austri and T. Nihei, *New cosmological and experimental constraints on the CMSSM*, *JHEP* **08** (2001) 024 [hep-ph/0106334] [INSPIRE].

[98] Y. Daikoku, *Muon anomalous magnetic dipole moment in the* μ *problem solvable extra* U(1) *models*, hep-ph/0107305 [INSPIRE].

[99] R. Adhikari, E. Ma and G. Rajasekaran, *Supersymmetric model of muon anomalous magnetic moment and neutrino masses*, *Phys. Rev. D* **65** (2002) 077703 [hep-ph/0108167] [INSPIRE].

[100] X.-J. Wang and M.-L. Yan, *Noncommutative QED and muon anomalous magnetic moment*, *JHEP* **03** (2002) 047 [hep-th/0109095] [INSPIRE].

[101] W. de Boer, M. Huber, C. Sander and D.I. Kazakov, *A global fit to the anomalous magnetic moment,* $b \to X/s\gamma$ *and Higgs limits in the constrained MSSM*, *Phys. Lett. B* **515** (2001) 283 [INSPIRE].

[102] N. Kersting, *Muon* $g-2$ *from noncommutative geometry*, *Phys. Lett. B* **527** (2002) 115 [hep-ph/0109224] [INSPIRE].

[103] Y.-F. Zhou and Y.-L. Wu, *Lepton flavor changing scalar interactions and muon* $g-2$, *Eur. Phys. J. C* **27** (2003) 577 [hep-ph/0110302] [INSPIRE].

[104] M. Endo and T. Moroi, *Muon magnetic dipole moment and Higgs mass in supersymmetric* SU(5) *models*, *Phys. Lett. B* **525** (2002) 121 [hep-ph/0110383] [INSPIRE].

[105] G. Cacciapaglia, M. Cirelli and G. Cristadoro, *Muon anomalous magnetic moment in a calculable model with one extra dimension*, *Nucl. Phys. B* **634** (2002) 230 [hep-ph/0111288] [INSPIRE].

[106] E. Ma and D.P. Roy, *Anomalous neutrino interaction, muon* $g-2$, *and atomic parity nonconservation*, *Phys. Rev. D* **65** (2002) 075021 [hep-ph/0111385] [INSPIRE].

[107] G.-C. Cho, N. Haba and J. Hisano, *The Stau exchange contribution to muon* $g-2$ *in the decoupling solution*, *Phys. Lett. B* **529** (2002) 117 [hep-ph/0112163] [INSPIRE].

[108] S.C. Park and H.S. Song, *Muon anomalous magnetic moment and the stabilized Randall-Sundrum scenario*, *Phys. Lett. B* **506** (2001) 99 [hep-ph/0103072] [INSPIRE].

[109] C.S. Kim, J.D. Kim and J.-H. Song, *Muon anomalous magnetic moment* $(g-2)$*(muon) and the Randall-Sundrum model*, *Phys. Lett. B* **511** (2001) 251 [hep-ph/0103127] [INSPIRE].

[110] K. Agashe, N.G. Deshpande and G.H. Wu, *Can extra dimensions accessible to the SM explain the recent measurement of anomalous magnetic moment of the muon?*, *Phys. Lett. B* **511** (2001) 85 [hep-ph/0103235] [INSPIRE].

JHEP09(2021)080

[111] X. Calmet and A. Neronov, *Kaluza-Klein theories and the anomalous magnetic moment of the muon*, *Phys. Rev. D* **65** (2002) 067702 [hep-ph/0104278] [INSPIRE].

[112] T. Appelquist and B.A. Dobrescu, *Universal extra dimensions and the muon magnetic moment*, *Phys. Lett. B* **516** (2001) 85 [hep-ph/0106140] [INSPIRE].

[113] P.K. Das, *Muon anomalous magnetic moment and a lower bound on Higgs mass due to stabilized radion in the Randall-Sundrum model*, *Int. J. Mod. Phys. A* **21** (2006) 5205 [hep-ph/0407041] [INSPIRE].

[114] Z.-H. Xiong and J.M. Yang, *Muon anomalous magnetic moment in technicolor models*, *Phys. Lett. B* **508** (2001) 295 [hep-ph/0102259] [INSPIRE].

[115] X. Calmet, H. Fritzsch and D. Holtmannspotter, *The anomalous magnetic moment of the muon and radiative lepton decays*, *Phys. Rev. D* **64** (2001) 037701 [hep-ph/0103012] [INSPIRE].

[116] Y.-B. Dai, C.-S. Huang and A. Zhang, $g-2$ *in composite models of leptons*, *J. Phys. G* **28** (2002) 139 [hep-ph/0103317] [INSPIRE].

[117] C.-x. Yue, Q.-j. Xu and G.-l. Liu, *Topcolor assisted technicolor models and muon anomalous magnetic moment*, *J. Phys. G* **27** (2001) 1807 [hep-ph/0103084] [INSPIRE].

[118] F. Tabbakh, J.-J. Liu and W.-G. Ma, *Muon* $g-2$ *in the littlest Higgs model*, *Commun. Theor. Phys.* **45** (2006) 894 [INSPIRE].

[119] M. Blanke, A.J. Buras, B. Duling, A. Poschenrieder and C. Tarantino, *Charged lepton flavour violation and* $(g-2)(\mu)$ *in the littlest Higgs model with T-parity: a clear distinction from supersymmetry*, *JHEP* **05** (2007) 013 [hep-ph/0702136] [INSPIRE].

[120] E.O. Iltan and H. Sundu, *Anomalous magnetic moment of muon in the general two Higgs doublet model*, *Acta Phys. Slov.* **53** (2003) 17 [hep-ph/0103105] [INSPIRE].

[121] M. Krawczyk, *The new* $(g-2)$ *for muon measurement and limits on the light Higgs bosons in 2HDM (II)*, hep-ph/0103223 [INSPIRE].

[122] F. Larios, G. Tavares-Velasco and C.P. Yuan, *A very light CP odd scalar in the two Higgs doublet model*, *Phys. Rev. D* **64** (2001) 055004 [hep-ph/0103292] [INSPIRE].

[123] M. Krawczyk, *Precision muon g-2 results and light Higgs bosons in the 2HDM(II)*, *Acta Phys. Polon. B* **33** (2002) 2621 [hep-ph/0208076] [INSPIRE].

[124] D. Chakraverty, D. Choudhury and A. Datta, *A nonsupersymmetric resolution of the anomalous muon magnetic moment*, *Phys. Lett. B* **506** (2001) 103 [hep-ph/0102180] [INSPIRE].

[125] U. Mahanta, *Implications of BNL measurement of* $\delta a(\mu)$ *on a class of scalar leptoquark interactions*, *Eur. Phys. J. C* **21** (2001) 171 [hep-ph/0102176] [INSPIRE].

[126] T. Huang, Z.H. Lin, L.Y. Shan and X. Zhang, *Muon anomalous magnetic moment and lepton flavor violation*, *Phys. Rev. D* **64** (2001) 071301 [hep-ph/0102193] [INSPIRE].

[127] S.N. Gninenko and N.V. Krasnikov, *The muon anomalous magnetic moment and a new light gauge boson*, *Phys. Lett. B* **513** (2001) 119 [hep-ph/0102222] [INSPIRE].

[128] K.R. Lynch, *Extended electroweak interactions and the muon* $g-2$, *Phys. Rev. D* **65** (2002) 053006 [hep-ph/0108080] [INSPIRE].

[129] S. Baek, N.G. Deshpande, X.G. He and P. Ko, *Muon anomalous* $g-2$ *and gauged L(muon)–L(tau) models*, *Phys. Rev. D* **64** (2001) 055006 [hep-ph/0104141] [INSPIRE].

JHEP09(2021)080

[130] E. Ma, D.P. Roy and S. Roy, *Gauged L(mu)–L(tau) with large muon anomalous magnetic moment and the bimaximal mixing of neutrinos*, *Phys. Lett. B* **525** (2002) 101 [hep-ph/0110146] [INSPIRE].

[131] B. Murakami, *The Impact of lepton flavor violating Z' bosons on muon $g-2$ and other muon observables*, *Phys. Rev. D* **65** (2002) 055003 [hep-ph/0110095] [INSPIRE].

[132] M. Pospelov, *Secluded* U(1) *below the weak scale*, *Phys. Rev. D* **80** (2009) 095002 [arXiv:0811.1030] [INSPIRE].

[133] J.H. Heo, *About a peculiar* U(1)*: Z' discovery limit, muon anomalous magnetic moment, Electron electric dipole moment*, *Phys. Rev. D* **80** (2009) 033001 [arXiv:0811.0298] [INSPIRE].

[134] C.-S. Huang and W. Liao, *$(g-2)(\mu)$ and CP asymmetries in $B^0(d,s) \to \ell^+\ell^-$ and $b \to s\gamma$ in SUSY models*, *Phys. Lett. B* **538** (2002) 301 [hep-ph/0201121] [INSPIRE].

[135] E. Kiritsis and P. Anastasopoulos, *The anomalous magnetic moment of the muon in the D-brane realization of the standard model*, *JHEP* **05** (2002) 054 [hep-ph/0201295] [INSPIRE].

[136] P. Das and U. Mahanta, *Testable muon $g-2$ contribution due to a light stabilized radion in the Randall-Sundrum model*, *Nucl. Phys. B* **644** (2002) 395 [hep-ph/0202193] [INSPIRE].

[137] S. Baek, P. Ko and J.-h. Park, *Muon anomalous magnetic moment from effective supersymmetry*, *Eur. Phys. J. C* **24** (2002) 613 [hep-ph/0203251] [INSPIRE].

[138] U. Chattopadhyay and P. Nath, *Interpreting the new Brookhaven muon $(g-2)$ result*, *Phys. Rev. D* **66** (2002) 093001 [hep-ph/0208012] [INSPIRE].

[139] M. Byrne, C. Kolda and J.E. Lennon, *Updated implications of the muon anomalous magnetic moment for supersymmetry*, *Phys. Rev. D* **67** (2003) 075004 [hep-ph/0208067] [INSPIRE].

[140] Y.G. Kim, T. Nihei, L. Roszkowski and R. Ruiz de Austri, *Upper and lower limits on neutralino WIMP mass and spin independent scattering cross-section, and impact of new (g-2)(mu) measurement*, *JHEP* **12** (2002) 034 [hep-ph/0208069] [INSPIRE].

[141] S. Baek, P. Ko and W.Y. Song, *SUSY breaking mediation mechanisms and $(g-2)(\mu)$, $B \to X_s\gamma$, $B \to X_s\ell^+\ell^-$ and $B_s \to \mu^+\mu^-$*, *JHEP* **03** (2003) 054 [hep-ph/0208112] [INSPIRE].

[142] S.P. Martin and J.D. Wells, *Superconservative interpretation of muon $g-2$ results applied to supersymmetry*, *Phys. Rev. D* **67** (2003) 015002 [hep-ph/0209309] [INSPIRE].

[143] G.G. Boyarkina and O.M. Boyarkin, *The $(g-2)_\mu$ anomaly, Higgs bosons and heavy neutrinos*, *Phys. Rev. D* **67** (2003) 073023 [arXiv:2104.08640] [INSPIRE].

[144] H. Chavez, C.N. Ferreira and J.A. Helayel-Neto, *Physics beyond the standard model: focusing on the muon anomaly*, *Phys. Rev. D* **74** (2006) 033006 [hep-ph/0410373] [INSPIRE].

[145] K. Sawa, *Muon anomalous magnetic moment due to the brane stretching effect*, *Phys. Rev. D* **73** (2006) 025010 [hep-ph/0506190] [INSPIRE].

[146] J.A.R. Cembranos, A. Dobado and A.L. Maroto, *Dark matter clues in the muon anomalous magnetic moment*, *Phys. Rev. D* **73** (2006) 057303 [hep-ph/0507066] [INSPIRE].

[147] T. Hambye, K. Kannike, E. Ma and M. Raidal, *Emanations of dark matter: muon anomalous magnetic moment, radiative neutrino mass, and novel leptogenesis at the TeV scale*, *Phys. Rev. D* **75** (2007) 095003 [hep-ph/0609228] [INSPIRE].

JHEP09(2021)080

[148] O.M. Boyarkin, G.G. Boyarkina and V.V. Makhnach, $(g-2)_\mu$ *anomaly within the left-right symmetric model*, *Phys. Rev. D* **77** (2008) 033004 [arXiv:2104.06320] [INSPIRE].

[149] J.-P. Aguilar, D. Greynat and E. De Rafael, *Muon anomaly from lepton vacuum polarization and the Mellin-Barnes representation*, *Phys. Rev. D* **77** (2008) 093010 [arXiv:0802.2618] [INSPIRE].

[150] A. Hektor, Y. Kajiyama and K. Kannike, *Muon anomalous magnetic moment and lepton flavor violating tau decay in unparticle physics*, *Phys. Rev. D* **78** (2008) 053008 [arXiv:0802.4015] [INSPIRE].

[151] F. Domingo and U. Ellwanger, *Constraints from the muon $g-2$ on the parameter space of the NMSSM*, *JHEP* **07** (2008) 079 [arXiv:0806.0733] [INSPIRE].

[152] C. Biggio, *The contribution of fermionic seesaws to the anomalous magnetic moment of leptons*, *Phys. Lett. B* **668** (2008) 378 [arXiv:0806.2558] [INSPIRE].

[153] Y. Adachi, C.S. Lim and N. Maru, *Lower bound for compactification scale from muon $g-2$ in the gauge-Higgs unification*, *Nucl. Phys. B* **839** (2010) 52 [arXiv:0904.1695] [INSPIRE].

[154] K. Cheung, O.C.W. Kong and J.S. Lee, *Electric and anomalous magnetic dipole moments of the muon in the MSSM*, *JHEP* **06** (2009) 020 [arXiv:0904.4352] [INSPIRE].

[155] L. Hofer, U. Nierste and D. Scherer, *Resummation of* $\tan\beta$*-enhanced supersymmetric loop corrections beyond the decoupling limit*, *JHEP* **10** (2009) 081 [arXiv:0907.5408] [INSPIRE].

[156] T. Fukuyama, H. Sugiyama and K. Tsumura, *Constraints from muon $g-2$ and LFV processes in the Higgs triplet model*, *JHEP* **03** (2010) 044 [arXiv:0909.4943] [INSPIRE].

[157] C.M. Ho and T.W. Kephart, *Electron and muon $g-2$ contributions from the T' Higgs sector*, *Phys. Lett. B* **687** (2010) 201 [arXiv:1001.3696] [INSPIRE].

[158] A. Crivellin, J. Girrbach and U. Nierste, *Yukawa coupling and anomalous magnetic moment of the muon: an update for the LHC era*, *Phys. Rev. D* **83** (2011) 055009 [arXiv:1010.4485] [INSPIRE].

[159] S. Heinemeyer, D. Stöckinger and G. Weiglein, *Two loop SUSY corrections to the anomalous magnetic moment of the muon*, *Nucl. Phys. B* **690** (2004) 62 [hep-ph/0312264] [INSPIRE].

[160] S. Heinemeyer, D. Stöckinger and G. Weiglein, *Electroweak and supersymmetric two-loop corrections to* $(g-2)(\mu)$, *Nucl. Phys. B* **699** (2004) 103 [hep-ph/0405255] [INSPIRE].

[161] T.-F. Feng, X.-Q. Li, L. Lin, J. Maalampi and H.-S. Song, *The two-loop supersymmetric corrections to lepton anomalous magnetic and electric dipole moments*, *Phys. Rev. D* **73** (2006) 116001 [hep-ph/0604171] [INSPIRE].

[162] S. Marchetti, S. Mertens, U. Nierste and D. Stöckinger, $\tan\beta$*-enhanced supersymmetric corrections to the anomalous magnetic moment of the muon*, *Phys. Rev. D* **79** (2009) 013010 [arXiv:0808.1530] [INSPIRE].

[163] P. von Weitershausen, M. Schafer, H. Stöckinger-Kim and D. Stöckinger, *Photonic SUSY two-loop corrections to the muon magnetic moment*, *Phys. Rev. D* **81** (2010) 093004 [arXiv:1003.5820] [INSPIRE].

[164] H.G. Fargnoli, C. Gnendiger, S. Paßehr, D. Stöckinger and H. Stöckinger-Kim, *Non-decoupling two-loop corrections to* $(g-2)_\mu$ *from fermion/sfermion loops in the MSSM*, *Phys. Lett. B* **726** (2013) 717 [arXiv:1309.0980] [INSPIRE].

[165] H. Fargnoli, C. Gnendiger, S. Paßehr, D. Stöckinger and H. Stöckinger-Kim, *Two-loop corrections to the muon magnetic moment from fermion/sfermion loops in the MSSM: detailed results*, *JHEP* **02** (2014) 070 [arXiv:1311.1775] [INSPIRE].

JHEP09(2021)080

[166] G.-C. Cho, K. Hagiwara, Y. Matsumoto and D. Nomura, *The MSSM confronts the precision electroweak data and the muon $g-2$*, *JHEP* **11** (2011) 068 [arXiv:1104.1769] [INSPIRE].

[167] M. Endo, K. Hamaguchi, S. Iwamoto, K. Nakayama and N. Yokozaki, *Higgs mass and muon anomalous magnetic moment in the* U(1) *extended MSSM*, *Phys. Rev. D* **85** (2012) 095006 [arXiv:1112.6412] [INSPIRE].

[168] M. Endo, K. Hamaguchi, S. Iwamoto and N. Yokozaki, *Higgs mass and muon anomalous magnetic moment in supersymmetric models with vector-like matters*, *Phys. Rev. D* **84** (2011) 075017 [arXiv:1108.3071] [INSPIRE].

[169] M. Endo, K. Hamaguchi, S. Iwamoto and N. Yokozaki, *Higgs mass, muon $g-2$, and LHC prospects in gauge mediation models with vector-like matters*, *Phys. Rev. D* **85** (2012) 095012 [arXiv:1112.5653] [INSPIRE].

[170] M. Ibe, S. Matsumoto, T.T. Yanagida and N. Yokozaki, *Heavy squarks and light sleptons in gauge mediation — from the viewpoint of* 125 *GeV Higgs boson and muon $g-2$*, *JHEP* **03** (2013) 078 [arXiv:1210.3122] [INSPIRE].

[171] J.E. Kim, *Inverted effective supersymmetry with combined Z' and gravity mediation, and muon anomalous magnetic moment*, *Phys. Rev. D* **87** (2013) 015004 [arXiv:1208.5484] [INSPIRE].

[172] M. Endo, K. Hamaguchi, S. Iwamoto and T. Yoshinaga, *Muon $g-2$ vs. LHC in supersymmetric models*, *JHEP* **01** (2014) 123 [arXiv:1303.4256] [INSPIRE].

[173] M. Ibe, T.T. Yanagida and N. Yokozaki, *Muon $g-2$ and* 125 *GeV Higgs in split-family supersymmetry*, *JHEP* **08** (2013) 067 [arXiv:1303.6995] [INSPIRE].

[174] S. Akula and P. Nath, *Gluino-driven radiative breaking, Higgs boson mass, muon $g-2$, and the Higgs diphoton decay in supergravity unification*, *Phys. Rev. D* **87** (2013) 115022 [arXiv:1304.5526] [INSPIRE].

[175] H.-B. Zhang, T.-F. Feng, S.-M. Zhao and T.-J. Gao, *Lepton-flavor violation and $(g-2)_\mu$ in the $\mu\nu$SSM*, *Nucl. Phys. B* **873** (2013) 300 [*Erratum ibid.* **879** (2014) 235] [arXiv:1304.6248] [INSPIRE].

[176] M. Endo, K. Hamaguchi, T. Kitahara and T. Yoshinaga, *Probing Bino contribution to muon $g-2$*, *JHEP* **11** (2013) 013 [arXiv:1309.3065] [INSPIRE].

[177] G. Bhattacharyya, B. Bhattacherjee, T.T. Yanagida and N. Yokozaki, *A practical GMSB model for explaining the muon $(g-2)$ with gauge coupling unification*, *Phys. Lett. B* **730** (2014) 231 [arXiv:1311.1906] [INSPIRE].

[178] J.L. Evans, M. Ibe, K.A. Olive and T.T. Yanagida, *One-loop anomaly mediated scalar masses and $(g-2)_m u$ in pure gravity mediation*, *Eur. Phys. J. C* **74** (2014) 2775 [arXiv:1312.1984] [INSPIRE].

[179] S. Iwamoto, T.T. Yanagida and N. Yokozaki, *CP-safe gravity mediation and muon $g-2$*, *PTEP* **2015** (2015) 073B01 [arXiv:1407.4226] [INSPIRE].

[180] J. Kersten, J.-h. Park, D. Stöckinger and L. Velasco-Sevilla, *Understanding the correlation between $(g-2)_\mu$ and $\mu \to e\gamma$ in the MSSM*, *JHEP* **08** (2014) 118 [arXiv:1405.2972] [INSPIRE].

[181] I. Gogoladze, F. Nasir, Q. Shafi and C.S. Un, *Nonuniversal gaugino masses and muon $g-2$*, *Phys. Rev. D* **90** (2014) 035008 [arXiv:1403.2337] [INSPIRE].

JHEP09(2021)080

[182] M. Badziak, Z. Lalak, M. Lewicki, M. Olechowski and S. Pokorski, *Upper bounds on sparticle masses from muon $g-2$ and the Higgs mass and the complementarity of future colliders*, *JHEP* **03** (2015) 003 [arXiv:1411.1450] [INSPIRE].

[183] K. Kowalska, L. Roszkowski, E.M. Sessolo and A.J. Williams, *GUT-inspired SUSY and the muon $g-2$ anomaly: prospects for LHC 14 TeV*, *JHEP* **06** (2015) 020 [arXiv:1503.08219] [INSPIRE].

[184] J. Chakrabortty, A. Choudhury and S. Mondal, *Non-universal Gaugino mass models under the lamppost of muon $(g-2)$*, *JHEP* **07** (2015) 038 [arXiv:1503.08703] [INSPIRE].

[185] B.P. Padley, K. Sinha and K. Wang, *Natural supersymmetry, muon $g-2$, and the last crevices for the top squark*, *Phys. Rev. D* **92** (2015) 055025 [arXiv:1505.05877] [INSPIRE].

[186] M. Bach, J.-h. Park, D. Stöckinger and H. Stöckinger-Kim, *Large muon $(g-2)$ with TeV-scale SUSY masses for $\tan\beta \to \infty$*, *JHEP* **10** (2015) 026 [arXiv:1504.05500] [INSPIRE].

[187] K. Harigaya, T.T. Yanagida and N. Yokozaki, *Muon $g-2$ in focus point SUSY*, *Phys. Rev. D* **92** (2015) 035011 [arXiv:1505.01987] [INSPIRE].

[188] D. Chowdhury and N. Yokozaki, *Muon $g-2$ in anomaly mediated SUSY breaking*, *JHEP* **08** (2015) 111 [arXiv:1505.05153] [INSPIRE].

[189] S. Khalil and C.S. Un, *Muon anomalous magnetic moment in SUSY B-L model with inverse seesaw*, *Phys. Lett. B* **763** (2016) 164 [arXiv:1509.05391] [INSPIRE].

[190] M.A. Ajaib, B. Dutta, T. Ghosh, I. Gogoladze and Q. Shafi, *Neutralinos and sleptons at the LHC in light of muon $(g-2)_\mu$*, *Phys. Rev. D* **92** (2015) 075033 [arXiv:1505.05896] [INSPIRE].

[191] K. Harigaya, T.T. Yanagida and N. Yokozaki, *Higgs boson mass of 125 GeV and $g-2$ of the muon in a gaugino mediation model*, *Phys. Rev. D* **91** (2015) 075010 [arXiv:1501.07447] [INSPIRE].

[192] I. Gogoladze, Q. Shafi and C.S. Ün, *Reconciling the muon $g-2$, a 125 GeV Higgs boson, and dark matter in gauge mediation models*, *Phys. Rev. D* **92** (2015) 115014 [arXiv:1509.07906] [INSPIRE].

[193] F.V. Flores-Baez, M. Gómez Bock and M. Mondragón, *Muon $g-2$ through a flavor structure on soft SUSY terms*, *Eur. Phys. J. C* **76** (2016) 561 [arXiv:1512.00902] [INSPIRE].

[194] A.S. Belyaev, J.E. Camargo-Molina, S.F. King, D.J. Miller, A.P. Morais and P.B. Schaefers, *A to Z of the muon anomalous magnetic moment in the MSSM with Pati-Salam at the GUT scale*, *JHEP* **06** (2016) 142 [arXiv:1605.02072] [INSPIRE].

[195] T. Li, S. Raza and K. Wang, *Constraining natural SUSY via the Higgs coupling and the muon anomalous magnetic moment measurements*, *Phys. Rev. D* **93** (2016) 055040 [arXiv:1601.00178] [INSPIRE].

[196] N. Okada and H.M. Tran, *125 GeV Higgs boson mass and muon $g-2$ in 5D MSSM*, *Phys. Rev. D* **94** (2016) 075016 [arXiv:1606.05329] [INSPIRE].

[197] A. Kobakhidze, M. Talia and L. Wu, *Probing the MSSM explanation of the muon $g-2$ anomaly in dark matter experiments and at a 100 TeV pp collider*, *Phys. Rev. D* **95** (2017) 055023 [arXiv:1608.03641] [INSPIRE].

[198] G. Bélanger, J. Da Silva and H.M. Tran, *Dark matter in U(1) extensions of the MSSM with gauge kinetic mixing*, *Phys. Rev. D* **95** (2017) 115017 [arXiv:1703.03275] [INSPIRE].

JHEP09(2021)080

[199] T. Fukuyama, N. Okada and H.M. Tran, *Sparticle spectroscopy of the minimal* SO(10) *model*, *Phys. Lett. B* **767** (2017) 295 [arXiv:1611.08341] [INSPIRE].

[200] A. Choudhury, S. Rao and L. Roszkowski, *Impact of LHC data on muon* $g-2$ *solutions in a vectorlike extension of the constrained MSSM*, *Phys. Rev. D* **96** (2017) 075046 [arXiv:1708.05675] [INSPIRE].

[201] K. Hagiwara, K. Ma and S. Mukhopadhyay, *Closing in on the chargino contribution to the muon* $g-2$ *in the MSSM: current LHC constraints*, *Phys. Rev. D* **97** (2018) 055035 [arXiv:1706.09313] [INSPIRE].

[202] M. Endo, K. Hamaguchi, S. Iwamoto and T. Kitahara, *Muon* $g-2$ *vs LHC Run 2 in supersymmetric models*, *JHEP* **04** (2020) 165 [arXiv:2001.11025] [INSPIRE].

[203] M. Chakraborti, S. Heinemeyer and I. Saha, *Improved* $(g-2)_\mu$ *measurements and supersymmetry*, *Eur. Phys. J. C* **80** (2020) 984 [arXiv:2006.15157] [INSPIRE].

[204] S.-I. Horigome, T. Katayose, S. Matsumoto and I. Saha, *Leptophilic fermion WIMP — Role of future lepton colliders*, arXiv:2102.08645 [INSPIRE].

[205] W. Yin and N. Yokozaki, *Splitting mass spectra and muon* $g-2$ *in Higgs-anomaly mediation*, *Phys. Lett. B* **762** (2016) 72 [arXiv:1607.05705] [INSPIRE].

[206] B. Zhu, R. Ding and T. Li, *Higgs mass and muon anomalous magnetic moment in the MSSM with gauge-gravity hybrid mediation*, *Phys. Rev. D* **96** (2017) 035029 [arXiv:1610.09840] [INSPIRE].

[207] M. Hussain and R. Khalid, *Understanding the muon anomalous magnetic moment in light of a flavor symmetry-based minimal supersymmetric standard model*, *PTEP* **2018** (2018) 083B06 [arXiv:1704.04085] [INSPIRE].

[208] X. Ning and F. Wang, *Solving the muon* $g-2$ *anomaly within the NMSSM from generalized deflected AMSB*, *JHEP* **08** (2017) 089 [arXiv:1704.05079] [INSPIRE].

[209] M. Frank and O. Özdal, *Exploring the supersymmetric* $\mathrm{U}(1)_{B-L} \times \mathrm{U}(1)_R$ *model with dark matter, muon* $g-2$ *and* Z' *mass limits*, *Phys. Rev. D* **97** (2018) 015012 [arXiv:1709.04012] [INSPIRE].

[210] E. Bagnaschi et al., *Likelihood analysis of the pMSSM11 in light of LHC* 13 *TeV data*, *Eur. Phys. J. C* **78** (2018) 256 [arXiv:1710.11091] [INSPIRE].

[211] C. Li, B. Zhu and T. Li, *Naturalness, dark matter, and the muon anomalous magnetic moment in supersymmetric extensions of the standard model with a pseudo-Dirac gluino*, *Nucl. Phys. B* **927** (2018) 255 [arXiv:1704.05584] [INSPIRE].

[212] G. Pozzo and Y. Zhang, *Constraining resonant dark matter with combined LHC electroweakino searches*, *Phys. Lett. B* **789** (2019) 582 [arXiv:1807.01476] [INSPIRE].

[213] Z. Altın, O. Özdal and C.S. Un, *Muon* $g-2$ *in an alternative quasi-Yukawa unification with a less fine-tuned seesaw mechanism*, *Phys. Rev. D* **97** (2018) 055007 [arXiv:1703.00229] [INSPIRE].

[214] M. Chakraborti, U. Chattopadhyay and S. Poddar, *How light a higgsino or a wino dark matter can become in a compressed scenario of MSSM*, *JHEP* **09** (2017) 064 [arXiv:1702.03954] [INSPIRE].

[215] T.T. Yanagida and N. Yokozaki, *Muon* $g-2$ *in MSSM gauge mediation revisited*, *Phys. Lett. B* **772** (2017) 409 [arXiv:1704.00711] [INSPIRE].

JHEP09(2021)080

[216] A. Choudhury, L. Darmé, L. Roszkowski, E.M. Sessolo and S. Trojanowski, *Muon $g-2$ and related phenomenology in constrained vector-like extensions of the MSSM*, *JHEP* **05** (2017) 072 [arXiv:1701.08778] [INSPIRE].

[217] M. Endo, K. Hamaguchi, S. Iwamoto and K. Yanagi, *Probing minimal SUSY scenarios in the light of muon $g-2$ and dark matter*, *JHEP* **06** (2017) 031 [arXiv:1704.05287] [INSPIRE].

[218] K. Wang, F. Wang, J. Zhu and Q. Jie, *The semi-constrained NMSSM in light of muon $g-2$, LHC, and dark matter constraints*, *Chin. Phys. C* **42** (2018) 103109 [arXiv:1811.04435] [INSPIRE].

[219] G. Bhattacharyya, T.T. Yanagida and N. Yokozaki, *An extended gauge mediation for muon $(g-2)$ explanation*, *Phys. Lett. B* **784** (2018) 118 [arXiv:1805.01607] [INSPIRE].

[220] P. Cox, C. Han and T.T. Yanagida, *Muon $g-2$ and dark matter in the minimal supersymmetric standard model*, *Phys. Rev. D* **98** (2018) 055015 [arXiv:1805.02802] [INSPIRE].

[221] P. Cox, C. Han, T.T. Yanagida and N. Yokozaki, *Gaugino mediation scenarios for muon $g-2$ and dark matter*, *JHEP* **08** (2019) 097 [arXiv:1811.12699] [INSPIRE].

[222] J.-L. Yang, T.-F. Feng, Y.-L. Yan, W. Li, S.-M. Zhao and H.-B. Zhang, *Lepton-flavor violation and two loop electroweak corrections to $(g-2)_\mu$ in the B-L symmetric SSM*, *Phys. Rev. D* **99** (2019) 015002 [arXiv:1812.03860] [INSPIRE].

[223] H.M. Tran and H.T. Nguyen, *GUT-inspired MSSM in light of muon $g-2$ and LHC results at $\sqrt{s} = 13$ TeV*, *Phys. Rev. D* **99** (2019) 035040 [arXiv:1812.11757] [INSPIRE].

[224] F. Wang, K. Wang, J.M. Yang and J. Zhu, *Solving the muon $g-2$ anomaly in CMSSM extension with non-universal gaugino masses*, *JHEP* **12** (2018) 041 [arXiv:1808.10851] [INSPIRE].

[225] M. Abdughani, K.-I. Hikasa, L. Wu, J.M. Yang and J. Zhao, *Testing electroweak SUSY for muon $g-2$ and dark matter at the LHC and beyond*, *JHEP* **11** (2019) 095 [arXiv:1909.07792] [INSPIRE].

[226] W. Kotlarski, D. Stöckinger and H. Stöckinger-Kim, *Low-energy lepton physics in the MRSSM: $(g-2)_\mu$, $\mu \to e\gamma$ and $\mu \to e$ conversion*, *JHEP* **08** (2019) 082 [arXiv:1902.06650] [INSPIRE].

[227] X.-X. Dong, S.-M. Zhao, H.-B. Zhang and T.-F. Feng, *The two-loop corrections to lepton MDMs and EDMs in the EBLMSSM*, *J. Phys. G* **47** (2020) 045002 [arXiv:1901.07701] [INSPIRE].

[228] M. Ibe, M. Suzuki, T.T. Yanagida and N. Yokozaki, *Muon $g-2$ in split-family SUSY in light of LHC Run II*, *Eur. Phys. J. C* **79** (2019) 688 [arXiv:1903.12433] [INSPIRE].

[229] J.-L. Yang, T.-F. Feng and H.-B. Zhang, *Electron and muon $(g-2)$ in the B-LSSM*, *J. Phys. G* **47** (2020) 055004 [arXiv:2003.09781] [INSPIRE].

[230] T.T. Yanagida, W. Yin and N. Yokozaki, *Muon $g-2$ in Higgs-anomaly mediation*, *JHEP* **06** (2020) 154 [arXiv:2001.02672] [INSPIRE].

[231] C. Han, M.L. López-Ibáñez, A. Melis, O. Vives, L. Wu and J.M. Yang, *LFV and $(g-2)$ in non-universal SUSY models with light higgsinos*, *JHEP* **05** (2020) 102 [arXiv:2003.06187] [INSPIRE].

JHEP09(2021)080

[232] J. Cao, J. Lian, L. Meng, Y. Yue and P. Zhu, *Anomalous muon magnetic moment in the inverse seesaw extended next-to-minimal supersymmetric standard model*, *Phys. Rev. D* **101** (2020) 095009 [arXiv:1912.10225] [INSPIRE].

[233] M. Yamaguchi and W. Yin, *A novel approach to finely tuned supersymmetric standard models: The case of the non-universal Higgs mass model*, *PTEP* **2018** (2018) 023B06 [arXiv:1606.04953] [INSPIRE].

[234] T.T. Yanagida, W. Yin and N. Yokozaki, *Flavor-safe light squarks in Higgs-anomaly mediation*, *JHEP* **04** (2018) 012 [arXiv:1801.05785] [INSPIRE].

[235] Y. Shimizu and W. Yin, *Natural split mechanism for sfermions: $N = 2$ supersymmetry in phenomenology*, *Phys. Lett. B* **754** (2016) 118 [arXiv:1509.04933] [INSPIRE].

[236] W. Yin, *Fixed point and anomaly mediation in partially $N = 2$ supersymmetric standard models*, *Chin. Phys. C* **42** (2018) 013104 [arXiv:1609.03527] [INSPIRE].

[237] L.-H. Su, S.-M. Zhao, X.-X. Dong, D.-D. Cui, T.-F. Feng and H.-B. Zhang, *The two-loop contributions to muon MDM in $\mathrm{U}(1)_X$ SSM*, *Eur. Phys. J. C* **81** (2021) 433 [arXiv:2012.04824] [INSPIRE].

[238] R.S. Hundi, S. Roy and S. SenGupta, *Muon $(g-2)$ from the bulk neutrino field in a warped extra dimensional model*, *Phys. Rev. D* **86** (2012) 036014 [arXiv:1206.5137] [INSPIRE].

[239] E. Megias, M. Quirós and L. Salas, *$g_\mu - 2$ from vector-like leptons in warped space*, *JHEP* **05** (2017) 016 [arXiv:1701.05072] [INSPIRE].

[240] A. Doff and C. Siqueira, *Composite Higgs models, technicolor and the muon anomalous magnetic moment*, *Phys. Lett. B* **754** (2016) 294 [arXiv:1512.03256] [INSPIRE].

[241] D.K. Hong and D.H. Kim, *Composite (pseudo) scalar contributions to muon $g-2$*, *Phys. Lett. B* **758** (2016) 370 [arXiv:1602.06628] [INSPIRE].

[242] A. Broggio, E.J. Chun, M. Passera, K.M. Patel and S.K. Vempati, *Limiting two-Higgs-doublet models*, *JHEP* **11** (2014) 058 [arXiv:1409.3199] [INSPIRE].

[243] T. Han, S.K. Kang and J. Sayre, *Muon $g-2$ in the aligned two Higgs doublet model*, *JHEP* **02** (2016) 097 [arXiv:1511.05162] [INSPIRE].

[244] L. Wang and X.-F. Han, *A light pseudoscalar of 2HDM confronted with muon g-2 and experimental constraints*, *JHEP* **05** (2015) 039 [arXiv:1412.4874] [INSPIRE].

[245] V. Ilisie, *New Barr-Zee contributions to $(g-2)_\mu$ in two-Higgs-doublet models*, *JHEP* **04** (2015) 077 [arXiv:1502.04199] [INSPIRE].

[246] T. Abe, R. Sato and K. Yagyu, *Lepton-specific two Higgs doublet model as a solution of muon $g-2$ anomaly*, *JHEP* **07** (2015) 064 [arXiv:1504.07059] [INSPIRE].

[247] E.J. Chun, Z. Kang, M. Takeuchi and Y.-L.S. Tsai, *LHC τ-rich tests of lepton-specific 2HDM for $(g-2)_\mu$*, *JHEP* **11** (2015) 099 [arXiv:1507.08067] [INSPIRE].

[248] L. Wang, S. Yang and X.-F. Han, *$h \to \mu\tau$ and muon $g-2$ in the alignment limit of two-Higgs-doublet model*, *Nucl. Phys. B* **919** (2017) 123 [arXiv:1606.04408] [INSPIRE].

[249] E.J. Chun and J. Kim, *Leptonic precision test of leptophilic two-Higgs-doublet model*, *JHEP* **07** (2016) 110 [arXiv:1605.06298] [INSPIRE].

[250] T. Abe, R. Sato and K. Yagyu, *Muon specific two-Higgs-doublet model*, *JHEP* **07** (2017) 012 [arXiv:1705.01469] [INSPIRE].

JHEP09(2021)080

[251] A. Cherchiglia, P. Kneschke, D. Stöckinger and H. Stöckinger-Kim, *The muon magnetic moment in the 2HDM: complete two-loop result*, *JHEP* **01** (2017) 007 [arXiv:1607.06292] [INSPIRE].

[252] A. Cherchiglia, D. Stöckinger and H. Stöckinger-Kim, *Muon $g-2$ in the 2HDM: maximum results and detailed phenomenology*, *Phys. Rev. D* **98** (2018) 035001 [arXiv:1711.11567] [INSPIRE].

[253] L. Wang, J.M. Yang, M. Zhang and Y. Zhang, *Revisiting lepton-specific 2HDM in light of muon $g-2$ anomaly*, *Phys. Lett. B* **788** (2019) 519 [arXiv:1809.05857] [INSPIRE].

[254] X.-F. Han, T. Li, L. Wang and Y. Zhang, *Simple interpretations of lepton anomalies in the lepton-specific inert two-Higgs-doublet model*, *Phys. Rev. D* **99** (2019) 095034 [arXiv:1812.02449] [INSPIRE].

[255] E.J. Chun, J. Kim and T. Mondal, *Electron EDM and muon anomalous magnetic moment in two-Higgs-doublet models*, *JHEP* **12** (2019) 068 [arXiv:1906.00612] [INSPIRE].

[256] S. Iguro, Y. Omura and M. Takeuchi, *Testing the 2HDM explanation of the muon $g-2$ anomaly at the LHC*, *JHEP* **11** (2019) 130 [arXiv:1907.09845] [INSPIRE].

[257] L. Wang and Y. Zhang, *μ-τ-philic Higgs doublet model confronted with the muon $g-2$, τ decays, and LHC data*, *Phys. Rev. D* **100** (2019) 095005 [arXiv:1908.03755] [INSPIRE].

[258] D. Sabatta, A.S. Cornell, A. Goyal, M. Kumar, B. Mellado and X. Ruan, *Connecting muon anomalous magnetic moment and multi-lepton anomalies at LHC*, *Chin. Phys. C* **44** (2020) 063103 [arXiv:1909.03969] [INSPIRE].

[259] S. Jana, V.P.K. and S. Saad, *Resolving electron and muon $g-2$ within the 2HDM*, *Phys. Rev. D* **101** (2020) 115037 [arXiv:2003.03386] [INSPIRE].

[260] F.J. Botella, F. Cornet-Gomez and M. Nebot, *Electron and muon $g-2$ anomalies in general flavour conserving two Higgs doublets models*, *Phys. Rev. D* **102** (2020) 035023 [arXiv:2006.01934] [INSPIRE].

[261] L. Delle Rose, S. Khalil and S. Moretti, *Explaining electron and muon $g-2$ anomalies in an aligned 2-Higgs doublet model with right-handed neutrinos*, *Phys. Lett. B* **816** (2021) 136216 [arXiv:2012.06911] [INSPIRE].

[262] S.-P. Li, X.-Q. Li, Y.-Y. Li, Y.-D. Yang and X. Zhang, *Power-aligned 2HDM: a correlative perspective on $(g-2)_{e,\mu}$*, *JHEP* **01** (2021) 034 [arXiv:2010.02799] [INSPIRE].

[263] N. Ghosh and J. Lahiri, *Generalized 2HDM with wrong-sign lepton Yukawa coupling, in light of $g_\mu - 2$ and lepton flavor violation at the future LHC*, arXiv:2103.10632 [INSPIRE].

[264] T. Mondal and H. Okada, *Inverse seesaw and $(g-2)$ anomalies in $B-L$ extended two Higgs doublet model*, arXiv:2103.13149 [INSPIRE].

[265] D. Das, C. Hati, G. Kumar and N. Mahajan, *Towards a unified explanation of $R_{D^{(*)}}$, R_K and $(g-2)_\mu$ anomalies in a left-right model with leptoquarks*, *Phys. Rev. D* **94** (2016) 055034 [arXiv:1605.06313] [INSPIRE].

[266] E. Coluccio Leskow, G. D'Ambrosio, A. Crivellin and D. Müller, *$(g-2)\mu$, lepton flavor violation, and Z decays with leptoquarks: Correlations and future prospects*, *Phys. Rev. D* **95** (2017) 055018 [arXiv:1612.06858] [INSPIRE].

[267] K. Kowalska, E.M. Sessolo and Y. Yamamoto, *Constraints on charmphilic solutions to the muon $g-2$ with leptoquarks*, *Phys. Rev. D* **99** (2019) 055007 [arXiv:1812.06851] [INSPIRE].

[268] I. Doršner, S. Fajfer and O. Sumensari, *Muon $g-2$ and scalar leptoquark mixing*, *JHEP* **06** (2020) 089 [arXiv:1910.03877] [INSPIRE].

JHEP09(2021)080

[269] A. Crivellin, D. Mueller and F. Saturnino, *Correlating $h \to \mu^+\mu^-$ to the anomalous magnetic moment of the muon via leptoquarks*, *Phys. Rev. Lett.* **127** (2021) 021801 [arXiv:2008.02643] [INSPIRE].

[270] V. Gherardi, D. Marzocca and E. Venturini, *Low-energy phenomenology of scalar leptoquarks at one-loop accuracy*, *JHEP* **01** (2021) 138 [arXiv:2008.09548] [INSPIRE].

[271] K.S. Babu, P.S.B. Dev, S. Jana and A. Thapa, *Unified framework for B-anomalies, muon $g-2$ and neutrino masses*, *JHEP* **03** (2021) 179 [arXiv:2009.01771] [INSPIRE].

[272] A. Crivellin, C. Greub, D. Müller and F. Saturnino, *Scalar leptoquarks in leptonic processes*, *JHEP* **02** (2021) 182 [arXiv:2010.06593] [INSPIRE].

[273] J. Heeck and W. Rodejohann, *Gauged L_μ–L_τ symmetry at the electroweak Scale*, *Phys. Rev. D* **84** (2011) 075007 [arXiv:1107.5238] [INSPIRE].

[274] W. Altmannshofer, S. Gori, M. Pospelov and I. Yavin, *Neutrino trident production: a powerful probe of new physics with neutrino beams*, *Phys. Rev. Lett.* **113** (2014) 091801 [arXiv:1406.2332] [INSPIRE].

[275] W. Altmannshofer, M. Carena and A. Crivellin, *L_μ–L_τ theory of Higgs flavor violation and $(g-2)_\mu$*, *Phys. Rev. D* **94** (2016) 095026 [arXiv:1604.08221] [INSPIRE].

[276] G. Bélanger, C. Delaunay and S. Westhoff, *A dark matter relic from muon anomalies*, *Phys. Rev. D* **92** (2015) 055021 [arXiv:1507.06660] [INSPIRE].

[277] W. Altmannshofer, C.-Y. Chen, P.S. Bhupal Dev and A. Soni, *Lepton flavor violating Z' explanation of the muon anomalous magnetic moment*, *Phys. Lett. B* **762** (2016) 389 [arXiv:1607.06832] [INSPIRE].

[278] G.-y. Huang, F.S. Queiroz and W. Rodejohann, *Gauged L_μ–L_τ at a muon collider*, *Phys. Rev. D* **103** (2021) 095005 [arXiv:2101.04956] [INSPIRE].

[279] S.N. Gninenko, N.V. Krasnikov and V.A. Matveev, *Muon $g-2$ and searches for a new leptophobic sub-GeV dark boson in a missing-energy experiment at CERN*, *Phys. Rev. D* **91** (2015) 095015 [arXiv:1412.1400] [INSPIRE].

[280] T. Araki, F. Kaneko, T. Ota, J. Sato and T. Shimomura, *MeV scale leptonic force for cosmic neutrino spectrum and muon anomalous magnetic moment*, *Phys. Rev. D* **93** (2016) 013014 [arXiv:1508.07471] [INSPIRE].

[281] A. Biswas, S. Choubey and S. Khan, *FIMP and muon $(g-2)$ in a $\mathrm{U}(1)_{L_\mu - L_\tau}$ model*, *JHEP* **02** (2017) 123 [arXiv:1612.03067] [INSPIRE].

[282] A. Kamada, K. Kaneta, K. Yanagi and H.-B. Yu, *Self-interacting dark matter and muon $g-2$ in a gauged $\mathrm{U}(1)_{L_\mu - L_\tau}$ model*, *JHEP* **06** (2018) 117 [arXiv:1805.00651] [INSPIRE].

[283] S.N. Gninenko and N.V. Krasnikov, *Probing the muon $g_\mu - 2$ anomaly, L_μ–L_τ gauge boson and dark matter in dark photon experiments*, *Phys. Lett. B* **783** (2018) 24 [arXiv:1801.10448] [INSPIRE].

[284] S. Patra, S. Rao, N. Sahoo and N. Sahu, *Gauged $\mathrm{U}(1)_{L_\mu - L_\tau}$ model in light of muon $g-2$ anomaly, neutrino mass and dark matter phenomenology*, *Nucl. Phys. B* **917** (2017) 317 [arXiv:1607.04046] [INSPIRE].

[285] D.W.P.d. Amaral, D.G. Cerdeno, P. Foldenauer and E. Reid, *Solar neutrino probes of the muon anomalous magnetic moment in the gauged $\mathrm{U}(1)_{L_\mu - L_\tau}$*, *JHEP* **12** (2020) 155 [arXiv:2006.11225] [INSPIRE].

[286] A. Bodas, R. Coy and S.J.D. King, *Solving the electron and muon $g-2$ anomalies in Z' models*, arXiv:2102.07781 [INSPIRE].

JHEP09(2021)080

[287] Y. Daikoku and H. Okada, *Lepton anomalous magnetic moments in an S_4 flavor-symmetric extra* U(1) *model*, arXiv:2011.10374 [INSPIRE].

[288] H. Davoudiasl, H.-S. Lee and W.J. Marciano, *Muon anomaly and dark parity violation*, *Phys. Rev. Lett.* **109** (2012) 031802 [arXiv:1205.2709] [INSPIRE].

[289] H. Davoudiasl, H.-S. Lee and W.J. Marciano, *Dark side of Higgs diphoton decays and muon* $g-2$, *Phys. Rev. D* **86** (2012) 095009 [arXiv:1208.2973] [INSPIRE].

[290] H. Davoudiasl, H.-S. Lee and W.J. Marciano, *Muon* $g-2$*, rare kaon decays, and parity violation from dark bosons*, *Phys. Rev. D* **89** (2014) 095006 [arXiv:1402.3620] [INSPIRE].

[291] H.-S. Lee, *Muon* $g-2$ *anomaly and dark leptonic gauge boson*, *Phys. Rev. D* **90** (2014) 091702 [arXiv:1408.4256] [INSPIRE].

[292] G. Mohlabeng, *Revisiting the dark photon explanation of the muon anomalous magnetic moment*, *Phys. Rev. D* **99** (2019) 115001 [arXiv:1902.05075] [INSPIRE].

[293] K. Kannike, M. Raidal, D.M. Straub and A. Strumia, *Anthropic solution to the magnetic muon anomaly: the charged see-saw*, *JHEP* **02** (2012) 106 [*Erratum ibid.* **10** (2012) 136] [arXiv:1111.2551] [INSPIRE].

[294] R. Dermisek and A. Raval, *Explanation of the muon* $g-2$ *anomaly with vectorlike leptons and its implications for Higgs decays*, *Phys. Rev. D* **88** (2013) 013017 [arXiv:1305.3522] [INSPIRE].

[295] S. Raby and A. Trautner, *Vectorlike chiral fourth family to explain muon anomalies*, *Phys. Rev. D* **97** (2018) 095006 [arXiv:1712.09360] [INSPIRE].

[296] Z. Poh and S. Raby, *Vectorlike leptons: muon* $g-2$ *anomaly, lepton flavor violation, Higgs boson decays, and lepton nonuniversality*, *Phys. Rev. D* **96** (2017) 015032 [arXiv:1705.07007] [INSPIRE].

[297] J. Kawamura, S. Okawa and Y. Omura, *Current status and muon* $g-2$ *explanation of lepton portal dark matter*, *JHEP* **08** (2020) 042 [arXiv:2002.12534] [INSPIRE].

[298] M. Frank and I. Saha, *Muon anomalous magnetic moment in two-Higgs-doublet models with vectorlike leptons*, *Phys. Rev. D* **102** (2020) 115034 [arXiv:2008.11909] [INSPIRE].

[299] A.S. De Jesus, S. Kovalenko, F.S. Queiroz, C. Siqueira and K. Sinha, *Vectorlike leptons and inert scalar triplet: Lepton flavor violation,* $g-2$*, and collider searches*, *Phys. Rev. D* **102** (2020) 035004 [arXiv:2004.01200] [INSPIRE].

[300] M. Endo and S. Mishima, *Muon* $g-2$ *and CKM unitarity in extra lepton models*, *JHEP* **08** (2020) 004 [arXiv:2005.03933] [INSPIRE].

[301] D. Huang, A.P. Morais and R. Santos, *Anomalies in B-meson decays and the muon* $g-2$ *from dark loops*, *Phys. Rev. D* **102** (2020) 075009 [arXiv:2007.05082] [INSPIRE].

[302] E.J. Chun and T. Mondal, *Explaining* $g-2$ *anomalies in two Higgs doublet model with vector-like leptons*, *JHEP* **11** (2020) 077 [arXiv:2009.08314] [INSPIRE].

[303] R. Dermisek, K. Hermanek, N. McGinnis and N. McGinnis, *Highly enhanced contributions of heavy Higgs bosons and new leptons to muon* $g-2$ *and prospects at future colliders*, *Phys. Rev. Lett.* **126** (2021) 191801 [arXiv:2011.11812] [INSPIRE].

[304] R. Dermisek, K. Hermanek and N. McGinnis, *Muon* $g-2$ *in two Higgs doublet models with vectorlike leptons*, arXiv:2103.05645 [INSPIRE].

JHEP09(2021)080

[305] C.-Y. Chen, H. Davoudiasl, W.J. Marciano and C. Zhang, *Implications of a light "dark Higgs" solution to the $g_\mu - 2$ discrepancy*, *Phys. Rev. D* **93** (2016) 035006 [arXiv:1511.04715] [INSPIRE].

[306] W.J. Marciano, A. Masiero, P. Paradisi and M. Passera, *Contributions of axionlike particles to lepton dipole moments*, *Phys. Rev. D* **94** (2016) 115033 [arXiv:1607.01022] [INSPIRE].

[307] M. Bauer, M. Neubert and A. Thamm, *LHC as an axion factory: probing an axion explanation for $(g-2)_\mu$ with exotic Higgs decays*, *Phys. Rev. Lett.* **119** (2017) 031802 [arXiv:1704.08207] [INSPIRE].

[308] J. Liu, C.E.M. Wagner and X.-P. Wang, *A light complex scalar for the electron and muon anomalous magnetic moments*, *JHEP* **03** (2019) 008 [arXiv:1810.11028] [INSPIRE].

[309] M. Bauer, M. Neubert, S. Renner, M. Schnubel and A. Thamm, *Axionlike particles, lepton-flavor violation, and a new explanation of a_μ and a_e*, *Phys. Rev. Lett.* **124** (2020) 211803 [arXiv:1908.00008] [INSPIRE].

[310] C. Cornella, P. Paradisi and O. Sumensari, *Hunting for ALPs with lepton flavor violation*, *JHEP* **01** (2020) 158 [arXiv:1911.06279] [INSPIRE].

[311] W. Abdallah, R. Gandhi and S. Roy, *Understanding the MiniBooNE and the muon and electron $g-2$ anomalies with a light Z' and a second Higgs doublet*, *JHEP* **12** (2020) 188 [arXiv:2006.01948] [INSPIRE].

[312] P. Escribano and A. Vicente, *Ultralight scalars in leptonic observables*, *JHEP* **03** (2021) 240 [arXiv:2008.01099] [INSPIRE].

[313] D. Buttazzo, P. Panci, D. Teresi and R. Ziegler, *Xenon1T excess from electron recoils of non-relativistic Dark Matter*, *Phys. Lett. B* **817** (2021) 136310 [arXiv:2011.08919] [INSPIRE].

[314] R.S. Hundi, *Constraints from neutrino masses and muon $(g-2)$ in the bilinear R-parity violating supersymmetric model*, *Phys. Rev. D* **83** (2011) 115019 [arXiv:1101.2810] [INSPIRE].

[315] J.-H. Huh and B. Kyae, $\mathrm{U}(1)_{B_1+B_2-2L_1}$ *mediation for the natural SUSY and the anomalous muon $g-2$*, *Phys. Lett. B* **726** (2013) 729 [arXiv:1306.1321] [INSPIRE].

[316] N. Okada, S. Raza and Q. Shafi, *Particle spectroscopy of supersymmetric* SU(5) *in light of* 125 *GeV Higgs and muon $g-2$ data*, *Phys. Rev. D* **90** (2014) 015020 [arXiv:1307.0461] [INSPIRE].

[317] C. Kelso, P.R.D. Pinheiro, F.S. Queiroz and W. Shepherd, *The muon anomalous magnetic moment in the reduced minimal 3-3-1 model*, *Eur. Phys. J. C* **74** (2014) 2808 [arXiv:1312.0051] [INSPIRE].

[318] K.S. Babu, I. Gogoladze, Q. Shafi and C.S. Ün, *Muon $g-2$,* 125 *GeV Higgs boson, and neutralino dark matter in a flavor symmetry-based MSSM*, *Phys. Rev. D* **90** (2014) 116002 [arXiv:1406.6965] [INSPIRE].

[319] D. Cogollo, *Muon anomalous magnetic moment in a* $\mathrm{SU}(4) \otimes \mathrm{U}(1)_N$ *model*, *Int. J. Mod. Phys. A* **30** (2015) 1550038 [arXiv:1409.8115] [INSPIRE].

[320] M. Adeel Ajaib, I. Gogoladze and Q. Shafi, *GUT-inspired supersymmetric model for $h \to \gamma\gamma$ and the muon $g-2$*, *Phys. Rev. D* **91** (2015) 095005 [arXiv:1501.04125] [INSPIRE].

[321] D. T. Binh, D. T. Huong, L. T. Hue and H. N. Long, *Anomalous magnetic moment of muon in economical 3-3-1 model*, *Commun. Phys.* **25** (2015) 29.

JHEP09(2021)080

[322] A. Hektor, K. Kannike and L. Marzola, *Muon $g-2$ and galactic centre γ-ray excess in a scalar extension of the 2HDM type-X*, *JCAP* **10** (2015) 025 [arXiv:1507.05096] [INSPIRE].

[323] D. Cogollo, *Exotic leptons: collider and muon magnetic moment constraints*, *Int. J. Mod. Phys. A* **30** (2015) 1550187 [arXiv:1508.01492] [INSPIRE].

[324] B. Allanach, F.S. Queiroz, A. Strumia and S. Sun, *Z' models for the LHCb and $g-2$ muon anomalies*, *Phys. Rev. D* **93** (2016) 055045 [*Erratum ibid.* **95** (2017) 119902] [arXiv:1511.07447] [INSPIRE].

[325] J. Chakrabortty, P. Ghosh, S. Mondal and T. Srivastava, *Reconciling $(g-2)_\mu$ and charged lepton flavor violating processes through a doubly charged scalar*, *Phys. Rev. D* **93** (2016) 115004 [arXiv:1512.03581] [INSPIRE].

[326] E. Jin Chun, *Solving the muon anomaly in two Higgs doublet models*, *Nuovo Cim. C* **38** (2016) 136 [INSPIRE].

[327] G. Bélanger and C. Delaunay, *A dark sector for $g_\mu-2$, R_K and a diphoton resonance*, *Phys. Rev. D* **94** (2016) 075019 [arXiv:1603.03333] [INSPIRE].

[328] M. Nishida and K. Yoshioka, *Higgs boson mass and muon $g-2$ with strongly coupled vector-like generations*, *Phys. Rev. D* **94** (2016) 095022 [arXiv:1605.06675] [INSPIRE].

[329] D.K. Hong, D.H. Kim and C.S. Shin, *Clockwork graviton contributions to muon $g-2$*, *Phys. Rev. D* **97** (2018) 035014 [arXiv:1706.09376] [INSPIRE].

[330] A. Crivellin, M. Hoferichter and P. Schmidt-Wellenburg, *Combined explanations of $(g-2)_{\mu,e}$ and implications for a large muon EDM*, *Phys. Rev. D* **98** (2018) 113002 [arXiv:1807.11484] [INSPIRE].

[331] S.-P. Li, X.-Q. Li and Y.-D. Yang, *Muon $g-2$ in a U(1)-symmetric two-Higgs-doublet model*, *Phys. Rev. D* **99** (2019) 035010 [arXiv:1808.02424] [INSPIRE].

[332] G.-L. Liu and Q.-G. Zeng, *Muon $g-2$ anomaly confronted with the Higgs global data in the left-right twin Higgs models*, *Eur. Phys. J. C* **79** (2019) 612 [arXiv:1811.04777] [INSPIRE].

[333] C.-H. Chen and T. Nomura, *Influence of an inert charged Higgs boson on the muon $g-2$ and radiative neutrino masses in a scotogenic model*, *Phys. Rev. D* **100** (2019) 015024 [arXiv:1903.03380] [INSPIRE].

[334] M. Badziak and K. Sakurai, *Explanation of electron and muon $g-2$ anomalies in the MSSM*, *JHEP* **10** (2019) 024 [arXiv:1908.03607] [INSPIRE].

[335] A. Datta, J.L. Feng, S. Kamali and J. Kumar, *Resolving the $(g-2)_\mu$ and B anomalies with leptoquarks and a dark Higgs boson*, *Phys. Rev. D* **101** (2020) 035010 [arXiv:1908.08625] [INSPIRE].

[336] M. Endo and W. Yin, *Explaining electron and muon $g-2$ anomaly in SUSY without lepton-flavor mixings*, *JHEP* **08** (2019) 122 [arXiv:1906.08768] [INSPIRE].

[337] A.E. Cárcamo Hernández, S.F. King, H. Lee and S.J. Rowley, *Is it possible to explain the muon and electron $g-2$ in a Z' model?*, *Phys. Rev. D* **101** (2020) 115016 [arXiv:1910.10734] [INSPIRE].

[338] C.-X. Liu, H.-B. Zhang, J.-L. Yang, S.-M. Zhao, Y.-B. Liu and T.-F. Feng, *Higgs boson decay $h \to Z\gamma$ and muon magnetic dipole moment in the $\mu\nu$SSM*, *JHEP* **04** (2020) 002 [arXiv:2002.04370] [INSPIRE].

[339] L. Calibbi, M.L. López-Ibáñez, A. Melis and O. Vives, *Muon and electron $g-2$ and lepton masses in flavor models*, *JHEP* **06** (2020) 087 [arXiv:2003.06633] [INSPIRE].

JHEP09(2021)080

[340] C.-H. Chen and T. Nomura, *Electron and muon $g-2$, radiative neutrino mass, and $\ell' \to \ell\gamma$ in a $\mathrm{U}(1)_{e-\mu}$ model*, *Nucl. Phys. B* **964** (2021) 115314 [arXiv:2003.07638] [INSPIRE].

[341] C.-K. Chua, *Data-driven study of the implications of anomalous magnetic moments and lepton flavor violating processes of e, μ and τ*, *Phys. Rev. D* **102** (2020) 055022 [arXiv:2004.11031] [INSPIRE].

[342] S. Saad, *Combined explanations of $(g-2)_\mu$, $R_{D^{(*)}}$, $R_{K^{(*)}}$ anomalies in a two-loop radiative neutrino mass model*, *Phys. Rev. D* **102** (2020) 015019 [arXiv:2005.04352] [INSPIRE].

[343] J.T. Acuña, M. Fabbrichesi and P. Ullio, *Phenomenological consequences of an interacting multicomponent dark sector*, *Phys. Rev. D* **102** (2020) 083009 [arXiv:2005.04146] [INSPIRE].

[344] M. Frank, Y. Hiçyılmaz, S. Moretti and O. Özdal, *Leptophobic Z' bosons in the secluded UMSSM*, *Phys. Rev. D* **102** (2020) 115025 [arXiv:2005.08472] [INSPIRE].

[345] B. Dutta, S. Ghosh and T. Li, *Explaining $(g-2)_{\mu,e}$, the KOTO anomaly and the MiniBooNE excess in an extended Higgs model with sterile neutrinos*, *Phys. Rev. D* **102** (2020) 055017 [arXiv:2006.01319] [INSPIRE].

[346] K.-F. Chen, C.-W. Chiang and K. Yagyu, *An explanation for the muon and electron $g-2$ anomalies and dark matter*, *JHEP* **09** (2020) 119 [arXiv:2006.07929] [INSPIRE].

[347] X. Liu, Y. Li, T. Li and B. Zhu, *The light sgoldstino phenomenology: explanations for the muon $(g-2)$ deviation and KOTO anomaly*, *JHEP* **10** (2020) 197 [arXiv:2006.08869] [INSPIRE].

[348] I. Doršner, S. Fajfer and S. Saad, *$\mu \to e\gamma$ selecting scalar leptoquark solutions for the $(g-2)_{e,\mu}$ puzzles*, *Phys. Rev. D* **102** (2020) 075007 [arXiv:2006.11624] [INSPIRE].

[349] R. Nagai and N. Yokozaki, *Lepton flavor violations in SUSY models for muon $g-2$ with right-handed neutrinos*, *JHEP* **01** (2021) 099 [arXiv:2007.00943] [INSPIRE].

[350] C. Arbeláez, R. Cepedello, R.M. Fonseca and M. Hirsch, *$(g-2)$ anomalies and neutrino mass*, *Phys. Rev. D* **102** (2020) 075005 [arXiv:2007.11007] [INSPIRE].

[351] A. Abdullahi, M. Hostert and S. Pascoli, *A dark seesaw solution to low energy anomalies: MiniBooNE, the muon $(g-2)$, and BaBar*, *Phys. Lett. B* **820** (2021) 136531 [arXiv:2007.11813] [INSPIRE].

[352] S. Jana, P.K. Vishnu, W. Rodejohann and S. Saad, *Dark matter assisted lepton anomalous magnetic moments and neutrino masses*, *Phys. Rev. D* **102** (2020) 075003 [arXiv:2008.02377] [INSPIRE].

[353] N. Chakrabarty, *Doubly charged scalars and vector-like leptons confronting the muon $g-2$ anomaly and Higgs vacuum stability*, arXiv:2010.05215 [INSPIRE].

[354] H. Banerjee, B. Dutta and S. Roy, *Supersymmetric gauged $\mathrm{U}(1)_{L_\mu - L_\tau}$ model for electron and muon $(g-2)$ anomaly*, *JHEP* **03** (2021) 211 [arXiv:2011.05083] [INSPIRE].

[355] S.Q. Dinh and H.M. Tran, *Muon $g-2$ and semileptonic B decays in BDW model with gauge kinetic mixing*, arXiv:2011.07182 [INSPIRE].

[356] V.G. Baryshevsky and P.I. Porshnev, *Pseudoscalar corrections to spin motion equation, search for electric dipole moment and muon magnetic $(g-2)$ factor*, arXiv:2012.11751 [INSPIRE].

[357] M.J. Ramsey-Musolf and J.C. Vasquez, *Left-right symmetry and electric dipole moments. A global analysis*, *Phys. Lett. B* **815** (2021) 136136 [arXiv:2012.02799] [INSPIRE].

JHEP09(2021)080

[358] N. Chen, B. Wang and C.-Y. Yao, *The collider tests of a leptophilic scalar for the anomalous magnetic moments*, arXiv:2102.05619 [INSPIRE].

[359] G.-L. Liu, F. Wang and W. Wang, *The lepton flavor changing decays and one-loop muon anomalous magnetic moment in the extended mirror twin Higgs models*, arXiv:2012.09986 [INSPIRE].

[360] J. Aebischer, W. Dekens, E.E. Jenkins, A.V. Manohar, D. Sengupta and P. Stoffer, *Effective field theory interpretation of lepton magnetic and electric dipole moments*, arXiv:2102.08954 [INSPIRE].

[361] J. Cao, Y. He, J. Lian, D. Zhang and P. Zhu, *Electron and muon anomalous magnetic moments in the inverse seesaw extended NMSSM*, arXiv:2102.11355 [INSPIRE].

[362] S. Fajfer, J.F. Kamenik and M. Tammaro, *Interplay of new physics effects in* $(g-2)_\ell$ *and* $h \to \ell^+\ell^-$ *— lessons from SMEFT*, *JHEP* **06** (2021) 099 [arXiv:2103.10859] [INSPIRE].

[363] W. Yin and W. Yin, *Radiative lepton mass and muon* $g-2$ *with suppressed lepton flavor and CP-violations*, arXiv:2103.14234 [INSPIRE].

[364] A. Greljo, P. Stangl and A.E. Thomsen, *A model of muon anomalies*, arXiv:2103.13991 [INSPIRE].

[365] M. Abdullah, B. Dutta, S. Ghosh and T. Li, $(g-2)_{\mu,e}$ *and the ANITA anomalous events in a three-loop neutrino mass model*, *Phys. Rev. D* **100** (2019) 115006 [arXiv:1907.08109] [INSPIRE].

[366] M.J. Baker, P. Cox and R.R. Volkas, *Radiative muon mass models and* $(g-2)_\mu$, *JHEP* **05** (2021) 174 [arXiv:2103.13401] [INSPIRE].

[367] A. Freitas, J. Lykken, S. Kell and S. Westhoff, *Testing the muon* $g-2$ *anomaly at the LHC*, *JHEP* **05** (2014) 145 [*Erratum ibid.* **09** (2014) 155] [arXiv:1402.7065] [INSPIRE].

[368] L. Calibbi, P. Paradisi and R. Ziegler, *Lepton flavor violation in flavored gauge mediation*, *Eur. Phys. J. C* **74** (2014) 3211 [arXiv:1408.0754] [INSPIRE].

[369] F.S. Queiroz and W. Shepherd, *New physics contributions to the muon anomalous magnetic moment: a numerical code*, *Phys. Rev. D* **89** (2014) 095024 [arXiv:1403.2309] [INSPIRE].

[370] C. Biggio, M. Bordone, L. Di Luzio and G. Ridolfi, *Massive vectors and loop observables: the* $g-2$ *case*, *JHEP* **10** (2016) 002 [arXiv:1607.07621] [INSPIRE].

[371] C. Biggio and M. Bordone, *Minimal muon anomalous magnetic moment*, *JHEP* **02** (2015) 099 [arXiv:1411.6799] [INSPIRE].

[372] K. Kowalska and E.M. Sessolo, *Expectations for the muon* $g-2$ *in simplified models with dark matter*, *JHEP* **09** (2017) 112 [arXiv:1707.00753] [INSPIRE].

[373] P. Athron, C. Balázs, A. Fowlie and Y. Zhang, *Model-independent analysis of the DAMPE excess*, *JHEP* **02** (2018) 121 [arXiv:1711.11376] [INSPIRE].

[374] H. Banerjee, P. Byakti and S. Roy, *Supersymmetric gauged* $\mathrm{U}(1)_{L_\mu - L_\tau}$ *model for neutrinos and the muon* $(g-2)$ *anomaly*, *Phys. Rev. D* **98** (2018) 075022 [arXiv:1805.04415] [INSPIRE].

[375] C.-W. Chiang, M. Takeuchi, P.-Y. Tseng and T.T. Yanagida, *Muon* $g-2$ *and rare top decays in up-type specific variant axion models*, *Phys. Rev. D* **98** (2018) 095020 [arXiv:1807.00593] [INSPIRE].

[376] L. Calibbi, R. Ziegler and J. Zupan, *Minimal models for dark matter and the muon* $g-2$ *anomaly*, *JHEP* **07** (2018) 046 [arXiv:1804.00009] [INSPIRE].

JHEP09(2021)080

[377] P. Das, M.K. Das and N. Khan, *The FIMP-WIMP dark matter and muon $g-2$ in the extended singlet scalar model*, arXiv:2104.03271 [INSPIRE].

[378] M.A. Buen-Abad, J. Fan, M. Reece and C. Sun, *Challenges for an axion explanation of the muon $g-2$ measurement*, arXiv:2104.03267 [INSPIRE].

[379] F. Wang, L. Wu, Y. Xiao, J.M. Yang and Y. Zhang, *GUT-scale constrained SUSY in light of new muon $g-2$ measurement*, *Nucl. Phys. B* **970** (2021) 115486 [arXiv:2104.03262] [INSPIRE].

[380] M. Abdughani, Y.-Z. Fan, L. Feng, Y.-L.S. Tsai, L. Wu and Q. Yuan, *A common origin of muon $g-2$ anomaly, Galaxy Center GeV excess and AMS-02 anti-proton excess in the NMSSM*, *Sci. Bull.* **66** (2021) 2170 [arXiv:2104.03274] [INSPIRE].

[381] C.-H. Chen, C.-W. Chiang and T. Nomura, *Muon $g-2$ in two-Higgs-doublet model with type-II seesaw mechanism*, arXiv:2104.03275 [INSPIRE].

[382] S.-F. Ge, X.-D. Ma and P. Pasquini, *Probing the dark axion portal with muon anomalous magnetic moment*, arXiv:2104.03276 [INSPIRE].

[383] M. Cadeddu, N. Cargioli, F. Dordei, C. Giunti and E. Picciau, *Muon and electron $g-2$ and proton and cesium weak charges implications on dark Zd models*, *Phys. Rev. D* **104** (2021) 011701 [arXiv:2104.03280] [INSPIRE].

[384] V. Brdar, S. Jana, J. Kubo and M. Lindner, *Semi-secretly interacting axion-like particle as an explanation of Fermilab muon $g-2$ measurement*, *Phys. Lett. B* **820** (2021) 136529 [arXiv:2104.03282] [INSPIRE].

[385] J. Cao, J. Lian, Y. Pan, D. Zhang and P. Zhu, *Improved $(g-2)_\mu$ measurement and singlino dark matter in the general NMSSM*, arXiv:2104.03284 [INSPIRE].

[386] M. Chakraborti, S. Heinemeyer and I. Saha, *The new "MUON G-2" result and supersymmetry*, arXiv:2104.03287 [INSPIRE].

[387] M. Ibe, S. Kobayashi, Y. Nakayama and S. Shirai, *Muon $g-2$ in gauge mediation without SUSY CP problem*, arXiv:2104.03289 [INSPIRE].

[388] P. Cox, C. Han and T.T. Yanagida, *Muon $g-2$ and co-annihilating dark matter in the MSSM*, arXiv:2104.03290 [INSPIRE].

[389] K.S. Babu, S. Jana, M. Lindner and V.P. K, *Muon $g-2$ anomaly and neutrino magnetic Moments*, arXiv:2104.03291 [INSPIRE].

[390] C. Han, *Muon $g-2$ and CP-violation in MSSM*, arXiv:2104.03292 [INSPIRE].

[391] S. Heinemeyer, E. Kpatcha, I. Lara, D.E. López-Fogliani, C. Muñoz and N. Nagata, *The new $(g-2)_\mu$ result and the $\mu\nu$SSM*, arXiv:2104.03294 [INSPIRE].

[392] L. Calibbi, M.L. López-Ibáñez, A. Melis and O. Vives, *Implications of the muon $g-2$ result on the flavour structure of the lepton mass matrix*, arXiv:2104.03296 [INSPIRE].

[393] D.W.P. Amaral, D.G. Cerdeño, A. Cheek and P. Foldenauer, *Distinguishing $\mathrm{U}(1)_{L_\mu - L_\tau}$ from $\mathrm{U}(1)_{L_\mu}$ as a solution for $(g-2)_\mu$ with neutrinos*, arXiv:2104.03297 [INSPIRE].

[394] Y. Bai and J. Berger, *Muon $g-2$ in lepton portal dark matter*, arXiv:2104.03301 [INSPIRE].

[395] S. Baum, M. Carena, N.R. Shah and C.E.M. Wagner, *The tiny $(g-2)$ muon wobble from small-μ supersymmetry*, arXiv:2104.03302 [INSPIRE].

[396] W. Yin, *Muon $g-2$ anomaly in anomaly mediation*, *JHEP* **06** (2021) 029 [arXiv:2104.03259] [INSPIRE].

JHEP09(2021)080

[397] D. Anselmi et al., *Fake doublet solution to the muon anomalous magnetic moment*, *Phys. Rev. D* **104** (2021) 035009 [arXiv:2104.03249] [INSPIRE].

[398] T. Nomura and H. Okada, *Explanations for anomalies of muon anomalous magnetic dipole moment, $b \to s\mu\bar{\mu}$, and radiative neutrino masses in a leptoquark model*, *Phys. Rev. D* **104** (2021) 035042 [arXiv:2104.03248] [INSPIRE].

[399] M. Van Beekveld, W. Beenakker, M. Schutten and J. De Wit, *Dark matter, fine-tuning and $(g-2)_\mu$ in the pMSSM*, arXiv:2104.03245 [INSPIRE].

[400] H.-X. Wang, L. Wang and Y. Zhang, *muon $g-2$ anomaly and μ-τ-philic Higgs doublet with a light CP-even component*, arXiv:2104.03242 [INSPIRE].

[401] Y. Gu, N. Liu, L. Su and D. Wang, *Heavy bino and slepton for muon $g-2$ anomaly*, *Nucl. Phys. B* **969** (2021) 115481 [arXiv:2104.03239] [INSPIRE].

[402] B. Zhu and X. Liu, *Probing the flavor-specific scalar mediator for the muon $(g-2)$ deviation, the proton radius puzzle and the light dark matter production*, arXiv:2104.03238 [INSPIRE].

[403] J.C. Criado, A. Djouadi, N. Koivunen, K. Müürsepp, M. Raidal and H. Veermäe, *Confronting spin-3/2 and other new fermions with the muon $g-2$ measurement*, *Phys. Lett. B* **820** (2021) 136491 [arXiv:2104.03231] [INSPIRE].

[404] G. Arcadi, L. Calibbi, M. Fedele and F. Mescia, *Muon $g-2$ and B-anomalies from Dark Matter*, *Phys. Rev. Lett.* **127** (2021) 061802 [arXiv:2104.03228] [INSPIRE].

[405] X.-F. Han, T. Li, H.-X. Wang, L. Wang and Y. Zhang, *Lepton-specific inert two-Higgs-doublet model confronted with the new results for muon and electron g-2 anomalies and multi-lepton searches at the LHC*, arXiv:2104.03227 [INSPIRE].

[406] S. Iwamoto, T.T. Yanagida and N. Yokozaki, *Wino-Higgsino dark matter in the MSSM from the $g-2$ anomaly*, arXiv:2104.03223 [INSPIRE].

[407] M. Endo, K. Hamaguchi, S. Iwamoto and T. Kitahara, *Supersymmetric interpretation of the muon $g-2$ anomaly*, *JHEP* **07** (2021) 075 [arXiv:2104.03217] [INSPIRE].

[408] A. Crivellin and M. Hoferichter, *Consequences of chirally enhanced explanations of $(g-2)_\mu$ for $h \to \mu\mu$ and $Z \to \mu\mu$*, *JHEP* **07** (2021) 135 [arXiv:2104.03202] [INSPIRE].

[409] A.E. Cárcamo Hernández, C. Espinoza, J. Carlos Gómez-Izquierdo and M. Mondragón, *Fermion masses and mixings, dark matter, leptogenesis and $g-2$ muon anomaly in an extended 2HDM with inverse seesaw*, arXiv:2104.02730 [INSPIRE].

[410] M. Chakraborti, L. Roszkowski and S. Trojanowski, *GUT-constrained supersymmetry and dark matter in light of the new $(g-2)_\mu$ determination*, *JHEP* **05** (2021) 252 [arXiv:2104.04458] [INSPIRE].

[411] M. Passera, W.J. Marciano and A. Sirlin, *The muon $g-2$ and the bounds on the Higgs boson mass*, *Phys. Rev. D* **78** (2008) 013009 [arXiv:0804.1142] [INSPIRE].

[412] A. Crivellin, M. Hoferichter, C.A. Manzari and M. Montull, *Hadronic vacuum polarization: $(g-2)_\mu$ versus global electroweak fits*, *Phys. Rev. Lett.* **125** (2020) 091801 [arXiv:2003.04886] [INSPIRE].

[413] A. Keshavarzi, W.J. Marciano, M. Passera and A. Sirlin, *Muon $g-2$ and $\Delta\alpha$ connection*, *Phys. Rev. D* **102** (2020) 033002 [arXiv:2006.12666] [INSPIRE].

[414] E. de Rafael, *Constraints between $\Delta\alpha_{\rm had}(M_Z^2)$ and $(g_\mu-2)_{\rm HVP}$*, *Phys. Rev. D* **102** (2020) 056025 [arXiv:2006.13880] [INSPIRE].

JHEP09(2021)080

[415] B. Malaescu and M. Schott, *Impact of correlations between a_μ and $\alpha_{\rm QED}$ on the EW fit*, *Eur. Phys. J. C* **81** (2021) 46 [arXiv:2008.08107] [INSPIRE].

[416] PLANCK collaboration, *Planck 2018 results. VI. Cosmological parameters*, *Astron. Astrophys.* **641** (2020) A6 [*Erratum ibid.* **652** (2021) C4] [arXiv:1807.06209] [INSPIRE].

[417] PARTICLE DATA GROUP collaboration, *Review of particle physics*, *Phys. Rev. D* **98** (2018) 030001 [INSPIRE].

[418] G.F. Giudice, P. Paradisi and M. Passera, *Testing new physics with the electron $g-2$*, *JHEP* **11** (2012) 113 [arXiv:1208.6583] [INSPIRE].

[419] J.A. Coarasa Perez, A. Mendez and J. Solà, *Higgs triplet effects in purely leptonic processes*, *Phys. Lett. B* **374** (1996) 131 [hep-ph/9511297] [INSPIRE].

[420] J.F. Gunion, J. Grifols, A. Mendez, B. Kayser and F.I. Olness, *Higgs bosons in left-right symmetric models*, *Phys. Rev. D* **40** (1989) 1546 [INSPIRE].

[421] W.-C. Chiu, C.-Q. Geng and D. Huang, *Correlation between muon $g-2$ and $\mu \to e\gamma$*, *Phys. Rev. D* **91** (2015) 013006 [arXiv:1409.4198] [INSPIRE].

[422] C. Kelso, H.N. Long, R. Martinez and F.S. Queiroz, *Connection of $g-2_\mu$, electroweak, dark matter, and collider constraints on 331 models*, *Phys. Rev. D* **90** (2014) 113011 [arXiv:1408.6203] [INSPIRE].

[423] CMS collaboration, *Searches for electroweak production of charginos, neutralinos, and sleptons decaying to leptons and W, Z, and Higgs bosons in pp collisions at 8 TeV*, *Eur. Phys. J. C* **74** (2014) 3036 [arXiv:1405.7570] [INSPIRE].

[424] A.V. Kuznetsov, N.V. Mikheev and A.V. Serghienko, *The third type of fermion mixing in the lepton and quark interactions with leptoquarks*, *Int. J. Mod. Phys. A* **27** (2012) 1250062 [arXiv:1203.0196] [INSPIRE].

[425] D. Hanneke, S. Fogwell and G. Gabrielse, *New measurement of the electron magnetic moment and the fine structure constant*, *Phys. Rev. Lett.* **100** (2008) 120801 [arXiv:0801.1134] [INSPIRE].

[426] H. Merkel et al., *Search at the Mainz microtron for light massive gauge bosons relevant for the muon $g-2$ anomaly*, *Phys. Rev. Lett.* **112** (2014) 221802 [arXiv:1404.5502] [INSPIRE].

[427] BABAR collaboration, *Search for a dark photon in e^+e^- collisions at BaBar*, *Phys. Rev. Lett.* **113** (2014) 201801 [arXiv:1406.2980] [INSPIRE].

[428] NA48/2 collaboration, *Search for the dark photon in π^0 decays*, *Phys. Lett. B* **746** (2015) 178 [arXiv:1504.00607] [INSPIRE].

[429] S.N. Gninenko, D.V. Kirpichnikov, M.M. Kirsanov and N.V. Krasnikov, *Combined search for light dark matter with electron and muon beams at NA64*, *Phys. Lett. B* **796** (2019) 117 [arXiv:1903.07899] [INSPIRE].

[430] M. Escudero, D. Hooper, G. Krnjaic and M. Pierre, *Cosmology with a very light L_μ–L_τ gauge boson*, *JHEP* **03** (2019) 071 [arXiv:1901.02010] [INSPIRE].

[431] E.J. Chun and T. Mondal, *Searching for a light Higgs boson via the Yukawa process at lepton colliders*, *Phys. Lett. B* **802** (2020) 135190 [arXiv:1909.09515] [INSPIRE].

[432] M. Bauer and M. Neubert, *Minimal leptoquark explanation for the $R_{D^{(*)}}$, R_K , and $(g-2)_\mu$ anomalies*, *Phys. Rev. Lett.* **116** (2016) 141802 [arXiv:1511.01900] [INSPIRE].

JHEP09(2021)080

[433] O. Popov and G.A. White, *One leptoquark to unify them? Neutrino masses and unification in the light of $(g-2)_\mu$, $R_{D^{(\star)}}$ and R_K anomalies*, *Nucl. Phys. B* **923** (2017) 324 [arXiv:1611.04566] [INSPIRE].

[434] W. Buchmüller, R. Ruckl and D. Wyler, *Leptoquarks in lepton-quark collisions*, *Phys. Lett. B* **191** (1987) 442 [*Erratum ibid.* **448** (1999) 320] [INSPIRE].

[435] I. Bigaran and R.R. Volkas, *Getting chirality right: Single scalar leptoquark solutions to the $(g-2)_{e,\mu}$ puzzle*, *Phys. Rev. D* **102** (2020) 075037 [arXiv:2002.12544] [INSPIRE].

[436] S.P. Martin, *A supersymmetry primer*, *Adv. Ser. Direct. High Energy Phys.* **18** (1998) 1 [hep-ph/9709356] [INSPIRE].

[437] J.M. Arnold, B. Fornal and M.B. Wise, *Phenomenology of scalar leptoquarks*, *Phys. Rev. D* **88** (2013) 035009 [arXiv:1304.6119] [INSPIRE].

[438] F.S. Queiroz, K. Sinha and A. Strumia, *Leptoquarks, dark matter, and anomalous LHC events*, *Phys. Rev. D* **91** (2015) 035006 [arXiv:1409.6301] [INSPIRE].

[439] W. Dekens, J. de Vries, M. Jung and K.K. Vos, *The phenomenology of electric dipole moments in models of scalar leptoquarks*, *JHEP* **01** (2019) 069 [arXiv:1809.09114] [INSPIRE].

[440] CMS collaboration, *Search for leptoquarks coupled to third-generation quarks in proton-proton collisions at $\sqrt{s} = 13$ TeV*, *Phys. Rev. Lett.* **121** (2018) 241802 [arXiv:1809.05558] [INSPIRE].

[441] CMS collaboration, *Constraints on models of scalar and vector leptoquarks decaying to a quark and a neutrino at $\sqrt{s} = 13$ TeV*, *Phys. Rev. D* **98** (2018) 032005 [arXiv:1805.10228] [INSPIRE].

[442] ALEPH et al. collaborations, *Precision electroweak measurements on the Z resonance*, *Phys. Rept.* **427** (2006) 257 [hep-ex/0509008] [INSPIRE].

[443] P. Arnan, D. Becirevic, F. Mescia and O. Sumensari, *Probing low energy scalar leptoquarks by the leptonic W and Z couplings*, *JHEP* **02** (2019) 109 [arXiv:1901.06315] [INSPIRE].

[444] F. Staub, *From superpotential to model files for FeynArts and CalcHep/CompHEP*, *Comput. Phys. Commun.* **181** (2010) 1077 [arXiv:0909.2863] [INSPIRE].

[445] F. Staub, *Automatic calculation of supersymmetric renormalization group equations and self energies*, *Comput. Phys. Commun.* **182** (2011) 808 [arXiv:1002.0840] [INSPIRE].

[446] F. Staub, *SARAH 3.2: Dirac gauginos, UFO output, and more*, *Comput. Phys. Commun.* **184** (2013) 1792 [arXiv:1207.0906] [INSPIRE].

[447] F. Staub, *SARAH 4: a tool for (not only SUSY) model builders*, *Comput. Phys. Commun.* **185** (2014) 1773 [arXiv:1309.7223] [INSPIRE].

[448] B.C. Allanach, *SOFTSUSY: a program for calculating supersymmetric spectra*, *Comput. Phys. Commun.* **143** (2002) 305 [hep-ph/0104145] [INSPIRE].

[449] B.C. Allanach, P. Athron, L.C. Tunstall, A. Voigt and A.G. Williams, *Next-to-minimal SOFTSUSY*, *Comput. Phys. Commun.* **185** (2014) 2322 [*Erratum ibid.* **250** (2020) 107044] [arXiv:1311.7659] [INSPIRE].

[450] G. Degrassi and G.F. Giudice, *QED logarithms in the electroweak corrections to the muon anomalous magnetic moment*, *Phys. Rev. D* **58** (1998) 053007 [hep-ph/9803384] [INSPIRE].

[451] FCC collaboration, *HE-LHC: the high-energy Large Hadron Collider: future circular collider conceptual design report volume 4*, *Eur. Phys. J. ST* **228** (2019) 1109 [INSPIRE].

JHEP09(2021)080

[452] T. Behnke et al., *The International Linear Collider technical design report — Volume 1: executive summary*, arXiv:1306.6327 [INSPIRE].

[453] M. Aicheler et al., *A multi-TeV linear collider based on CLIC technology: CLIC conceptual design report*, CERN-2012-007 (2012).

[454] CEPC Study Group collaboration, *CEPC conceptual design report. Volume 1: accelerator*, arXiv:1809.00285 [INSPIRE].

[455] FCC collaboration, *FCC-ee: the lepton collider: Future Circular Collider conceptual design report. Volume 2*, *Eur. Phys. J. ST* **228** (2019) 261 [INSPIRE].

[456] FCC collaboration, *FCC-hh: the hadron collider: Future Circular Collider conceptual design report. Volume 3*, *Eur. Phys. J. ST* **228** (2019) 755 [INSPIRE].

[457] A. Crivellin, D. Müller and F. Saturnino, *Leptoquarks in oblique corrections and Higgs signal strength: status and prospects*, *JHEP* **11** (2020) 094 [arXiv:2006.10758] [INSPIRE].

[458] I. Doršner and A. Greljo, *Leptoquark toolbox for precision collider studies*, *JHEP* **05** (2018) 126 [arXiv:1801.07641] [INSPIRE].

[459] S. Bar-Shalom, J. Cohen, A. Soni and J. Wudka, *Phenomenology of TeV-scale scalar Leptoquarks in the EFT*, *Phys. Rev. D* **100** (2019) 055020 [arXiv:1812.03178] [INSPIRE].

[460] G. Hiller, D. Loose and I. Nišandžić, *Flavorful leptoquarks at hadron colliders*, *Phys. Rev. D* **97** (2018) 075004 [arXiv:1801.09399] [INSPIRE].

[461] B.C. Allanach, T. Corbett and M. Madigan, *Sensitivity of future hadron colliders to leptoquark pair production in the di-muon di-jets channel*, *Eur. Phys. J. C* **80** (2020) 170 [arXiv:1911.04455] [INSPIRE].

[462] W. Altmannshofer, S. Gori, H.H. Patel, S. Profumo and D. Tuckler, *Electric dipole moments in a leptoquark scenario for the B-physics anomalies*, *JHEP* **05** (2020) 069 [arXiv:2002.01400] [INSPIRE].

[463] P. Asadi, R. Capdevilla, C. Cesarotti and S. Homiller, *Searching for leptoquarks at future muon Colliders*, arXiv:2104.05720 [INSPIRE].

[464] G.-Y. Huang, S. Jana, F.S. Queiroz and W. Rodejohann, *Probing the $R_{K^{(*)}}$ anomaly at a muon Collider*, arXiv:2103.01617 [INSPIRE].

[465] ALEPH collaboration, *Search for charginos nearly mass degenerate with the lightest neutralino in e^+e^- collisions at center-of-mass energies up to 209 GeV*, *Phys. Lett. B* **533** (2002) 223 [hep-ex/0203020] [INSPIRE].

[466] DELPHI collaboration, *Searches for supersymmetric particles in e^+e^- collisions up to 208 GeV and interpretation of the results within the MSSM*, *Eur. Phys. J. C* **31** (2003) 421 [hep-ex/0311019] [INSPIRE].

[467] F. del Aguila, J. de Blas and M. Pérez-Victoria, *Effects of new leptons in electroweak precision data*, *Phys. Rev. D* **78** (2008) 013010 [arXiv:0803.4008] [INSPIRE].

[468] S. Kraml et al., *SModelS: a tool for interpreting simplified-model results from the LHC and its application to supersymmetry*, *Eur. Phys. J. C* **74** (2014) 2868 [arXiv:1312.4175] [INSPIRE].

[469] F. Ambrogi et al., *SModelS v1.1 user manual: Improving simplified model constraints with efficiency maps*, *Comput. Phys. Commun.* **227** (2018) 72 [arXiv:1701.06586] [INSPIRE].

[470] J. Dutta, S. Kraml, A. Lessa and W. Waltenberger, *SModelS extension with the CMS supersymmetry search results from Run 2*, *LHEP* **1** (2018) 5 [arXiv:1803.02204] [INSPIRE].

JHEP09(2021)080

[471] F. Ambrogi et al., *SModelS v1.2: long-lived particles, combination of signal regions, and other novelties*, *Comput. Phys. Commun.* **251** (2020) 106848 [arXiv:1811.10624] [INSPIRE].

[472] T. Sjöstrand, S. Mrenna and P.Z. Skands, *PYTHIA 6.4 physics and manual*, *JHEP* **05** (2006) 026 [hep-ph/0603175] [INSPIRE].

[473] T. Sjöstrand et al., *An introduction to PYTHIA 8.2*, *Comput. Phys. Commun.* **191** (2015) 159 [arXiv:1410.3012] [INSPIRE].

[474] A. Buckley, *PySLHA: a Pythonic interface to SUSY Les Houches Accord data*, *Eur. Phys. J. C* **75** (2015) 467 [arXiv:1305.4194] [INSPIRE].

[475] M. Drees, H. K. Dreiner, J. S. Kim, D. Schmeier and J. Tattersall, *Checkmate: Confronting your favourite new physics model with LHC data*, *Comput. Phys. Commun.* **187** (2015) 227.

[476] D. Dercks, N. Desai, J.S. Kim, K. Rolbiecki, J. Tattersall and T. Weber, *CheckMATE 2: from the model to the limit*, *Comput. Phys. Commun.* **221** (2017) 383 [arXiv:1611.09856] [INSPIRE].

[477] A.L. Read, *Presentation of search results: the CL(s) technique*, *J. Phys. G* **28** (2002) 2693 [INSPIRE].

[478] M. Cacciari and G.P. Salam, *Dispelling the N^3 myth for the k_t jet-finder*, *Phys. Lett. B* **641** (2006) 57 [hep-ph/0512210] [INSPIRE].

[479] M. Cacciari, G.P. Salam and G. Soyez, *The anti-k_t jet clustering algorithm*, *JHEP* **04** (2008) 063 [arXiv:0802.1189] [INSPIRE].

[480] M. Cacciari, G.P. Salam and G. Soyez, *FastJet user manual*, *Eur. Phys. J. C* **72** (2012) 1896 [arXiv:1111.6097] [INSPIRE].

[481] DELPHES 3 collaboration, *DELPHES 3, a modular framework for fast simulation of a generic collider experiment*, *JHEP* **02** (2014) 057 [arXiv:1307.6346] [INSPIRE].

[482] CMS collaboration, *Search for new physics in events with two soft oppositely charged leptons and missing transverse momentum in proton-proton collisions at $\sqrt{s} = 13$ TeV*, *Phys. Lett. B* **782** (2018) 440 [arXiv:1801.01846] [INSPIRE].

[483] N. Arkani-Hamed, A. Delgado and G.F. Giudice, *The well-tempered neutralino*, *Nucl. Phys. B* **741** (2006) 108 [hep-ph/0601041] [INSPIRE].

[484] CMS collaboration, *Searches for long-lived charged particles in pp collisions at $\sqrt{s} = 7$ and 8 TeV*, *JHEP* **07** (2013) 122 [arXiv:1305.0491] [INSPIRE].

[485] ATLAS collaboration, *Search for direct production of charginos, neutralinos and sleptons in final states with two leptons and missing transverse momentum in pp collisions at $\sqrt{s} = 8$ TeV with the ATLAS detector*, *JHEP* **05** (2014) 071 [arXiv:1403.5294] [INSPIRE].

[486] CMS collaboration, *Constraints on the pMSSM, AMSB model and on other models from the search for long-lived charged particles in proton-proton collisions at $\sqrt{s} = 8$ TeV*, *Eur. Phys. J. C* **75** (2015) 325 [arXiv:1502.02522] [INSPIRE].

[487] ATLAS collaboration, *Search for electroweak production of supersymmetric particles in final states with two or three leptons at $\sqrt{s} = 13$ TeV with the ATLAS detector*, *Eur. Phys. J. C* **78** (2018) 995 [arXiv:1803.02762] [INSPIRE].

[488] CMS collaboration, *Search for supersymmetric partners of electrons and muons in proton-proton collisions at $\sqrt{s} = 13$ TeV*, *Phys. Lett. B* **790** (2019) 140 [arXiv:1806.05264] [INSPIRE].

JHEP09(2021)080

[489] CMS collaboration, *Search for heavy stable charged particles with* $12.9\,fb^{-1}$ *of 2016 data*, CMS-PAS-EXO-16-036 (2016).

[490] ATLAS collaboration, *Search for electroweak production of charginos and sleptons decaying into final states with two leptons and missing transverse momentum in* $\sqrt{s} = 13$ *TeV pp collisions using the ATLAS detector*, *Eur. Phys. J. C* **80** (2020) 123 [arXiv:1908.08215] [INSPIRE].

[491] S. Kraml et al., *SModelS: a tool for interpreting simplified-model results from the LHC and its application to supersymmetry*, *Eur. Phys. J. C* **74** (2014) 2868 [arXiv:1312.4175] [INSPIRE].

[492] C.K. Khosa, S. Kraml, A. Lessa, P. Neuhuber and W. Waltenberger, *Smodels database update v1.2.3*, arXiv:2005.00555.

[493] J. Alwall et al., *The automated computation of tree-level and next-to-leading order differential cross sections, and their matching to parton shower simulations*, *JHEP* **07** (2014) 079 [arXiv:1405.0301] [INSPIRE].

[494] G. Bélanger, F. Boudjema, A. Goudelis, A. Pukhov and B. Zaldivar, *MicrOMEGAs5.0: freeze-in*, *Comput. Phys. Commun.* **231** (2018) 173 [arXiv:1801.03509] [INSPIRE].

[495] F. Feroz and M.P. Hobson, *Multimodal nested sampling: an efficient and robust alternative to MCMC methods for astronomical data analysis*, *Mon. Not. Roy. Astron. Soc.* **384** (2008) 449 [arXiv:0704.3704] [INSPIRE].

[496] F. Feroz, M.P. Hobson and M. Bridges, *MultiNest: an efficient and robust Bayesian inference tool for cosmology and particle physics*, *Mon. Not. Roy. Astron. Soc.* **398** (2009) 1601 [arXiv:0809.3437] [INSPIRE].

[497] F. Feroz, M.P. Hobson, E. Cameron and A.N. Pettitt, *Importance nested sampling and the MultiNest algorithm*, *Open J. Astrophys.* **2** (2019) 10 [arXiv:1306.2144] [INSPIRE].

[498] J. Buchner et al., *X-ray spectral modelling of the agn obscuring region in the cdfs: Bayesian model selection and catalogue*, *Astron. Astrophys.* **564** (2014) A125.

[499] CMS collaboration, *Searches for long-lived charged particles*, *Eur. Phys. C* **80** (2020) 572 [arXiv:2004.11305].

[500] CMS collaboration, *Search for electroweak production of charginos, neutralinos, and sleptons using leptonic final states in pp collisions at* 8 *TeV*, *Eur. Phys. J. C* **80** (2020) 123 [arXiv:1908.08215].

[501] CMS collaboration, *Search for selectrons and smuons at* $\sqrt{s} = 13$ *TeV*, CMS-PAS-SUS-17-009 (2017).

[502] PLANCK collaboration, *Planck 2015 results. XIII. Cosmological parameters*, *Astron. Astrophys.* **594** (2016) A13 [arXiv:1502.01589] [INSPIRE].

[503] G. Degrassi and G.F. Giudice, *QED logarithms in the electroweak corrections to the muon anomalous magnetic moment*, *Phys. Rev. D* **58** (1998) 053007 [hep-ph/9803384] [INSPIRE].

[504] L. Lopez Honorez, E. Nezri, J.F. Oliver and M.H.G. Tytgat, *The inert doublet model: an archetype for dark matter*, *JCAP* **02** (2007) 028 [hep-ph/0612275] [INSPIRE].

[505] P. Athron, J.M. Cornell, F. Kahlhoefer, J. McKay, P. Scott and S. Wild, *Impact of vacuum stability, perturbativity and XENON1T on global fits of* $\mathbb{Z}_2$ *and* $\mathbb{Z}_3$ *scalar singlet dark matter*, *Eur. Phys. J. C* **78** (2018) 830 [arXiv:1806.11281] [INSPIRE].

[506] XENON collaboration, *First dark matter search results from the XENON1T experiment*, *Phys. Rev. Lett.* **119** (2017) 181301 [arXiv:1705.06655] [INSPIRE].

JHEP09(2021)080

[507] XENON collaboration, *Dark matter search results from a one ton-year exposure of XENON1T*, *Phys. Rev. Lett.* **121** (2018) 111302 [arXiv:1805.12562] [INSPIRE].

[508] GAMBIT Dark Matter Workgroup collaboration, *DarkBit: a GAMBIT module for computing dark matter observables and likelihoods*, *Eur. Phys. J. C* **77** (2017) 831 [arXiv:1705.07920] [INSPIRE].

[509] GAMBIT collaboration, *Global analyses of Higgs portal singlet dark matter models using GAMBIT*, *Eur. Phys. J. C* **79** (2019) 38 [arXiv:1808.10465] [INSPIRE].

[510] M. Cirelli, N. Fornengo and A. Strumia, *Minimal dark matter*, *Nucl. Phys. B* **753** (2006) 178 [hep-ph/0512090] [INSPIRE].

[511] P. Athron, D. Harries, R. Nevzorov and A.G. Williams, *Dark matter in a constrained E_6 inspired SUSY model*, *JHEP* **12** (2016) 128 [arXiv:1610.03374] [INSPIRE].

[512] T. Moroi, *The Muon anomalous magnetic dipole moment in the minimal supersymmetric standard model*, *Phys. Rev. D* **53** (1996) 6565 [*Erratum ibid.* **56** (1997) 4424] [hep-ph/9512396] [INSPIRE].

[513] T. Aoyama, M. Hayakawa, T. Kinoshita and M. Nio, *Tenth-order QED contribution to the electron $g-2$ and an improved value of the fine structure constant*, *Phys. Rev. Lett.* **109** (2012) 111807 [arXiv:1205.5368] [INSPIRE].

[514] T. Aoyama, T. Kinoshita and M. Nio, *Revised and improved value of the QED tenth-order electron anomalous magnetic moment*, *Phys. Rev. D* **97** (2018) 036001 [arXiv:1712.06060] [INSPIRE].

[515] R.H. Parker, C. Yu, W. Zhong, B. Estey and H. Müller, *Measurement of the fine-structure constant as a test of the Standard Model*, *Science* **360** (2018) 191 [arXiv:1812.04130] [INSPIRE].

[516] L. Morel, Z. Yao, P. Cladé and S. Guellati-Khélifa, *Determination of the fine-structure constant with an accuracy of 81 parts per trillion*, *Nature* **588** (2020) 61 [INSPIRE].

[517] P. Athron, J.-h. Park, T. Steudtner, D. Stöckinger and A. Voigt, *Precise Higgs mass calculations in (non-)minimal supersymmetry at both high and low scales*, *JHEP* **01** (2017) 079 [arXiv:1609.00371] [INSPIRE].

[518] T. Kwasnitza, D. Stöckinger and A. Voigt, *Improved MSSM Higgs mass calculation using the 3-loop FlexibleEFTHiggs approach including x_t-resummation*, *JHEP* **07** (2020) 197 [arXiv:2003.04639] [INSPIRE].

[519] S.-M. Zhao, T.-F. Feng, H.-B. Zhang, B. Yan and X.-J. Zhan, *The corrections from one loop and two-loop Barr-Zee type diagrams to muon MDM in BLMSSM*, *JHEP* **11** (2014) 119 [arXiv:1405.7561] [INSPIRE].

[520] CMS collaboration, *Search for electroweak production of charginos and neutralinos in multilepton final states in proton-proton collisions at $\sqrt{s} = 13$ TeV*, *JHEP* **03** (2018) 166 [arXiv:1709.05406] [INSPIRE].

[521] ATLAS collaboration, *Search for direct production of electroweakinos in final states with one lepton, missing transverse momentum and a Higgs boson decaying into two b-jets in pp collisions at $\sqrt{s} = 13$ TeV with the ATLAS detector*, *Eur. Phys. J. C* **80** (2020) 691 [arXiv:1909.09226] [INSPIRE].

[522] A. Canepa, T. Han and X. Wang, *The search for electroweakinos*, *Ann. Rev. Nucl. Part. Sci.* **70** (2020) 425 [arXiv:2003.05450] [INSPIRE].

JHEP09(2021)080

[523] CMS collaboration, *Combined search for electroweak production of charginos and neutralinos in proton-proton collisions at* $\sqrt{s} = 13$ *TeV*, *JHEP* **03** (2018) 160 [arXiv:1801.03957] [INSPIRE].

[524] ATLAS collaboration, *Search for the direct production of charginos and neutralinos in final states with tau leptons in* $\sqrt{s} = 13$ *TeV pp collisions with the ATLAS detector*, *Eur. Phys. J. C* **78** (2018) 154 [arXiv:1708.07875] [INSPIRE].

[525] CMS collaboration, *Search for new phenomena in final states with two opposite-charge, same-flavor leptons, jets, and missing transverse momentum in pp collisions at* $\sqrt{s} = 13$ *TeV*, *JHEP* **03** (2018) 076 [arXiv:1709.08908] [INSPIRE].

[526] ATLAS collaboration, *Search for chargino-neutralino production using recursive jigsaw reconstruction in final states with two or three charged leptons in proton-proton collisions at* $\sqrt{s} = 13$ *TeV with the ATLAS detector*, *Phys. Rev. D* **98** (2018) 092012 [arXiv:1806.02293] [INSPIRE].

[527] ATLAS collaboration, *Search for chargino-neutralino production with mass splittings near the electroweak scale in three-lepton final states in* $\sqrt{s} = 13$ *TeV pp collisions with the ATLAS detector*, *Phys. Rev. D* **101** (2020) 072001 [arXiv:1912.08479] [INSPIRE].

[528] ATLAS collaboration, *Searches for electroweak production of supersymmetric particles with compressed mass spectra in* $\sqrt{s} = 13$ *TeV pp collisions with the ATLAS detector*, *Phys. Rev. D* **101** (2020) 052005 [arXiv:1911.12606] [INSPIRE].

[529] CMS collaboration, *Search for supersymmetry with a compressed mass spectrum in the vector boson fusion topology with 1-lepton and 0-lepton final states in proton-proton collisions at* $\sqrt{s} = 13$ *TeV*, *JHEP* **08** (2019) 150 [arXiv:1905.13059] [INSPIRE].

[530] GAMBIT collaboration, *ColliderBit: a GAMBIT module for the calculation of high-energy collider observables and likelihoods*, *Eur. Phys. J. C* **77** (2017) 795 [arXiv:1705.07919] [INSPIRE].

[531] GAMBIT collaboration, *GAMBIT: the global and modular beyond-the-standard-model inference tool*, *Eur. Phys. J. C* **77** (2017) 784 [*Addendum ibid.* **78** (2018) 98] [arXiv:1705.07908] [INSPIRE].

[532] GAMBIT Models Workgroup collaboration, *SpecBit, DecayBit and PrecisionBit: GAMBIT modules for computing mass spectra, particle decay rates and precision observables*, *Eur. Phys. J. C* **78** (2018) 22 [arXiv:1705.07936] [INSPIRE].

[533] GAMBIT collaboration, *Comparison of statistical sampling methods with ScannerBit, the GAMBIT scanning module*, *Eur. Phys. J. C* **77** (2017) 761 [arXiv:1705.07959] [INSPIRE].

[534] GAMBIT Flavour Workgroup collaboration, *FlavBit: a GAMBIT module for computing flavour observables and likelihoods*, *Eur. Phys. J. C* **77** (2017) 786 [arXiv:1705.07933] [INSPIRE].

[535] GAMBIT collaboration, *Combined collider constraints on neutralinos and charginos*, *Eur. Phys. J. C* **79** (2019) 395 [arXiv:1809.02097] [INSPIRE].

[536] J. Bramante, N. Desai, P. Fox, A. Martin, B. Ostdiek and T. Plehn, *Towards the final word on neutralino dark matter*, *Phys. Rev. D* **93** (2016) 063525 [arXiv:1510.03460] [INSPIRE].

[537] L. Roszkowski, E.M. Sessolo and S. Trojanowski, *WIMP dark matter candidates and searches — current status and future prospects*, *Rept. Prog. Phys.* **81** (2018) 066201 [arXiv:1707.06277] [INSPIRE].

JHEP09(2021)080

[538] J.R. Ellis, T. Falk and K.A. Olive, *Neutralino-Stau coannihilation and the cosmological upper limit on the mass of the lightest supersymmetric particle*, *Phys. Lett. B* **444** (1998) 367 [hep-ph/9810360] [INSPIRE].

[539] J.R. Ellis, T. Falk, K.A. Olive and M. Srednicki, *Calculations of neutralino-stau coannihilation channels and the cosmologically relevant region of MSSM parameter space*, *Astropart. Phys.* **13** (2000) 181 [*Erratum ibid.* **15** (2001) 413] [hep-ph/9905481] [INSPIRE].

[540] T. Nihei, L. Roszkowski and R. Ruiz de Austri, *Exact cross-sections for the neutralino slepton coannihilation*, *JHEP* **07** (2002) 024 [hep-ph/0206266] [INSPIRE].

[541] K. Harigaya, K. Kaneta and S. Matsumoto, *Gaugino coannihilations*, *Phys. Rev. D* **89** (2014) 115021 [arXiv:1403.0715] [INSPIRE].

[542] XENON100 collaboration, *Dark matter results from* 225 *live days of XENON100 data*, *Phys. Rev. Lett.* **109** (2012) 181301 [arXiv:1207.5988] [INSPIRE].

[543] PandaX-II collaboration, *Dark matter results from first* 98.7 *days of data from the PandaX-II experiment*, *Phys. Rev. Lett.* **117** (2016) 121303 [arXiv:1607.07400] [INSPIRE].

[544] LUX collaboration, *Results from a search for dark matter in the complete LUX exposure*, *Phys. Rev. Lett.* **118** (2017) 021303 [arXiv:1608.07648] [INSPIRE].

[545] T. Bringmann, J. Edsjö, P. Gondolo, P. Ullio and L. Bergström, *DarkSUSY 6: an advanced tool to compute dark matter properties numerically*, *JCAP* **07** (2018) 033 [arXiv:1802.03399] [INSPIRE].

[546] P. Huang and C.E.M. Wagner, *Blind spots for neutralino dark matter in the MSSM with an intermediate m_A*, *Phys. Rev. D* **90** (2014) 015018 [arXiv:1404.0392] [INSPIRE].

[547] L. Calibbi, I. Galon, A. Masiero, P. Paradisi and Y. Shadmi, *Charged slepton flavor post the* 8 *TeV LHC: a simplified model analysis of low-energy constraints and LHC SUSY searches*, *JHEP* **10** (2015) 043 [arXiv:1502.07753] [INSPIRE].

[548] M. Chakraborti, S. Heinemeyer and I. Saha, *Improved $(g-2)_\mu$ measurements and wino/higgsino dark matter*, arXiv:2103.13403 [INSPIRE].

[549] J.L. Feng, K.T. Matchev and T. Moroi, *Focus points and naturalness in supersymmetry*, *Phys. Rev. D* **61** (2000) 075005 [hep-ph/9909334] [INSPIRE].

[550] J.L. Feng, K.T. Matchev and T. Moroi, *Multi-TeV scalars are natural in minimal supergravity*, *Phys. Rev. Lett.* **84** (2000) 2322 [hep-ph/9908309] [INSPIRE].

[551] J.R. Ellis, K.A. Olive and P. Sandick, *Phenomenology of GUT-less supersymmetry breaking*, *JHEP* **06** (2007) 079 [arXiv:0704.3446] [INSPIRE].

[552] J.C. Costa et al., *Likelihood Analysis of the Sub-GUT MSSM in Light of LHC 13-TeV Data*, *Eur. Phys. J. C* **78** (2018) 158 [arXiv:1711.00458] [INSPIRE].

[553] M. Beneke, R. Szafron and K. Urban, *Sommerfeld-corrected relic abundance of wino dark matter with NLO electroweak potentials*, *JHEP* **02** (2021) 020 [arXiv:2009.00640] [INSPIRE].

[554] H. Baer, V. Barger, D. Sengupta and X. Tata, *Is natural higgsino-only dark matter excluded?*, *Eur. Phys. J. C* **78** (2018) 838 [arXiv:1803.11210] [INSPIRE].

[555] O. Buchmueller et al., *The CMSSM and NUHM1 after LHC Run 1*, *Eur. Phys. J. C* **74** (2014) 2922 [arXiv:1312.5250] [INSPIRE].

[556] P. Bechtle et al., *Killing the CMSSM softly*, *Eur. Phys. J. C* **76** (2016) 96 [arXiv:1508.05951] [INSPIRE].

JHEP09(2021)080

[557] C. Han, K.-i. Hikasa, L. Wu, J.M. Yang and Y. Zhang, *Status of CMSSM in light of current LHC Run-2 and LUX data*, *Phys. Lett. B* **769** (2017) 470 [arXiv:1612.02296] [INSPIRE].

[558] GAMBIT collaboration, *Global fits of GUT-scale SUSY models with GAMBIT*, *Eur. Phys. J. C* **77** (2017) 824 [arXiv:1705.07935] [INSPIRE].

[559] LUX-ZEPLIN collaboration, *Projected WIMP sensitivity of the LUX-ZEPLIN dark matter experiment*, *Phys. Rev. D* **101** (2020) 052002 [arXiv:1802.06039] [INSPIRE].

[560] XENON collaboration, *Projected WIMP sensitivity of the XENONnT dark matter experiment*, *JCAP* **11** (2020) 031 [arXiv:2007.08796] [INSPIRE].

[561] CLICdp, CLIC collaboration, *The Compact Linear Collider (CLIC) — 2018 Summary Report*, arXiv:1812.06018 [INSPIRE].

[562] R. Capdevilla, D. Curtin, Y. Kahn and G. Krnjaic, *Discovering the physics of $(g-2)_\mu$ at future muon colliders*, *Phys. Rev. D* **103** (2021) 075028 [arXiv:2006.16277] [INSPIRE].

[563] D. Buttazzo and P. Paradisi, *Probing the muon $g-2$ anomaly at a muon collider*, arXiv:2012.02769 [INSPIRE].

[564] W. Yin and M. Yamaguchi, *Muon $g-2$ at multi-TeV muon collider*, arXiv:2012.03928 [INSPIRE].

[565] R. Capdevilla, D. Curtin, Y. Kahn and G. Krnjaic, *A no-lose theorem for discovering the new physics of $(g-2)_\mu$ at muon colliders*, arXiv:2101.10334 [INSPIRE].

[566] K. Cheung and Z.S. Wang, *Physics potential of a muon-proton collider*, *Phys. Rev. D* **103** (2021) 116009 [arXiv:2101.10476] [INSPIRE].

[567] T. Han, S. Li, S. Su, W. Su and Y. Wu, *Heavy Higgs bosons in 2HDM at a muon collider*, arXiv:2102.08386 [INSPIRE].

[568] J-PARC G-2 collaboration, *New $g-2$ experiment at J-PARC*, *Chin. Phys. C* **34** (2010) 745 [INSPIRE].

[569] M. Abe et al., *A new approach for measuring the muon anomalous magnetic moment and electric dipole moment*, *PTEP* **2019** (2019) 053C02 [arXiv:1901.03047] [INSPIRE].

[570] G. Abbiendi et al., *Measuring the leading hadronic contribution to the muon g-2 via μe scattering*, *Eur. Phys. J. C* **77** (2017) 139 [arXiv:1609.08987] [INSPIRE].

[571] P. Banerjee et al., *Theory for muon-electron scattering @ 10 ppm: A report of the MUonE theory initiative*, *Eur. Phys. J. C* **80** (2020) 591 [arXiv:2004.13663] [INSPIRE].

[572] H. H. Patel, *Package-x 2.0: A mathematica package for the analytic calculation of one-loop integrals*, *Comput. Phys. Commun.* **218** (2017) 66.

[573] K. Fujikawa, B.W. Lee and A.I. Sanda, *Generalized renormalizable gauge formulation of spontaneously broken gauge theories*, *Phys. Rev. D* **6** (1972) 2923 [INSPIRE].

JHEP09(2021)080